АВТОМАТИКА
и
ТЕЛЕМЕХАНИКА

Vol. 21, No. 3, March, 1960

Translation Published November, 1960

SOVIET INSTRUMENTATION AND
CONTROL TRANSLATION SERIES

Automation and Remote Control

(The Soviet Journal *Avtomatika i Telemekhanika* in English Translation)

■ This translation of a Soviet journal on automatic control is published as a service to American science and industry. It is sponsored by the Instrument Society of America under a grant in aid from the National Science Foundation, continuing a program initiated by the Massachusetts Institute of Technology.

SOVIET INSTRUMENTATION AND CONTROL TRANSLATION SERIES

■ This translation of the Soviet Journal *Avtomatika i Telemekhanika* is published and distributed at nominal subscription rates under a grant in aid to the Instrument Society of America from the National Science Foundation. This translated journal, and others in the Series (see back cover), will enable American scientists and engineers to be informed of work in the fields of instrumentation, measurement techniques, and automatic control reported in the Soviet Union.

The original Russian articles are translated by competent technical personnel. The translations are on a cover-to-cover basis, permitting readers to appraise for themselves the scope, status,and importance of the Soviet work.

Publication of *Avtomatika i Telemekhanika* in English translation started under the present auspices in April, 1958, with Russian Vol. 18, No. 1 of January, 1957. The program has been continued with the translation and printing of the 1958, 1959, and 1960 issues.

Transliteration of the names of Russian authors follows the system known as the British Standard. This system has recently achieved wide adoption in the United Kingdom, and is currently being adopted by a large number of scientific journals in the United States.

All views expressed in the translated material are intended to be those of the original authors, and not those of the translators, nor the Instrument Society of America.

Readers are invited to submit communications on the quality of the translations and the content of the articles to ISA headquarters. Pertinent correspondence will be published in the "Letters" section of the ISA Journal. Space will also be made available in the ISA Journal for such replies as may be received from Russian authors to comments or questions by American readers.

1960 Volume 21 Subscription Prices:

Per year (12 issues), starting with Vol. 21, No. 1

General: United States and Canada	$35.00
Elsewhere	38.00
Libraries of nonprofit academic institutions:	
United States and Canada	$17.50
Elsewhere	20.50
Single issues to everyone, each	$ 6.00

1957 Volume 18, 1958 Volume 19, and 1959 Volume 20 issues also available. Prices upon request.

See back cover for combined subscription to entire Series.

Subscriptions and requests for information on back issues should be addressed to the:

Instrument Society of America
313 Sixth Avenue, Pittsburgh 22, Penna.

Translated and printed by Consultants Bureau Enterprises, Inc.

Automation and Remote Control

A translation of Avtomatika i Telemekhanika, a publication of the Academy of Sciences of the USSR

Russian Original Dated March, 1960

Vol. 21, No. 3, pp. 195-302 November, 1960

CONTENTS

ESTIMATING THE EFFECT OF QUANTIZATION BY LEVEL ON THE PROCESSES IN AUTOMATIC DIGITAL SYSTEMS

Ya. Z. Tsypkin

(Moscow)

Translated from Avtomatika i Telemekhanika, Vol. 21, No. 3, pp. 281-285, March, 1960
Original article submitted July 28, 1959

An estimate is given of the effect of the level-quantization interval in automatic digital systems whose continuous portions contain both constant and variable parameters.

INTRODUCTION

In automatic digital systems (ADS) at least one quantity is subject to quantization by level and by time. The quantization process consists in fixing previously given discrete levels at discrete moments of time. Level-quantization interval σ_z is determined by the accuracy, and time-quantization interval T by the speed of action, of the digital devices which belong to the automatic system.

The effect of the time-quantization interval was studied earlier [1,2]. An estimate of the effect of the level-quantization interval was made in [3] on the basis of the canonical forms of equations. Due to this, the results of the estimation process were obtained in an unnecessarily complicated form. Moreover, it is not possible to concur with all the conclusions of [3].

Below, we present a simple way of estimating the effect of the level-quantization interval which is not related to the canonical forms of equations, and which is valid for ADS with constant and with variable parameters.

1. Equivalent Scheme of an ADS

We consider the ADS scheme shown on Fig. 1. The functional schematic of the device (AD) for analog-to-digital conversion (Fig. 2, a) may be presented in the form of a series connection of a pulse element and a relay element with a multistep characteristic (Fig. 2,b).

In its turn, the relay element can be presented in the form of a parallel connection of an amplifying element with gain k = 1 and a nonlinear element (Fig. 2, c) whose characteristic Ψ equals the difference between a linear and the relay characteristic.

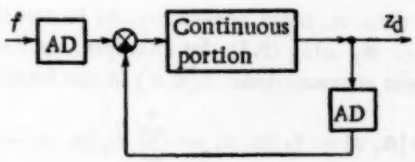

Fig. 1.

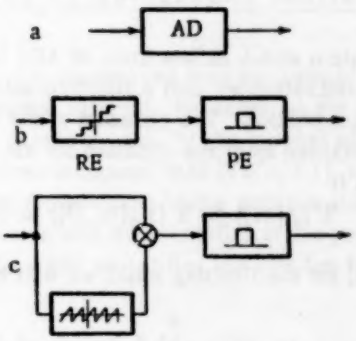

Fig. 2.

By using this representation of the AD converter, we can replace the ADS scheme by the equivalent scheme of a limiting sampled-data system in which the effect of the level quantization is taken into account by the stimuli applied to it via the nonlinear element with characteristic Ψ. In Fig. 3, a, this system is represented

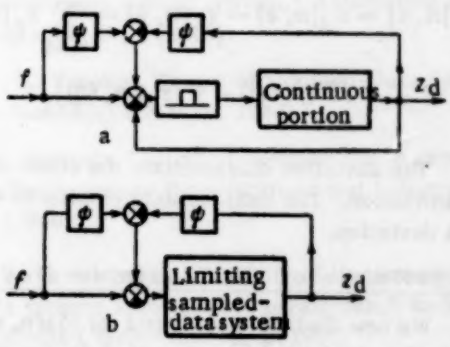

Fig. 3.

as a sampled-data system with a linear feedback path; on Fig. 3, b, the feedback path is included in the limiting system.

We denote the impulse characteristic of the closed linear sampled-data system, which can also contain variable

parameters, by $k_c[n, m, \epsilon]$. Methods of determining $k_c[n, m, \epsilon]$ were described in [4]. If there are no variable parameters, then

$$k_c[n, m, \varepsilon] = k_c[n - m, \varepsilon]. \tag{1.1}$$

By using the impulse characteristic, we can write the equation of the ADS of Fig. 3, b in the form

$$z_d[n, \varepsilon] = \sum_{m=0}^{n} k_c[n, m, \varepsilon]\{[\Psi(f[m]) - \Psi(z_d[m, 0])] + f[m]\}. \tag{1.2}$$

2. Deviations Engendered by Level Quantization

A system which differs from an ADS by its absence of level quantization we call a limiting automatic sampled-data system (ASDS). The equation of the limiting ASDS can be obtained from the equation for the ADS (1.2) by setting in it

$$\Psi(f[m]) \equiv \Psi(z_d[m, 0]) \equiv 0. \tag{2.1}$$

Thus, for the limiting ASDS we will have

$$z_s[n, \varepsilon] = \sum_{m=0}^{n} k_c[n, m, \varepsilon] f[m] \tag{2.2}$$

or

$$z_s[n, \varepsilon] = \sum_{m=0}^{n} k_c[n, n - m, \varepsilon] f[n - m]. \tag{2.3}$$

The difference between $z_d[n, \epsilon]$ and $z_s[n, \epsilon]$, defining the effect of level quantization, may be presented on the basis of (1.2) and (2.2), in the form

$$\delta z[n, \varepsilon] = z_d[n, \varepsilon] - z_s[n, \varepsilon] = \sum_{m=0}^{n} k_c[n, m, \varepsilon] \{\Psi(f[m]) - \Psi(z_d[m, 0])\}. \tag{2.4}$$

The deviation characterizes the effect of level quantization. The next problem consists in estimating this deviation.

3. Estimate of the Maximum Deviation

We now find an upper bound for $|\delta z[n, \epsilon]|$. By replacing, in the left member of (2.4), the absolute magnitude of the sum by the sum of the absolute magnitudes, we get

$$|\delta z[n, \varepsilon]| \leqslant \sum_{m=0}^{n} |k_c[n, m, \varepsilon]| \{|\Psi(f[m])| + |\Psi(z_d[m, 0])|\}. \tag{3.1}$$

But the difference between the linear and the relay characteristics or, what amounts to the same thing, between the nonquantized and the quantized quantities, may not, in absolute magnitude, exceed half the quantization interval $\sigma/2$. Therefore,

$$|\Psi(f[m])| \leqslant \frac{\sigma}{2}, \quad |\Psi(z_d[m, 0])| \leqslant \frac{\sigma}{2}. \tag{3.2}$$

By using these inequalities, and replacing the left member of (3.1) by the maximum value, we obtain

$$\max|\delta z[n, \varepsilon]| \leqslant \sum_{m=0}^{n} |k_c[n, m, \varepsilon]|\,\sigma \tag{3.3}$$

or, after replacing the variable of summation m by n–m,

$$\max|\delta z[n, \varepsilon]| \leqslant \sum_{m=0}^{n} |k_c[n, n - m, \varepsilon]|\,\sigma. \tag{3.4}$$

On the basis of (1.1), for an ADS with constant parameters we obtain from (3.3) and (3.4), respectively,

$$\max|\delta z[n, \varepsilon]| \leqslant \sum_{m=0}^{n} |k_c[n - m, \varepsilon]|\,\sigma \tag{3.5}$$

or

$$\max|\delta z[n, \varepsilon]| \leqslant \sum_{m=0}^{n} |k_c[m, \varepsilon]|\,\sigma. \tag{3.6}$$

Thus, the process' maximum deviation engendered by level quantization does not exceed the sum of the absolute values of the impulse characteristic of the limiting ASDS multiplied by the quantization interval.

An estimate of the steady-state deviation is found from (3.4), (3.6) if the limit of summation n tends to ∞.

For an ADS with constant parameters, the estimate of the steady-state deviation is the greatest possible one.

This estimate corresponds to the maximum possible accumulation in the limiting ASDS for stimuli which are modulus-limited, and is the discrete analog of the accumulation problem of B. V. Bulgakov.

4. Comparison of Some Properties of the Limiting ASDS and the ADS

If a step function stimulus

$$f[n] = \begin{cases} 1 & \text{for } n \geqslant 0, \\ 0 & \text{for } n < 0, \end{cases}$$

is applied to the limiting ASDS, its reaction is determined by its time or, more accurately, by its transient characteristic. By using (2.3), for example, we can present the transient characteristic $h[n, \epsilon]$ in the form

$$h[n, \varepsilon] = z_s[n, \varepsilon] = \sum_{m=0}^{n} k_c[n, n - m, \varepsilon]. \tag{4.1}$$

The steady-state characteristic will be

$$h_{ste}[n, \varepsilon] = \sum_{m=0}^{\infty} k_c[n, n-m, \varepsilon]. \quad (4.2)$$

It is a function of n and ϵ. For an ADS with constant parameters,

$$h_{ste}[n, \varepsilon] = h(\varepsilon) = \sum_{m=0}^{\infty} k_c[m, \varepsilon] \quad (4.3)$$

is a function of ϵ only. If the ASDS is designed to reproduce the stimuli applied to it then, in general,

$$h_{ste}[n, \varepsilon] = h(\varepsilon) \leqslant 1. \quad (4.4)$$

We assume that the impulse characteristic of the limiting ASDS, $k_c[n, n-m, \epsilon]$, for given n and ϵ and arbitrary m, is nonnegative, i.e.,

$$k_c[n, n-m, \varepsilon] \geqslant 0, \quad (4.5)$$

so that we shall have, from (3.4) and (4.1),

$$\max|\delta z[n, \varepsilon]| \leqslant \sum_{m=0}^{n} k_c[n, n-m, \varepsilon]\sigma = h[n, \varepsilon]\sigma. \quad (4.6)$$

Thus, in this case the maximum deviation at the given moment of time which is engendered by the level quantization does not exceed the quantity equal to the product of the quantization interval by the value of the characteristic at that same moment of time.

The estimate of the steady-state deviation will have the form

$$\max|\delta z_{ste}[n, \varepsilon]| \leqslant \sum_{m=0}^{\infty} k_c[n, n-m, \varepsilon]\sigma = h_{ste}[n, \varepsilon]\sigma. \quad (4.7)$$

Let us consider in somewhat more detail an ADS with constant parameters. For it, the [(4.5)] that $k_c[m, \epsilon] \geq 0$ is equivalent to the condition that $h[n, \epsilon]$ be monotonic for ϵ = const. By taking into account that $h[n, \epsilon] \leq h_{ste}[n, \epsilon] = h(\epsilon)$, we find that

$$\max|\delta z[n, \varepsilon]| \leqslant h[n, \varepsilon]\sigma < h_{ste}[n, \varepsilon]\sigma = h(\varepsilon)\sigma \quad (4.8)$$

or, by taking (4.4) into account,

$$\max|\delta z[n, \varepsilon]| \leqslant \sigma. \quad (4.9)$$

Thus, for a monotonic characteristic, the deviation due to level quantization does not exceed the quantization interval. In this case, and only in this case, we can deduce the stability of the ADS from the stability of the limiting ASDS. If the characteristic is not monotonic, i.e., the impulse characteristic changes sign, the sum of the absolute values of the impulse characteristic may significantly exceed unity, and instead of (4.6) we shall therefore have

$$\max|\delta z[n, \varepsilon]| \leqslant \alpha\sigma. \quad (4.10)$$

where $\alpha > 1$. Under these conditions, it is possible to have, in an ADS with constant parameters, an autooscillatory mode with an "amplitude" not exceeding $\alpha\sigma$. The greater the oscillation of the characteristic $h[n, \epsilon]$ for ϵ = const, i.e., the greater the oscillation of the limiting ASDS, the greater will be the "amplitude" of the autooscillatory modes possible in the ADS.

Thus, in spite of the assertion made in [3], it is, strictly speaking, impossible in this case to conclude that the ADS is stable from the fact that the limiting ASDS is stable.

The result just derived does not depend on the size of the quantization interval. However, as the quantization interval σ decreases, i.e., as the number of places in the digital devices increases, $\max|\delta z[n, \epsilon]|$ will increase and, despite the presence of the possible autooscillations, their amplitude will be so small that the processes in the ADS and the ASDS will differ less and less from each other.

The estimates given above allow one to determine the maximum quantization interval for which the difference of the processes in the ADS and the ASDS will not exceed a given magnitude.

LITERATURE CITED

1. Ya. Z. Tsypkin, "Frequency method of analyzing discontinuous control systems," Avtomatika i Telemekhanika 19, 1 (1958).
2. Ya. Z. Tsypkin, Theory of Sampled-Data Systems [in Russian] (Fizmatgiz, 1958).
3. J. E. Bertram, "Effect of quantization in sampled-feedback systems," Applications and Industry No. 38 (1958).
4. G. P. Tartakovskii, "Stability of linear sampled-data systems with variable parameters," Radiotekhnika i Elektronika 2, 1 (1957).

DETERMINATION OF THE OPTIMAL IMPULSIVE RESPONSE FUNCTION IN THE PRESENCE OF INTERNAL NOISE

P. S. Matveev

(Moscow)

Translated from Avtomatika i Telemekhanika, Vol. 21, No. 3, pp. 286-292, March, 1960
Original article submitted May 8, 1959

The problem of determining the optimal transfer function [1, 2] is generalized to the cases when the input stimuli are applied to n different elements of a servosystem and to systems with variable parameters.

In [1, 2] a solution was given to the problem of determining the optimal impulsive response function for cases when input stimuli are applied to two different elements of a servosystem. The aim of the present work is to generalize the results obtained in [1, 2] to the case when the stimuli are applied to n elements of a servosystem, and to systems with variable parameters.

1. Determination of the Impulsive Response Function in the Class of Systems with Constant Parameters

We assume that the servosystem has n elements to which stimuli are applied, whereby a controlling signal

$$y(t) = g(t) + m(t), \tag{1}$$

is applied to one basic element, where g(t) is a given function of time, with

$$g(t) = \sum_{i=0}^{r} g_i t^i, \tag{2}$$

and m(t) is a stationary random function.

In addition, noise n(t), in the form of a stationary random function, is superimposed on the controlling signal. To the remaining n − 1 elements of the servosystem (Fig. 1), stimuli are applied in the form of stationary random functions $u_1(t), u_2(t), \ldots, u_{n-1}(t)$. We assume for simplicity that $m(t), n(t), u_1(t), u_2(t), \ldots, u_{n-1}(t)$ have zero mean values and are mutually uncorrelated. We also assume that the transfer functions $W_1(p), W_2(p), \ldots, W_{n-1}(p)$ [or the corresponding impulsive response functions $b_1(t), b_2(t), \ldots, b_{n-1}(t)$] are known. What is not known is the transfer function $W_c(p)$ (impulsive response function) of the correcting device. We initially determine the optimal impulsive response function k(t) of the closed system from which, by using well-known methods [2, 3], we can easily determine the transfer function $W_c(p)$ of the correcting device. The problem may be formulated in the following way: from given correlation functions $R_m(\tau), R_n(\tau), R_{u_1}(\tau), R_{u_2}(\tau), \ldots, R_{u_{n-1}}(\tau)$ [spectral densities $S_m(\omega), S_n(\omega), S_{u_1}(\omega), S_{u_2}(\omega), \ldots, S_{u_{n-1}}(\omega)$], given duration T of the transient response, given reproduction operator H(p), error coefficients C_l and transfer functions $W_1(p), W_2(p), \ldots, W_{n-1}(p)$, to find the impulsive response function k(t) such that the mean-square error will be a minimum.

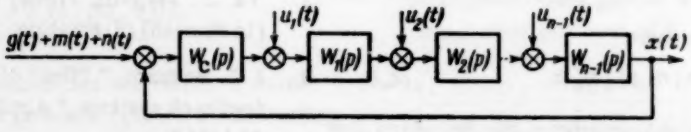

Fig. 1.

It is easily shown that the scheme shown on Fig. 2, for n = 3, is equivalent to the scheme of Fig. 1. This scheme will be used for the subsequent argument. Then [4], the system's output quantity can be written in the following way:

$$x(t) = \int_0^T [g(t-\tau) + m(t-\tau) + n(t-\tau)]\, k(\tau)\, d\tau - \int_0^T k(\tau)\, d\tau \int_{-\infty}^{\infty} b_1(\sigma)\, d\sigma \int_{-\infty}^{\infty} u_1(t-\tau-\sigma-\mu)\, b_2(\mu)\, d\mu - \tag{3}$$

$$-\int_0^T k(\tau)\,d\tau\int_{-\infty}^{\infty} u_2(t-\tau-\sigma)\,b_2(\sigma)\,d\sigma+\int_{-\infty}^{\infty} b_1(\tau)\,d\tau\int_{-\infty}^{\infty} u_1(t-\tau-\sigma)\,b_2(\sigma)\,d\sigma$$

$$+\int_{-\infty}^{\infty} u_2(t-\tau)\,b_2(\tau)\,d\tau,$$

where

$$k(\tau)=N(t)+\sum_{j=0}^{q} E_j\,\delta^{(j)}(t)+\sum_{j=0}^{q}\delta^{(j)}(t-T)\quad(0<t<T). \tag{4}$$

Let the ideal system be required to reproduce at its output the signal

$$h(t)=H_g(p)\,g(t)+H(p)\,m(t), \tag{5}$$

where

$$H(p)=\sum_{i=0}^{r}\frac{H_i}{i!}\,p^i,\quad H_g(p)=H(p)-\sum_{j=0}^{r}\frac{C_j}{j!}\,p^j\quad(i\neq j). \tag{6}$$

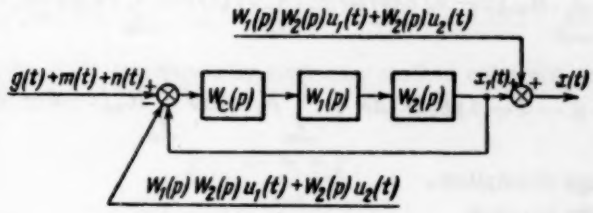

Fig. 2

Here, for convenience, we have introduced the operator $H_g(p)$ which simultaneously takes into account the operation of reproducing g(t) and the errors with which it is reproduced.

Then the reproduction error can be written in the form

$$\varepsilon(t)=h(t)-x(t).$$

If it now be required that the mean error of reproduction equal zero, then [2, 4, 5] we are led to limitations of k(t) of the form

$$\mu_\nu=(-1)^\nu\int_0^T\tau^\nu k(\tau)\,d\tau\quad(\nu=0,1,2,\ldots,r) \tag{7}$$

or

$$H_i=(-1)^\nu\int_0^T\tau^i k(\tau)\,d\tau,\quad -C_j=(-1)\int_0^T\tau^j k(\tau)\,d\tau\quad(j\neq i=0,1,2,\ldots,r), \tag{8}$$

If (8) holds, the reproduction error can be written in the following way:

$$\varepsilon(t)=\int_{-\infty}^{\infty} m(t-\tau)\,x(\tau)\,d\tau-\int_0^T k(\tau)\,d\tau\,[m(t-\tau)+n(t-\tau)-$$

$$-\int_{-\infty}^{\infty} b_1(\sigma)\,d\tau\int_{-\infty}^{\infty} u_1(t-\tau-\sigma-\mu)\,b_2(\mu)\,d\mu-\int_{-\infty}^{\infty} u_2(t-\tau-\sigma)\,b_2(\sigma)\,d\sigma\Big]- \tag{9}$$

$$-\int_{-\infty}^{\infty} b_1(\tau)\,d\tau\int_{-\infty}^{\infty} u_1(t-\tau-\sigma)\,b_2(\sigma)\,d\sigma-\int_{-\infty}^{\infty} u_2(t-\tau)\,b_2(\tau)\,d\tau,$$

where

$$x(t) = \frac{1}{2\pi} \int_{-\infty}^{\infty} H(j\omega)\, e^{j\omega t}\, d\omega.$$

Further, by using the same arguments as in [2, 4, 5, 6], we obtain the necessary and sufficient condition for the minimum average value of the square of (9), when (7) holds, in the form of an integral equation

$$\int_0^T \Big[R_m(\tau-\theta) + R_n(\tau-\theta) + \int_{-\infty}^{\infty} b_1(\sigma)\,d\sigma \int_{-\infty}^{\infty} b_2(\mu)\,d\mu \int_{-\infty}^{\infty} b_1(\lambda)\,d\lambda \times \int_{-\infty}^{\infty} R_{u_1}(\tau+\sigma+\mu-\theta-\lambda-\eta)\, b_2(\eta)\,d\eta + \int_{-\infty}^{\infty} b_2(\sigma)\,d\sigma \int_{-\infty}^{\infty} R_{u_2}(\tau+\sigma-\theta-\lambda)\, b_2(\lambda)\,d\lambda\Big] k(\theta)\,d\theta = \tag{10}$$

$$= \int_{-\infty}^{\infty} R_m(\tau-\theta)\, x(\theta)\,d\theta + \int_{-\infty}^{\infty} b_1(\sigma)\,d\sigma \int_{-\infty}^{\infty} b_2(\mu)\,d\mu \int_{-\infty}^{\infty} b_1(\theta)\,d\theta \int_{-\infty}^{\infty} R_{u_1}(\tau+\sigma+\mu-\theta-\lambda)\, b_2(\lambda)\,d\lambda + \int_{-\infty}^{\infty} b_2(\sigma)\,d\sigma \int_{-\infty}^{\infty} R_{u_2}(\tau+\sigma-\theta)\, b_2(\theta)\,d\theta + \sum_{i=0}^{r} \gamma_i \tau^i,$$

where the γ_i are Lagrange multipliers.

We now introduce the notation

$$R^*_{u_1}(\tau-\theta) = \int_{-\infty}^{\infty} b_1(\sigma)\,d\sigma \int_{-\infty}^{\infty} b_2(\mu)\,d\mu \int_{-\infty}^{\infty} b_1(\lambda)\,d\lambda \times \int_{-\infty}^{\infty} R_{u_1}(\tau+\sigma+\mu-\theta-\lambda-\eta)\, b_2(\eta)\,d\eta, \tag{11}$$

$$R^*_{u_2}(\tau-\theta) = \int_{-\infty}^{\infty} b_2(\sigma)\,d\sigma \int_{-\infty}^{\infty} R_{u_2}(\tau+\sigma-\theta-\lambda)\, b_2(\lambda)\,d\lambda. \tag{12}$$

With the use of the notation of (11) and (12), (10) can be presented in the following form:

$$\int_0^T [R_m(\tau-\theta) + R_n(\tau-\theta) + R^*_{u_1}(\tau-\theta) + R^*_{u_2}(\tau-\theta)]\, k(\theta)\,d\theta =$$

$$= \int_{-\infty}^{\infty} R_m(\tau-\theta)\, x(\theta)\,d\theta + R^*_{u_1}(\tau) + R^*_{u_2}(\tau) + \sum_{i=0}^{r} \gamma_i \tau^i \quad (0 \leqslant \tau \leqslant T). \tag{13}$$

Equation (13) does not differ in form from the integral equations obtained in [2, 4, 5, 6] and, therefore, the same methods of solution may be used for the determination of k(τ). Obviously, integral equation (13) is easily generalized to the case of n inputs. For this, integral equation (13) can be written in the form

$$\int_0^T [R_m(\tau-\theta) + R_n(\tau-\theta) + R^*_{u_1}(\tau-\theta) + R^*_{u_2}(\tau-\theta) + \ldots + R_{u_{(n-1)}}(\tau-\theta)]\, k(\theta)\,d\theta = \int_{-\infty}^{\infty} R_m(\tau-\theta)\, x(\theta)\,d\theta + R^*_{u_1}(\tau) + R^*_{u_2}(\tau) + \ldots + R^*_{u_{(n-1)}}(\tau-\theta) + \sum_{i=0}^{r} \gamma_i \tau^i \quad (0 \leqslant \tau \leqslant T). \tag{14}$$

If the correlation function $R_m(\tau) + R_n(\tau) + R^*_{u_1}(\tau) + \ldots + R^*_{u_{(n-1)}}(\tau)$ corresponds to a rational-fraction spectral density

$$S(\omega)=\frac{a_0+a_1\omega^2+\ldots+a_k\omega^{2k}}{b_0+b_1\omega^2+\ldots+b_l\omega^{2l}}=\frac{M(\omega)M^*(\omega)}{L(\omega)L^*(\omega)}, \tag{15}$$

then, by using the same arguments as in [5], we can shown that the impulsive response function is defined by the expression *

$$k(t)=\sum_{i=0}^{r}A_i t^i+\sum_{i=1}^{2k}B_i e^{\lambda_i t}+\sum_{j=0}^{q}E_j\delta^{(j)}(t)+\sum_{j=0}^{q}D_j\delta^{(j)}(t-T)+$$

$$+L(p)L^*(p)M^{-1}(p)M^{*-1}(p)\Big[\int_{-\infty}^{\infty}R_m(t-\tau)\varkappa(\tau)\,d\tau+$$

$$+R^*_{u_1}(t)+R^*_{u_2}(t)+\ldots+R^*_{u_{(n-1)}}(t)\Big]\quad(0\leqslant t\leqslant T), \tag{16}$$

where q= l–k–1 and L(p) and M(p) equal L (ω) and M(ω) for p = jω, which are easily determined from the spectral density of (15).

The unknowns A_i, B_i, E_j, D_j in (16) are determined as in [5]. Further, by the usual methods [3], the transfer function of the closed system was determined and later, also, the transfer function of the correcting device.

2. Determination of the Impulsive Response Function in the Class of Systems with Variable Parameters

We assume that the system (Fig. 3) is acted upon by stationary random noise n(t) and signal y(t) = g(t) + m(t) consisting of the given function of time

$$g(t)=\sum_{i=0}^{r}g_i t^i, \tag{17}$$

where the g_i are unknown coefficients and the t^i are known functions of time, plus the stationary random function m(t). To the system's second element there is applied a disturbing stimulus in the form of the stationary random function u(t).

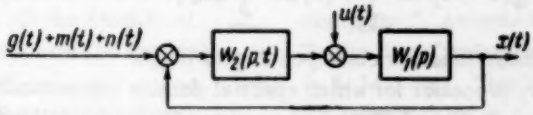

Fig. 3.

The problem solved below may be formulated as follows: from given correlation functions $R_m(\tau)$, $R_n(\tau)$, and $R_u(\tau)$ (spectral densities) and given object transfer function $W_1(p)$, to find the servosystem's impulsive response function such that the system will provide an exact reproduction of g(t) at each moment of time t > 0 and a minimum dispersion of the random process at the system's output at each moment of time.

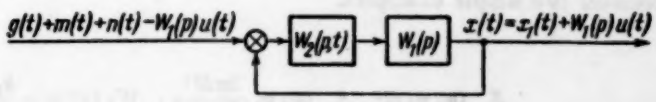

Fig. 4.

It may be shown that the scheme of Fig. 4 is equivalent to that shown on Fig. 3. Henceforth, the scheme of Fig. 4 will be used.

The reproduction error of the system (Fig. 3) can be given in the form

$$\epsilon(t)=g(t)+m(t)-x(t)=[1+W_1(p)W_2(p,t)]^{-1}[g(t)+m(t)-Q(t)]-$$
$$-[1+W_1(p)W_2(p,t)]^{-1}W_1(p)W_2(p,t)n(t), \tag{18}$$

where $$Q(t)=W_1(p)u(t).$$

The reproduction error of the system given by Fig. 4 may be written in the form

* An analogous generalization can also be made for the case when g(t) is a harmonic function [4].

$$\varepsilon_1(t) = g(t) + m(t) - Q(t) - x_1(t) =$$
$$= [1 + W_1(p)\,W_2(p, t)]^{-1}[g(t) + m(t) - Q(t)] -$$
$$-[1 + W_1(p)\,W_2(p, t)]^{-1} W_1(p)\,W_2(p, t)\,n(t). \tag{19}$$

By comparing (18) and (19), we find that $\epsilon(t) = \epsilon_1(t)$ and, consequently, just as in [4, 7], the reproduction error can be written in the form

$$\varepsilon(t) = g(t) + m(t) - Q(t) - x(t) = g(t) + m(t) - Q(t) -$$
$$-\int_{-\infty}^{t} [g(\tau) + m(\tau) - Q(\tau) + n(\tau)]\,k(t, \tau)\,d\tau \quad (t \geqslant \tau). \tag{20}$$

The requirement that there be no bias, i.e., zero dynamic error, leads to r + 1 conditions of the form

$$t^i = \int_0 \tau^i k(t, \tau)\,d\tau. \tag{21}$$

If (21) holds, the expression for the error has the form

$$\varepsilon(t) = m(t) - Q(t) - \int_{-\infty}^{t} [m(\tau) - Q(\tau) + n(\tau)]\,k(t, \tau)\,d\tau. \tag{22}$$

It may be shown [7] that the necessary and sufficient condition for a minimum mean value of the square of (22) amounts to this-that the impulsive response function $k(t, \tau)$ satisfy the integral equation

$$\int_{-\infty} [R_m(\tau - \theta) + R_n(\tau - \theta) + R_Q(\tau - \theta)]\,k(t, \theta)\,d\theta$$
$$= \sum_{i=0}^{r} \gamma_i \tau^i + R_m(t) + R_Q(t), \tag{23}$$

where

$$R_Q(\tau - \theta) = \int_{-\infty}^{\infty} b(\sigma)\,d\sigma \int_{-\infty}^{\infty} R_u(\tau + \sigma - \theta - \lambda)\,b(\lambda)\,d\lambda, \tag{24}$$

and $b(\tau)$ is the impulsive response function corresponding to $W_1(p)$.

For the class of stationary processes for which spectral density corresponding to $R_m(\tau) + R_n(\tau) + R_Q(\tau)$ can be given in the form of (15), the solution of (23) can be written [7] in the following form:

$$k(t, \tau) = \sum_{i=1}^{k} B_i(t)\,e^{\lambda_i \tau} + \sum_{i=0}^{r} A_i(t)\,\tau^i + \sum_{j=0}^{q} E_j\,\delta^{(j)}(t - \tau)$$
$$+ L(p)\,L^*(p)\,M^{-1}(p)\,M^{*-1}(p)\,[R_m(t) + R_Q(t)] \quad (t \geqslant \tau). \tag{25}$$

The rest of the argument is the same as in Section 1 of this paper.

In conclusion, we consider two simple examples.

Example 1. Let

$$S_{u_1}(\omega) = N^2, \quad S_{u_2}(\omega) = \frac{2\alpha M^2}{\omega^2 + \alpha^2}, \quad W_1(p) = \frac{k_1}{p + \tau_1}, \quad W_2 = \frac{k_2}{p + \tau_2},$$
$$H(p) = H_g(p) = 1, \quad g(t) = g_0 + g_1 t.$$

Then [3],

$$S^*_{u_1}(\omega) = |W_1(j\omega)|^2\,|W_2(j\omega)|^2\,S_{u_1}(\omega) = \frac{k_1^2 k_2^2 N^2}{(\omega^2 + \tau_1^2)(\omega^2 + \tau_2^2)},$$

$$S^*_{u_2}(\omega) = |W_2(j\omega)|^2\,S_{u_2}(\omega) = \frac{2\alpha k_2^2 M^2}{(\omega^2 + \tau_2^2)(\omega^2 + \alpha^2)},$$

$$S(\omega) = S^*_{u_1}(\omega) + S^*_{u_2}(\omega) = \frac{k_2^2}{\omega^2 + \tau_2^2}\left[\frac{(2\alpha M^2 + k_1^2 N^2)\,\omega^2 + 2\alpha\tau_1^2 M^2 + 2\alpha^2 k_1^2 N^2}{(\omega^2 + \alpha^2)(\omega^2 + \tau_1^2)}\right].$$

On the basis of (16), the impulsive response function will have the form

$$k(t) = A_0 + A_1 t + B_1 e^{\lambda_1 t} + B_2 e^{\lambda_2 t} + E_0 \delta(t) + E_1 \delta'(t) + D_0 \delta(t-T) + D_1 \delta'(t-T) + L(p) L^*(p) M^{-1}(p) M^{*-1}(p) [R^*_{u_1}(t) + R^*_{u_2}(t)],$$

where

$$M(p) M^*(p) = k_2^2 [-(2\alpha M^2 + k_1^2 N^2) p^2 + 2\alpha \tau_1^2 M^2 + 2\alpha^2 k_1^2 N^2],$$

$$L(p) L^*(p) = (\tau_2^2 - p^2)(\alpha^2 - p^2)(\tau_1^2 - p^2)$$

and λ_1 and λ_2 are the roots of the equation $M(\lambda) M^*(\lambda) = 0$.

The expressions for $R^*_{u_1}(t)$ and $R^*_{u_2}(t)$ are determined from (11) and (12).

Example 2. Let

$$g(t) = g_0 + g_1 t, \quad S_u(\omega) = N^2, \quad W_1(p) = \frac{k_1}{p+\tau}.$$

Then, $$S^*_u(\omega) = |W_1(j\omega)|^2 S_u(\omega) = \frac{k_1^2 N^2}{\omega^2 + \tau^2}.$$

On the basis of (25), we have

$$k(t, \tau) = A_0(t) + A_1(t)\tau + E_0(t)\delta(t-\tau) + D_0(t)\delta(t-\tau) + L(p) L^*(p) M^{-1}(p) M^{*-1}(p) R^*_u(t),$$

where $$M(p) M^*(p) = k_1^2 N^2, \quad L(p) L^*(p) = \tau^2 - p^2.$$

LITERATURE CITED

1. M. Pelegren, Statistical Design of Servosystems [Russian translation] (IL 1957).
2. P. S. Matveev, Method of Synthesizing Correcting Devices for Servosystems with Given Requirements on Quality Dynamic Accuracy in the Presence of Noise. Dissertation [in Russian] (1958).
3. V. V. Solodovnikov, Introduction to the Statistical Dynamics of Automatic Control Systems [in Russian] (Gostekhizdat, 1952).
4. P. S. Stimuli, Method of Determining the Optimal Impulsive Response function for One Class of Stimulii, Avtomatika i Telemekhanika 20, 1 (1959).
5. V. V. Solodovnikov and P. S. Matveev, Synthesis of Correcting Devices for Servo Systems in the Presence of Noise with Given Requirements on Dynamic Accuracy, Avtomatika i Telemekhanika 16, 3 (1955).
6. L. A. Zadeh and S. R. Ragazzini, "An extension of Wiener's Theory of Prediction," J. Appl. Phys. 21, No.7 (1950).
7. A. M. Batkov, "Analysis and synthesis of linear automatic control systems by the use of analog computers," Automatic Control and Computing Technology [in Russian] (Mashgiz, 1958).
8. P. S. Matveev, "Synthesis of correcting devices for servosystems in the presence of noise," Avtomatika i Telemekhanika, 20, 6 (1959).
9. N. Wiener, Extrapolation, Interpolation and Smoothing of Stationary Time Series (John Wiley, New York, 1949).

ON THE AUTOOSCILLATIONS OF A DYNAMIC TABLE PLATFORM

G. P. Miroshnichenko

(Moscow)

Translated from Avtomatika i Telemekhanika, Vol. 21, No. 3, pp. 293-300, March 1960
Original article submitted December 1, 1959

Determined in this paper are several properties of the motion of the platform of a single-axis dynamic table with an asynchronous motor with a tubular rotor, as well as the conditions under which autooscillations will arise when there is dry friction in the bearings.

In the design and testing of autopilots, one uses tables, that is, dynamic models comprised of a device with a platform on which the autopilot's sensitive element is placed. The platform turns about its center of mass in accordance with the aircraft's law of motion.

Tables may be divided into two classes.

a) Tables whose drives work like a servosystem at whose input a signal from an electronic computer is applied. The errors of such tables, given a small coefficient of friction, are basically determined by the inertia of the drive and the platform.

b) Tables which operate on the principle of dynamic similarity. The output element of such a table is the platform on which torques act which are proportional to the aerodynamic torques acting on the aircraft. The coefficient of similarity equals the ratio of the inertial torques relative to the corresponding axes of the platform (with the autopilot's sensitive element mounted on it) and the aircraft. In this case, the platform's moment of inertia is, in some scale, the aircraft's moment of inertia. The table's viscous friction can be taken into account by the proper decrease of the aerodynamic damping. In this case, the table's errors are principally determined by the presence of dry friction, which may introduce significant distortions in the simulation of certain modes, for example, motion at high altitudes where the damping is small.

Therefore, the study of the effect of friction and of other factors causing distortions in dynamic similarity, including the autooscillations to be studied here, is of practical interest, the more so since tuning of the coefficient of static stability a_2 is carried out by measuring the frequency of the platform's autooscillations.

A single-axis mechanical dynamic table was used by Oppelt [1]. The theory of such tables was developed by him.

In the present paper, the nonlinear problem is solved by a method similar to that of A. A. Andronov.

The single-axis dynamic table is represented by a mathematical two-dimensional model leading, in one case, to Milne's equation and, in the other to Liénard's equation.

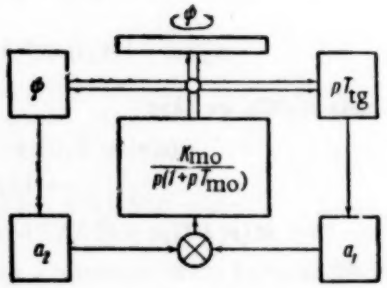

Fig. 1.

The table (Fig. 1) consists of a platform turned by an asynchronous motor with a tubular rotor whose transfer function (if the motor is considered as a linear link) is $k_{mo}/p(1 + pT_{mo})$, where k_{mo} and T_{mo} are the motor's gain and time constant, equal to the aircraft's time constant, and p is the Laplace operator.

On the motor's shaft are fitted the slider of potentiometer ψ and a tachometer generator with gain k_{tg}. The signals are applied to the motor's control winding via dividers a_2 and a_1 and a summing device. However, in actuality the motor has a nonlinear characteristic. In the absence of any signal to the control winding, with a sufficiently weak impulse about its axis, the rotor slowly turns and stops (due to the dry friction), and for a sufficiently strong impulse, the rotor begins to rotate more rapidly. For certain values of a_1 and a_2, after a shock (an impulse about the rotor's axis) there is set up an autooscillation whose frequency can be varied by varying a_2.

For investigating the autooscillation, one must find the nonlinear motor equation.

The adjustment of the table (Fig. 1) under the system to be studied consists of a sequential regulation of the table parameters to quantities defined by the equations of motion of the aircraft relative to the axis under consideration.

Let us consider, in the Liénard plane $\{\psi, \omega\}$, where $\omega = \dot{\psi}$, the phase trajectory and its mathematical expressions, which correspond to the nontrivial steady-state platform modes. It is known [2] that, for a two-dimensional system, such modes can only be periodic.

We denote by I the total moment of inertia of the platform and load with respect to the motor axis, by M_{ro} the rotational torque applied to the motor's rotor and by $M_{fr}(\omega)$ the dry frictional torque in the bearings and platform reducer. By using Newton's second law, we can write the platform's equation of motion in the form

$$I\dot{\omega} = M_{ro} + M_{fr}. \qquad (1)$$

If we express the dry frictional torque in terms of the platform's weight G and the constant frictional coefficient with respect to the motor's axis $k > 0$, we get

$$M_{fr}(\omega) = \begin{cases} -kG & \text{for } \omega > 0, \\ M_{ro} & \text{for } \omega = 0, \\ kG & \text{for } \omega < 0. \end{cases} \qquad (2)$$

By applying a signal depending on ω to the motor's control winding, we can obtain the artificial damping torque $a_1\omega$, where a_1 is the damping coefficient. A torque depending on ω also arises as the result of the voltage induced in the control winding when the rotor moves, from viscous friction in the bearing, from air friction of the rotating parts, etc.

By denoting this torque by $f(\omega)\omega$, and by ignoring the lag in the motor's control winding, we write the expression for the rotational torque:

$$M_{ro} = [a_1 + \varphi(\omega)]\omega + a_2\psi, \qquad (3)$$

where $a_1 > 0$ and $a_2 > 0$, and the function $\varphi(\omega)$ is even, bounded and continuous, together with its first two derivatives, in each finite segment $\{\omega_1, \omega_2\}$.

It has been experimentally established that there exists an angular platform velocity ω_0 such that

$$\varphi(\omega) < 0 \text{ for } |\omega| < \omega_0, \ \varphi(\omega) =$$

$$= 0 \text{ for } |\omega| = \omega_0, \ \varphi(\omega) > 0 \text{ for } |\omega| > \omega_0. \qquad (4)$$

Moreover, $\varphi(\omega)$ does not decrease for $\omega > 0$ and does not increase for $\omega < 0$.

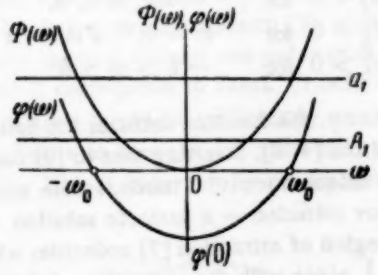

Fig. 2.

By adding and subtracting $\varphi(0)$ in (3), and by denoting [(Fig. 2)] $\Phi(\omega) \equiv \varphi(\omega) - \varphi(0)$, $A_1 \equiv a_1 + \varphi(0)$, we obtain

$$M_{ro} = [A_1 + \Phi(\omega)]\omega + a_2\psi. \qquad (5)$$

It is essential to note that the function $\Phi(\omega)$ is even and positive-definite, i.e., $\Phi(\omega) > 0$ for $\omega \neq 0$ and $\Phi(0) = 0$. At the same time, $A_1 > 0$ for $|a_1| > |\varphi(0)|$, $A_1 < 0$ for $|a_1| < |\varphi(0)|$ and $A_1 > \varphi(0)$ since $a_1 > 0$.

By substituting (5) in (1), we get

$$I\dot{\omega} + [A_1 + \Phi(\omega)]\omega + a_2\psi = M_{fr}(\omega). \qquad (6)$$

The investigation of (6) breaks down into two cases:

1) $A_1 \geq 0$, i.e., $a_1 \geq -\varphi(0)$, $(a_1 \geq 0)$;

2) $A_1 < 0$, i.e., $a_1 < -\varphi(0)$.

Case 1. $(A_1 \geq 0)$. If, with this, $M_{fr}(\omega) \equiv 0$, then (6) reduces to a form considered by Milne [3] and Sansone [4].

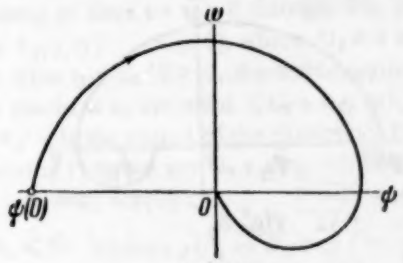

Fig. 3.

We now consider the phase trajectory for $M_{fr}(\omega) \equiv 0$. If $D = A_1^2 - 4Ia_2 \geq 0$, then the solution $\psi \equiv \psi(t)$, $[\psi(0) \neq 0]$ cannot have more than one zero in the time interval $t[0, \infty]$, which corresponds to a stable node (Fig. 3).

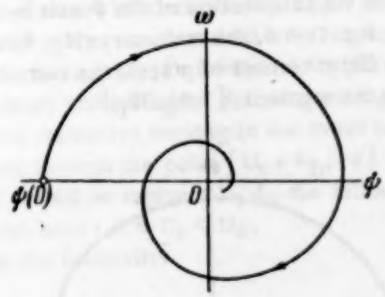

Fig. 4.

In the opposite case for $D < 0$, all solutions oscillate, and the phase trajectory corresponds to a stable focus (Fig. 4). With this, if we denote neighboring zeros of $\psi(t)$ by t_s and t_{s+1}, $t_s < t_{s+1}$, then the Milne-Sansone inequality holds:

$$t_{s+1} - t_s \leqslant \frac{2(\pi - \alpha_0)}{\nu},$$

where $\nu^2 = -D/4I^2 > 0$ and α_0 is an arc between 0 and $\pi/2$ such that $\tan\alpha_0 = \nu I/A_1$.

Consequently, if $T_0 = 2\pi/\nu$ is the period of the platform's free oscillations for $\Phi(\omega) \equiv 0$, and $T = t_{s+1} - t_{s-1}$ is the period of free oscillations for $\Phi(\omega) \not\equiv 0$ then, since $t_{s+1} - t_{s-1} \leq 2(t_{s+1} - t_s)$, we obtain the inequality

$$T \leqslant T_0\left(1 - \frac{\alpha_0}{\pi}\right). \qquad (7)$$

For example, for $a_1 = -\varphi(0)$ (i.e., for $A_1 = 0$), $\alpha_0 = \pi/2$, and the period T satisfies the obvious relationship $T < T_0$, since the case $T = T_0$ occurs only for $\Phi(\omega) \equiv 0$.

We now consider the phase trajectory corresponding to (6) for $M_{fr} \neq 0$. Motion is possible if the angle of the platform's initial position $\psi(0)[\dot{\psi} = 0]$ lies outside the angle of stagnant dry friction — the segment

$\{-\psi_{fr},\ \psi_{fr}\}$, where $\psi_{fr} = KG/a_2$, that is, if $|\psi(0)| > \psi$. In this case, for constructing the trajectory we can use (6), in which the point $\{-\psi_{fr},\ 0\}$ is chosen for the origin of coordinates for the upper half-plane (since for $\omega > 0$, $-\psi_{fr} = \text{const}$) and, for the lower half-plane, the point $\{\psi_{fr},\ 0\}$ is chosen (since for $\omega < 0$, $\psi_{fr} = \text{const}$).

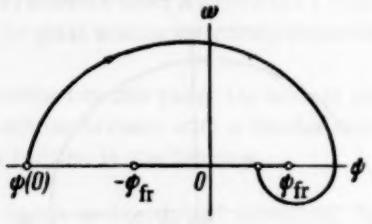

Fig. 5.

Then, on the basis of [3] and [4], in the case $D \geq 0$ the trajectory (Fig. 5) will consist of not more than two pieces, the second of which abuts the segment $(-\psi_{fr},\ \psi_{fr})$. The initial conditions will be the point $\{\psi(0) + \psi_{fr},\ 0\}$ for the upper piece and the point $\{\psi(t_1) - \psi_{fr},\ 0\}$ for the lower piece, where t_1 is the moment of time corresponding to the intersection of the ψ axis by the trajectory. For $D < 0$, the trajectory (Fig. 6) will consist of a finite number of pieces, the last one of which abuts the segment $\{-\psi_{fr},\ \psi_{fr}\}$.

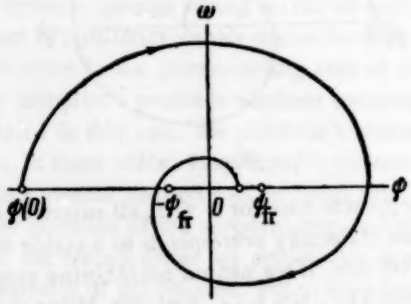

Fig. 6.

For each piece of the trajectory in the case under consideration ($M_{fr}(\omega) \not\equiv 0$), (7) is valid. Consequently, the dry friction does not change the period T of free oscillations, but increases the decrement of damping in such fashion that the radius vector ρ ($\rho^2 = \psi^2 + \omega^2$) during one period T is additionally decreased by the amount $2\psi_{fr}$. Thus, if the radius vector is decreased by $\Delta\rho_{M_{fr}=0}$ for $M_{fr}(\omega) \equiv 0$, then for $M_{fr}(\omega) \not\equiv 0$, it is decreased by $\Delta\rho_{M_{fr}\not\equiv 0} = \rho_{t=T} - \rho_{t=0} = \Delta\rho_{M_{fr}=0} - 2\psi_{fr}$.

From the last relationship (for arbitrary D) and from the Archimedean axiom follows the finitude of the number of previously mentioned arcs, the last of which abuts the segment $\{-\psi_{fr},\ \psi_{fr}\}$

Case 2. ($A_1 < 0$). If we introduce into (6) the function

$$F(\omega) = \frac{1}{\mu}[A_1 + \Phi(\omega)]\,\omega,$$

where μ is the angular frequency of the undamped free oscillations, $\mu^2 = a_2/I$, we get

$$\dot{\omega} + \mu F(\omega) + \mu^2\psi = \frac{1}{I} M_{fr}(\omega). \tag{8}$$

For $M_{fr} \equiv 0$ we obtain, by differentiating (8),

$$\ddot{\omega} + \mu f(\omega)\dot{\omega} + \mu^2\omega = 0, \tag{9}$$

where

$$f(\omega) \equiv F\frac{\partial F}{\partial \omega} \equiv \frac{1}{\mu}[a_1 + \varphi(\omega) + \varphi'(\omega)\omega].$$

For sufficiently small ω, $\omega\,\varphi'(\omega) \approx 0$ and

$$f(\omega) = \frac{1}{\mu}[a_1 + \varphi(\omega)], \tag{10}$$

but with our condition that $-\omega_0 < \omega < \omega_0$, $\varphi(\omega) < 0$.

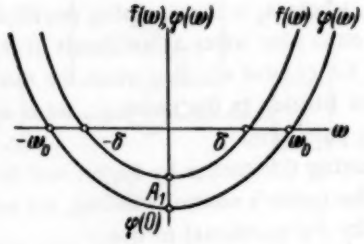

Fig. 7.

Since $A_1 = a_1 + \varphi(0) < 0$, and $\varphi(\omega)$ is continuous, then, for neighboring values of ω, $a_1 + \varphi(\omega) < 0$ and, consequently, $f(\omega) < 0$ for some ω (Fig. 7).

Since, by our assumptions, $\varphi(\omega)$ and $\varphi'(\omega)$ are continuous and bounded, $f(\omega)$ is continuous and satisfies the Lipschitz condition (guaranteeing existence and uniqueness) and, moreover since $\varphi(\omega)$ satisfies (4), then $f(\omega)$, for increasing ω, intersects the axis of abscissas at some point δ and, for decreasing ω, at the point $-\delta$, i.e.,

$$\begin{aligned} &f(\omega) < 0 \text{ for } && -\delta < \omega < \delta, \\ &f(\omega) = 0 \text{ for } && \omega = \delta, \quad \omega = -\delta \\ &f(\omega) > 0 \text{ for } && -\delta > \omega > \delta. \end{aligned} \tag{11}$$

Consequently, the function satisfies the Sansone-Massera condition [4, 6], asserting that to (9) there corresponds a unique nontrivial mode, stable according to the Lyapunov criterion — a periodic solution — a cycle whose region of attraction [7] coincides with the entire $\{\omega, \dot{\omega}\}$ plane with the exception of the origin of coordinates.

From whence it follows [5] that the homogeneous equation corresponding to (8):

$$\dot{\omega} + \mu F(\omega) + \mu^2\psi = 0 \tag{12}$$

also has a unique nontrivial mode — a stable cycle. The phase trajectory of (10) contains a cycle which intersects an arbitrary half-line —the ray $\overline{OA}$ — in the unique point B (Fig. 8).

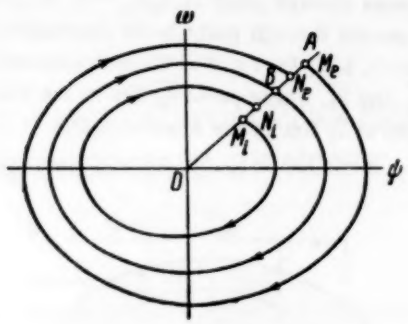

Fig. 8.

Let M_1 be an interior point of the segment $\overline{OB}$ of ray $\overline{OA}$. Then the trajectory passing through M_1 at time $t = t_0 = 0$ intersects $\overline{OB}$ in the point N_1 at time $t' > 0$, where $\overline{ON}_1 > \overline{OM}_1$. The last inequality follows from Bendixon's theorem [8]. Analogously, if M_e is an exterior point of ray $\overline{OA}$, i.e., $\overline{OM}_e > \overline{OB}$, then the trajectory defines another point N_e, where $\overline{OM}_e > \overline{ON}_e$.

We consider the phase trajectory of (8) for a sufficiently small coefficient k of dry friction. We assume that the stagnant angle-segment $\{-\psi_{fr}, \psi_{fr}\}$ — lies inside the region bounded by the arcs of trajectory $\overset{\frown}{M_1N_1}$ and by the segment $\overline{M_1N_1}$. As in the first case, each trajectory consists of a segment, or segments, lying in the upper ($\omega > 0$) and lower ($\omega < 0$) half-planes. The equations of these segments are led to the form of (10) by changing the variable ψ — translating the origin of coordinates to the point $\{\psi_{fr}, 0\}$ for the transition from the upper to the lower half-plane, and to the point $\{0, -\psi_{fr}\}$ for the converse transition. We assume that the friction angle $2\psi_{fr}$ is so small that the interior $\overset{\frown}{M_1N_1}$ and exterior $\overset{\frown}{M_eN_e}$ trajectories are so little deformed, that the inequalities $\overline{OM}_1 < \overline{ON}_1$ and $\overline{OM}_e > \overline{ON}_e$ retain their validity.

Since the continuous dependency of the trajectory on the initial conditions is retained, each point of the closed segment $\overline{M_1M_e}$ can be put into correspondence with a point of segment $\overline{N_1N_e}$, lying strictly interior to $\overline{M_1M_e}$. On the basis of the Bolya-Brauer theorem [9], with such a correspondence there is at least one point of the segment $\overline{M_1M_e}$ which corresponds to itself. It defines the periodic mode described by (9) for sufficiently small k. However, it is impossible to assert in this case that such a mode will be unique. This is borne out by the following example:

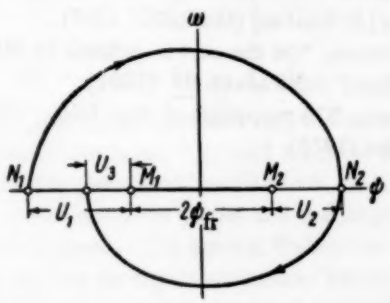

Fig. 9.

Let there exist an interval of variation of the angular velocity $\{-\Omega_0, \Omega_0\}$ such that $\Phi(\omega) = 0$ for $|\omega| < |\Omega_0|$. We then consider the trajectory defined by the equation

$$I\omega + A_1\omega + a_2\psi = M_{fr}(\omega) \qquad (13)$$

and passing at time $t = t_0 = 0$ through the point $\{-(U_1 + \psi_{fr}), 0\}$ (Fig. 9), where $U_1 > 0$ and $\psi_{fr} = kG/a_2$.

At time $t_1 = T_0/2 > 0$, the trajectory intersects the axis of abscissas in the point $\{U_2 + \psi_{fr}\ 0\}$. Here, $T_0 = 2\pi/\nu$ is the period of the platform's free oscillations.

Solving (13), we get $U_2 + 2\psi_{fr} = U_1 \exp(-A_1\pi/2I\nu)$, where $A_1 = a_1 + \varphi(0) < 0$, $\nu = \frac{\sqrt{-D}}{2I}$ and $D = A_1^2 - 4Ia_2 < 0$. Whence, $U_2 = U_1 \exp\left(-\frac{\pi A_1}{\sqrt{-D}}\right) - 2\psi_{fr}$.

Motion is possible for $U_2 > 0$, i.e., for

$$U_1 \exp\left(-\frac{\pi A_1}{\sqrt{-D}}\right) > 2\psi_{fr}$$

or

$$U_1 > 2\psi_{fr} \exp\left(\frac{\pi A_1}{\sqrt{-D}}\right).$$

Since the laws of motion in the upper ($\omega > 0$) and lower ($\omega < 0$) half-planes are identical with respect to their own centers of rotation, M_1 (for $\omega > 0$) and M_2 (for $\omega < 0$), it is then necessary and sufficient that, for the representative point of the trajectory moving in the lower half-plane and passing through the point $\{U_2 + \psi_{fr}, 0\}$ at time $t_1 = T_0/2$ to fall on segment $\overline{N_1M_1}$, the following two inequalities hold: $0 < U_3 < U_2$.

From the inequality

$$U_3 = U_2 \exp\left(-\frac{\pi A_1}{\sqrt{-D}}\right) - 2\psi_{fr} =$$

$$= \left[U_1 \exp\left(-\frac{\pi A_1}{\sqrt{-D}}\right) - 2\psi_{fr}\right] \exp\left(-\frac{\pi A_1}{\sqrt{-D}}\right) -$$

$$- 2\psi_{fr} < U_1$$

follows

$$U_1 < \frac{2\psi_{fr}}{\exp\left(-\frac{\pi A_1}{\sqrt{-D}}\right) - 1}.$$

From the inequality $U_3 > 0$ follows

$$U_2 > \frac{2\psi_{fr}}{\exp\left(-\frac{\pi A_1}{\sqrt{-D}}\right)} \quad \text{or}$$

$$U_1 > \frac{2\psi_{fr}\left[1 + \exp\left(\frac{\pi A_1}{\sqrt{-D}}\right)\right]}{\exp\left(-\frac{\pi A_1}{\sqrt{-D}}\right)}.$$

Whence,

$$\frac{1 + \exp\left(\frac{\pi A_1}{\sqrt{-D}}\right)}{\exp\left(-\frac{\pi A_1}{\sqrt{-D}}\right)} 2\psi_{fr} < U_1 < \frac{1}{\exp\left(-\frac{\pi A_1}{\sqrt{-D}}\right) - 1} 2\psi_{fr}. \qquad (14)$$

For $U_1 > \dfrac{2\psi_{fr}}{\exp\left(-\dfrac{\pi A_1}{\sqrt{-D}}\right)-1}$ the representative point falls on the segment $\{-\psi_{fr}, \psi_{fr}\}$, and motion ceases.

For $U_1 < \dfrac{1+\exp\left(\dfrac{\pi A_1}{\sqrt{-D}}\right)}{\exp\left(-\dfrac{\pi A_1}{\sqrt{-D}}\right)}$ the representative point falls on the ray defined by the inequality $\psi < -(U_1 + \psi_{fr})$; the system will oscillate.

From the single-valuedness and continuous dependency on the initial conditions of the solution of (13) there flows the existence of a nontrivial steady-state mode-cycle with fixed frequency $f = \nu/2\pi$ and with oscillation spread of $\Psi = |\psi_{min}| + |\psi_{max}|$, where

$$|\psi_{min}| = U_1 + \psi_{fr} = \frac{2\psi_{fr}}{\exp\left(-\dfrac{\pi A_1}{\sqrt{-D}}\right)-1} + \psi_{fr},$$

$$|\psi_{max}| = U_2 + \psi_{fr} = \frac{2\psi_{fr}}{1+\exp\left(\dfrac{\pi A_1}{\sqrt{-D}}\right)} - \psi_{fr}.$$

From whence,

$$\Psi = \frac{2\psi_{fr}\left[\exp\left(-\dfrac{2\pi A_1}{\sqrt{-D}}\right)+1\right]}{\exp\left(-\dfrac{2\pi A_1}{\sqrt{-D}}\right)-1}. \qquad (15)$$

This mode is unstable in the strong sense, according to the Lyapunov criterion, i.e., both on the interior and the exterior sides of the region, the orbits of this mode are limited. The topological picture of the interior portion of the domain is a set of trajectories consisting of a finite number of rays, the last one of which abuts the resting segment $\overline{M_1M_2}$. The exterior side consists of trajectories swept out with the cycle's orbits.

In the example considered, it is natural to assume that, for sufficiently large values of the distance R of the representative point from the origin of coordinates ($R^2 = \psi^2 + \omega^2$), there will appear additional dissipative torques applied to the table's platform. The mathematical form of these torques can be found if we start from the assumption that coefficient A_1 of viscous friction in (13) varies as a function of R according to the law

$$A_1 = \begin{cases} a_1 + \varphi(0) < 0 & \text{for} \quad R < \frac{1}{2}\Psi + \varepsilon, \\ E > 0 & \text{for} \quad R \geqslant \frac{1}{2}\Psi + \varepsilon, \end{cases}$$

where ϵ and E are certain fixed positive numbers.

We consider two trajectories (Fig. 10), the first of which passes through point S_1, $\overline{S_1N_1} = \epsilon$, at time $t = t_0 = 0$ and the second through point S_2 for decreasing time parameter t, i.e., for $t < 0$. These trajectories define two points $\overline{S_1}$ and $\overline{S_2}$, where point $\overline{S_1}$ lies to the left of point S_1, and point $\overline{S_2}$ lies in the interval S_2N_1.

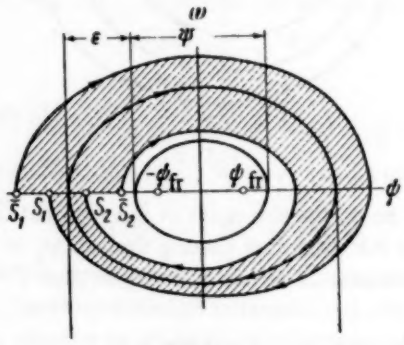

Fig. 10.

Based on what has been said, we conclude that there exists a periodic mode which lies in the hashed portion of the figure. Since all the $R < \Psi/2 + \epsilon$ define points lying on trajectories swept out with unstable orbits, and since all $R > \Psi + \epsilon$ define points corresponding to damped motion ($A_1 > 0$), then $R = \Psi + \epsilon$ defines a point lying on the trajectory corresponding to a stable cycle with spread $\Psi_1 = \Psi + 2\epsilon$ and frequency f.

The author wishes to thank B. V. Shirokorad for his aid in the preparation of this paper.

LITERATURE CITED

1. F. Oppelt, "Airplane navigation for straight-line flights," Luftfahrtforschung 14, 4/5 (1938).
2. V. V. Nemytskii, "On steady-state modes in three-dimensional autonomous dynamic systems," Vestnik MGU, Ser. Matem. No. 1 (1957).
3. W. E. Milne, "Damped vibrations," Univ. Oregon Publ. 2, No. 2 (1923).
4. G. Sansone, Ordinary Differential Equations. 2 [Russian translation] (IL, 1954).
5. I. M. Babakov, Theory of Oscillations [in Russian] (Gostekhizdat, 1958).
6. L. L. Massera, "On a theorem of G. Sansone on Lienard's equation," Boll. unione matematica Italiana 4, 3, 9 (1954).
7. V. I. Zubov, The Method of A. M. Lyapunov and Its Use [in Russian] (Izd. LGU, 1957).
8. I. Bendixon, "On the curves defined by differential equations," Acta Math. 24 (1901).
9. J. Brauer, "On mappings of manifolds," Math. Annalen (1912).

PHASE-LOCK AUTOMATIC FREQUENCY CONTROL OPERATION IN THE PRESENCE OF NOISE

V. I. Tikhonov

(Moscow)

Translated from Avtomatika i Telemekhanika, Vol. 21, pp. 301-309, March , 1960
Original article submitted May 20, 1959

It is established, by means of the two-dimensional Fokker-Planck equation, that due to external and internal fluctuations the mean frequencies of the fundamental and the synchronized generators in a standard phase-lock automatic frequency control scheme do not equal each other. An approximate method is suggested for computing the mean difference of the generators' frequencies and its dispersion.

INTRODUCTION

In [1] there was considered the effect of noise on the operation of a simplified circuit of a phase-lock automatic frequency control scheme (a phase-locked oscillator, henceforth denoted by PLO) in which the low-frequency filter was considered to be ideal. In this work, the circuit was described by a nonlinear first-order differential equation.

In actual PLO circuits, one may use, as a low-frequency filter, either a low-frequency amplifier or a series-connected RC network. The voltage from this latter filter is applied to a reactive tube.

If it is possible to approximate the low-frequency amplifier's frequency characteristic by the frequency characteristic of the RC network, then the operation of the PLO scheme will be described by the two equations [1]

$$\dot{\varphi} = \Delta_0 - su + \dot{\psi}, \tag{1}$$

$$RC\dot{u} + u = \frac{1}{2}\mu A_2 [(A_1 + E_l)\sin\varphi - E_s\cos\varphi]. \tag{2}$$

We now adopt the following nomenclature:

$$\varphi = \Phi_2 - \Phi_1,\ \dot{\psi} = \dot{\theta}_2 - \dot{\theta}_1,\ \Delta_0 = \omega_{l_0} - \omega_0; \tag{3}$$

μ is the transformation coefficient of the phase detector, s is the reactive tube's transconductance, ω_{l0} is the mean frequency of the locked (synchronized) generator for $u(t) = 0$. With this, the expressions for the oscillations of the fundamental and the locked generators take the form

$$u_f(t) = A_1\cos\Phi_1 = A_1\cos(\omega_0 t + \theta_1),$$
$$u_l(t) = A_2\sin\Phi_2 = A_2\sin(\omega t + \theta_2), \tag{4}$$

where A_1 and A_2 are constant amplitudes, ω_0 and ω are the mean frequencies, $\theta_1(t)$ and $\theta_2(t)$ are the random phases of the generators' oscillations, resulting from the noise of the generators' tubes and the impedance losses of their elements. The normal fluctuation noise $n(t)$, whose spectral density is symmetric about frequency ω_0, is described in the form of a quasi-harmonic oscillation

$$n(t) = E(t)\cos(\omega_0 t + \theta),\ E_l(t) = E(t)\cos(\theta - \theta_1),$$
$$E_s(t) = E(t)\sin(\theta - \theta_1). \tag{5}$$

By differentiating (1) with respect to time, and then substituting the expressions for $\dot{u}$ from (2) and for u from (1), we obtain

$$\ddot{\varphi} + \alpha\dot{\varphi} + \alpha\Delta\sin\varphi = \alpha\Delta_0 + \xi(t,\ \varphi), \tag{6}$$

where

$$\alpha = \frac{1}{RC},\quad \Delta = \frac{1}{2}\mu s A_1 A_2,\quad \xi(t,\ \varphi) =$$
$$= \ddot{\psi} + \alpha\dot{\psi} + \frac{\alpha\Delta}{A_1}(E_s\cos\varphi - E_l\sin\varphi).$$

Nonlinear second-order differential equation (6), with a specific random function in the right member, describes the operation of a PLO scheme when one has taken into account the natural instability of the generators' frequencies and the presence of fluctuation noise in the fundamental generator's channel.

It should be mentioned that the investigation of (6) is of interest apart from its connection with the concrete problem being considered here. Such equations describe many physical systems. Thus, for example, an analogous equation holds for a pendulum acted upon by random disturbances and, under certain conditions, for a gyroscope as well [2].

The basic purpose of the present paper is to compute the mean difference $\bar{\dot{\varphi}}$ of the fundamental and locked generators' frequencies, which is of the greatest practical interest. Here and in the sequel, a superscript bar denotes the operation of averaging over the set of different realizations.

The Two-Dimensional Fokker-Planck Equation

We use the Fokker-Planck equation to solve our problem. It is well known [3] that for the investigation of the behavior of a system with time constant τ_s on which there acts a stationary random disturbance $\zeta(t)$ with correlation time $\tau_c \ll \tau_s$, one can use the apparatus of Markov processes and, in particular, the Fokker-Planck equation. By the correlation time we understand the quantity $\tau_c = \int_{-\infty}^{\infty} |R_\zeta(\tau)|\,d\tau$, where $R_\zeta(\tau)$ is the autocorrelation function of $\zeta(t)$.

We assume that this condition holds for the system described by the differential equation

$$\ddot{x} = F(\dot{x},\ x,\ \zeta(t)), \tag{7}$$

If we consider, instead of the nonlinear differential equation (7), the equivalent system of two first-order equations $\dot{x} = y$, $\dot{y} = F(y, x, \zeta(t))$, we may then, by employing the usual procedure [4, 5], find that the two-dimensional probability density $w_2(\dot{x}, x, t)$ for $\underline{x}$ and $\underline{\dot{x}}$ must satisfy the following two-dimensional Fokker-Planck equation:

$$\dot{w}_2 = -\dot{x}\frac{\partial w_2}{\partial x} - \frac{\partial}{\partial \dot{x}}\left\{\left(\overline{F} + \int_{-\infty}^{0} K\left[\frac{\partial F}{\partial \dot{x}},\ F_\tau\right] d\tau\right) w_2\right\} + \\ + \frac{\partial^2}{\partial \dot{x}^2}\left\{w_2 \int_{-\infty}^{0} K[F,\ F_\tau]\, d\tau\right\}. \tag{8}$$

Here, in computing $\overline{F}$ and the integrand correlation functions, denoted by the symbol K, the arguments $\underline{x}$ and $\underline{\dot{x}}$ are considered fixed.

In seeking the solution of (8), it is necessary to add to it the initial and boundary conditions, which are determined by the physics of the concrete problem. Certainly, the probability density $w_2(\dot{x}, x, t)$ must satisfy the normalization condition. By giving some distribution, $w_2(\dot{x}, x, t_0) = w_{20}(\dot{x}, x)$, at some initial moment, we then find, by solving (8), the subsequent deformation of this distribution for $t > t_0$. If the random functions $x(t)$ and $\dot{x}(t)$ can assume all possible values between plus and minus infinity then, as the boundary conditions, one should use the convergence of the probability density to zero as $x, \dot{x} \to \pm\infty$, i.e., $w_2(\pm\infty, \pm\infty, t) = 0$. If the random functions $x(t)$ and $\dot{x}(t)$ assume values which are limited to a certain region, then it is necessary to seek the solution of (8) only in this region. In the problem we are considering, (6), we shall use, as the boundary condition, the condition that the probability density be periodic in φ.

If we limit consideration to a stationary solution of (8), when the probability density w_2 does not depend explicitly on time, i.e., $\dot{w}_2 = 0$, we then obtain the following Fokker-Planck equation for the stationary state:

$$\frac{\partial^2}{\partial \dot{x}^2}\left\{w_2 \int_{-\infty}^{0} K[F,\ F_\tau]\, d\tau\right\} - \frac{\partial}{\partial \dot{x}}\left\{\left(\overline{F} + \int_{-\infty}^{0} K\left[\frac{\partial F}{\partial \dot{x}},\ F_\tau\right] d\tau\right) w_2\right\} - \dot{x}\frac{\partial w_2}{\partial x} = 0. \tag{9}$$

As applied to (6), it is now necessary to set

$$F = \alpha\Delta_0 - \alpha\dot{\varphi} - \alpha\Delta\sin\varphi + \xi(t,\ \varphi), \quad x = \varphi. \tag{10}$$

We now compute the individual quantities which enter into (9). It can be shown [6] that

$$\overline{\xi(t,\ \varphi)} = \overline{\ddot{\Psi}} + \alpha\overline{\dot{\Psi}} + \frac{\alpha\Delta}{A_1}\left(\overline{E}_s\cos\varphi - \overline{E}_l\sin\varphi\right) = 0.$$

Therefore,

$$\overline{F} = \alpha\Delta_0 - \alpha\dot{\varphi} - \alpha\Delta\sin\varphi,$$

$$K[F,\ F_\tau] = \overline{[F - \overline{F}]\,[F_\tau - \overline{F}_\tau]} = \overline{\xi(t,\ \varphi)\,\xi(t+\tau,\ \varphi)} =$$

$$= \overline{[\ddot{\psi} + \alpha\dot{\psi} + \frac{\alpha\Delta}{A_1}(E_s\cos\varphi - E_l\sin\varphi)][\ddot{\psi}_\tau + \alpha\dot{\psi}_\tau + \frac{\alpha\Delta}{A_1}(E_{s\tau}\cos\varphi - E_{l\tau}\sin\varphi)]} =$$

$$= \overline{\ddot{\psi}\,\ddot{\psi}_\tau} + 2\alpha\,\overline{\dot{\psi}\,\ddot{\psi}_\tau} + \alpha^2\,\overline{\dot{\psi}\,\dot{\psi}_\tau} + \left(\frac{\alpha\Delta}{A_1}\right)^2\sigma^2 r(\tau),$$

where it is assumed that the correlation function of the noise $n(t)$ has the form

$$k_n(\tau) = \sigma^2 r(\tau)\cos\omega_0\tau.$$

From (10) we also have

$$\frac{\partial F}{\partial \dot{\varphi}} = -\alpha, \qquad \frac{\partial F}{\partial \dot{\varphi}} - \frac{\overline{\partial F}}{\partial \dot{\varphi}} = 0, \qquad K\left[\frac{\partial F}{\partial \dot{\varphi}},\ F_\tau\right] = 0$$

By substituting the individual quantities in (9), we obtain the following definitive form of the Fokker-Planck equation which describes the stationary operating mode in the PLO system under consideration:

$$K_2\frac{\partial^2 w_2}{\partial \dot{\varphi}^2} - \frac{\partial}{\partial \dot{\varphi}}\{(\alpha\Delta_0 - \alpha\dot{\varphi} - \alpha\Delta\sin\varphi)\,w_2\} - \dot{\varphi}\frac{\partial w_2}{\partial \varphi} = 0. \tag{11}$$

Here,

$$K_2 = \int_{-\infty}^{0} \overline{(\ddot{\psi}\ \ddot{\psi}_\tau + 2\alpha\ddot{\psi}\ \dot{\psi}_\tau + \alpha^2\dot{\psi}\ \dot{\psi}_\tau + \left(\frac{\alpha\Delta}{A_1}\right)^2\sigma^2 r(\tau)\}}\, d\tau. \tag{12}$$

Second-order partial differential Eq. (11) is linear and of parabolic type. Its general solution depends on two arbitrary constants, which are defined by the condition that the probability density be normalized and be periodic in φ, i.e.,

$$\int_0^{2\pi}\int_{-\infty}^{\infty} w_2(\dot{\varphi}, \varphi)\, d\dot{\varphi} d\varphi = 1, \quad w_2(\dot{\varphi}, \varphi + 2\pi) = w_2(\dot{\varphi}, \varphi). \tag{13}$$

An exact solution of (11) for (13) exists only in the particular case when the initial mistuning of the generators equals zero: $\Delta_0 = 0$. We easily convince ourselves that the solution of the equation

$$K_2 \frac{\partial^2 w_2}{\partial \dot{\varphi}^2} + \frac{\partial}{\partial \dot{\varphi}}\{(\alpha\dot{\varphi} + \alpha\Delta\sin\varphi) w_2\} - \dot{\varphi}\frac{\partial w_2}{\partial \varphi} = 0, \tag{14}$$

satisfying (13) has the form

$$w_2(\dot{\varphi}, \varphi) = \sqrt{\frac{\alpha}{2\pi K_2}}\, \frac{1}{2\pi I_0\left(\frac{\alpha^2\Delta}{K_2}\right)} \exp\left[-\frac{\alpha\dot{\varphi}^2}{2K_2} + \frac{\alpha^2\Delta}{K_2}\cos\varphi\right], \tag{15}$$

where $I_0(z)$ is a Bessel function of zero order and imaginary argument.

From (15) we find the one-dimensional probability density for the frequency difference $\dot{\varphi}$:

$$w(\dot{\varphi}) = \int_{-\pi}^{\pi} w_2(\dot{\varphi}, \varphi)\, d\varphi = \sqrt{\frac{\alpha}{2\pi K_2}} \exp\left(-\frac{\alpha\dot{\varphi}^2}{2K_2}\right). \tag{16}$$

From this we easily obtain

$$\bar{\dot{\varphi}} = 0, \ \sigma_{\dot{\varphi}}^2 = \overline{\dot{\varphi}^2} = \frac{1}{\alpha} K_2 \int_{-\infty}^{0} \left\{RC\ \overline{\ddot{\psi}\ddot{\psi}_\tau} + \frac{1}{RC}\overline{\dot{\psi}\dot{\psi}_\tau} + \frac{1}{RC}\left(\frac{\Delta\sigma}{A_1}\right)^2 r(\tau)\right\} d\tau. \tag{17}$$

In many practical cases one can neglect the generators natural fluctuations in comparison with the external noise. Then, the basic role in (17) will be played by the last term in the integrand.

Thus, if the initial mistuning of the generators at the moment when the PLO is switched in is zero, then the average frequencies of the fundamental and locked generators remain equal to each other during PLO operation, and the dispersion of the frequency difference $\sigma^2\phi$, as is obvious from (17), increases with increasing intensity of the external noise σ^2 and the generators' natural fluctuations, and decreases with increasing time constant of the RC filter. These results are comprehensible physically.

In the sequel we shall consider approximately the cases when, in (11), the initial mistuning of the generators is different from zero ($\Delta_0 \neq 0$).

Approximate Method of Solving the Fokker-Planck Equation

It is difficult to find a solution in compact form of (11) which satisfies (13). Below, we present an approximate method of solving (11).

We shall seek a solution in the form of a series:

$$w_2(\dot{\varphi}, \varphi) = \sum_{n=0}^{\infty} w^{(n)}(\dot{\varphi})\, L_n(\varphi), \tag{18}$$

where the functions $L_n(\varphi)$ are to be defined, and

$$w(\dot{\varphi}) = \exp\left(-\frac{\alpha\dot{\varphi}^2}{2K_2}\right). \tag{19}$$

By direct differentiation, we easily convince ourselves that the following recursion formulas are valid for the derivatives of the function $w(\dot{\varphi})$:

$$\dot{\varphi} w^{(n)}(\dot{\varphi}) = -\frac{1}{\alpha} K_2 w^{(n+1)}(\dot{\varphi}) - n w^{(n-1)}(\dot{\varphi}) \quad (n = 0, 1, 2, \ldots). \tag{20}$$

By substituting the expression for $w_2(\dot{\varphi}, \varphi)$ from (18) in (11), then using (20) and collecting similar terms, we obtain

$$\frac{1}{\alpha} K_2 \sum_{n=0}^{\infty} w^{(n+1)}(\dot{\varphi}) L_n'(\varphi) - \alpha(\Delta_0 - \Delta \sin\varphi) \sum_{n=0}^{\infty} w^{(n+1)}(\dot{\varphi}) L_n(\varphi) =$$

$$= \alpha \sum_{n=0}^{\infty} n w^{(n)}(\dot{\varphi}) L_n(\varphi) - \sum_{n=0}^{\infty} n w^{(n-1)}(\dot{\varphi}) L_n'(\varphi)$$

or

$$\sum_{n=0}^{\infty} w^{(n+1)}(\dot{\varphi}) L_n'(\varphi) - \frac{\alpha^2}{K_2}(\Delta_0 - \Delta \sin\varphi) \sum_{n=0}^{\infty} w^{(n+1)}(\dot{\varphi}) L_n(\varphi) =$$

$$= \frac{\alpha^2}{K_2} \sum_{n=0}^{\infty} n w^{(n)}(\dot{\varphi}) L_n(\varphi) - \frac{\alpha}{K_2} \sum_{n=0}^{\infty} n w^{(n-1)}(\dot{\varphi}) L_n'(\varphi). \tag{21}$$

By equating coefficients of like orders of the derivatives $w^{(n)}(\dot{\varphi})$, we obtain the following system of differential equations for the definition of the $L_n(\varphi)$:

$$\begin{aligned}
&L_1'(\varphi) = 0,\\
&L_0'(\varphi) - \frac{\alpha^2}{K_2}(\Delta_0 - \Delta\sin\varphi) L_0(\varphi) = \frac{\alpha^2}{K_2} L_1(\varphi) - 2\frac{\alpha}{K_2} L_2'(\varphi),\\
&L_1'(\varphi) - \frac{\alpha^2}{K_2}(\Delta_0 - \Delta\sin\varphi) L_1(\varphi) = 2\frac{\alpha^2}{K_2} L_2(\varphi) - 3\frac{\alpha}{K_2} L_3'(\varphi),\\
&L_2'(\varphi) - \frac{\alpha^2}{K_2}(\Delta_0 - \Delta\sin\varphi) L_2(\varphi) = 3\frac{\alpha^2}{K_2} L_3(\varphi) - 4\frac{\alpha}{K_2} L_4'(\varphi),\\
&\cdots\cdots\cdots\cdots\cdots\cdots\cdots\cdots
\end{aligned} \tag{22}$$

In general,

$$L_{n-1}'(\varphi) - \frac{\alpha^2}{K_2}(\Delta_0 - \Delta\sin\varphi) L_{n-1}(\varphi) = n\frac{\alpha^2}{K_2} L_n(\varphi) - (n+1)\frac{\alpha}{K_2} L_{n+1}'(\varphi).$$

We may suggest the following order for solving (22). The equations are solved successively, starting with the first, whereby, in solving each successive equation, we ignore the last terms in the right member, containing derivatives of higher-order functions $L_n(\varphi)$.

For an approximate estimate of the value of the mean frequency difference of the generators, we shall henceforth limit ourselves to computing the first two functions, $L_0(\varphi)$ and $L_1(\varphi)$. From the first equation of (22) we have that $L_1 = c = \text{const}$. By neglecting the term containing $L_2'(\varphi)$ in the second equation, we obtain the following differential equation for defining $L_0(\varphi)$:

$$L_0'(\varphi) - \frac{\alpha^2}{K_2}(\Delta_0 - \Delta\sin\varphi) L_0(\varphi) = \frac{\alpha^2}{K_2} c.$$

The solution of this equation, as we easily convince ourselves, can be written in the form

$$L_0(\varphi) = c\frac{\alpha^2}{K_2} \exp(D_0\varphi + D\cos\varphi) \int_{\varphi_0}^{\varphi} \exp(-D_0\gamma - D\cos\gamma)\, d\gamma,$$

where φ_0 is some arbitrary constant and

$$D_0 = \frac{\alpha^2\Delta_0}{K_2}, \quad D = \frac{\alpha^2\Delta}{K_2}. \tag{23}$$

Thus, in our approximation, we obtain the following solution of (11):

$$\begin{aligned}
&w_2(\dot{\varphi}, \varphi) = w(\dot{\varphi}) L_0(\varphi) + w'(\dot{\varphi}) L_1(\varphi) =\\
&= c\frac{\alpha}{K_2} \exp\left(-\frac{\alpha\dot{\varphi}^2}{2K_2}\right)\left\{-\dot{\varphi} + \alpha\exp(D_0\varphi + D\cos\varphi)\int_{\varphi_0}^{\varphi} \exp(-D_0\gamma - D\cos\gamma)\, d\gamma\right\}.
\end{aligned} \tag{24}$$

To satisfy the condition for periodicity (13), it is necessary that the following equation hold:

$$\exp(D_0\varphi + 2\pi D_0 + D\cos\varphi) \int_{\varphi_0}^{\varphi+2\pi} \exp(-D_0\gamma - D\cos\gamma)\, d\gamma =$$

$$= \exp(D_0\varphi + D\cos\varphi) \int_{\varphi_0}^{\varphi} \exp(-D_0\gamma - D\cos\gamma)\, d\gamma.$$

From this equation, the following relationship derives:

$$\int_{\varphi_0}^{\varphi} \exp(-D_0\gamma - D\cos\gamma)\,d\gamma = \frac{\exp(2\pi D_0)}{1-\exp(2\pi D_0)} \int_{\varphi}^{\varphi+2\pi} \exp(-D_0\gamma - D\cos\gamma)\,d\gamma, \tag{25}$$

which permits the arbitrary constant φ_0 to be eliminated.

To determine the second arbitrary constant c, we use the normalization condition

$$\int_0^{2\pi}\int_{-\infty}^{\infty} w_2(\dot\varphi, \varphi)\,d\dot\varphi d\varphi = c\alpha\sqrt{\frac{2\pi\alpha}{K_2}}\,\frac{\exp(2\pi D_0)}{1-\exp(2\pi D_0)}\int_0^{2\pi}\exp(D_0\varphi + D\cos\varphi)\,d\varphi \times$$
$$\times \int_{\varphi}^{\varphi+2\pi}\exp(-D_0\gamma - D\cos\gamma)\,d\gamma = 1. \tag{26}$$

It can be shown [1, 7] that

$$J = \int_0^{2\pi}\exp(D_0\varphi + D\cos\varphi)\,d\varphi \int_{\varphi}^{\varphi+2\pi}\exp(-D_0\gamma - D\cos\gamma)\,d\gamma =$$
$$= 4\pi^2\exp(-\pi D_0)\,|I_{iD_0}(D)|^2,$$

where $I_{i\nu}(z)$ is a Bessel function of imaginary order and imaginary argument. Therefore, we obtain from (26)

$$c = \frac{1}{4\pi\alpha^2}\sqrt{\frac{K_2}{2\pi\alpha}}\,\frac{1-\exp(2\pi D_0)}{\exp(\pi D_0)}\,|I_{iD_0}(D)|^{-2} \tag{27}$$

By using (25) and (27), we can write the approximate expression for the probability density in its definitive form:

$$w_2(\dot\varphi, \varphi) = \sqrt{\frac{1}{2\pi\alpha K_2}}\,\frac{1-\exp(2\pi D_0)}{4\pi^2\exp(\pi D_0)}\,|I_{iD_0}(D)|^{-2}\exp\left(-\frac{\alpha\dot\varphi^2}{2K_2}\right)\times$$
$$\times\left\{-\dot\varphi + \alpha\,\frac{\exp(2\pi D_0)}{1-\exp(2\pi D_0)}\exp(D_0\varphi + D\cos\varphi)\int_{\varphi}^{\varphi+2\pi}\exp(-D_0\gamma - D\cos\gamma)\,d\gamma\right\}. \tag{28}$$

It is easily verified that this formula goes over into the exact formula (15) for zero initial mistuning ($D_0 = 0$). This attests to the fact that the suggested approximate method of solving the Fokker-Planck equation gives logically-noncontradictory results.

By integrating (28) over φ and $\dot\varphi$ between the proper limits, we obtain the one-dimensional probability densities for, respectively, $\dot\varphi$ and φ:

$$w(\dot\varphi) = \left\{\sqrt{\frac{\alpha}{2\pi K_2}} - \dot\varphi\sqrt{\frac{2\pi}{\alpha K_2}}\,\frac{1-\exp(2\pi D_0)}{4\pi^2\exp(\pi D_0)}\,|I_{iD_0}(D)|^{-2}\right\}\exp\left(-\frac{\alpha\dot\varphi^2}{2K_2}\right), \tag{29}$$

$$w(\varphi) = \frac{1}{4\pi^2}\exp(\pi D_0)\,|I_{iD_0}(D)|^{-2}\exp(D_0\varphi + D\cos\varphi)\int_{\varphi}^{\varphi+2\pi}\exp(-D_0\gamma - D\cos\gamma)\,d\gamma. \tag{30}$$

The last formula for the probability density of φ coincides in form with that obtained in [1]. The difference consists in this, that here the coefficients D_0 and D depend on the low-frequency filter's passband [cf. (23)]. This fact also gives us some confidence that, in taking only the first two functions in (22) into account, we obtain results which are in qualitative agreement with those obtained in [1].

By using (29), we find the average difference of the generators' frequencies and the dispersion of this difference:

$$\dot{\bar\varphi} = \bar\omega - \omega_0 = \frac{K_2}{2\pi\alpha^2}\,\frac{\exp(2\pi D_0) - 1}{\exp(\pi D_0)}\,|I_{iD_0}(D)|^{-2} = \Delta_0\,\frac{\operatorname{sh}\pi D_0}{\pi D_0}\,I_{iD_0}(D)|^{-2},\ \sigma^2_{\dot\varphi} \approx \frac{1}{\alpha}K_2. \tag{31}$$

For $D_0 = 0$, these formulas coincide with (17).

Particular Examples

Let the external noise n(t) be obtained as the result of the action of a sufficiently wide-band fluctuation on a narrow-band oscillatory loop with resonant frequency ω_0 and, consequently, let the noise have correlation function

$$k_n(\tau) = \sigma^2 e^{-\beta|\tau|}\cos\omega_0\tau.$$

We assume that we may ignore the natural instability of the frequencies of the fundamental and locked generators in comparison with the noise n(t). Then,

$$K_2 = \left(\alpha\Delta\frac{\sigma}{A_1}\right)^2\int_{-\infty}^{0} e^{\beta\tau}\,d\tau = \frac{1}{\beta}\left(\alpha\Delta\frac{\sigma}{A_1}\right)^2.$$

By substituting this value of K_2 in (23) and (31), we get

$$D_0 = \frac{\beta\Delta_0}{\Delta^2}\left(\frac{A_1}{\sigma}\right)^2, \quad D = \frac{\beta}{\Delta}\left(\frac{A_1}{\sigma}\right)^2,$$

$$-\Delta = \frac{1}{2}\mu s A_1 A_2, \quad \sigma_{\dot\varphi}^2 = \frac{\alpha}{\beta}\Delta^2\left(\frac{\sigma}{A_1}\right)^2. \qquad (32)$$

In the given concrete case, D_0 and D do not depend on α. With this, as is clear from (32) and (31), the dispersion of the frequencies' difference depends on α, but the average discrepancy of the frequencies does not depend on α. This last result is seemingly a consequence of the approximate solution of (11). Recently, A. G. Zhuravlev showed that, although the term containing $L_2(\varphi)$ in (18) for the probability density does not of itself give a correction to the mean frequency difference, its being taken into account does result in the function $L_0(\varphi)$ assuming a different form:

$$L_0(\varphi) = C\frac{\alpha}{K_2}\frac{\exp(2\pi D_0)}{1-\exp(2\pi D_0)}\exp\times$$
$$\times(D_0\varphi + D\cos\varphi)\int_{\varphi}^{\varphi+2\pi}(\alpha-\Delta\cos\gamma)\times \qquad (33)$$
$$\times\exp(-D_0\gamma - D\cos\gamma)\,d\gamma.$$

We now make some numerical estimates. It is known [8] that, in the absence of noise, the maximum voltage at the phase detector's output can not exceed twice the magnitude of the least of the applied voltages. We replaced the phase detector by a device implementing multiplication of the voltages $u_f(t)$ and $u_l(t)$. In accordance with what has been said, for $A_2 > A_1$, the maximum value of the voltage at the multiplier's output is determined by the relationship

$$U_{max} = \frac{1}{2}\mu A_1 A_2 \leqslant 2A_1.$$

We take $u_{out} \approx 0.5U_{max}$, i.e., $\mu A_1 A_2/2 \approx A_1$. Whence $\mu \approx 2/A_2$ and $\Delta \approx sA_1$.

The parameters of the PLO scheme are so chosen that stable operation is guaranteed. As follows from [9], for $\Delta_0/\Delta \lesssim 0.6$, stability is guaranteed if the following inequality holds:

$$\sqrt{\frac{1}{RC\Delta}} \geqslant \frac{\pi}{4}\frac{\Delta_0}{\Delta}. \qquad (34)$$

Let $A_1 \approx 1$v, s = 0.1 kg/v, $\alpha = 20\ \text{sec}^{-1}$, $\beta = 300\ \text{sec}^{-1}$, $\Delta_0/\Delta = 0.5$. With these parameters, Ineq. (34) holds and, simultaneously, the conditions hold for the applicability of the Fokker-Planck equation. Then, $\Delta \approx sA_1 = 100$ cps, $D_0 = 1.5(A_1/\sigma)^2$, $D = 3(A_1/\sigma)^2$ and $\sigma_{\dot\varphi}^2 \approx 700(\sigma/A_1)^2$. By using the graphs of I. G. Akopyan, given in [1], we get

$$\bar\omega - \omega_0 \approx 35\text{cps}, \quad \sigma_{\dot\varphi} \approx 36\text{ cps for } \left(\frac{A_1}{\sigma}\right)^2 \approx 0.7,$$

$$\bar\omega - \omega_0 \approx 10\text{cps}, \quad \sigma_{\dot\varphi} \approx 18\text{ cps for } \left(\frac{A_1}{\sigma}\right)^2 \approx 2.0.$$

From what has been considered above, we may draw the following conclusions:

1. From (32) and the quantitative estimates adduced, it is clear that, when the conditions hold for the applicability of the Fokker-Planck equation ($\alpha \ll \beta$), the mean frequency difference and its mean square decrease as the ratio A_1/σ increases. For sufficiently small signal-to-noise ratios, the average frequency difference may turn out to be significantly less than the mean square value, and it is necessary to take it into account.

2. When stability condition (34) holds, a decrease of the time constant RC provides a shorter duration of the PLO's transient response, but the dispersion of the frequency difference is thereby increased. Therefore, the requirements of short establishment time and high noise immunity are, in a very definite sense, contradictory.

In conclusion, I wish to thank R. L. Stratonovich for his interest in the present work.

LITERATURE CITED

1. V. I. Tikhonov, "Influence of noise on phase-locked oscillator operation," Avtomatika i Telemekhanika 20, 9 (1959).
2. N. N. Bogolyubov and Yu. A. Mitropol'skii, Asymptotic Methods in Nonlinear Oscillation Theory [in Russian] (Fizmatgiz, 1958).
3. P. I. Kuznetsov, R. L. Stratonovich, and V. I. Tikhonov, "Correlation function in the theory of Brownian motion," Zhur. Eksp. i Teor. Fiz. 26, 2 (1954).
4. Wang Ming-chen and G. E. Uhlenbeck, On the theory of the Brownian motion, Rev. Mod. Phys. 17, No. 2-3 (1945).
5. H. A. Kramers, "Brownian motion in a field of force and the diffusion model of chemical reactions," Physics 7, No. 4 (1940).
6. V. I. Tikhonov, "Effect of natural fluctuations on self-excited oscillator operation," Vestnik MGU 2, 53 (1957).
7. R. L. Stratonovich, "Self-excited oscillator synchronization in the presence of noise," Radiotekhnika i Élektronika 3, 4 (1958).
8. M. R. Kaplanov and V. A. Levin, Phase-Lock Automatic Frequency Control [in Russian] (Gosénergoizdat, 1956).
9. Yu. N. Bakaev, "Investigation of inertial systems of television synchronization," Radiotekhnika i Élektronika 3, 2 (1958).

ANALYSIS OF A TWO-POSITION COMPENSATING CONTROL SYSTEM UNDER CONSTANT PROLONGED DISTURBANCES

A. I. Cherepanov

(Pert')

Translated from Avtomatika i Telemekhanika, Vol. 21, No. 3, pp. 310-316, March, 1960
Original article submitted October 28, 1959

It is shown that the simplified graphico-analytic method developed in [1] for computing the processes in a two-position regulator may be employed for analyzing the processes in two-position compensating control systems [2] under constant prolonged disturbances.

In [2] of this author there was described a new method for improving the quality of the processes in a two-position regulator by the use of a special relay-type correcting device. The basic advantage of this method in comparison with prior ones [3, 4, 5, 8] is that, with essentially reduced amplitude of controlled quantity oscillations, of temperature for example, it provides the minimum increase in the required number of switchings of the object's heater in and out of the system, computed on the basis of a nonsymmetric mode of operation.

It should be mentioned that, at the present, of all the types of two-position compensating controllers, those with thermoelectric correcting (compensating) devices have been most widely used [6, 7].

However, electromechanical correcting devices have certain advantages: e.g., such devices can be used both in regulators which employ some electrical means of measuring the controlled parameter and in many industrial two-position regulators of dilatometric, bimetallic, or magnometric types which use some nonelectric means of measuring the controlled quantity. Moreover, the use of an electromechanical correcting device permits the employment of the regulator's measuring portion for measuring or recording the true temperature in the object. When a thermoelectric device is used, it is necessary to have an additional intrument for this purpose, since the action of the device distorts the output signal of the measuring portion.

Simple formulas were obtained in [2] for calculating the correcting device's adjustment parameters and the basic parameters of the compensating control process in the steady state. It was noted in [2] that the character of the possible disturbances in the system should be taken into account in choosing the correcting device's parameters.

In the present paper we provide an analysis of the processes with disturbances in a two-position control system with an electromechanical correcting device. The possibility is demonstrated of the existence in such a system of complex periodic motions, somewhat similar to those considered in [5, 8]. Recommendations are given for the choice of the adjustment parameters of the correcting device which will provide the very best quality processes given the disturbances.

As in [2], the analysis is made by means of a simplified graphico-analytic method of calculating the two-position controller's processes [1], thanks to which the formulas obtained are simple, and may be used without difficulty for engineering computations.

By the adjustment parameters of the correcting device we shall understand the following quantities: t_0t_1 is the duration of the make state of contact K-1, t_{bre} is the duration of the break state of contact K-1, $t_{bre} = t_1t_2$, t_{mak} is the total duration of the make state of contact K-1 during one disk rotation, $t_{mak} = t_0t_1 + t_0t_3 - t_1t_2$, t_{ro} is the time for one complete disk rotation, $t_{ro} = t_0t_3$.

1. Pulse Repetition Period as a Function of the Load

The distinguishing feature of a two-position control system with an electromechanical correcting device is that the repetition period of the pulses of heat admission to the object, for invariant adjustment parameters, depends on the load. This is achieved due to the use in the device of two controlling disks, one of which switches in the flow of energy to the object at a definite previously specified time while the other disk returns the first disk to its initial position in the time following a positive deviation of the parameter from its given value*. With this, if the magnitude of the energy efflux changes within certain limits, for example, if it increases, then the new switching in of the relay's motor would occur somewhat earlier than for the previous value of the efflux. The pulses switching in the influx would have the same duration, but their repetition frequency would increase, and the correction process would not be disrupted.

Figure 1, a shows the graph of the process in a two-position controller with compensation, where the influx multiplicity is $n_1 = 8$, and the degree of correction is $k = 2.86$. In Fig. 1 and in the sequel, we adopt the nomemclature: $\Delta\vartheta$ is the deviation of the controlled parameter (temperature), $\Delta\vartheta'$ is the deviation of the object's controlled temperature with compensation

* For a more detailed description of the correcting device's operation, cf. [2].

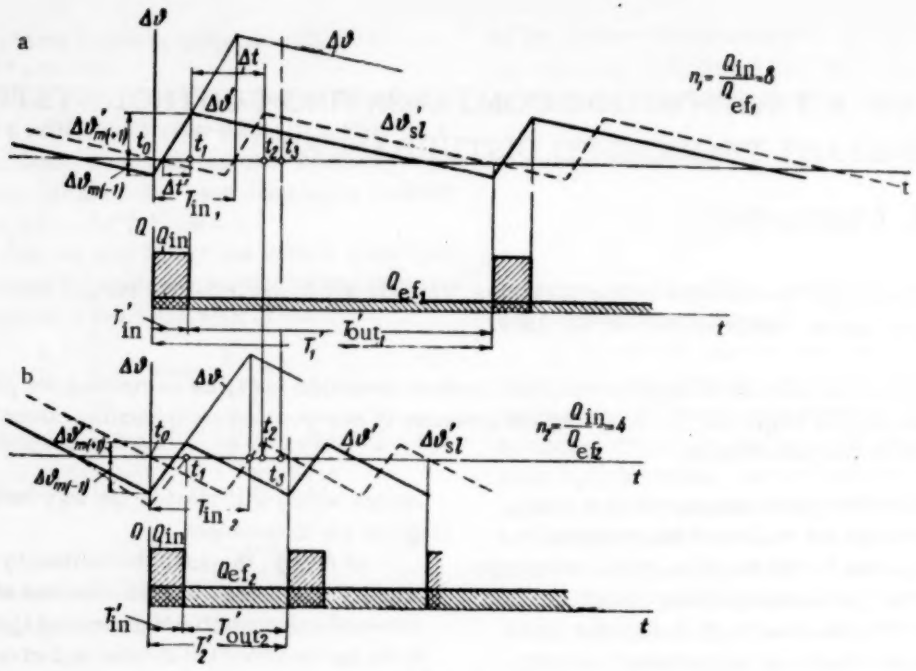

Fig. 1.

(correction), $\Delta\vartheta_{se}$ is the temperature deviation of the sensitive element with compensation, $\Delta\vartheta'_{m(+)}$ is the positive amplitude of the deviation with compensation, $\Delta\vartheta_{m(-)}$ is the negative deviation amplitude, Q_{in} is the influx of heat, Q_{ef} is the efflux of heat, T_{in} is the duration of switching in for control without correction, T'_{in} is the duration of switching in when the corrective device is used, T_{out} is the duration of switching out, T is the period of oscillation, t_0 is the moment of switching in, t_1 is the moment of switching the influx off when correction is used, t_2 is the moment of the new making of controlling contact K-1, t_3 is the moment of disk cessation, Δt is the system's lag time, $\Delta t'$ is the residual lag time when correction is used.

Figure 1,b shows the control process in the same system when the heat efflux is increased twofold, i.e., for $n_2 = 4$. As is clear from the graph, the correction process is not disrupted. The duration of switching in of the heater, T'_{in}, remains as before. The duration of switching out T'_{out_1} is decreased, and becomes equal to T'_{out_2}. The positive amplitude of the deviation is also decreased. The negative deviation amplitude $\Delta\vartheta_{m(-)}$ increases, as with ordinary two-position controllers. The period of influx switching in is shortened to T'_2. The total amplitude of the oscillations, $\Delta\vartheta_{m(+)} + \Delta\vartheta_{m(-)}$ is somewhat decreased.

It may be seen from a comparison of Fig. 1, a and b that the degree of correction k became larger in the second case: k = 6.2.

We now find the dependence of the variation in the degree of correction k on the magnitude of the influx multiplicity n for a constant (given) duration of switching in T'_{in}. As is known [2],

$$k = \frac{\Delta t}{\Delta t'}. \tag{1}$$

The quantity $\Delta t'$ can be expressed in terms of the duration of switching in T'_{in} and the influx multiplicity n by use of the formula [2]

$$T'_{in} = \Delta t' \frac{Q_{in}}{Q_{in} - Q_{ef}} + (\Delta t - \Delta t') \frac{Q_{ef}}{Q_{in} - Q_{ef}}. \tag{2}$$

From (2) we obtain

$$\Delta t' = T'_{in} - \Delta t \frac{1}{n-1}. \tag{3}$$

By substituting (3) in (1), we find that

$$k = \frac{\Delta t}{T'_{in} - \Delta t \frac{1}{n-1}}. \tag{4}$$

From (4) one can calculate the degree of correction for various values of influx multiplicity n and switching in duration T'_{in}.

Equation (4) shows that, for some value of n, the denominator vanishes and k becomes infinite.

This value of n will be, in some sense, a critical one; we denote it by n_{cr}†. Obviously,

$$n_{cr} = 1 + \frac{\Delta t}{T'_{in}}. \tag{5}$$

When the influx multiplicity has the value n_{cr}, the temperature in the object during the given time T'_{in} rises exactly to the given limit. For values of n less than n_{cr}, the temperature in the object during the switching in time T'_{in} does not attain the given value, and the normal course of the correction process is disrupted.

† In [2] n_{cr} has a different connotation.

For the case shown on Fig. 1,a, the calculated value of $n_{cr} = 3$. On Fig. 1,b, the dashed line represents the temperature variations in the object for this value n = 3. The calculated value of n_{cr} is well borne out by the graph.

2. Complex Periodic Motions

As was shown in the previous section, the correction process can proceed normally for disturbances up to some value n_{cr}. With this, as the disturbance increases (the value of n decreases) there will be an increase of the negative amplitude and a decrease of the positive amplitude. The given condition ($n > n_{cr}$) for the guarantee of normal correction process is necessary but not sufficient. As is clear from Figs. 2, 3, and 4, it is necessary, for the normal flow of the correction process, that the following additional conditions be met:

$$t_2 > T_{in} , \quad t_{ro} < T'. \qquad (6)$$

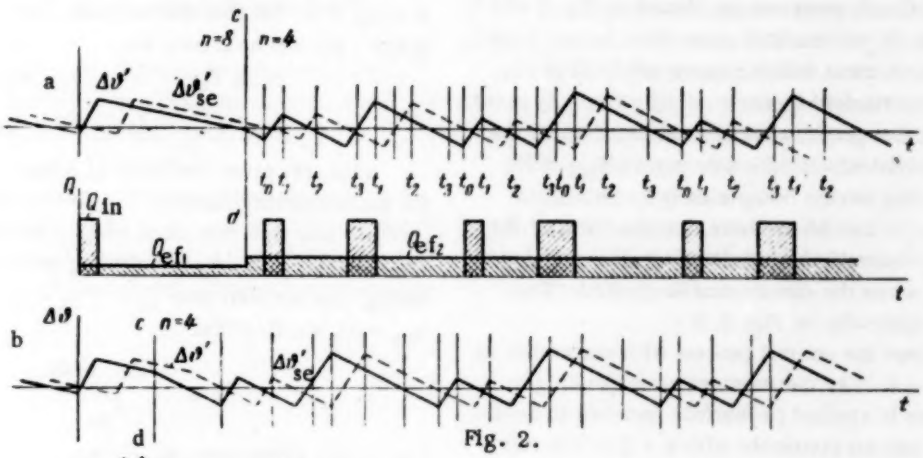

Fig. 2.

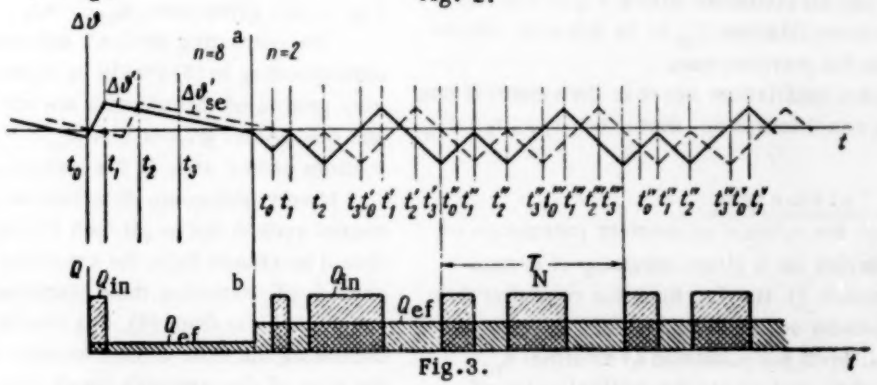

Fig. 3.

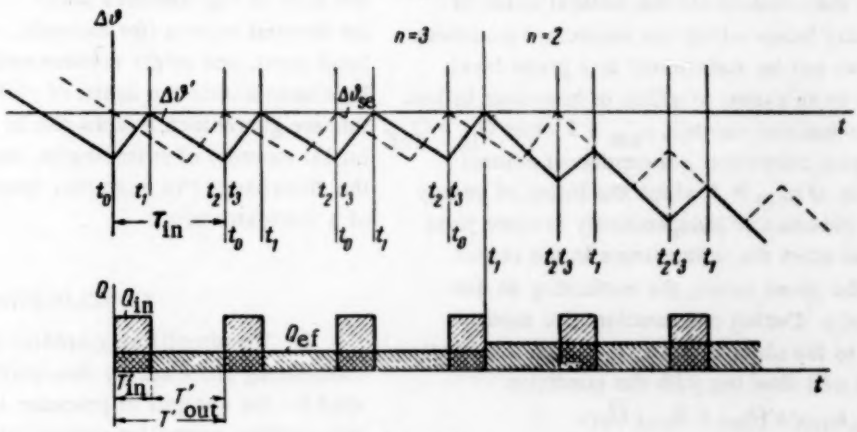

Fig. 4.

Thus, in the system under consideration, the repetition period of the influx switching-in pulses depends on the load, and the correction process flows normally only for influx multiplicities greater than the critical value.

For values of influx multiplicity $n < n_{cr}$, the normal course of the correction process is disrupted, and there arise complex periodic temperature oscillations in the system, examples of which are considered in the following section.

If the correcting device's parameters, selected so as to permit processing of the greatest possible disturbances be so chosen that inequalities (6) are transgressed for values of $\underline{n}$ higher than n_{cr}, then complex periodic motions, similar to those considered in [5, 8], will arise in the system.

Examples of such processes are shown in Fig. 2 and 3. Figure 2, a shows the process with correction for n = 8 up to line cd. At the moment which corresponds to line cd, and instantaneous twofold increase of efflux (n = 4) occurs. As is clear from the graph, after several oscillations the process is reestablished with the new period T_N. With this, the correcting device completes two revolutions during a period. It can be assumed that the form of the postdisturbance -reestablished oscillations does not depend on the moment when the disturbance is applied. This is confirmed graphically on Fig. 2, b.

Figure 3 shows the control process with correction up to line ab for n = 8. At the moment corresponding to ab, a disturbance is applied (a fourfold increase in heat efflux) and the process continues with n = 2. The new period of complex oscillations T_N is, in this case, somewhat less than in the previous case.

Thus, complex oscillations occur in the system if one of the following conditions is not met: $n > n_{cr}$, $t_2 > T_{in}$, $t_{ro} < T'$.

3. Optimal Parameters

We now seek the optimal adjustment parameters of the correcting device for a given accuracy of control (degree of correction $\underline{k}$), starting from the condition that the correction process not be disrupted for the very greatest disturbance, i.e., from the condition of minimal n_{cr}.

By n_{cm} we shall understand the critical value of influx multiplicity below which the controlled parameter (temperature) can not be maintained at a given level. This occurs due to an excess of efflux of heat over influx. For ordinary two-position control, $n_{cm} = 1$ when $Q_{in} = Q_{ef}$. For regulation with correction, disruption of control occurs for a value of $n_{cm} > 1$, since the influx of energy to the object is switched off independently at some time t_{bre}. In the case when the temperature in the object remains below the given value, the correcting device works continuously. During one rotation, the amount of heat applied to the object equals $Q_{in} t_{mak}$. An equal quantity of heat will flow out with the condition

$$Q_{in} t_{mak} = (t_{bre} + t_{mak}) \overline{Q}_{ef},$$

where $\overline{Q}_{ef}$ is the critical value of heat efflux. If $Q_{ef} > \overline{Q}_{ef}$, then the temperature does not rise to the given level.

From whence we find n_{cm} as

$$n_{cm} = \frac{Q_{in}}{\overline{Q}_{ef}} = \frac{t_{mak} + t_{bre}}{t_{mak}} = 1 + \frac{t_{bre}}{t_{mak}}.$$

It is clear that $t_{mak} = t_{ro} - t_{bre}$. We finally obtain

$$n_{cm} = 1 + \frac{t_{bre}}{t_{ro} - t_{bre}} \qquad (7)$$

or

$$n_{cm} = \frac{f}{f-1}, \quad \text{where} \quad f = \frac{t_{ro}}{t_{bre}}.$$

We have (5) for n_{cr}. Figure 4 shows the control process for the critical value of influx multiplicity $n = n_{cr} = 3$. For this critical case, as is clear from the graph, (6) can hold only for

$$t_2 = T_{in} \quad \text{for} \quad n_{cr},$$
$$t_{ro} = T' = T_{in} \quad \text{for} \quad n_{cr}. \qquad (8)$$

Thus, (8) gives the optimal adjustment parameters for the correcting device.

We now find the value of n_{cm} for the case of optimal adjustment. By substituting (8) in (7), and by taking into account that $t_{ro} = T'_{in} + t_{bre}$ and that $t_{bre} = \Delta t$, we find that

$$n_{cm} = \frac{T'_{in} + \Delta t}{T'_{in}}, \qquad (9)$$

i.e., in the given case, $n_{cm} = n_{cr}$.

The correcting device's adjustment parameters corresponding to (8) should be taken in those cases when very protracted disturbances are not observed in practice and $\underline{n}$ is always greater than n_{cr}. We note that complex motions cannot arise in the system under these conditions.

If very protracted disturbances are possible in the control system ($n < n_{cr}$), then the device's parameters should be chosen from the condition that the system be capable of processing these disturbances.

As is clear from (8), this can be achieved by increasing the time of disk rotation t_{ro} or by decreasing the time of the contact's break state t_{bre}. In practice, for thermal objects (for example, of the dessicator hood type), one might recommend that the rotation time be chosen within the limits of (0.6 to 0.7)T', since with this are guaranteed a rapid rise in temperature at the initial moment of switching in, and good processing of the disturbance (for example, upon opening the door of a dessicator hood).

CONCLUSIONS

1. The simplified graphico-analytic theory of calculating processes in two-position controllers may be used for the analysis of processes with disturbances in two-position controller systems with time correction.

2. The distinguishing feature of the two-position control system with an electromagnetic correcting device is that the pulse repetition period (the mark-space ratio) depends on the load.

3. Under definite conditions, complex periodic motions of the controlled quantity (temperature) arise in the system.

4. With optimal adjustment parameters of the correcting device, normal course of the correction process is guaranteed for the very greatest disturbances.

LITERATURE CITED

1. A. A. Kampe-Hemm, Two-position Control Dynamics [in Russian] (Gosénergoizdat, 1955).
2. A. I. Cherepanov, "On improving the quality of two-position control," Avtomatika i Telemekhanika 19, 5 (1958).
3. A. A. Kampe-Hemm, "Correcting devices with differential switching in of thermocouples, and their use with two-position controllers," Priborostroenie No.11 (1956).
4. A. A. Kampe-Hemm, "Comparative analysis of several improved methods of two-position control," Avtomatika i Telemekhanika, 17, 8 (1956).
5. A. S. Alekseev, "Two-position temperature controllers with advance zones," Collection: In Commemoration of Aleksandr Aleksandrovich Andronov [in Russian] (Izd. AN SSSR, 1955).
6. A. A. Kampe-Hemm, "The use of thermoelectric isodrome correcting devices for improving the quality of two-position temperature control," Avtomatika i Telemekhanika, 19, 5 (1958).
7. A. A. Kampe-Hemm and A. N. Trusov, "Simple methods of increasing the accuracy of two-position temperature controllers," Collection: Heat-Engineering Instruments and Controllers. 3 [in Russian] (1956).
8. A. S. Alekseev, Two-Position Temperature Controllers with Advance Zones. Dissertation [in Russian] (Gor'kii, 1954).

ON THE ERRORS OF AN INTERPOLATING DEVICE FOR A GIVEN CIRCULAR MOTION

V. V. Karibskii

(Moscow)

Translated from Avtomatika i Telemekhanika, Vol. 21, No. 3, pp. 317-322, March, 1960
Original article submitted July 7, 1959

An algorithm for a digital interpolating device for a given circular motion is described. A theoretical investigation of the interpolation errors is given. A brief description of the device's circuit is provided.

Today, in various domains of technology, the necessity arises of so controlling an object that it moves along a given trajectory. Frequently this is implemented by means of sampled-data servosystems. Each system controls the motion corresponding to one coordinate and, at each input pulse, there results a translation by unit length in the scale chosen, this length being called the value of the pulse. The pulses for each coordinate axis must be distributed in accordance with a given trajectory of the object's motion. Distribution of the pulses is ordinarily implemented by means of special digital computers.

In the present paper we consider the design principles, and estimate the errors, of a device of this type which provides motion along a circle.

The equation for a circle centered at the origin has the form

$$x^2 + y^2 = R^2, \qquad (1)$$

where x and y are the current coordinate values and R is the circle's radius.

We assume that the motion begins at point A with coordinates x = 0, y = R (Fig. 1), and must proceed clockwise about the circle.

We now find the value of x^2 for which the coordinate y is decreased by unity, i.e., becomes equal to y-1, for which we substitute the new value of the coordinate y in (1):

$$x_1^2 = R^2 - (y-1)^2.$$

By taking into account that y = R, we get $x_1^2 = 2R-1$.

Analogously, we can find the values of $x_2^2, x_3^2, \ldots$ x_k^2 for which there are corresponding changes of the coordinate y by 2, 3, . . ., k units. Knowing these values, we can find the corresponding differences, which will have the form

$$\begin{aligned} x_1^2 &= 2R-1, \\ x_2^2 - x_1^2 &= 2R-3, \\ &\cdots\cdots\cdots \\ x_k^2 - x_{k-1}^2 &= 2R-(2k-1) \quad (k=1, 2, 3, \ldots). \end{aligned} \qquad (2)$$

Based on the formulas obtained, we can suggest the following method of constructing a circle. First, we must vary the coordinate x until the value of x_1^2 equals 2R-1 and, as soon as this happens, we must change y by one unit, after which we change the coordinate x until the difference $x_2^2 - x_1^2$ becomes equal to 2R-3, at which time we again change y by one unit, etc. It is obvious that, in this case, the approximation error is nowhere larger than unity. However, due to the discreteness of the system's operation, such a method is not implementable, since translations of less than the value of a pulse are impossible. Consequently, R and the quantity x_k^2 are integers. However, the quantity x_k may be expressed by a noninteger at points where y_k is expressed by an integer, and conversely. We shall, therefore, in moving from point A, vary coordinate x by unity and then compute the value of x^2. As soon as the coordinate x reaches the integral value x_{i-m} for which the condition $x_{i-m}^2 \geq 2R-1$ holds, we change coordinate y by unity and determine whether the condition holds that

$$\Delta_1 = x_{i-m}^2 - (2R-1) \geqslant 2R-3.$$

If so, then a unit increment of coordinate x at the given point of the circle corresponds to an increment of coordinate y greater than, or equal to, two units. Therefore, coordinate y should be changed by one unit, the quantity $\Delta_2 = x_{i-m}^2 - (2R-1) - (2R-3)$ computed, and the condition $\Delta_2 \geq (2R-5)$ verified, etc. Such operations are carried out until the condition $\Delta_k < 2R-[2(k+1)-1]$ begins to hold. As soon as this happens, we again change coordinate x by unity and then compute the increment of x^2 obtained, with account being taken of the residue, i.e., in this case $x_{i+1-m}^2 - x_{i-m}^2 + \Delta_k$ where $x_{i+1-m} - x_{i-m} = 1$. If now the following condition holds:

$$x_{i+1-m}^2 - x_{i-m}^2 + \Delta_k \geqslant 2R - [2(k+1)-1], \qquad (2')$$

then coordinate y should be changed by one unit, and the process just described should be repeated. The sequence of actions described above and (2') comprise the algorithm in accordance with which the scheme described at the end of this paper operates. In this case, naturally, coordinate y will be changed by one unit somewhat later than the time when x reaches a value corresponding to a one-unit change of y, rather than simultaneously. As a result, the circle will be approximated by a broken line with an

error. We now estimate this error. For this, we prove that, with the method chosen, varying the magnitude of $\underline{x}$ by unity at any point x_i in the interval $0 < x < R/\sqrt{2}$ cannot give rise to a change of the quantity $x^2_{i+1} - x^2_i$ greater

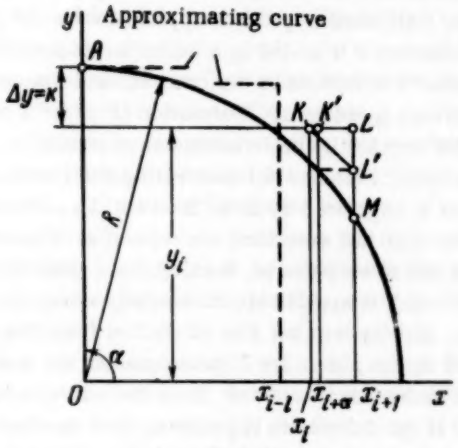

Fig. 1.

than what is necessary to change $\underline{y}$ by one unit.

A. With motion along an approximating curve in accordance with the method we have adopted, let the moving point reach point K (Fig. 1) where, at this moment, coordinate $\underline{x}$ is changed by x_i units and coordinate $\underline{y}$ by $\underline{k}$ units. Then, a subsequent increment of coordinate $\underline{x}$ by one unit engenders the increment

$$x_{i+1}^2 - x_i^2 = 2x_i + 1. \qquad (3)$$

For coordinate y_i to be changed by one unit, with the condition that $\Delta_k = 0$ at point K, it is necessary that the following equation hold:

$$x_{i+1}^2 - x_i^2 = 2R - [2(k+1) - 1]. \qquad (4)$$

It follows from this that for all relationships of $\underline{x}$ and $\underline{y}$ which satisfy the condition

$$2R - (2k+1) \geqslant 2x_i + 1, \qquad (5)$$

an increment of one unit in coordinate $\underline{x}$ will give rise to an increment of coordinate $\underline{y}$ equal to or less than unity if, at these points, it can be assumed that $\Delta_k = 0$. After transformation, (5) assumes the form

$$R - k \geqslant x_i + 1 \qquad (6)$$

or, taking into account that $y_i = R - k$,

$$y_i \geqslant x_{i+1}. \qquad (7)$$

For $\underline{x}$ equal to y_i, a unit increment of coordinate $\underline{x}$ engenders, for $\Delta_k = 0$, a unit increment of coordinate $\underline{y}$, which corresponds to an angle of 45 degrees, or $x = R/\sqrt{2}$. In other words, for motion from point A to point K, each unit change of coordinate $\underline{x}$ engenders a smaller variation in $\underline{y}$. Only, when, as the result of successive variations of $\underline{x}$ by unity, coordinate $\underline{x}$ becomes equal to coordinate $\underline{y}$ at the preceding point does the coordinate $\underline{y}$ also change by unity.

B. We now determine the maximum possible deviation of the approximating curve along the axis of ordinates from the given circle in the interval $0 < x < R/\sqrt{2}$, with account being taken of the Δ_k. Let the motion begin at point A (Fig. 1) and be directed clockwise, with the coordinate $\underline{x}$ being given a unit increment. By virtue of what has already been proved, each unit increment of coordinate $\underline{x}$ requires a variation of coordinate $\underline{y}$ by a quantity less than unity.

However, in accordance with the method chosen for constructing the circle, this change does not occur until the resulting increment of x^2 satisfies the condition $x^2 \geq 2R-1$. This means that, for such a value of $\underline{x}$, the deviation along the axis of ordinates of the approximating curve from the given one is $\delta_y \geq 1$. Let such a point, where the condition $x^2 > 2R-1$ holds, be the point with abscissa x_{i-m}. Then, at the point x_{i-m-1} where $x_{i-m} - x_{i-m-1} = 1$, $\delta_y < 1$. But by virtue of the fact that on this segment a unit increment of coordinate $\underline{x}$ cannot engender an increment of coordinate $\underline{y}$ by more than unity, the transition from point x_{i-m-1} to point x_{i-m} can increase δ_y by at most unity. Thus, the resulting error along the axis of ordinates can lie within the limits $0 \leq \delta_y < 2$. It should be kept in mind that, after transition to the point with coordinates (x_{i-m}, y_{i-m}), there occurs a change of $\underline{y}$ by unity, and δ_y becomes less than unity.

By an analogous argument we can successively check each value of $\underline{x}$ in the given interval, coming to the same conclusion each time.

We now consider the very worst case. Let the moving point be at point K with coordinates (x_i, y_i) such that the next increment of coordinate $\underline{x}$ by unity engenders the incrementation of $\underline{y}$ by unity for $\Delta_k = 0$, i.e., $x^2_{i+1} - x^2_i = 2R-(2k+1) = 2y_i - 1$, where $\underline{k}$ is the number of units by which coordinate $\underline{y}$ was changed at the moment of transition to point K. We assume that, at the moment of transition to point K, the total accumulated increment is $x^2_i - x^2_{i-l}$, where x_{i-l} is the abscissa of the point at which the last change of $\underline{y}$ occurred, or that the magnitude of the residual Δ_k, if we hit point K after the latest change by unity of coordinate $\underline{y}$ rather than $\underline{x}$, had the maximum possible value $\Delta_{k\,max}$. In accordance with the algorithm for the operation of the scheme, $\Delta_{k\,max}$ must, at point K, be at least one unit less than $2y_i - 1$, i.e., must satisfy the equation $\Delta_{k\,max} = 2y_i - 2$.

In making the transition from point K to point L, the residual $\Delta_{k\,max}$ increases by $2y_i - 1$, as a result of which coordinate $\underline{y}$ changes by unity and executes a transition to point L'. However, the residual at point L', $\Delta_{k+1} = \Delta_{k\,max}$, turns out to be larger than the quantity, $2(y_i - 1) - 1$, necessary for changing the ordinate of point L' by unity. As a result of this, a transition occurs to point M, and the following residual is formed:

$$\Delta_{k+2} = 2y_i - 2 - 2(y_i - 1) + 1 = 1.$$

A third change of coordinate $\underline{y}$ by unity can only occur for the condition $2(y_i - 2) - 1 = 1$, i.e., for $y_i = 3$.

By taking (7) into account, we can write $x_{i+1} \leq y_i = 3$. It follows from this that variation of coordinate $\underline{y}$ at

point L by three units in succession is only possible for $R = \sqrt{2}\, x_{i+1} \leq 3\sqrt{2}$. For all values of $R > 3\sqrt{2}$, change of coordinate $\underline{y}$ at point L can occur only by two units. For large R ($R \approx 100$), the magnitude of $2(y_i - 2) - 1 \gg 1$ and, by neglecting unity in comparison with $2(y_i - 2) - 1$, we can assume that in the worst case the change of coordinate $\underline{y}$ is by exactly two units, and point M lies on the circle. Thus, the maximum error, equal to two, will be at point L.

If the order of applying incrementation is somewhat varied, this error can be reduced to unity. For this, we shall first carry out all the computations and then, when it becomes clear that a unit incrementation in $\underline{y}$ must occur, we execute it simultaneously with the incrementation in $\underline{x}$ which was giving rise to it. In the actual scheme, this leads to motion at an angle of 45 degrees from point K to point L' (Fig. 1). As a result, the error in coordinate $\underline{y}$, equal to δ_y, will everywhere be less than unity. The expression for $\underline{x}$ in terms of $\underline{y}$ which is obtained from the equation of the circle coincides with the expression for $\underline{y}$ in terms of $\underline{x}$. Therefore, all the argument already given for $\underline{x}$ is also valid for $\underline{y}$ within the limits of variation of angle α from 0 to 45°, i.e., for variation of α within the limits $R \geq x \geq R/\sqrt{2}$, and the approximating curve is symmetric about the line passing through the first quadrant at a 45° angle. At the limits of the interval $0 < x \leq R/\sqrt{2}$, the radial error at any point $\underline{x}$ will equal

$$\delta_R = \sqrt{(\sqrt{R^2 - x^2} + \delta y)^2 + x^2} - R. \qquad (8)$$

The error δ_y equals the difference between the true value $\underline{y}$ corresponding to a given $\underline{x}$ and the next larger integer if $\underline{y}$ itself is not an integer.

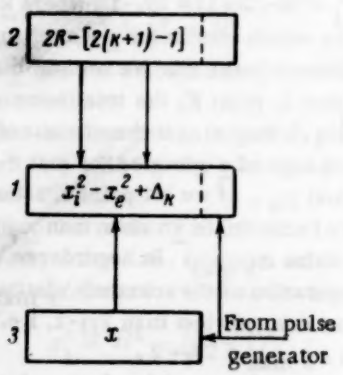

Fig. 2.

Figure 2 shows the simplified block schematic of the interpolating computer which operates in accordance with the principles described above. The circuit consists of counter 3, to which quantity $\underline{x}$ is fed, adder 1 which stores the current value of the difference $x_i^2 - x_l^2 + \Delta_k$, and adder 2 which stores the current value of $2R - [2(k+1)-1]$. The dashed lines on Fig. 2 mark off the adders' least significant places. If the motion is clockwise, starting from point A (Fig. 1) then, before operations commence, the counter and adder 1 are set to zero and the number 2R-1 is placed in adder 2. Then, from the pulse generator, one pulse is applied to the $\underline{x}$ counter, storing a "1" in the counter and in adder 1. From the contents of the adder 1 the number 2R-1 is subtracted and, if the difference formed in adder 1 is negative, the number 2R-1 is added to it, and one pulse is applied along the $\underline{x}$ axis. The sign of the difference is staticized in the sign bit of adder 1. After this, another pulse is applied to the counter, and the number 3 is added into adder 1. As a result, the number 2 is formed in the counter, and the number 4 (2^2) is formed in adder 1. Formation in adder 1 of the square of the number is implemented automatically, thanks to a special scheme for connecting the counter with adder 1, suggested by B. L. Ermilov [1]. Then the arithmetic acts just described are repeated. If the difference turns out to be positive, then addition does not occur, one pulse each is applied simultaneously along the $\underline{x}$ and $\underline{y}$ axes, and the number 2 is subtracted from the contents of adder 2, i.e., in adder 2 there remains the number 2R-3. This number is subtracted from the contents of adder 1 and, if the difference is positive, then another pulse is applied along the $\underline{y}$ axis, and the number 2 is again subtracted from the contents of adder 2, etc., until the difference becomes negative. As soon as the difference does become negative, addition again ensues, and the next pulse is applied from the pulse generator to the counter, etc.

If motion begins from some arbitrary point with coordinates $[x_0, y_0]$, then the initial establishment of values must be the following: in the counter the number x_0 is established, in adder 1 the number $x_0^2 - R^2 + y_0$, and, in adder 2, the number $2y_0 - 1$, where y_0 is the value of $\underline{y}$ corresponding to the value x_0 and rounded off to the next higher integer.

For processing the complete circle, the initial established values and the direction of motion along the axes are changed in making the transition from one quadrant to the next.

Thus, by means of addition and subtraction, comparisons are made in the scheme proposed of the quantities $x_{j+1}^2 - x_j^2 + \Delta k$ with the quantities $2y_j - 1$, where x_j and y_j are the coordinates of any point of the approximating broken line. In a comparison the indication (sign of the difference) is developed which is used for controlling the distribution of the generator pulses along the $\underline{x}$ and $\underline{y}$ axes in correspondence with the given law of motion (circular). With such a computational algorithm for circular motion there occurs a variation of the path velocity by a factor of $\sqrt{2}$ which, in the majority of cases, is admissible. Moreover, by using velocity feedback, one can so control the frequency of the pulse generator that the velocity can be kept constant and equal to a given value. (For a more detailed description of the scheme, cf. [2].)

The scheme suggested by B. L. Ermilov [3] operates by such a mathematical algorithm, but with the use of another computational algorithm, the mathematical

algorithm not being described in general form. The scheme of B. L. Ermilov consists of two counters and one adder of the accumulative type. Pulses from the generator are applied to the x axis and to the input of one of the counters, forming the quantity x in it; with this, the quantity x^2 is formed in the adder. The adder's overflow pulses are applied along the y axis. By means of the second counter, each overflow pulse introduces the quantity $2^n-(2y_j-1)$ into the adder, where n is the number of places in the adder, adding this number to the number remaining in the adder after transmission of the overflow unit. If the overflow pulse does not give rise to a second overflow pulse then, from the first counter, the number 2x-1 continues to be added with the arrival of each generator pulse until overflow again occurs, whereby since $x = 1, 2, 3, \ldots, x^2$ is formed.

Since, on the segments of the circle where the coordinate x is close to R, there are emitted $\sqrt{2R-1}$ successive overflow pulses with the frequency of the scheme's elements' operation, there occurs a sharp change in the path velocity. Indeed, the generator's frequency must be approximately $\sqrt{2R-1}$ times less than the frequency of the overflow pulses so that $\sqrt{2R-1}$ overflow pulses can be disseminated between any two generator pulses. As a result, motion at the beginning of the processing of a quadrant of the circle (from 90 to 45°) will occur with a velocity smaller by a factor of $\sqrt{2R-1}$ than that at the end. Such a sharp variation of path velocity in cases when the device is designed to guide a cutting tool is inadmissible. It should be mentioned that control of the path velocity by variation of the generator frequency is not possible in the scheme given, since the frequency of the overflow pulses does not depend on the generator frequency.

SUMMARY

1. For constructing a circle, we use the derived formula $x_{j+1}^2 - x_j^2 + \Delta_k \geqslant 2R - [2(k+1) - 1]$.

2. In constructing a circle in accordance with the computational algorithm suggested, there occurs no accumulation of errors, and one obtains an absolute radial approximation error δ_R which is less than one unit in the chosen scale.

3. The scheme suggested makes it possible to control path velocity by varying the pulse generator's frequency.

LITERATURE CITED

1. B. L. Ermilov, "Certain types of digital function generators," paper given at the Conference on the Theory and Application of Discrete Automatic Systems [in Russian] (Moscow, 1958).
2. V. V. Karibskii, "An interpolating device for giving circular motion," Priborostroenie 2 (1960).
3. B. L. Ermilov, "Sampled-data device for the automatic control of circular motion," Claim No. 604342/26 of Aug. 19 (1958).

EXPERIMENTAL INVESTIGATION OF RUBBER-FABRIC MEMBRANE CHARACTERISTICS

G. T. Berezovets and Chou Ching-leng

(Moscow)

Translated from Avtomatika i Telemekhanika, Vol. 21, No. 3, pp. 323-332, March, 1960
Original article submitted September 3, 1959

The results are given of an experimental investigation of rubber-fabric membrane characteristics, these membranes being used in pneumoautomation devices.

1. Aim and Methodology of the Investigation

Modern pneumoautomation devices, designed for the regulation and control of various continuous productive processes, are constructed on the principle of force compensation.

As one of their basic physical elements, these devices usually contain either bellows or rubber-fabric membranes. The pneumatic instruments of unified aggregate systems (UAS), produced domestically, as well as the instruments of the majority of foreign companies —Moore, Sunvic, Taylor, Bristol, Brown, Electroflo, DRD, etc. are constructed with membranes. The membranes delimit the individual pneumatic chambers inside the instruments, and it is on the membranes that forces from the compressed air in these chambers are balanced.

Such indicators of quality of operation of modern pneumatic devices as their accuracy and sensitivity, as well as their static and dynamic characteristics, depend to a large extent on the properties and characteristics of their membranes.

There are many works in the literature on the investigation of metallic membranes, but there are only a few works [1-4] devoted to the investigation of rubber-fabric membranes. In connection with this, and because precisely these rubber-fabric membranes have attained their greatest dissemination in pneumatic devices for the control and regulation of productive processes, the necessity for a more careful investigation of these membranes arose.

The membranes investigated had plane and conic profiles (Fig. 1, a and b), prepared from brand 1520 caprone, from glass cloth and TD cloth covered with brand 44-9 rubber, and also included corrugated membranes of AM-93 rubber, used in UAS instruments (Fig. 1, c).

The experimental investigation was to determine the following characteristics:

1) the dependence of the membrane's effective area on its travel, $F_e = f(S)$;

2) the dependence of the membrane's effective area on the pressure drop across it, $F_e = f(\Delta p)$;

3) the membrane's hysteresis.

In addition, we determined the effect of the membrane's geometry, of the dimensions of its rigid center, and of the material's quality on the course of the characteristics $F_e = f(S)$ and $F_e = f(\Delta p)$, investigated the stability of membrane operation, and determined the possible skewing of the membrane which might arise during its operation.

The experiments were carried out on stands specially developed for this purpose, in which atmospheric pressure acted on one side of the membrane and, on the other side, compressed air or a vacuum, the magnitudes of which were controlled.

The forces arising from the pressure drops acting on the membranes were equalized by weights attached to the membranes' rigid centers. The membrane characteristics were taken off for the following weight sizes: 0.540, 0.728, 4.62, 8.85, 13.09, and 17.32 kg. A cathetometer measured the membrane displacements.

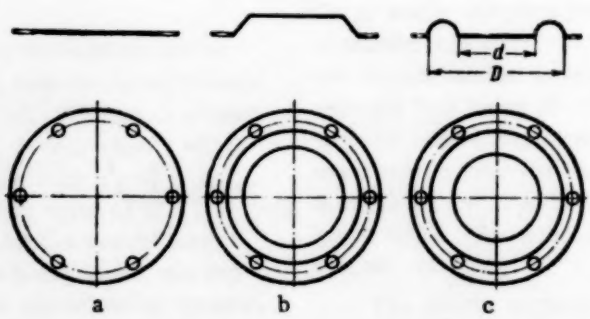

Fig. 1. Forms of the membranes investigated.

For measuring skewing, pressure was introduced into a chamber over the membrane, with a long pointer attached to the membrane's rigid center on the load side. Membrane skewing was determined by the position of the end of the pointer fixed to a scale under the pointer. The scale was a uniform lattice of concentric circles and radial lines. Angles were read off from the radial lines, while the displacement of the pointer's end from the center was read off from the concentric circles.

The magnitude of the membranes' effective area was computed from the formula

$$F_e = \frac{G}{\Delta p},$$

where F_e is the magnitude of the effective area in cm^2, G is the size of the weight placed at the membrane's rigid center, in kg, and Δp is the pressure drop across the membrane, in kg/cm^2.

For the testing of the plane and conical membranes we used rigid centers of two sizes: d = 20 mm and d = 45 mm; the diameter D of the seals of these membranes was the same for all, and equal to 60 mm. A corrugated membrane (Fig. 1, c) was tested with a rigid center d = 45 mm and a value of D equal to 62 mm.

EXPERIMENTAL RESULTS

Stability of Membrane Characteristics and Membrane Skewing

The characteristic $F_e = f(S)$, for new membranes, was only stabilized after the membrane had operated under pressure for several hours. The characteristics of one and the same membrane, in an unchanged set-up, may be repeated only in the case when they are taken off, one after another, without any interruption in membrane operation. Membrane characteristics taken off after an interruption in operation are initially unstable, but then, after some time, are stabilized and begin to coincide with each other; but they almost never coincide exactly with the characteristics taken off before the interruption. The difference between these effective area characteristics can reach 10 to 12 %.

With a readjustment of the membrane, the characteristics taken off before and after the readjustment never coincide. As the pressure drop acting on the membrane becomes larger, the characteristics become more stable.

In investigating membrane skewing, it was observed that they are unstable, but depend basically on the membrane's positioning and, particularly, on the presence of nonconcentricity between the membrane's rigid center and the seal's circle.

Figure 2 shows part of the scale plus the graphs of the motion of the end of the pointer for two different positionings of one and the same membrane. The solid line shows the course of the pointer as the pressure in the chamber over the membrane was increased (forward travel), and the dashed lines show it for decreasing pressure (reverse travel). It was established that the skewing angle between the plane of the flapper, fixed on the membrane's rigid center, and the plane of the nozzle's face end, which this flapper must cover, can oscillate, for different membranes, from 0.5° to 1.5°.

Investigation of Plane Membranes

A comparison of the characteristics $F_e = f(S)$, taken off for membranes prepared of caprone, glass cloth, and TD cloth, led to the following conclusions:

a) the membranes of TD cloth possessed the greatest hysteresis; for them, the relative magnitude of the maximum hysteresis per effective area ΔF_h can reach 18 %, while for membranes of glass cloth, having minimum hysteresis, it was about 7 to 8 % (computing ΔF_h

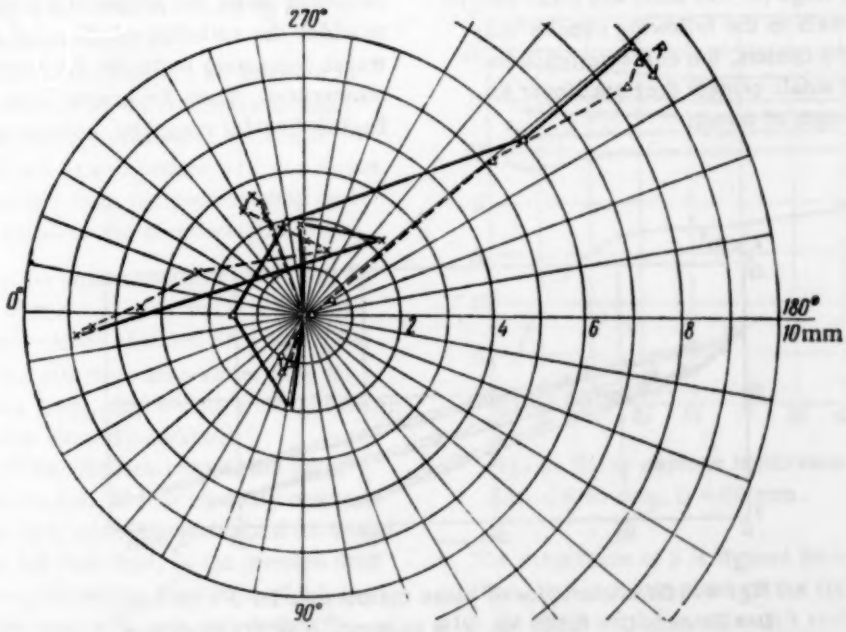

Fig. 2. Graphs characterizing the skewing of a membrane's rigid center.

as the maximum absolute value of the hysteresis divided by the maximum value of effective area $F_{e\ max}$ for forward travel of the membrane);

b) for one and the same pressure drop on the membrane (i.e., for one and the same value of F_e), the least travel was observed in glass cloth membranes; the travels of membranes of caprone and TD cloth were almost identical, and were larger than the travels of glass cloth membranes.

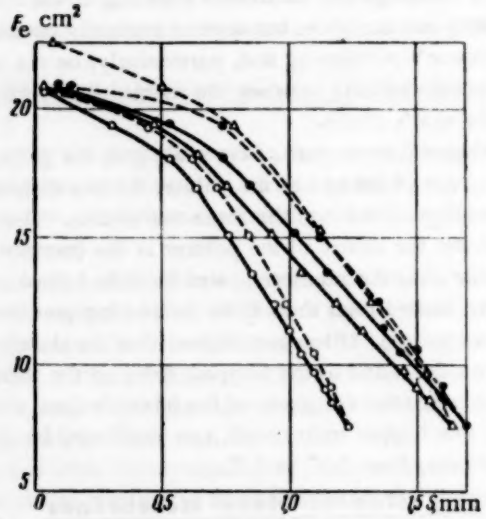

Fig. 3. Characteristics of plane membranes for d = 45 mm, D = 60 mm, G = 0.540 kg. Solid lines are for forward travel, dashed lines for reverse travel; ● is caprone, △ is TD cloth, ○ is glass cloth.

A comparison of plane membrane characteristics (Figs. 3 and 4) with large (d = 45 mm) and small (d = 20 mm) rigid centers leads to the following conclusions:

a) for large rigid centers, the characteristics are nonlinear, while for small centers they are linear for almost the entire length of travel;

b) with small centers, the hysteresis per area equals 1.6 to 2%, i.e., is much less than for membranes with large centers, in which it may oscillate between 7 and 18 %;

c) when the rigid center is decreased, the membrane travel is increased, but not by the same amount: in caprone membranes this increase is about 53 % of the travel for d = 45 mm and, for glass cloth membranes, about 23 %;

d) as the diameter of the rigid center is varied from 45 to 20 mm, or as its area varies from 16.2 to 3.2 cm², the maximum effective area F_e (with S = 0) is varied, for all the membranes, approximately from 21 to 12 cm².

Figure 5 shows the characteristics $F_e = f(S)$ for plane caprone membranes with a large rigid center (d = 45 mm), taken off for weights of different magnitudes.

By considering the characteristics obtained, one can establish the following regularities in their behavior;

1. The larger the weight, i.e., the greater the initial value of the drop necessary for the membrane to begin to move, the greater is the steepness of the characteristic $F_e = f(S)$ as the pressure drop thereafter increases, i.e., the less does the effective area change over the course of the membrane's travel.

This is explained by the circumstance that, with a large weight, there is a large pressure drop across the membrane even before it begins to move, under the action of which pressure drop the membrane's free surface is deformed, forming a semispherical crimp. With a further increase in pressure drop, a motion begins which is analogous to the motion of a crimped (corrugated) membrane.

The formation of crimps in plane membranes occurring under the action of a pressure drop (thanks to which the variation of effective area as a function of travel decreases) increases the possibility of using plane membranes. Thus, for example, in the regulators of the English Sunvic company, instead of using doubled

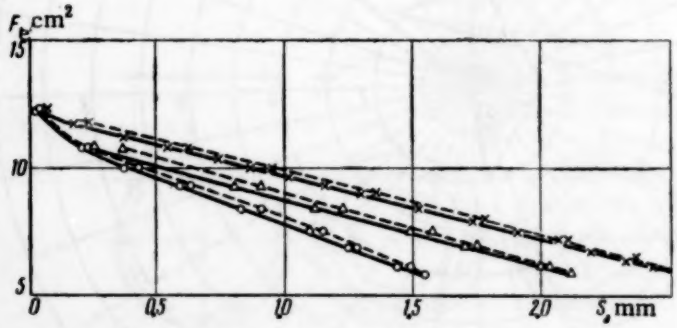

Fig. 4. Characteristics of plane membranes for d = 20 mm, D = 60 mm, G = 0.540 kg. × is caprone, △ is TD cloth and ○ is glass cloth.

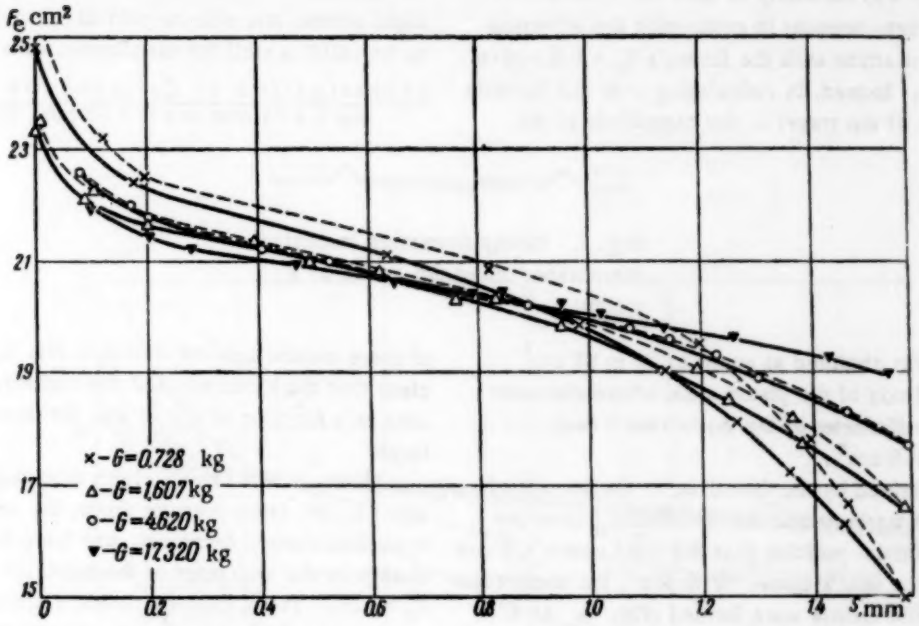

Fig. 5. Plane caprone membrane characteristics, taken off for different weights. d = 45 mm, D = 60 mm.

corrugated membranes with atmospheric pressure between them, as is done in the UAS blocks, doubled plane membranes are used, with the pressure between them being obtained from the supply channel. Since the supply pressure is necessarily greater than the pressure in any of the regulator chambers, crimps are always formed under the action of this pressure.

2. The greater the size of the weight, the less the hystersis per area ΔF_h : if ΔF_h = 3.6 % for a weight G = 0.728 kg, then ΔF_h = 0.2% for G = 4.62 kg and, for G = 8.85 kg, it vanishes completely.

The decrease in hysteresis observed for increase in weight is explained by this, that the internal frictional force which engenders the phenomenon of hysteresis becomes vanishingly small in comparison with the forces generated in the membrane from the pressure drop on it which is necessary to equalize the given weight.

3. Figure 6 shows the characteristic $F_e = f(\Delta p)$ for a caprone membrane with d = 45 mm and D = 60 mm, constructed for different values of travel S* . It is clear from the graphs that the effective area varies only for small values of pressure drop, after which, with increasing pressure drop, it remains virtually constant.

This means that if the displacement of the membrane is severely limited, i.e., if it is virtually clamped into the position when it is initially established for values of travel of S = 0.4 to 0.8 mm then, as the pressure drop across the membrane varies within the limits of 0.1 to 1 kg/cm², the effective area will vary very insignificantly. The explanation of this fact is very important, since it opens up the possibility of such an establishment of initial membrane position in devices for which deviations of effective membrane area should be minimal.

Investigation of Membranes with Conic Profiles

In the investigation of membranes with conic profiles, it was established that, with small weights

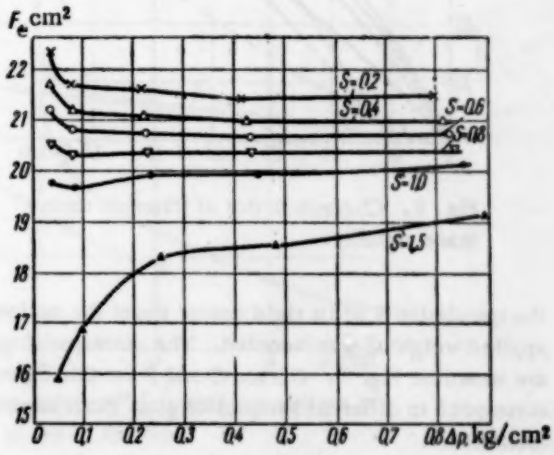

Fig. 6. Plane caprone membrane characteristics. d = 45 mm, D = 60 mm.

* The magnitude of S is figured from the neutral position, in which the plane of the rigid center coincides with the plane of the membrane's seal. An increase in the travel S corresponds to a displacement of the membrane upward from the neutral position.

(G = 0.540 g), it was necessary to take the membrane's natural rigidity into account in computing the effective area, since calculations with the formula $F_e = G/\Delta p$ give incorrect results. Indeed, in calculating with this formula for small values of the travel S, the magnitude of the effective area was obtained as equal to 30 to 35 cm^2, while the magnitude of the piston area, whose diameter would equal the diameter of the membrane's seal, equalled only 28.8 cm^2.

This is explained by the fact that, in the process of taking off the characteristics, the membrane was so established in its initial position that the rigid center's plane coincided with the seal's plane. With this, the membrane was deformed, and crimps were formed (Fig. 7). As a result, a force Q arose, resulting from the membrane's inherent rigidity, which counteracted the weight G applied to the membrane.

An experiment was specially carried out to determine the inherent rigidity of conical and corrugated membranes, in which the free membrane was gradually loaded, and

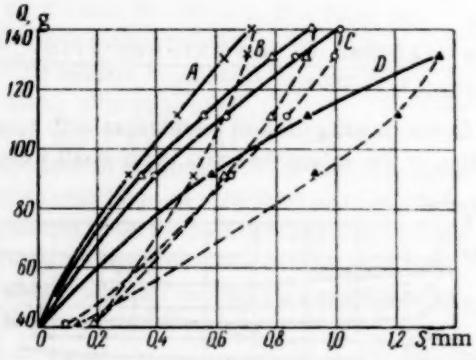

Fig. 8. Characteristics of inherent membrane rigidity.

the translation S of its rigid center under the action of the applied weight Q was recorded. The corresponding graphs are shown on Fig. 8. Curves C and D on this figure correspond to different samples of glass cloth conical membranes.

It is clear from these graphs that, for small weights, the force Q becomes commensurable with the magnitude of the weight G, so that the computation of the effective area in this case can be carried out with the formula $F_e = (G-Q)/\Delta p$.

All the fundamental regularities observed in the testing of plane membranes, both with respect to the behavior of the characteristics $F_e = f(S)$ and $F_e = f(\Delta p)$ for different weights and for different diameters of the rigid center, and with respect to hysteresis, turned out to be valid as well for membranes with conical profiles.

Investigation of Crimped UAS Membranes

For d = 45 mm and D = 62 mm, the characteristics

Fig. 7. Crimp formation in conical membranes under the action of a weight.

of these membranes are shown in Fig. 9, from which it is clear that the hysteresis and the variation of effective area as a function of travel are, for small weights, very large.

However, for large weights (starting with G = 4.62 kg), i.e., for large pressure drops, the amount of hysteresis sharply decreases, and there is a simultaneous change in the character of the behavior of characteristic $F_e = f(S)$. These characteristics, starting with a travel of about S = 0.45 mm, become practically linear and, what is particularly important, steep.

The magnitude of a UAS membrane's effective area strongly depends on the position of the rigid center with respect to the plane of the membrane's seal. This is particularly apparent for small weights. Figure (10) shows the characteristics of a UAS membrane for d = 45 mm and D = 62 mm, taken off for weights of G = 0.540 kg and G = 17.32 kg, and for various distances h of the membrane's rigid center from the seal plane. Characteristics A correspond to the neutral position, when h = 0; characteristics B correspond to h = -2 mm, i.e., to a position of the membrane below the neutral position, and characteristics C correspond to the position when h = 2 mm, i.e., the membrane is above the neutral position.

For UAS membranes we investigated the hysteresis as a function of the travel (Fig. 11). This confirmed the conclusion, given in [3], that the hysteresis decreases with decreasing travel.

In Fig. 8, given earlier, the characteristics Q = f (S) were given, from which the inherent membrane rigidity can be determined.

Characteristic A corresponds to the case when the UAS membrane is loaded on the side of crimp concavity, and characteristic B to the case when the load is on the convex side.

From a comparison of these characteristics it is clear that the membrane possesses different rigidity, depending on which side of the crimp the force is acting, specifically, the rigidity is greater in the case when the force acts on the crimp's concave side.

SUMMARY

From the experimental results, we may draw the following conclusions:

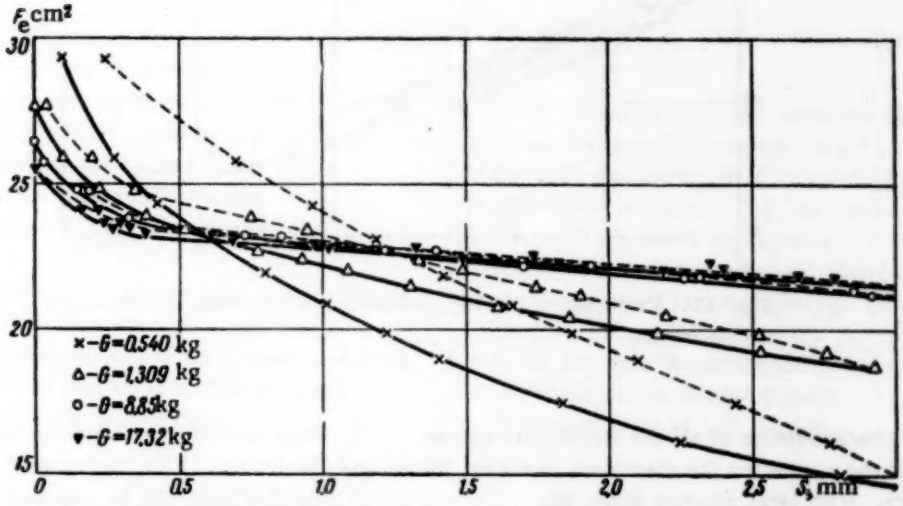

Fig. 9. Characteristics of UAS membranes, taken off for various weights. D = 62 mm, d = 45 mm.

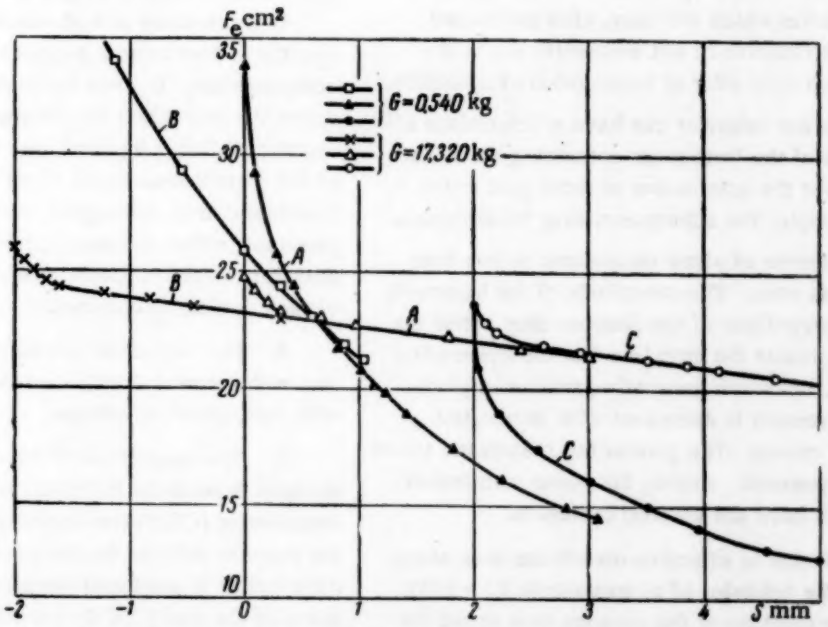

Fig. 10. UAS membrane characteristics, taken off for various positions of the UAS membrane with respect to the plane of the seal.

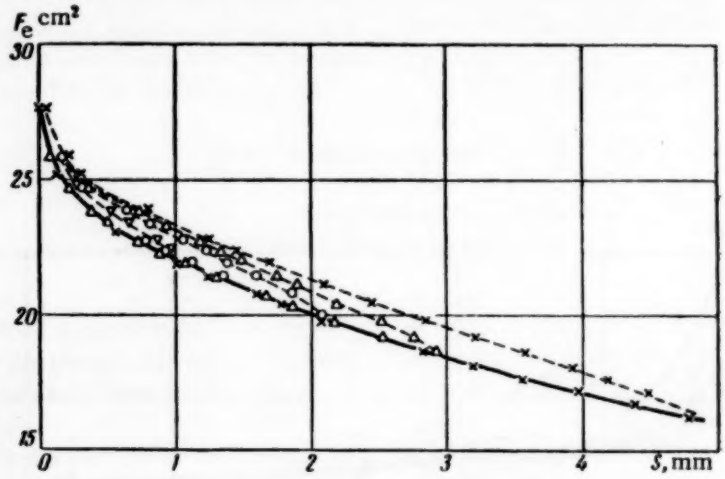

Fig. 11. Variation of the UAS membrane's hysteresis as a function of the travel.

1. The characteristics of all the membranes can be stable only in the case when the membrane is always found under pressure. With large pressure drops, the characteristics are more stable than with small ones. Interruptions in membrane operation lead to a confusion of its characteristics which are then, after protracted operation, again stabilized , but frequently not to the same value which held prior to interruption of operation.

Such membrane behavior can have a deleterious effect on the operation of the instrument containing the membrane and used for the automation of some productive process: for example, the adjustments may be disrupted.

2. The hysteresis of plane membranes is less than that of corrugated ones. The magnitude of the hysteresis depends on the magnitude of the pressure drop across the membrane: the greater the drop, the less the hysteresis ; with large drops, hysteresis generally vanishes in plane membranes. Hysteresis is decreased with decreasing membrane rigid center. The greater the membrane travel, the greater its hysteresis. Among the plane membranes, those of TD cloth have the greatest hysteresis.

3. The variation in effective membrane area along its travel, i.e., the behavior of characteristic $F_e = f(S)$, depends on the magnitude of the pressure drop across the membrane. For a given membrane travel, the greater the drop, the less the variation in the membrane's effective area.

4. The effective membrane area varies as a function of the drop; the less the drop, the greater this variation. However, starting with a drop of about 0.15 kg/cm², further increases in it lead to virtually no changes in effective area, i.e., it may be considered constant. This last statement is valid both for plane and for conical and corrugated membranes.

From whence the following important conclusion may be drawn : if the membrane's travel is limited, then its effective area will be constant for all practical purposes for variations of the pressure drop on it within the limits of 0.15 to 1 kg/cm².

It is precisely in such conditions that membranes operate in instruments designed on the principle of force compensation. In these instruments, the pressure drop across the individual membranes might vary within the limits of 0.2 to 1 kg/cm², and the static translation of the membranes equals about 0.05 mm. The effective membrane area, during the instrument's operating processes, either remains completely unchanged or changes only very slightly, thanks to which an increased accuracy of such devices is obtained.

5. The variations in effective area, both with travel and with pressure drop , are least of all in UAS membranes with semispherical crimps.

6. The magnitude of the membrane's effective area strongly depends on its initial establishment; this dependency is the more strongly pronounced, the less the pressure drop on the membrane. When the membrane's rigid center is displaced downward with respect to the plane of the seal ($h < 0$) the effective area increases in comparison with the case when the membrane is in the neutral position ($h = 0$) and, when the displacement is upward ($h > 0$), it decreases.

In connection with this, the accuracy of the initial placement of the membranes in UAS instruments plays an important role, since by it one determines the deviation of the effective area of one membrane from another. In isodrome regulators, for example, this is inadmissible, since it might lead to the appearance of residual nonuniformities.

7. Experiment showed that the formula usually given in the literature for calculating effective membrane area,

$$F_e = \frac{\pi}{12}(D^2 + Dd + d^2),$$

which does not take into account the variation in area as a function of travel and pressure drop, can be used only for determining the value of F_e for zero or very small travels of plane membranes, and only in the case when the membrane is established in the strictly neutral position (h = 0).

8. Calculating membrane characteristics from experimental data by the formula $F_e = G/\Delta p$ can be done only for large weights and, consequently, for large pressure drops. Calculations for small pressure drops give incorrect results, due to the fact that the membrane's inherent rigidity has not been taken into account.

The magnitude of the force arising from this rigidity is not a constant for different membranes, and may reach a magnitude of 300_g. If this force is commensurable with the magnitude of the weight, it is then necessary to take it into account in the calculations.

9. In certain devices of pneumoautomation, for example, lead blocks, where there are not very stringent requirements on the invariance of membrane effective area, doubled corrugated membranes can be replaced by doubled plane membranes with supply pressure between them.

LITERATURE CITED

1. V. L. Lossievskii, Automatic Regulators [in Russian] (Oborongiz, 1944).
2. V. V. Afanas'ev, "On the variations of effective area of rubber-fabric membranes," Systems, Devices, and Elements of Pneumohydraulic Automata [in Russian] (Izd. AN SSSR, 1959).
3. Yu. L. Mach and S. P. Stepanov, "The investigation of membrane characteristics," Systems, Devices, and Elements of Pneumohydraulic Automata [in Russian] (Izd. AN SSSR, 1959).
4. V. P. Temnyi, "Experimental determination of rubber-fabric membrane rigidity," Avtomatika i Telemekhanika 17, 11 (1956).

OPTIMAL FREQUENCY CONTROL OF ASYNCHRONOUS ELECTRIC MOTORS

Yu. P. Petrov

(Leningrad)

Translated from Avtomatika i Telemekhanika, Vol. 21, No. 3, pp. 333-339, March, 1960
Original article submitted November 25, 1959

The question is investigated as to which law should be followed in controlling voltage and frequency in asynchronous electric motors so as to provide optimal transient responses. The optimal control laws are derived for various requirements on the character of the transient response for the case when the impedance moment depends linearly on the rotational velocity*.

For those stands where it is possible arbitrarily to vary the frequency of the voltage supplying the executive asynchronous electric motors, the problem arises as to which law the frequency should be varied by so as to provide optimal motor operation in the transient states. Electric drives can be divided into two basic groups as a function of the requirements imposed on the character of their transient responses.

Electric drives of the first group must provide maximum translation of the executive mechanism in a given time for given values of initial and final rotational velocities. Electric drives of the second group must provide maximum change of rotational velocity of the executive mechanism in a given time.

As examples of the first group of electric drives, one may take traction motors while, as examples of the second group, one can adduce electric starting motors.

Optimal control laws, as we shall see below, will be different for the different groups of electric drives.

We shall start from the basic equation of electric drive dynamics:

$$M_{mo} - M_i = J \frac{dn}{dt}, \qquad (1)$$

where M_{mo} is the motor's rotational torque, M_i is the impedance torque, depending on rotational velocity, and J is the moment of inertia about the motor shaft of the motor and drive.

We now introduce relative units. As the unit rotational torque we take the maximum (tilting) torque M_{max}, corresponding to critical slipping; as the unit of rotational speed we take n_s, the synchronous velocity for the supply line's maximum frequency; as the time unit we take T_M, the mechanical time constant, numerically equal to the time for accelerating the drive zero up to the synchronous velocity for a constant rotational torque equal to the maximum; as the unit of current frequency in the rotor, we take f_{cr}, the critical frequency corresponding to tilting slipping; for the unit of current we take I_{cr}, the rotor current for critical slipping.

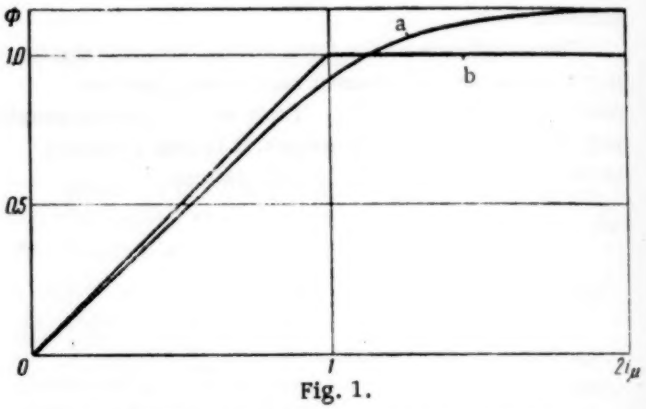

Fig. 1.

The relative units will be: for motor rotational torque, $M = M_{mo}/M_{max}$, for impedance moment, $\mu = M_i/M_{max}$, for time $\tau = t/T_M$, for rotor rotational speed, $\nu = n/n_s$, for rotor current frequency, $\omega = f_{rot}/f_{cr}$, for current $i = I/I_{cr}$ and, for stator frequency, $f = f_{st}/f_{max}$.

We make the following assumptions:

1. We shall replace the true motor magnetization curve a by the piecewise-linear curve b, consisting of two segments (Fig. 1).

2. We shall not take into account the electromagnetic transient response (the free component in the rotor current).

In relative units, the dynamics equation (1) takes the following form:

$$M - \mu = \frac{d\nu}{d\tau}. \qquad (2)$$

The rotational torque M and the heat dissipation in the rotor Q will be expressed by the formulas

$$M = \frac{2\Phi^2\omega}{1+\omega^2}, \qquad (3)$$

$$Q = \int_0^\tau \frac{2\Phi^2\omega^2}{1+\omega^2}\,d\tau \qquad (4)$$

* The basic propositions of this paper were presented on Sept. 29, 1958 at the All-Union Conference on the Theory and Applications of Discrete Automatic Systems (Section on Optimal System Theory).

where Φ is the motor's magnetic flux in relative units :

$$\Phi = \frac{\Phi_{mo}}{\Phi_{max}} .$$

The yield of electric drives of the first group will be proportional to the integral

$$\Delta\alpha = \int_0^\tau \nu d\tau, \qquad (5)$$

and that of the second group to the integral

$$\Delta\nu = \int_{\nu_1}^{\nu_2} d\nu = \int_0^\tau \nu' d\tau. \qquad (6)$$

In seeking an optimal control law, we should take into account the limitations imposed by the properties of the electric motors. The most important of these is the limitation of heating : the temperature of the winding must not exceed a limiting admissible value. Since the thermal transient responses in a motor flow much more slowly than the mechanical transient responses (heating time constants are measured in minutes [2]), one can ignore the heat emission during the start-up and braking times. With heat emission ignored, the heating limitation on the quantity of heat which can be generated in the rotor in a given time, i.e.,

$$\int_0^\tau \frac{2\Phi^2\omega^2}{1+\omega^2} d\tau \leqslant Q_0. \qquad (7)$$

With complete use of motor heating, (7) goes over into an equality. Steel saturation introduces a limitation on magnetic flux. With the assumptions we have made, this limitation, in relative units, is written in the form

$$0 \leqslant \Phi \leqslant 1. \qquad (8)$$

Finally, the motor's rotational speed is limited by the supply line's maximum frequency

$$\nu \leqslant \nu_{max} \qquad (9)$$

and, for $\mu = 0$,

$$\nu_{max} = 1.$$

Optimal Control Law for Electric Drives of the First Group

The optimal control problem for electric drives of the first group is formulated mathematically as follows : to find $\omega = \omega(\tau)$ and $\Phi^2 = \Phi^2(\tau)$ which maximize (5) for a given value of (4), for given relational equations (2) and (3) and given limitations (8) and (9). This is the general Lagrange problem of variational calculus, complicated by the fact that only one-sided variation is admissible here. Consequently [1], the functions sought, $\omega(\tau)$ and $\Phi^2(\tau)$, must :

1) either be extremal, i.e., satisfy the Euler equations

$$\frac{\partial F}{\partial \nu} - \frac{d}{d\tau}\frac{\partial F}{\partial \nu'} = 0, \qquad \frac{\partial F}{\partial \omega} - \frac{d}{d\tau}\frac{\partial F}{\partial \omega'} = 0, \qquad \frac{\partial F}{\partial \Phi^2} - \frac{d}{d\tau}\frac{\partial F}{\partial \Phi^{2\prime}} = 0$$

for the auxiliary function F :

$$F = \frac{2\Phi^2\omega^2}{1+\omega^2} - \lambda_0\nu + \lambda\left(\nu' + \mu - \frac{2\Phi^2\omega}{1+\omega^2}\right), \qquad (10)$$

where λ_0 and λ are Lagrange multipliers, with λ_0 constant and λ a function of τ ;

2) or be boundary curves, i.e., satisfy (8) or (9) with the equality signs;

3) or, finally, may consist of extremal segments plus segments of boundary curves.

We turn now to the search for extremals.

The first Euler equation leads to the expression

$$\lambda\frac{d\mu}{d\nu} - \lambda_0 = \frac{d\lambda}{d\tau}, \qquad (11)$$

from which, for $\mu = \mu_0 + k\nu$, we will have

$$\lambda = \frac{\lambda_0}{k} - C_1 e^{k\tau}, \qquad (12)$$

and, for the most important case when $\mu = \mu_0 = \text{const}$,

$$\lambda = C_2 - \lambda_0\tau. \qquad (13)$$

The second Euler equation, after some transformation, is written in the form

$$\frac{2\omega}{1-\omega^2} = \lambda. \qquad (14)$$

We note particularly that (14) does not contain Φ and is valid for any magnetic flux (in addition to the trivial case $\Phi = 0$).

To find the control law for magnetic flux, we use the third Euler equation.

By differentiation of F with respect to Φ^2, we get

$$\frac{\partial F}{\partial \Phi^2} = \frac{2\omega^2}{1+\omega^2} - \lambda\frac{2\omega}{1+\omega^2}. \qquad (15)$$

By substituting the value of λ from (14) in (15), we convince ourselves that $\partial F/\partial \Phi^2$ can not vanish and, consequently, $\Phi^2(\tau)$ which maximizes integral (5) can not be extremal, but is a boundary curve, i.e., $\Phi = 1$.

The optimal voltage control law is a control such that, with account taken of the voltage drop in the stator winding, the magnetic flux will be maintained constant.

The optimal laws of current frequency variation in the rotor will be :

for $\mu = \text{const}$,

$$\frac{2\omega}{1-\omega^2} = C_2 - \lambda_0\tau; \qquad (16)$$

for $\mu = \mu_0 + k\nu$

$$\frac{2\omega}{1-\omega^2} = \frac{\lambda_0}{k} - C_1 e^{k\tau}. \qquad (17)$$

For constant magnetic flux, the law of rotor frequency variation also determines the optimal law of variation of the motor's rotational torque as a function of time. By knowing the motor's torque and its mechanical time constant, we determine the rotor's speed of rotation and, thereby, the optimal law for supply frequency variation.

This law will be valid until the rotor's speed of rotation reaches its limiting value, bounded by (9). After reaching this limiting speed, one must transfer

Since the extremals must, at the junction point, coincide with the boundary curves tangent to them [1], then the equalitites $M = \mu$ and $d\nu/d\tau = 0$ must hold for the transition points.

Optimal Control Law for Electric Drives of the Second Group

The problem of optimal control for electric drives of the second group is formulated mathematically as follows: to find $\omega(\tau)$ and $\Phi^2(\tau)$ which maximize (6) for a given value of (4), for given relational equations (2) and (3) and given limitation (8). Thus, the optimal control problem for electric drives of the second group is analogous to that for those of the first group, with the sole difference that the auxiliary function will now have the form

$$F_1 = \frac{2\Phi^2\omega}{1+\omega^2} - \lambda_0\nu' + \lambda\left(\nu' + \mu - \frac{2\Phi^2\omega}{1+\omega^2}\right). \quad (18)$$

The first Euler equation is now written in the form

$$\lambda\frac{d\mu}{d\nu} = \frac{d\lambda}{d\tau}. \quad (19)$$

The second Euler equation will be

$$\frac{1}{1-\omega^2} = \lambda.$$

From the third Euler equation, with account taken of (8), we get, just as for electric drives of the first group, that the magnetic flux, for optimal control, must be maintained constant ($\Phi = 1$). For $\mu = \mu_0 + k\nu$ we obtain, from (19) and (14), the expression for the optimal control law for the current frequency in the rotor:

$$\frac{2\omega}{1-\omega^2} = C_3 e^{k\tau}. \quad (20)$$

It follows from this that the rotational torque must increase as the drive starts up. For $k = 0$, i.e., for $\mu = \text{const}$, it follows from (20) that $\omega = \text{const}$. Thus, we arrive at the important conclusion that, for constant impedance torque, the optimal control law for electric drives of the second group amounts to maintaining constant current frequency in the rotor, and consequently, constancy of the rotational torque. With this, the drives rotational speed will vary linearly and, consequently, the supply frequency must also vary as a linear function of time [6].

On the basis or the duality principle of variational calculus [1], all the optimal laws derived by us from the assumptions that the quantity of heat was given, and that it was required to provide the greatest translation (or change of speed), will also remain valid for the case when the translation and the time are given, and it is required to provide minimum dissipation. The same laws also remain valid when the time of translation and the heat dissipation are given, and it is required to provide the minimum time of translation.

The optimal control laws for asynchronous electric motors have great similarity to the optimal laws for dc motors [3-5]. If we compare the dependence of rotational torque on time for optimal control, then the optimal control law for dc motors turns out to be the limiting case of the optimal law for asynchronous motors with the condition that the latter's maximum torque tends to infinity. In an optimally controlled asynchronous motor, the frequency in the rotor is always less than critical, and the rotational torque fs less than maximal.

It should also be mentioned that the maximum torque of an optimally controlled asynchronous motor is larger than the maximum torque of a motor with a constant voltage on its terminal, since for critical slipping, due to the voltage drop in the stator winding, the motor's magnetic flux is less than the nominal value. With optimal control, when the magnetic flux is maintained constant, the maximum torque is 1.5 to 2 times greater than what is stated in the catalogs.

Figure 2 shows an example of optimal control for a motor in which critical slipping equals 0.2, the maximum torque multiplicity (for complete magnetic flux) equals 5, the mechanical time constant is $T_M = 1.82$ seconds, the impedance torque is constant and equal to the nominal value, and the electric drive falls in the first group.

Determination of the Coefficients in the Extremal Equations

We had found the extremal equations in a general form. For practical use of the optimal control laws found, it is necessary to know, in each concrete case, the coefficients in the extremal equations as functions of the given electric-drive parameters.

We consider electric drives of the first group, with constant impedance torques. Extremal (16) is known,

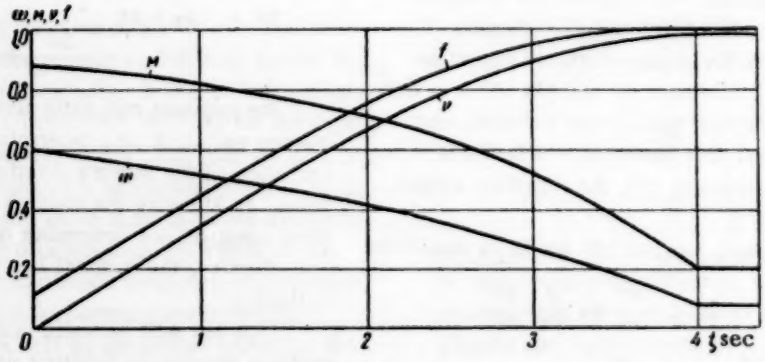

Fig. 2.

from control by extremals (16) or (17) to control by boundary curves, i.e., it is necessary to maintain $\nu = \nu_{max}$ and $M = \mu$ and, consequently, $\omega = const$. and we now derive useful auxiliary formulas. By carrying out a change of variables in (2), (3), and (4) on the basis of (16), and then integrating, we get

$$\nu_2 - \nu_1 = \frac{2}{\lambda_0}\left[\frac{1}{1-\omega^2}\right]_{\omega_2}^{\omega_1} - \mu\tau, \qquad (21)$$

$$Q = \frac{2}{\lambda_0}\left[\frac{\omega}{1-\omega^2} - \operatorname{arc\,tanh}\omega\right]_{\omega_2}^{\omega_1}. \qquad (22)$$

We recall the self-evident formula

$$\nu = f - s_{cr}\,\omega, \qquad (23)$$

where f is the stator frequency in relative units and s_{cr} is the critical slipping.

By using these formulas one can, on the basis of the given parameters of the electric drive and the characteristics of the transient response, find the coefficients in the extremal equations. For the example given, let it be required that the electric motor with critical slipping s_{cr} and impedance torque μ_0 start the drive, within time T_0, from initial speed $\nu_1 = 0$ to speed ν_2, corresponding to stator frequency $f = 1$. The dissipation during starting time T_0 must not exceed Q_0. The electric drive falls in the first group and, consequently, the optimal control problem is to provide maximum translation in time T_0. We know extremal (16). We determine the coefficients C_2 and λ_0 which appear in (16). We start by determining rotor frequency ω_2, corresponding to the end of the start-up period. From the equation

$$\frac{2\omega_2}{1+\omega_2^2} = \mu_0$$

we find ω_2, after which, from (23), we find $\nu_2 = 1 - s_{cr}\omega_2$.

Now, (21) and (22) give us a system of two equations for determining the two unknowns ω_1 and λ_0:

$$\nu_2 = \frac{2}{\lambda_0}\left[\frac{1}{1-\omega^2}\right]_{\omega_2}^{\omega_1} - \mu_0 T_0,$$

$$Q_0 = \frac{2}{\lambda_0}\left[\frac{\omega}{1-\omega^2} - \operatorname{arc\,tanh}\omega\right]_{\omega_2}^{\omega_1}.$$

Knowing ω_1, we determine the coefficient $C_2 = 2\omega_1/(1-\omega_1^2)$ in (16).

SUMMARY

1. For the frequency control of asynchronous motors, there exists an optimal control law of frequency as a function of time which provides maximum yield of the electric drive for given limitations on heating.

2. The optimal control law depends on the conditions imposed on the electric drive, and on the law of variation of the impedance torque. For electric drives of the first group, the optimal control law will be given by (17) and, for those in the second group, by (20). The voltage control law is the same for both groups, and amounts to maintaining the constancy of the motor's magnetic flux.

LITERATURE CITED

1. M. Lavrent'ev and L. Lyusternik, Fundamentals of Variational Calculus. 1 [in Russian] (ONTI, 1935).
2. I. A. Syromyatnikov, Operating Modes of Asynchronous Electric Motors [in Russian] (Gosénergoizdat, 1955).
3. K. I. Kozhevnikov, "Motor current diagrams for auxiliary mechanisms of rolling mills," Élektrichestvo No. 6 (1956).
4. E. A. Rozenman, "On optimal transient responses in systems with power limitations," Avtomatika i Telemekhanika 18, 6 (1957).
5. E. A. Rozenman, "On the limiting speed of response of servosystems with limitations on power, torque, and speed of the executive element," Avtomatika i Telemekhanika 19, 7 (1958).
6. A. A. Bulgakov, Frequency Control of Asynchronous Electric Motors [in Russian] (Izd. AN SSSR, 1955).

ON A DRIVE SCHEME WITH A GIVEN EQUATION OF MOTION*

I. A. Boguslavskii

(Moscow)

Translated from Avtomatika i Telemekhanika, Vol. 21, No. 3, pp. 340-343, March, 1960
Original article submitted May 15, 1959

A method is presented for the construction of a drive scheme with a given equation of motion wherein operational amplifiers are not employed.

In designing an automatic control system controlled by disturbances (cf. [1]) and also in various modelling schemes, it is frequently necessary to have a drive with a given equation of motion. This means that the drive's output coordinate x(t) (angular velocity, or angular displacement of the drive's output axis) must be related to the input coordinate f(t) (for example, with the arbitrarily varying angle of rotation of a potentiometer slider) by a given differential equation of the form

$$\sum_{k=0}^{n} a_k \frac{d^k x(t)}{dt^k} = \sum_{k=0}^{m} b_k \frac{d^k f(t)}{dt^k}. \qquad (1)$$

The problem just formulated is easily solved under the following conditions:

1) if the drive is shunted by a total feedback path for angle or for angular velocity such that the servosystem thus obtained follows, with high static and dynamic accuracy, the output coordinate x(t) by some input voltage u(t) and, consequently,

$$x(t) = ku(t), \qquad (2)$$

where k is a scale factor;

2) if, using operational amplifiers, one constructs an electronic scheme in which the output voltage u(t)** is related to the input f(t) by the equation obtained by replacing x(t) by ku(t) in (1).

However, in certain conditions of industrial usage, an electronic scheme may turn out to be inapplicable due to its complex voltage supply, zero drift of the operational amplifiers, etc. It is therefore advantageous to consider the possibility of replacing an electronic operational circuit by one composed of passive R and C elements (resistors and capacitors) which is free from the disadvantages mentioned above. However, a circuit of passive elements can be used directly only in solving certain special types of differential equations. For example, even for an equation which describes a simple oscillatory link, an RC circuit, as is well known, does not permit an accurate solution. In addition, the direct use of a circuit of passive elements (even in those cases where this is theoretically possible) is inconvenient in that a change in the coefficients of (1) requires, as a rule, a change in the parameters of all the passive elements. We shall show that a circuit with passive elements can be freed of the disadvantages cited if a voltage proportional to x(t) is applied to certain of its links. In this case, the drive, together with the basic direct negative feedback, is shunted by several indirect feedback paths (Fig. 1), and thus participates directly in the solution of (1). The servo amplifier which directly controls drive operation does not fall into the category of operational amplifiers due, for example, to the completely different requirements on gain stability.

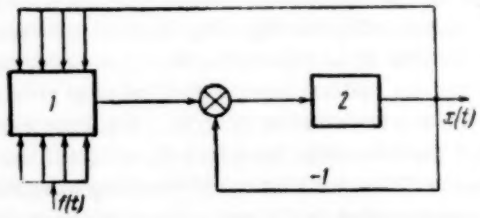

Fig. 1. 1 is the circuit of passive elements, 2) is the drive.

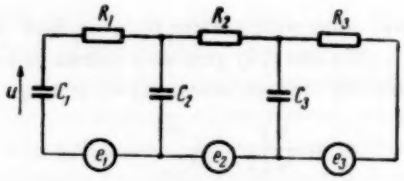

Fig. 2.

For simplicity, we present the proposed principle for drive design in the case when (1) has the form

$$(p^3 + a_2p^2 + a_1p + a_0)x(t) = (b_2p^2 + b_1p + b_0)f(t), \qquad (3)$$

where the a_i and b_i are given constant coefficients and $p = d/dt$.

*The material in this paper is contained in the author's paper at the Second All-Union Conference on Automatic Control Theory.

**Note that "u(t)" is used for both input and output voltage [translator's note].

In the general case, the circuit design is carried out analogously.

We consider the electric circuit (Fig. 2) in which the R_i and C_i are constant resistors and capacitors, chosen from technical considerations, and the e_i are certain voltage sources with zero internal impedance. In analyzing the circuit, for example, by the method of loop currents, we find that u, the voltage taken off capacitor C_1, satisfies the equation

$$(p^3 + A_2p^2 + A_1p + A_0)\,u = (B_2p^2 + = B_1p + B_0)\,e_1 + (D_1p + D_0)\,e_2 + C_0e_3, \quad (4)$$

where the A_i, B_i, D_i, and C_0 are constants, easily expressed in terms of the circuit parameters.

We require the holding of (2) and of the conditions

$$e_1 = \frac{1}{k}[k_{x1}x(t) + k_{f1}f(t)], \quad (5)$$

$$e_2 = \frac{1}{k}[k_{x2}x(t) + k_{f2}f(t)], \quad (6)$$

$$e_3 = \frac{1}{k}[k_{x3}x(t) + k_{f3}f(t)], \quad (7)$$

where the k_{xi} and k_{fi} are certain positive or negative constants, defined successively by the relationships

$$A_2 - B_2k_{x1} = a_2, \quad (8)$$

$$A_1 - B_1k_{x1} - D_1k_{x2} = a_1, \quad (9)$$

$$A_0 - B_0k_{x1} - D_0k_{x2} - C_0k_{x3} = a_0, \quad (10)$$

$$B_2k_{f1} = b_2, \quad (11)$$

$$B_1k_{f_1} + D_1k_{f_2} = b_1, \quad (12)$$

$$B_0k_{f_1} + D_0k_{f_2} + C_0k_{f_3} = b_0. \quad (13)$$

By a direct substitution of e_1, e_2, and e_3 in (4), we easily convince ourselves that, if (5)-(13) hold, x(t) and f(t) satisfy the original (3) and, consequently, the construction just described solves the problem posed. As was previously stated, (2) holds as the result of constructing a high-quality system for following x(t) by the voltage u(t). If x(t) is the angular velocity of the output shaft's rotation then, to realize (5), (6), and (7), with the shaft, in addition to the tachometer generator of the direct feedback path, there must be connected three dc tachometer generators whose output voltages are divided by special potentiometers in accordance with the coefficients k_{xi} and then introduced into the proper places in the circuit (Fig. 3). In addition, to the axis rotating to the angle f(t) there must be attached the sliders of three potentiometers with insulated voltage supplies and output voltage dividers operating in correspondence with coefficients k_{fi}. The practical values of R_1, R_2, and R_3 in Fig. 3 are not less than the order of the large divider impedances shunted by the internal impedances of the tachometer generators. Therefore, A_i, B_i, and C_i can be determined without the internal impedances of the voltage supplies being taken into account.

If x(t) is the angular rotation of the output shaft, then to it, in addition to the potentiometer of the direct feedback path, there are connected the sliders of three potentiometers with insulated voltage supplies and with the corresponding dividers. We emphasize that, for any change in the coefficients of (3), the parameters of the passive circuit (the quantities R_i and C_i) are not changed. When there are new values of the k_{xi} and the k_{fi}, only the positions of the divider sliders are subject to change. In an analogous manner, by the use of a passive circuit composed of n series-connected RC networks, n + 1 mutually insulated voltage supplies proportional to x (t), n insulated voltage sources proportional to f(t), and the corresponding number of dividers, one can construct a drive with equation of motion (1) for n > m. By having several circuits of passive elements and several drives with the corresponding number of insulated voltage sources proportional to their output coordinates, one can, by applying portions of these voltages to various points of the circuit, construct a system of drives with given

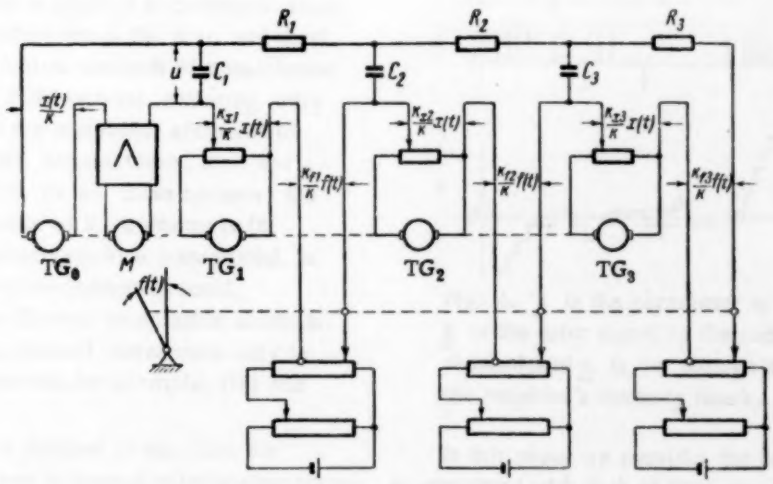

Fig. 3.

interrelationships of the equations of motion. The method described also applies, in an uncomplicated way, to the case when coefficients a_i and b_i of (1) are given functions of time, differentiable a definite number of times. For example, in (3) let $a_0 = a_0(t)$, $a_1 = a_1(t)$, and $a_2 = a_2(t)$.

Then, coefficients k_{xi} in (5)-(7) should be considered as unknown functions of time. As a simple verification, we show that x(t) will satisfy (1) for variable a_i if the functions $k_{xi}(t)$ are successively determined from the following relationships:

$$A_2 - B_2 k_{x1} = a_2(t),$$

$$A_1 - B_1 k_{x1} - 2B_2 \frac{dk_{x1}}{dt} - D_1 k_{x2} = a_1(t),$$

$$A_0 - B_0 k_{x1} - B_1 \frac{dk_{x1}}{dt} - B_2 \frac{d^2 k_{x1}}{dt^2} - D_0 k_{x2} - D_0 \frac{dk_{x2}}{dt} - C_0 k_{x3} = a_0(t).$$

If we, by using the proper elements, move the sliders of the dividers in accordance with the laws $k_{x1}(t)$, $k_{x2}(t)$, and $k_{x3}(t)$, we can implement the realization of a drive with equation of motion (3) for variable $a_0(t)$, $a_1(t)$ and $a_2(t)$.

The static accuracy of the solution of (1) by the drive is determined by the stability of the coefficient $\underline{k}$ in (2), the stability of the values of the R_i and C_i, and by the accuracy of positioning the dividers' sliders for the formation of coefficients k_{x1} and k_{f1}. The dynamic accuracy of the solution of (1) by the drive will be the higher, the wider is the frequency passband of the drive's servosystem, providing for the holding of (2), as compared with the bandwidth of the fundamental frequencies of the solution of Eq. (1).

LITERATURE CITED

1. V. S. Kulebakin, "On the basic problems and methods of increasing the quality of automatic control systems," in Proceedings of the Second All-Union Conference on Automatic Control Theory. 2 [in Russian] (Izd. AN SSSR, 1955).

ON THE NOISE IMMUNITY OF THE DISCRETE-INCREMENTAL METHOD OF INFORMATION TRANSMISSION

V. M. Baikovskii

(Moscow)

Translated from Avtomatika i Telemekhanika, Vol. 21, No. 3, pp. 344-358, March, 1960
Original article submitted August 28, 1959

The potential noise immunity (noise stability) of discrete-incremental modulation (DIM) with fluctuation noise is determined. Comparisons are made of the noise immunity of pulse-code modulation (PCM), deltamodulation(DM) and DIM. It is shown that, in a number of cases, the noise immunity of DIM is higher than of PCM and DM.

INTRODUCTION

In remote action telemetry systems, the communications channel is the most essential element, and determines the entire construction and, often, the accuracy of the system. This is true of telemetering apparatus in energy systems and gas and oil pipelines where it is necessary to transmit a series of parameters over distances of up to hundreds of kilometers. This is also characteristic of radiotelemetric systems, widely used in aviation for controlling various moving objects (including those used in space explorations), etc.

In designing such telemetry systems, the form of signal and the type of modulation are selected, not only from considerations of the best construction of the transforming devices, but also as a function of the channel's noise level and other characteristics.

Recently, many designers have been turning to discrete methods of transmitting data which, distinguished by their high equipment accuracy, permit high noise immunity to be attained. These methods acquire particular value from the broad development of digital technology.

Certain forms of discrete modulation had already been frequently considered as applied to communications problems. Pulse-code modulation is the first, and most highly developed, of the digital methods of transmission. There are many different PCM systems, differing only by the implementation of the individual elements of the apparatus: transformers, accumulators, etc. But there is one thing common to all these systems: the complete instantaneous value of a parameter (with account being taken of quantization) is transmitted, in coded form, along the communication channel.

There later appeared discrete modulation methods in which the signal in the channel corresponds only to the increment of the parameter, for example, DM and delta-PCM.

Recently, still another method of this class for transmitting information was suggested—digital-incremental modulation ("incremental coding") [1, 2, 3]. Incremental coding arose in connection with the desire to increase the efficiency of transmitting data along a channel by exploiting the statistical properties of the information to be transmitted. If the assumption in PCM is that each successive parameter value is not related to the previous one, in DIM the design is based on the assumption that there is a comparatively peaked (at least, nonflat) correlation function for the information.

The DIM operating principle is clearly elucidated in Fig. 1. The basic difference between this modulation method and those of PCM and DM is that here a signal is sent through the channel only at the moments when the measured quantity passes through a quantization level. If it stays within the limits of one quantization step, then no signal appears. Thus, transmission occurs irregularly: the more slowly the information changes, the more rarely are pulses sent through the channel.

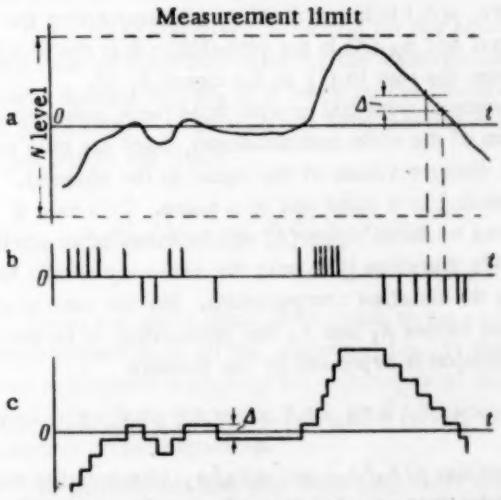

Fig. 1. a is the parameter to be transmitted b is the error signal in the communications channel, and c is the voltage at the output of the receiver's memory block.

In this paper we consider the noise immunity of DIM as compared with that of PCM and DM. As criteria for judging noise immunity of discrete telemetry systems, we adopt here the mathematical expectation of the error

(the mean error) and the dispersion of the error (the squared mean-square error). We have obviously made the assumption that the error's probability distribution function is sufficiently completely characterized by its first two moments.

Potential DIM Noise Immunity for One Particular Case

To estimate the effect of fluctuation noise on a discrete system for information transmission, it is convenient to use V. A. Kotel'nikov's theory of potential noise immunity. It consists essentially of the following:

Let the set of signals $\{A(t)\}$ be used for transmission. When signal $A_i(t)$ is sent, then, due to the action of noise, the following total quantity is applied to the receiver:

$$X(t) = A_i(t) + W(t), \qquad (1)$$

where W(t) is a normal fluctuation oscillation. Depending on the value of X(t), the receiver identifies it with (or assimilates it to) one of the possible signals $A_j(t)$ of $\{A(t)\}$ with some probability of error. The potential noise immunity defines the probability of signal distortion as the result of the action of noise, for reception by an ideal receiver.

An ideal receiver is characterized as one for which this probability of incorrect reproduction will be the least for a given form of signal (given energy) and a definite specific energy (per unit bandwidth) of the fluctuation noise. In other words, the ideal receiver reproduces the information, corresponding to that signal, which maximizes the expression

$$p(A_i)\, p_{A_i}(X). \qquad (2)$$

Here, $p(A_i)$ is the probability of transmitting the ith signal and $p_{A_i}(X)$ is the probability that the receiver reproduces the sum in (1) as the signal $A_i(t)$.

In systems with DM or with PCM (with pulse-by-pulse reception of the code combinations), there are only two possible discrete values of the signal in the channel, corresponding to a pulse and to a pause. This case is considered by Kotel'nikov [4] and in many other works [5, 6]. We therefore give only the necessary results here, omitting the detailed computations. For the case of only two signal values A_1 and A_2, the probability of an error in transmission is expressed by the formula

$$p_{\text{dis}} = p(A_1)\, p(A_2/A_1) + p(A_2)\, p(A_1/A_2). \qquad (3)$$

The quantities $p(A_1/A_2)$ and $p(A_2/A_1)$ characterize the probabilities that one signal transfers to the other as the result of the action of fluctuation noise. In correspondence with [4], they equal

$$p(A_2/A_1) = V(\alpha_{21}), \quad p(A_1/A_2) = V(\alpha_{12}), \qquad (4)$$

where

$$V(x) = \frac{1}{\sqrt{2\pi}} \int_x^\infty e^{-\frac{z^2}{2}}\, dz,$$

and

$$\alpha_{21} = \alpha + \frac{1}{2\alpha} \ln \frac{p(A_1)}{p(A_2)}, \quad \alpha_{12} = \alpha + \frac{1}{2\alpha} \ln \frac{p(A_2)}{p(A_1)}.$$

Thus, the potential noise immunity is defined by the two quantities: $p(A_1)/p(A_2)$ —the ratio of the a priori probabilities of the two signals—and the quantity α, which characterizes the ratio of the mean energy difference of these signals to the specific energy of the noise, i.e.,

$$\alpha = \sqrt{\frac{1}{2\sigma^2} \int_{-\frac{T}{2}}^{+\frac{T}{2}} [A_1(t) - A_2(t)]^2\, dt}. \qquad (5)$$

Here, T is the signal duration and σ is the specific energy of the noise (intensity), which is defined so that

$$\overline{W^2(t)} = \int_0^\infty \sigma^2(\omega)\, d\omega. \qquad (6)$$

Since the quantity to be transmitted in telemetry is always bounded by definite limits, then, on the average, over a sufficiently long interval of its variation, one can consider the appearances of pulses and pauses for DM and PCM to be equiprobable.

Consequently,

$$p(A_1) = p(A_2) = \frac{1}{2}, \qquad (7)$$

$$\alpha_{12} = \alpha_{21} = \alpha.$$

As a result, we obtain

$$p(A_1/A_2) = p(A_2/A_1) = V(\alpha). \qquad (8)$$

Discrete-incremental modulation differs from the foregoing in that the signal can assume three values. In the channel appear the values +1 or −1 when the measured quantity goes through a quantization level and the value 0, if the quantity does not go beyond the bounds of one quantization step. Thus, there are the signals $A_1(t) = +1$, $A_2(t) = 0$ and $A_3(t) = -1$, with probabilities $p(A_1)$, $p(A_2)$ and $p(A_3)$. With this, and for the same reasons as for (7), we can assume that $p(A_1) = p(A_3)$ and, moreover, that $p(A_2) > p(A_1) = p(A_3)$, since only in this case is DIM meaningful.

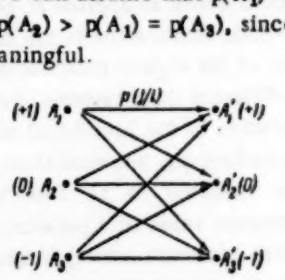

Fig. 2. Scheme of discrete channel (DIM).

The scheme for a channel with discrete-incremental modulation is shown in Fig. 2. According to this scheme, the probability of error for DIM may be found from the formula

$$p_{\text{er}} = \sum_{i=1}^{3} \sum_{j=1}^{3} p(A_i)\, p(A_j/A_i) \qquad (i \neq j). \qquad (9)$$

The values of the probabilities $p(A_j/A_i)$ depend on which pulse signs are used for transmission.

In its general form, the problem is difficult to solve even with three signals. It is impossible to find an expression for the probability of distortion in a simple and graphic form, convenient for computations and for comparisons with the analogous expressions for other systems. We therefore consider one simple special case of signal transmission by DIM, and we then show that the results obtained can be used for an approximate estimate of noise immunity in a number of other cases.

We assume that to signals $A_1(t)$ and $A_3(t)$ there correspond identical video pulses of different polarity. Let their transmission be implemented by the so-called synchronous method, i.e., the pulses can be applied to the channel only at regular time intervals, or multiples thereof. Therefore, the intervals between pulses are multiples of some quantity T_{min} chosen, just as in DM, from the condition that there be reproduced the portion of the information with the greatest steepness (the overshoot). In this case, the analysis of noise immunity (cf. the Appendix) allows us to construct, for the ternary channel characterized by the scheme of Fig. 2), the matrix of transition probabilities:

	A_1'	A_2'	A_3'
A_1	$1-V(\alpha')$	$V(\alpha')[1-V(\alpha''')]$	$V(\alpha')V(\alpha''')$
A_2	$V(\alpha'')$	$1-2V(\alpha'')$	$V(\alpha'')$
A_3	$V(\alpha')V(\alpha''')$	$V(\alpha')[1-V(\alpha''')]$	$1-V(\alpha')$

(10)

To determine the mathematical expectation and the dispersion of the error, it is necessary to find the "value" or the weight of each individual error ξ_{ij}. The "value" of an error for discrete-incremental modulation is easily determined if we turn back to Fig. 1.

When, under the action of noise, signal A_2 goes over to A_1, or A_3 goes over to A_2, the step function voltage in the receiver will be changed by quantity Δ, i.e., for $(A_2 \to A_1)$ and $(A_3 \to A_2)$, $\xi = +1$ and, analogously, for $(A_2 \to A_3)$ and $(A_1 \to A_2)$, $\xi = -1$. If $(A_3 \to A_1)$ or $(A_1 \to A_3)$, then $\xi = \pm 2$.

Since it was accepted that signals A_1 and A_3 are equiprobable, the system of signals is symmetric, and the average of the error equals zero:

$$MU_{er} = \sum_{i=1}^{3}\sum_{j=1}^{3} p(A_i)\, p(A_j/A_i)\, \xi_{ij} = 0 \qquad (i \neq j). \tag{11}$$

According to probability theory,

$$D\xi = M(\xi - M\xi)^2.$$

Thus, taking into account that $M\xi = 0$, we find that

$$DU_{er} = \Delta^2 D\xi = \Delta^2 M\xi^2. \tag{12}$$

By using (9), we find that

$$DU_{er} = \Delta^2\{2p(A_2)V(\alpha'') + 2p(A_1)V(\alpha')[1 - V(\alpha''')] + 8p(A_1)V(\alpha')V(\alpha'')\}. \tag{13}$$

We now introduce the concept of the probability p_n of a transition of the quantity to be transmitted through a quantization level. Obviously, this quantity depends on the character of the variation of the parameter to be transmitted. The steeper the correlation function, the smaller is the value of p_n. From what was said above, it follows that $p_n = 2p(A_1)$. By keeping in mind that $p(A_2) = 1-2p(A_1)$, and by denoting $p(A_2)/p(A_1) = K$, we obtain the final expression for the dispersion of the error for DIM:

$$DU_{er} = \Delta^2 p_n [KV(\alpha'') + V(\alpha') + 3V(\alpha')V(\alpha''')]. \tag{14}$$

It follows from (14) that the noise immunity of this type of modulation is connected with the statistical properties of the ensemble of possible communications. An analysis of this dependence was given in [2].

On the Approximate Estimate of Noise Immunity of DIM in the General Case

It is obvious that, in addition to the one considered other methods of DIM transmission can be used. However, of all the possible methods, the only interesting ones from the practical point of view are those which are characterized by small values of the probabilities $p(A_1/A_3)$ and $p(A_3/A_1)$.

The determination of an exact analytical expression for noise immunity for each case in even this limited class poses mathematical difficulties.

In [4] there was given a method for the approximate estimation of noise immunity for the transmission of several discrete signals. It is based on the theorem that the probability P of at least one of m possible outcomes B_i lies within the limits

$$p(B_i)_{max} \leqslant P \leqslant \sum_{k=1}^{m} p(B_i). \tag{15}$$

Here, the lower limit corresponds to the complete interrelationship of all the outcomes, i.e., to the case when one outcome implies the occurrence of all the others. To obtain the upper limit, it is necessary that the outcomes be incompatible.

As applied to DIM, this inequality takes the form

$$\sum_{i=1}^{3} p(A_i)\, p^*(A_j/A_i)_{max} \leqslant p_{dis} \leqslant \sum_{i=1}^{3}\sum_{j=1}^{3} p(A_i)\, p^*(A_j/A_i), \tag{16}$$

where each $p^*(A_j/A_i)$ is determined, in accordance with (4), for each pair of signals without taking account of the others.

We considered several methods of transmission: for example, sending, for the signals $A_1(t)$ and $A_3(t)$, radio pulses with orthogonal frequencies, unipolar orthogonal video pulse, etc. Analysis showed that, for identical p pulse energy, the bounds on the error given by (16) for many methods of DIM transmission virtually coincided with those obtained in the case considered above. With this, the upper and lower bounds are so close that the region of error has the form of a very narrow ribbon (Fig. 3). By keeping this in mind, we can assume that the value of the error found for synchronous transmission of different polarity pulses characterizes, with adequate accuracy, the noise immunity of a number of other forms of DIM transmission. Therefore, in making our subsequent comparisons of noise immunity for the three forms of modulation, we shall use (14) to define the error with DIM (the dashed line on Fig. 3).

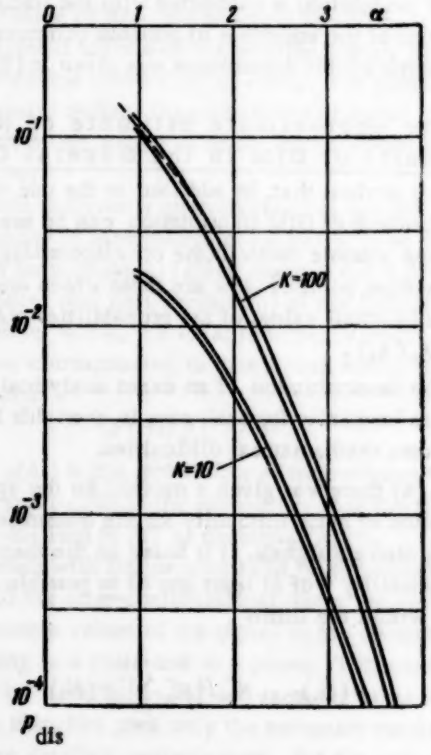

Fig. 3.

It was previously noted that the noise immunity of DIM is determined on the basis of the probabilities of suppression or of formation of false signals $A_1(t)$ and $A_3(t)$ (since $A_2(t) = 0$).

If we therefore replace the "ternary" ideal receiver by two, one of which receives $A_1(t)$ and $A_2(t)$ while the other receives $A_3(t)$ and $A_2(t)$, then the noise immunity will differ very little from the potential value. Computations show that the error arising with this is negligibly small. By taking this into account, we have the possibility, in making approximate estimates of noise immunity for DIM in many cases, to consider two identical binary channels separately. It is obvious that such an approach simplifies the selection of the most efficient methods of transmitting and receiving, and eases system design.

Comparison of Systems' Noise Immunity

For the comparisons, it is necessary to obtain expressions for the dispersion and mathematical expectation of the error for DM and PCM. With deltamodulation, the transition of one signal to the other in the channel (suppression of a pulse or the emergence of a false one) gives rise to a variation in the step function voltage in the receiver by the amount 2Δ. The error voltage with this can be expressed in the form $U_{er} = 2\Delta\xi$, where ξ is a random variable which assumes the values + 1 and − 1. Since these values are equiprobable, the mathematical expectation of the error equals zero:

$$MU_{er} = 2\Delta M\xi = 0. \tag{17}$$

The dispersion of the error may be determined as

$$DU_{er} = 4\Delta^2 D\xi; \tag{18}$$

since $M\xi = 0$, then $D\xi = M\xi^2$.

For deltamodulation,

$$M\xi^2 = 1\,\frac{1}{2}\,p(A_1/A_2) + 1\,\frac{1}{2}\,p(A_2/A_1). \tag{19}$$

By taking (8) into account, we obtain

$$D\xi = V(\alpha). \tag{20}$$

Thus, for DM

$$DU_{er} = 4\Delta^2 V(\alpha). \tag{21}$$

In the case of code modulation, the value of the error depends on which pulse in the code group will be distorted. The value of each individual pulse with ordinal number k in a code group of n pulses is found from the formula

$$N_k = 2^{k-1}\Delta. \tag{22}$$

Therefore, the error voltage is determined as

$$U_{er} = \sum_{k=1}^{n} 2^{k-1}\Delta\xi. \tag{23}$$

Here the random variable, when noise acts, takes the values + 1 and − 1 and, otherwise, the value zero.

Exactly as in the previous case, we find that $MU_{er} = 0$ and

$$DU_{er} = D\sum_{k=1}^{n} 2^{k-1}\Delta\xi = \sum_{k=1}^{n} (2^{k-1})^2\Delta^2 D\xi. \tag{24}$$

After some transformation, we find the formula for the dispersion of the error in the case of PCM:

$$DU_{er} = \frac{2^{2k}-1}{3}\,\Delta^2 V(\alpha). \tag{25}$$

A) The case of a given average transmitter power. We now consider the conditions under which the systems' noise immunity should be compared.

1. We assume that there is no filtering of the signal in the receiver, but simply its recording by a sufficiently

fast-acting reproducing device. We therefore carry out the comparison by using (14), (21), and (25).

2. We assume that all the systems are designed for transmitting information with identical upper-frequency bounds F_u.

3. We assume that the quality of transmission is identical for identical numbers of levels of partitioning, i.e., that the discreteness errors Δ are equal.

4. We assume that the mean transmitter power P_{av} and noise level σ are the same for all cases.

5. We assume that the bandwidth and, consequently the duration of the pulses in the channel, is identical for all the systems.

For simplicity, we shall assume that the pulses are rectangular. With this, the signal energy entering into Formula (6) will equal $P_p\tau$ (here, P_p is the transmitter's pulse power).

Then, for the quantity α we obtain the expression

$$\alpha = \frac{1}{\sigma}\sqrt{\frac{P_p}{2}\tau} = \frac{1}{\sigma}\sqrt{\frac{P_{av}}{2}T_i} \qquad (26)$$

for code and deltamodulation, and the expression

$$\alpha = \frac{1}{\sigma}\sqrt{\frac{P_p}{2}\tau} = \frac{1}{\sigma}\sqrt{\frac{P_{av}}{2}T_{av}} \qquad (27)$$

for discrete-incremental modulation.

Here, the quantity T_{av} is the average duration of the time interval between neighboring pulses. It depends on the statistics of the information to be transmitted and, obviously, is related to p_n. Finding this relationship analytically in the general case entails mathematical difficulties, so that the magnitude of T_{av} is determined from the corresponding distribution, taken off experimentally from recordings of information typical of the given telemetry system.

The implementation of this investigation for several parameters subject to telemetering in industry, in energetics in particular [2], showed that the distribution of the intervals between moments when the parameter changed levels is close to a Poisson distribution. Indeed, if it be assumed that the transition probability p_n on the time segment $\Delta t = T_{min}$ depends on the length of this segment, i.e., $p_n = p_0\Delta t$, and is unrelated to the behavior of the process on the remaining segments, then this distribution will be described by the expression

$$H(t) = p_0 e^{-p_0 t}\Delta t, \qquad (28)$$

and the magnitude of T_{av} can be found from the formula

$$T_{av} = \int_0^\infty t p_0 e^{-p_0 t} dt = \frac{1}{p_0}. \qquad (29)$$

Since we have agreed that $p_n = p_0 T_{min}$, then

$$T_{av} = \frac{T_{min}}{p_n}. \qquad (30)$$

In order to express the repetition period in terms of the quantity F_u for code modulation, we use the well-known relationship

$$f_i = 2F_u. \qquad (31)$$

The pulse repetition frequency, in the case of delta-modulation, is chosen, as was mentioned earlier, from considerations of reproducing the maximum slope in the information to be transmitted $\left|\,dS(t)/dt\,\right|_{max}$. Just as in (7) and (8), we use the simplified expression

$$|\Delta| \approx \left|\frac{dS(t)}{dt}\right|_{max} T_i = \Omega_u T_i. \qquad (32)$$

Thus, the repetition period for DM, or T_{min} for DIM, will equal

$$T_{iDM} = T_{min} = \frac{\Delta}{2\pi F_u}. \qquad (33)$$

On the basis of what has been said earlier, we can write the expressions defining the quantity α for all three forms of modulation:

$$\alpha_{DM} = \frac{1}{\sigma}\sqrt{\frac{P_{av}}{2F_u}}\sqrt{\frac{\Delta}{\pi}}, \qquad (34)$$

$$\alpha_{PCM} = \frac{1}{\sigma}\sqrt{\frac{P_{av}}{2F_u}}\sqrt{\frac{1}{2\lg_2\frac{1+\Delta}{\Delta}}}, \qquad (35)$$

where $\lg_2[(1+\Delta)/\Delta] = n$ is an integer;

$$\alpha_{DIM} = \frac{1}{\sigma}\sqrt{\frac{P_{av}}{2F_u}}\sqrt{\frac{\Delta}{2\pi}(k+2)}. \qquad (36)$$

Figure 4 shows the curves which characterize the potential noise immunity of the three forms of modulation considered, for two different values of Δ. It is clear from the figure that, for a given mean transmitter power,

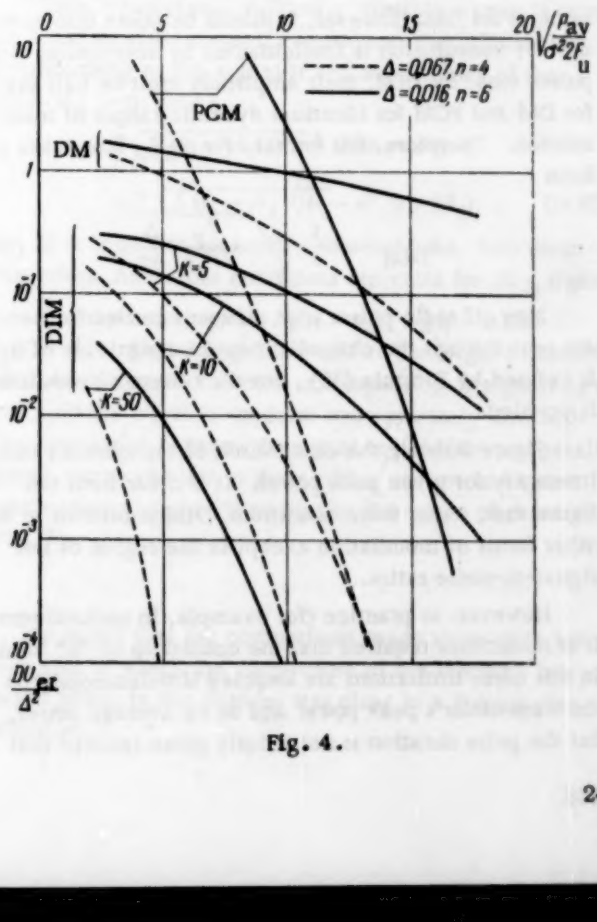

Fig. 4.

the noise immunity of a system with discrete-incremental modulation is always better than in a system with delta-modulation, and only sometimes worse than the noise immunity of a system with PCM. With this, pulse-code modulation turns out to have higher noise immunity than DIM for large numbers of levels to be transmitted and high transmitter power. For small signal-to-noise ratios, conversely, the dispersion of the error is less when DIM is used.

B) The case of given peak pulse power . We now compare the modulation forms we have been considering when the transmitter's peak power is given, retaining all the other conditions assumed under paragraph A.

In this case, (26) and (27) are changed. If we denote by q the mark-space ratio of the pulses, then these expressions will have the form:

$$\alpha_{PCM} = \frac{1}{\sigma}\sqrt{\frac{P_p}{2F_u q^2 \lg\frac{1+\Delta}{\Delta}}}, \qquad (37)$$

$$\alpha_{DM} = \frac{1}{\sigma}\sqrt{\frac{P_p \Delta}{2F_u q\pi}}. \qquad (38)$$

As for the value of α_{DIM}, we must consider two cases:

a) when the duration of the pulses and the interval T_{min} are rigidly related to the quantity q ;

b) when the following conditions are imposed on the pulse duration:

$$\tau \leqslant \frac{T_{av}}{q} \text{ and } \tau \leqslant T_{min}$$

In the first case, the magnitude of τ will be the same as for DM. However, it should be taken into account that, if transmission is implemented by heteropolar video pulses then, for DIM, their amplitude must be half that for DM and PCM for identical dynamic ranges of transmission. Therefore, the formula for α_{DIM} now takes the form

$$\alpha_{DIM} = \frac{1}{\sigma}\sqrt{\frac{P_p}{2F_u q}\frac{\Delta}{4\pi}}. \qquad (39)$$

Now, if radio pulses with different carrier frequencies are sent through the channel, then the magnitude of α_{DIM} is defined by Formula (38) , but the system's bandwidth is doubled.

Figure 5 shows the comparison of the system's noise immunity for given peak power. It is clear from the figure that, under these conditions, DIM is inferior to the other forms of modulation except in the region of low signal-to-noise ratios.

However, in practice (for example, in radiotelemetry) it is sometimes required that the conditions of "b" hold. In this case, limitations are imposed simultaneously on the transmitter's peak power and on its average power, but the pulse duration is not strictly given (except that

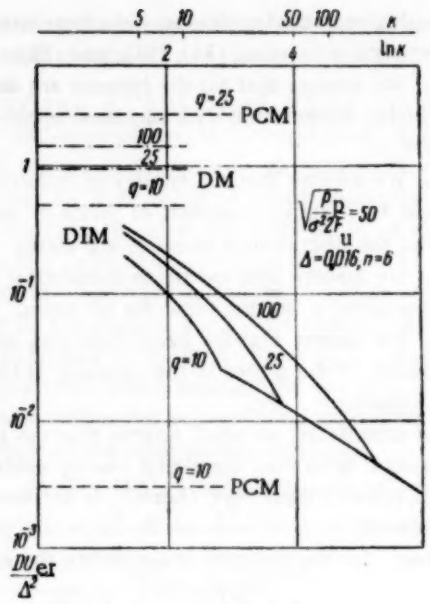

Fig. 5.

$\tau \leq T_{min}$). With this, the magnitude of α_{DIM} can be found from the formula

$$\alpha_{DIM} = \frac{1}{\sigma}\sqrt{\frac{P_p}{2F_u}\frac{\Delta}{4\pi}\frac{(K+2)}{2q}}. \qquad (40)$$

Thus, by increasing the duration of the pulses, one can improve the noise immunity of transmission and, simultaneously, reduce the required channel bandwidth. Broadening of the pulses is possible up to the point when the quantity $(K + 2)/2q$ becomes equal to unity, after which the magnitude of α_{DIM} must remain constant. The improvement of the noise immunity of DIM as a function of K for various admissible mark-space ratios is shown in Fig. 6 .

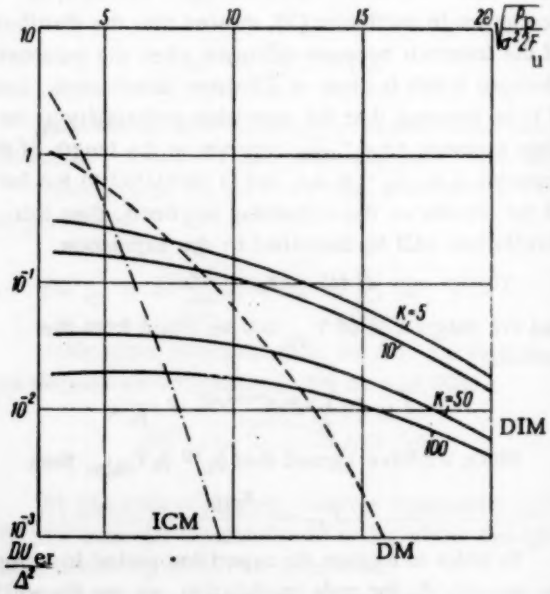

Fig. 6.

SUMMARY

1. The theory of potential noise immunity allows one to estimate the telemetering error with fluctuation noise for the discrete-incremental method of information transmission. An accurate and, at the same time, sufficiently simple expression for the probability of distortion with DIM could be found for only one special case—synchronous transmission of heteropolar pulses. However, this expression can be used for an approximate estimate of the error in a number of other cases.

2. If the signal-to-noise ratio is not very small and the probabilities $p(A_1/A_3)$ and $p(A_3/A_1)$ are much less than the remaining transition probabilities, then a communications channel with DIM may be considered as two individual binary channels, and transmission and reception methods can be chosen in correspondence with this.

3. Noise immunity of DIM is immediately related to the statistics of the messages to be transmitted: the greater the slope of the correlation function, the smaller the probability of error.

4. The comparison of the noise immunity of the discrete systems* showed that, for given average power, DIM is always better than DM, and is inferior to PCM only for high signal-to-noise ratios and large numbers of quantization levels.

5. For given peak power and pulse duration, DIM has a practical noise immunity which is comparable to that of DM and significantly worse than for PCM.

For a given mark-space ratio, a gain can be achieved only at the cost of widening the pulses.

APPENDIX

Computation of the Transition Probability Matrix for DIM with Synchronous Transmission of Heteropolar Pulses

We determine the noise immunity for the given particular case of transmission with three discrete signals. For this we return to the basic propositions of the theory of potential noise immunity and to the definition of the ideal receiver which was given previously. We recall that, by Kotel'nikov's theorem, a signal which is limited to the time T and whose energy is lumped into some frequency band F may be completely characterized by a finite number 2FT of its values. These values are considered as the coordinates of the signal vector in a multidimensional space. The length of the vector is determined by the signal's average power, and equals

$$\sqrt{\sum_{r=1}^{2FT} a_r^2} = \sqrt{\overline{A^2(t)}}. \qquad (A.1)$$

Here, the a_r are the signal values at 2FT points uniformly distributed in time. Analogously, the fluctuation noise is represented by a random vector of length

$$\sqrt{\frac{\sigma^2}{2T}\sum_{l=1}^{2FT}\theta_l}, \qquad (A.2)$$

where θ_l is a normal random variable for which

$$p(z < \theta < z + dz) = \frac{dz}{\sqrt{2\pi}} e^{-\frac{z^2}{2}} \qquad (A.3)$$

The terminus of the total vector, corresponding to the oscillation X(t) can, with some probability, fall at various points of space. Therefore, the problem of the receiver is the correct identification of the received signal X(t) with that one of the signals which was transmitted during time T. Thus, the receiver's design principle is characterized by some division or other of the entire signal space into regions of correct reception of each of the signals $A_i(t)$.

In particular, for an ideal receiver, the configuration of the regions is so determined that it must reproduce the signal with the maximum value of the probability described by (2). With transmission of $A_i(t)$, the probability that signal X(t) falls in region dv of the 2FT-dimensional space equals

$$p_{A_i}(X) = \frac{dv}{\left(\sqrt{\frac{\pi}{T}}\sigma\right)^{2FT}} \times$$

$$\times \exp\left(-\frac{T}{\sigma^2}\overline{[X(t) - A_i(t)]^2}\right). \qquad (A.4)$$

Therefore, the ideal signal, in receiving oscillation X(t), will reproduce that signal for which the quantity

$$\frac{T}{\sigma^2}\overline{[X(t) - A_j(t)]^2} - \ln p(A_j) \qquad (A.5)$$

will be minimal.

Thus, when signal $A_i(t)$ of n possible signals is sent, the ideal receiver correctly reproduces the information corresponding to this signal if n-1 inequalities of the following form hold:

$$T\overline{[X(t) - A_i(t)]^2} - \sigma^2 \ln p(A_i) \leqslant$$

$$\leqslant T\overline{[X(t) - A_j(t)]^2} - \sigma^2 \ln p(A_j). \qquad (A.6)$$

If at least one inequality does not hold, then distortion arises. Analogous conditions are valid for all n signals.

There are the signals $A_1(t) = +1$, $A_2(t) = 0$ and $A_3(t) = -1$. Signal $A_2(t)$ is found at the origin of coordinates, and the radius vectors corresponding to signals $A_1(t)$ and $A_3(t)$ are equal in modulus and oppositely directed. The boundaries between the signal regions are two parallel planes, perpendicular to these radius vectors and symmetrically located with respect to the origin of coordinates (Fig. 7).

* We recall that the comparisons made were valid for messages in which the distribution of the intervals between pulses in the channel was close to a Poisson distribution.

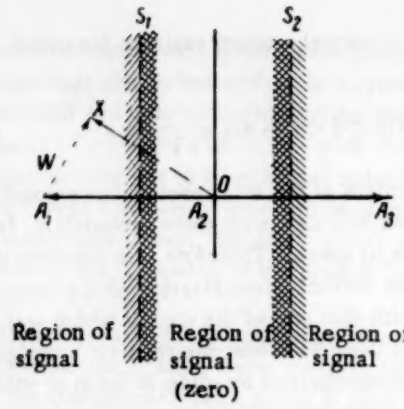

Fig. 7.

It is easily seen that, for distortion of signal $A_1(t)$, it suffices to violate just the one inequality

$$T\overline{[X(t)-A_1(t)]^2}-\sigma^2\ln p(A_1)<$$

$$<T\overline{[X(t)-A_3(t)]^2}-\sigma^2\ln p(A_3), \qquad (A.7)$$

since it is only possible to pass from the region of signal $A_3(t)$ to that of $A_1(t)$ by going through the region of signal $A_2(t)$.

We consider the inequality inverse to that of (A.7). By using (1), we may write

$$T\overline{[W(t)+A_1(t)-A_1(t)]^2}-\sigma^2\ln p(A_1)\geqslant$$

$$\geqslant T\overline{[W(t)+A_1(t)-A_2(t)]^2}-\sigma^2\ln p(A_2) \qquad (A.8)$$

or

$$T\overline{W^2(t)}\geqslant T\overline{W^2(t)}+2T\overline{W(t)[A_1(t)-A_2(t)]}+$$

$$+T\overline{[A_1(t)-A_2(t)]^2}-\sigma^2\ln\frac{p(A_2)}{p(A_1)}. \qquad (A.9)$$

By then taking into account that, in our case, $A_2(t)=0$, we use (2.60) of [1]:

$$\overline{W(t)A(t)}=\frac{\sigma}{\sqrt{2T}}\sqrt{\overline{A^2(t)}}\,\theta. \qquad (A.10)$$

Here, θ is the normal random variable of (A.3). After some transformation we obtain

$$0\geqslant\sigma\sqrt{2T}\sqrt{\overline{A^2(t)}}\,\theta_1+T\overline{A_1^2(t)}-\sigma^2\ln\frac{p(A_2)}{p(A_1)}. \qquad (A.11)$$

The probability that this inequality holds is $V(\alpha')$, so that

$$p_{\text{dis}}(A_1)=V(\alpha'). \qquad (A.12)$$

It is obvious here that

$$\alpha'=\frac{\sqrt{T\overline{A_1^2(t)}}}{\sigma\sqrt{2}}-\frac{\sigma}{\sqrt{2}\sqrt{T\overline{A_1^2(t)}}}\ln\frac{p(A_2)}{p(A_1)} \qquad (A.13)$$

By substituting $\alpha=\dfrac{\sqrt{T\overline{A_1^2(t)}}}{\sigma\sqrt{2}}$ and $\dfrac{p(A_2)}{p(A_1)}=K$,

we find

$$\alpha'=\alpha-\frac{1}{2\alpha}\ln K. \qquad (A.14)$$

Distortion of signal $A_2(t)$ corresponds to the holding of the inequalities

$$T\overline{[X(t)-A_2(t)]^2}-\sigma^2\ln p(A_2)\geqslant$$

$$\geqslant T\overline{[X(t)-A_1(t)]^2}-\sigma^2\ln p(A_1),$$

$$T\overline{[X(t)-A_2(t)]^2}-\sigma^2\ln p(A_2)\geqslant$$

$$\geqslant T\overline{[X(t)-A_3(t)]^2}-\sigma^2\ln p(A_3). \qquad (A.15)$$

It is easily shown that the probability of each inequality holding is the same for all, and equals

$$p(A_3/A_2)=p(A_1/A_2)=V(\alpha''), \qquad (A.16)$$

where

$$\alpha''=\alpha+\frac{1}{2\alpha}\ln K, \qquad (A.17)$$

and the probability

$$p_{\text{dis}}(A_2)=2V(\alpha''). \qquad (A.18)$$

Due to the symmetry of the system of three signals, we have

$$p_{\text{dis}}(A_3)=p_{\text{dis}}(A_1).$$

We can thus obtain the expression for the probability of error with discrete-incremental modulation in this particular case.

Since

$$p_{\text{er}}=\sum_{i=1}^{3}p(A_i)\,p_{\text{dis}}(A_i), \qquad (A.19)$$

then

$$p_{\text{er}}=2p(A_1)V(\alpha')+2p(A_2)V(\alpha''). \qquad (A.20)$$

Equation (A.20) characterizes the probability of distortion as a whole. For us to compute the errors, it is necessary to know the transition probabilities of each signal to the two others separately. For this, we consider in more detail the transmission of signals $A_1(t)$ and $A_3(t)$. Let signal $A_1(t)$ be transmitted. The probability that the ideal receiver reproduces precisely signal $A_1(t)$ at its output equals the probability of the simultaneous holding of the inequalities

$$p(A_1)\exp\left(-\frac{T}{\sigma^2}\overline{[X(t)-A_1(t)]^2}\right)\leqslant$$

$$\leqslant p(A_2)\exp\left(-\frac{T}{\sigma^2}\overline{[X(t)-A_2(t)]^2}\right),$$

$$p(A_2)\exp\left(-\frac{T}{\sigma^2}\overline{[X(t)-A_2(t)]^2}\right)\leqslant$$

$$\leqslant p(A_3)\exp\left(-\frac{T}{\sigma^2}\overline{[X(t)-A_3(t)]^2}\right). \qquad (A.21)$$

The probability that the first of these hold was already found earlier (A.12).

We consider the second inequality. We rewrite it in the form

$$T\overline{[X(t)-A_2(t)]^2}-\sigma^2\ln p(A_2)\leqslant$$

$$\leqslant T\overline{[X(t)-A_3(t)]^2}-\sigma^2\ln p(A_3). \qquad (A.22)$$

After multiplying out the parentheses and cancelling, we have

$$2T\overline{W(t)A_1(t)}+\overline{TA_1^2(t)}-\sigma^2\ln\frac{p(A_2)}{p(A_1)}\leqslant$$

$$\leqslant 2T\overline{W(t)[A_1(t)-A_3(t)]}+T\overline{[A_1(t)-A_3(t)]^2}. \qquad (A.23)$$

By taking into account that $|A_1(t)| = |A_3(t)|$ and $p(A_1) = p(A_3)$, we can write

$$2T\overline{W(t)A_1(t)}\leqslant 2T\overline{W(t)[A_1(t)-A_3(t)]}+$$

$$+3T\overline{A_1^2(t)}+\sigma^2\ln K. \qquad (A.24)$$

We now use Formula (A.10). Then,

$$\sqrt{2T}\sqrt{\overline{A_1^2(t)}}\,\theta_1\leqslant 2\sqrt{2T}\sqrt{\overline{A_1^2(t)}}\,\theta_{13}+$$

$$+3T\overline{A_1^2(t)}+\sigma^2\ln K. \qquad (A.25)$$

For the case considered, the quantities θ_1 and θ_{13} are equal, since they are the projections of one and the same vector on one and the same line. With this in mind, we obtain the inequality

$$0\leqslant 2\sqrt{2T}\sqrt{\overline{A_1^2(t)}}\,\theta_1+3T\overline{A_1^2(t)}+\sigma^2\ln K. \qquad (A.26)$$

The probability that this holds equals

$$1-V(\alpha'''), \qquad (A.27)$$

where

$$\alpha'''=3\alpha+\frac{1}{2\alpha}\ln K. \qquad (A.28)$$

The probability that the two inequalities in (A.21) hold simultaneously equals the product of the partial probabilities, i.e.,

$$p(A_2/A_1)=V(\alpha')[1-V(\alpha''')]. \qquad (A.29)$$

The probability of reproducing signal $A_3(t)$ instead of $A_1(t)$ is defined by the inequalities

$$p(A_1)\exp\left(-\frac{T}{\sigma^2}\overline{[X(t)-A_1(t)]^2}\right)<$$

$$<p(A_3)\exp\left(-\frac{T}{\sigma^2}\overline{[X(t)-A_3(t)]^2}\right),$$

$$p(A_2)\exp\left(-\frac{T}{\sigma^2}\overline{[X(t)-A_2(t)]^2}\right)\leqslant$$

$$\leqslant p(A_3)\exp\left(-\frac{T}{\sigma^2}\overline{[X(t)-A_3(t)]^2}\right). \qquad (A.30)$$

Since the regions of signals $A_3(t)$ and $A_1(t)$ do not have common boundaries, the first inequality should be replaced by the inequality

$$p(A_1)\exp\left(-\frac{T}{\sigma^2}\overline{[X(t)-A_1(t)]^2}\right)\leqslant$$

$$<p(A_2)\exp\left(-\frac{T}{\sigma^2}\overline{[X(t)-A_2(t)]^2}\right). \qquad (A.31)$$

After transformations analogous to those given above, we find† that

$$p(A_3/A_1)=V(\alpha')V(\alpha'''). \qquad (A.32)$$

Since $p(A_2/A_3)$ and $p(A_1/A_3)$ have the same value, it is then easy, from the data obtained, to construct the matrix of transition probabilities (10).

LITERATURE CITED

1. V. M. Baikovskii, R. R. Vasil'ev, and A. M. Petrovskii, "Application of the methods of information theory to the analysis and design of certain industrial telemetry systems," Otchet IAT AN SSSR (1956).
2. V. M. Baikovskii, "Discrete-incremental method of transmitting information in telemetering systems," Collection: Automatic Control [in Russian] (Izd AN SSSR, 1960).
3. J. Mass, "An incremental remote position control system," National Telemetering Conference (London, May, 1955).
4. V. A. Kotel'nikov, Theory of Potential Noise Immunity [in Russian] (Gosénergoizdat, 1956).
5. S. V. Borodich, "On the noise immunity of communications with pulse-code modulation," Radiotekhnika No. 5 (1949).
6. N. F. Zyuzev, "Noise immunity of deltamodulation for fluctuation noise," Trudy LKVVIA No. 136 (1955).
7. A. M. Petrovskii, "A method of computing noise immunity of a pulse communications system under fluctuation noise," Avtomatika i Telemekhanika 15, 2 (1954).
8. A. A. Kharkevich, Outlines of General Communication Theory [in Russian] (Gostekhizdat, 1954).

† Generally speaking, this can be obtained from simpler considerations, by taking into account (A.29) and that

$$p_{dis}(A_1)=p(A_2/A_1)+p(A_3/A_1).$$

FINITE AUTOMATA.II*

M. A. Aizerman, L. A. Gusev, L. I. Rozonoér,
I. M. Smirnova, and A. A. Tal'

(Moscow)

Translated from Avtomatika i Telemekhanika, Vol. 21, No. 3, pp. 359-368, March, 1960

In the second part of this work we continue the exposition of the authors' point of view on finite automata, the problems in the theory of finite automata, and the interrelationships of this theory with the ordinary theory of switching (in particular, relay contact) circuits. The general problem is posed of constructing automata operating in one time scale (i.e., with one partitioning of the continuous time axis into discrete points) from elements which operate in a different time scale. As examples of this type of system, we consider abstract neurons (neurons of the type proposed by McCulloch and Pitts) and neuron nets. Relay contact and, more generally, switching circuits are then simply one possible technical realization of abstract neuron nets.

6. Realizations of Automata Operating in a Given Time Scale from Automata Operating in a Different One

In the first part of this work it was assumed that both an automaton as a whole and all of the elements of which the automaton was assembled operate in one and the same time scale (the term "sequentiality" was used previously). As applied to the last remarks of section 5, related to technical realization, this meant, for example, that all the delay elements simultaneously received signals denoting the appearance of the next cycle (i.e., next moment of discrete time) from one and the same cycle transducer.

Here we shall be interested in the more general problem of constructing automata which operate in one time scale from automata operating in a different one.

We consider automaton A, defined by the equation

$$\varkappa(p) = F[\varkappa(p-1), \rho(p-1)], \qquad (1)$$

for which there is given partitioning of the time axis into cycles $t = 0,1,2,\ldots,p,\ldots$, defining the time scale T, and we construct a tape L of the states of this automaton which arise for some initial automaton state $\kappa(0) = \kappa_0$ and for some sequence of inputs $\rho = \rho(t)$. We transform this tape in the following way. From the sequence $t = 0, 1, 2, \ldots, p, \ldots$, we choose some increasing sequence of values of time $t_0, t_1, t_2, \ldots, t_l, \ldots$, and we pick out from the original tape those columns ρ, κ which correspond to the moments of time $t_0, t_1, \ldots t_l, \ldots$. The sequence of these columns, written in correspondence with the sequence of moments of time $t_0, t_1, \ldots, t_l, \ldots$, forms some new tape L^*. Still one more transformation may be carried out on tape L^* by recoding all the symbols written in row "κ"†. The recoding amounts to this, that all symbols from the $\{\kappa\}$ alphabet which appear on tape L^* are divided into groups, and each group is put into correspondence with some new symbol (which, in particular, may again be a symbol from the $\{\kappa\}$ alphabet). The symbols within any given group are not distinguished from each other, and one and the same new symbol corresponds to each of them. By replacing the symbols in column "κ" of tape L^* by the corresponding new symbols, we obtain tape L'.

It may certainly happen that there are contradictory triads on tapes L^* and L', although there were none on tape L. It is important to note that even if there are contradictory triads on tape L^*, it is possible that, thanks to the recoding, there will be none on tape L'. If there are contradictory triads on tape L', then this tape cannot be the state tape of any finite automaton. But if L' contains no contradictory triads, then it could have been obtained as the result of the operation of some finite automaton, operating in time scale T', defined by the sequence of moments of time $t_0, t_1, \ldots, t_i, \ldots$

We now assume that, for each possible state tape L of automaton A, it is possible to stipulate a sequence of moments of time $t_0, t_1, \ldots, t_i, \ldots$ and a method of recoding‡ such that the transformed tape L' would not contain contradictory triads. With this, let there be no contradictory triads even among the set of all the triads contained in the entire collection of transformed tapes. Then this set of transformed tapes can be considered as the

---

* For the first portion of this work, cf. Avtomatika i Telemekhnika No. 2 (1960).

† The symbols in row "ρ" will not be recoded although, to be sure, this is possible.

‡ For different tapes it is admissible to choose different sequences of time and different methods of coding (for example, the sequence of moments $t_0, t_1, \ldots, t_l, \ldots$ may be determined by the sequence of inputs $\rho(t)$ for which the given tape L was obtained; for an example of this type, see section 7 below). As a particular case, the sequence $t_0, t_1, \ldots, t_l, \ldots$ and the method of coding may be chosen independently of the appearance of any given tape.

set of state tapes of one and the same new finite automaton A', operating in the new time scale T'**. The alphabet $\{\kappa'\}$ of states of automaton A' is defined by the accepted method of recoding and contains, as is readily understandable, a number of symbols less than, or equal to, the number of symbols in alphabet $\{\kappa\}$. The alphabet $\{\rho'\}$ of inputs of automation A' is composed of all or some of the symbols of alphabet $\{\rho\}$. By numbering the moments of time $t = t_0, t_1, \ldots$ by the series of natural numbers $0, 1, \ldots, i, \ldots$ and by introducing the new time variable $t' = 0, 1, 2, \ldots, p', \ldots$, we can present the operation of the new automaton A' by an equation of the form

$$x'(p') = F'[x'(p'-1), \rho'(p'-1)],$$

where $p' = i$ if $p = t_i$.

The problem of constructing a given automaton A', operating in time scale T', from elements operating in time scale T reduces to the realization, based on these elements, of an automaton A which, although operating itself in time scale T, may nonetheless be used, with some coding system and with the proper choice of a "new time", as the automaton A', operating in time scale T'. Automaton A' may be represented as consisting of automaton A and a special "reading" device. This device records, for each state tape L of automaton A, the moments of time $t_0, t_1, \ldots, t_i, \ldots$, reads the symbols for the state and inputs of automaton A at these moments of time, and puts out the notation for these symbols in the adopted coding system††. In contradistinction to the cycle transducer which was discussed at the end of section 5, the reading-coding device just described in no way acts on the elements of automaton A.

Automata thus constructed, operating in time scale T', must themselves serve as elements for the construction of nets (section 5), mapping automata operating in the new time scale.

The transition from automaton A to the new automaton A' was implemented by transforming discrete time t to t' and alphabet $\{\kappa\}$ to $\{\kappa'\}$. As was stated earlier, because of the possibility of contradictory triads making an appearance, not each such transformation translates a finite automaton into another finite automaton. The problem arises as to what sort of transformation of discrete time, in conjunction with a recoding of symbols, does not take the device under consideration out of the class of finite automata. Closely related to this question is the question as to which class of device the aforementioned reading-coding device belongs to, and whether it is itself a finite automaton.

We note in conclusion that the contents of sections 5 and 6 reduce to the determination of different structures which are maps of one and the same automaton. What we are saying, essentially, is that different structures, thanks to recoding of states and transformations of time, may be mappings of equivalent automata.

7. Two Methods of Constructing Automata by Transforming Time Scales

Let there be a set of elements, consisting of arbitrary instantaneously acting binary logical transformers and of one-cycle delay element symbols from the alphabet $\{0,1\}$. We assume for simplicity that the cycles are defined by a partition of the continuous time axis into identical intervals of duration τ. It is required to construct, from this set, an automaton forming a given automaton A',

$$x(p') = F[x(p'-1), \rho(p'-1)] \qquad (2)$$

with alphabets $\{\kappa\}$ and $\{\rho\}$, operating in a time scale defined by a partitioning of the time axis into identical intervals of length $l\tau$ (l 0– is an integer), i.e., into an l-fold decelerated time scale.

It was shown in section 5 that a net, mapping any given automaton of any time scale T', can be constructed from a set containing any logical transformers and from delay elements of the same time scale T'. We are now given logical transformers and delay elements in time scale T. The problem thus reduces to the construction, from delay elements in time scale T, of delay elements in time scale T'.

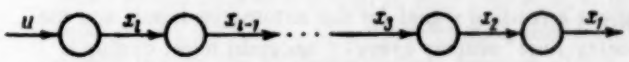

Fig. 1.

** A time scale is defined, not by giving a concrete partitioning of the time axis into equal or unequal intervals, but by giving a method which permits such a partitioning to be made in each concrete case. Thus, for example, the statement that each change of the input state means the beginning of a new cycle (i.e., defines a new discrete moment of time) thereby also determines the time scale, since for each concrete giving of the sequence of inputs it permits one to carry out a definite partitioning of the time axis into cycles.

Earlier, before there was any discussion of transformations of time scales, this remark would have been meaningless.

†† Since, for different tapes of automaton A (i.e., for different inputs and states of the automaton), different sequences of moments of time $t_0, t_1, \ldots t_p \ldots$ and different coding methods are permitted, then this device must, generally speaking, obtain signals as to the inputs and states of automaton A at each moment of time $t = 0, 1, 2, \ldots, p, \ldots$

This device is intended, essentially, for the representation of events. Specifically, it represents some event characterizing the operation of automaton A (for example, each change of state of A's input, the appearance of some state in automaton A itself, etc.) by putting out a reading signal at the moment when the event transpires.

For this purpose, we join l delay elements, operating in time scale T, in series so as to form a delay line (Fig. 1), which is described by the recursion formulas

$$x_1(p) = x_2(p-1),$$
$$x_2(p) = x_3(p-1),$$
$$\cdots\cdots\cdots\cdots$$
$$x_l(p) = u(p-1).$$

By eliminating from these relationships all the x_i except x_1, we obtain, for the delay line as a whole,

$$x_1(p) = u(p-l).$$

The delay line's output at time sl is uniquely determined by the input at time $(s-1)l$. Therefore, if we set $t' = s$ for $t = sl$, then such a delay line may be considered as a delay element operating in time scale T'.

We now construct an automaton by the assembly method (section 5) but now, instead of delay elements in time scale T, we connect, in each instance, a delay line as just described. The automaton thus constructed will operate in time scale T. But if we read the input symbols of this automaton, and the output of each delay line, only every $l\tau$ seconds, then we shall obtain the required automaton, operating in the time scale we require.

The reading-coding device of which we spoke earlier can, in the given case, be a time counter, which gives a reading signal for the automaton inputs and the delay lines' outputs every $l\tau$ seconds; here, coding is implemented automatically since only the delay lines' outputs are read, by virtue of which those states of automaton A which are not differentiated by the states of the terminal elements of all the delay lines are therewith lumped into one group.

We consider one particular case of the problem of realizing an automaton, operating in a given time scale, by means of an automaton operating in another time scale. This case is of interest in its own right, since it plays a basic role in the understanding of certain important technological methods of realizing finite automata in general, and switching circuits in particular.

We consider some automaton A, given by (1). At time t_0, let the input assume the state denoted by symbol ρ^0, and let the input state thereafter remain unchanged until time t_1. During the entire time $t_0 \leq t \leq t_1$, the automaton operates as an autonomous automaton, and its changes of state occur in correspondence with the equation

$$x(p) = F[x(p-1), \rho^0], \qquad t_0 < p \leqslant t_1. \qquad (3)$$

We now assume that, for each ρ^0, there exists a number $\underline{s}$ such that:

a) this autonomous automaton is decremented, i.e., its graph is such that, fron any initial state, it can reach one of several possible equilibrium states [i.e., a state which, by virtue of (3), is transformed into itself] within a finite number $\underline{h}$ $(h \leq s)$ of cycles, and

b) the following change of the automaton's input occurs only after the automaton has reached an equilibrium state, i.e., $t_1 - t_0 \geq s$.

At time $t = t_1$, input state ρ^0 is changed to ρ^1, which then remains unchanged until time $t = t_2$. There is then formed a new autonomous automaton

$$x(p) = F[x(p-1), \rho^1], \qquad t_1 < p \leqslant t_2,$$

about which we make the same two assumptions. Once again, after a time less than $t_2 - t_1$, the automaton reaches an equilibrium state, which may differ from the previous one. At time $t = t_2$, input ρ^1 is changed to ρ^2, etc.

We assume that the automaton's inputs and states are read only at the moments $t_0, t_1, t_2, \ldots, t_i, \ldots$, when the input states change. It is not necessary here to recode the states.

Tape L', written by the corresponding "reading" device,

t	t_0	t_1	t_2	$\ldots$
ρ	ρ^0	ρ^1	ρ^2	$\ldots$
x	$x(t_0)$	$x(t_1)$	$x(t_2)$	$\ldots$

does not contain contradictory triads, as is easily seen.

Therefore, tape L' can be considered, for any input sequence $\rho^0, \rho^1, \rho^2, \ldots$, as the result of the operation of the new automaton A', operating in time scale T' which is defined by the moments at which the inputs change. Serving as the states of automaton A' are the equilibrium states of the autonomous automata formed from automaton A for fixed (sustained) inputs.

It is immediately evident that the operation of automaton A' is completely independent of the time scale of automaton A. It is important only that automaton A operate sufficiently rapidly, i.e., that equilibrium is attained in it before a new cycle commences in automaton A'.

8. Abstract Neurons and Neuron Nets

The name "abstract neuron" is given to an element with a finite number of input lines and one output line, the states of which can be denoted by symbols from the alphabet $\{0, 1\}$; the symbol at the output is uniquely defined by the symbols at the inputs τ seconds previously, where τ is a given number.‡‡

Thus, a neuron is a combination of logical transformers and delay elements with lag time τ. The specific feature of neurons is that the logical transformers and delay elements cannot be distinguished from each other.

‡‡ The term "neuron" for these abstract elements is used for historical reasons, and is only slightly related to the physiological meaning of the term.

A neuron may be considered as an elementary finite automaton in which only two states are possible whereby, with a fixed input, an equilibrium state is reached in one cycle (the time between cycles is τ seconds).

Neurons are connected to each other, forming neuron nets. For the formation of a net, the states of several or all input lines of the neurons from some set are immediately identified with the output states of some neurons from the same set. In contradistinction to the nets treated in section 5, neuron nets do not contain symbol transformers, and the original elements are not any automata, but automata of a very special form, namely, neurons.

The logical functions which can be realized by one neuron can be most diverse. But in neurons of a given type only a completely concrete set of logical functions may be realized. By setting up a net from neurons of a given type, this net having one output line and several input lines, one can extend the set of realizable logical functions, in the sense that the state at the output of such a net will be a logical function of the input states, but with a delay, not of τ, but of $l\tau$ seconds, where l is an integer. We now assume that, for any logical function whatever, one can, from neurons of a given type, construct a net which realizes this function in not more than $\zeta\tau$ seconds. The least value of ζ which satisfies this condition will be called the index of the neuron. The number ζ depends on the logical capabilities of the neurons from which the net was set up. •••

It follows from what has been presented that, from neurons with a finite index ζ, one can construct any logical transformer but, in contradistinction to the transformers studied in previous sections, these will not be instantaneously acting; up to $\zeta\tau$ seconds will be required to implement a logical transformation.

A neuron net is a particular case of a net in the sense of section 5, so that any neuron net is therefore a finite automaton. The time scale of this finite automaton is determined by the partitioning of the continuous time axis into equal intervals of duration τ. Obviously, if one is considering the operation of an automaton in such a time scale, then neurons with index $\zeta > 1$ do not constitute a complete set. Indeed, in such a time scale it is impossible to construct from neurons even the simplest automaton.

$$x(p) = L[x(p-1), u(p-1)],$$

where L is a logical function for the realization of which more than one cycle is required (if $\zeta > 1$ then, by definition, such a function L exists).

Now, if the time scale is defined by a partitioning of the time axis into identical intervals equal or greater than $\zeta\tau$, then any automaton may be constructed from neurons with index ζ. In fact, any logical function is realized within $\zeta\tau$ seconds, as well as (by the use of feedback paths) a system of equations of the form

$$x_i(p') = L_i[x_1(p'-1), \ldots, x_n(p'-1);$$

$$u_1(p'-1), \ldots, u_s(p'-1)] \quad (i=1,\ldots,n),$$

where $p' = s$ if $p = s\zeta$, i.e., an abstract structure which is the mapping, as was shown in section 5, of any finite automaton of time scale p'.

By using automata operating in such a "uniform" time scale $\zeta\tau$, we can construct, from neurons, automata operating in other time scales. On the basis of the arguments given in sections 5-7, we can now give at least two methods for realizing such automata.

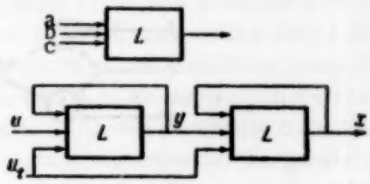

Fig. 2.

First method. From neurons with finite index ζ we can construct delay elements for the time defined by the externally supplied special cycle signals u_t. Figure 2 shows an example of a circuit of such elements, with input $\underline{u}$ and output $\underline{x}$. The transformers L shown on the circuit realize the following logical function with a delay $l\tau$ (where $l \leq \zeta$):

$$z = (a \,\&\, \bar{c}) \vee (b \,\&\, c).$$

In correspondence with this, the equations which describe the delay elements have the form

$$x(p) = [y(p-l) \,\&\, u_t(p-l)] \vee [x(p-l) \,\&\, \bar{u}_t(p-l)],$$

$$y(p) = [u(p-l) \,\&\, u_t(p-l)] \vee [y(p-l) \,\&\, \bar{u}_t(p-l)],$$

Correct operation of the scheme shown can be guaranteed in the case when the new cycle signal u_t lasts for l old cycles and, moreover, if input $\underline{u}$ does not change before signal u_t is applied. Figure 3 shows the changes in time of all the net coordinates for certain given changes in $\underline{u}$ and u_t. Figure 4 shows an example of a McCulloch-Pitts neuron net which realizes a delay element for a time defined by synchronizing input u_t.

From such delay elements and from logical transformers which, as was shown above, are constructed from the same neurons, one may construct any finite automaton, operating at a tempo defined by synchronizing input u_t.

••• It is certainly possible that $\zeta = \infty$, or that there exist logical functions which, in general, cannot be realized by neurons of the given type.

The McCulloch-Pitts neuron has index 2, since no more than 2τ seconds is required to realize any complete normal form in a net constructed of McCulloch-Pitts neurons.

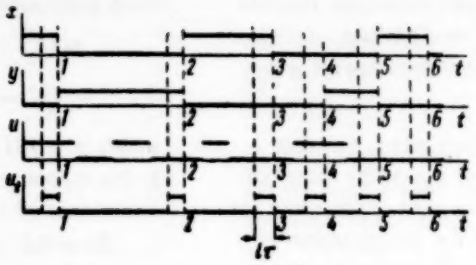

Fig. 3.

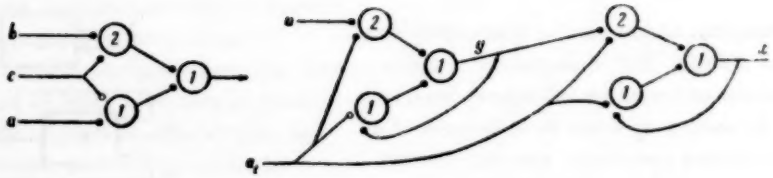

Fig. 4.

Second method . If it is necessary to construct an automaton whose time scale is defined by the changes in the input states, then one may use, in neuron circuits, the method of constructing automata from the equilibrium states of the corresponding autonomous automata (cf. section 7). Certainly, the first method is the more general; it is also valid in the given case, when the signals u_t are engendered by each change of input states in the automaton.

9. Relay Contact Circuits as Finite Automata

In the consideration of relay contact circuits there arise many important technological and scientific problems related to the peculiar features of this branch of technology. The problems alluded to will be briefly stated at the end of the present section. We, however, will not be interested here in these problems, however important they may be for the construction of actual relay contact circuits.

Here, we consider relay contact circuits only from the point of view of their special features which permit their assimilation to finite automata and which permit the use of the methods of the theory of finite automata in the construction of relay contact circuits. Therefore, we shall henceforth in this section consider an idealized model of a relay circuit.

By a relay we understand a device with a finite number of input lines and one output †††, and which satisfies the following two requirements :

a) each of the input lines and the output may have only two states, denoted by zero or unity;

b) the output state is some logical function of the states of the input lines with some time lag τ .

For example, in ordinary electromechanical relays with one winding, each relay has one input (the presence or absence of current in the winding) and realizes a logical function of one variable of the type " yes" (normally open relay contacts) or "no" (normally closed relay contacts). The lag of τ seconds is due to the relay's operating time.

In using relays with several windings, each relay has several inputs, and the character of the logical functions realized (with a delay of τ seconds) in the relays is determined by the special characteristics of the windings.

Individual relays are combined in a relay circuit by means of electrical circuits (contact circuits). These circuits define all or several inputs to relays as logical functions of the states of relay contacts and of contacts whose states depend on external stimuli . These logical functions are realized virtually instantaneously in practice. Therefore, the contact circuits play the role of the instantaneously acting logical transformers.

From what has been presented it follows that a relay is an ordinary neuron, the value of whose index ζ depends on which logic can be realized by means of one relay. A relay circuit differs from a neuron net only in its capability of being used as an instantaneously acting transformer. This difference is inessential, since the essential fact for a neuron net is that its time scale, as an automaton, is predetermined by the time τ — the neurons' lag.

Therefore, relay circuits are finite automata of the "neuron net" type, and everything presented in sections 6 and 7 applies to relay circuits as well. In particular,

††† Or two outputs, one of which is the negation of the other.

the two methods given in section 7 for constructing finite automata which operate in time scales different from the neurons' natural time scale, also define two possible ways of constructing relay circuits which map an arbitrary finite automaton whose time scale differs from the natural time scale of the relay circuit, as defined by the relays' time lag. Both these methods are used for synthesizing relay circuits. The first of these (with the construction of delay elements) is used most frequently in the construction of the so-called cyclical circuits. However, it is clear from section 7 that this method is a general one, valid for the relay realization of any finite automaton. As an example, Fig. 5 shows the schematic realization of a delay element for the time

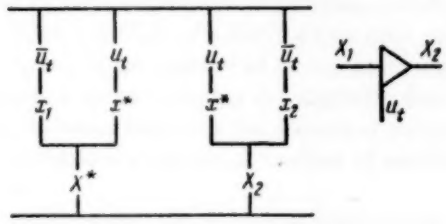

Fig. 5.

defined by synchronizing signal u_t, constructed from ordinary electromechanical relays. The second method, using the equilibrium states of the corresponding autonomous automata, is actually used in almost all sequential circuits.

Although relay circuits are one of the possible methods of technically realizing finite automata, specific analytical and synthesizing techniques are applied to them. This specificity is due, in particular, to the fact that the lag times in different relays of one circuit are not identical. Therefore, the time axis cannot be partitioned beforehand into equal cycles, thanks to which the analysis and synthesis of relay circuits requires that one obtain additional information which is not forthcoming from finite automata theory. Moreover, the differences in relay operating times might lead to relay competitions.

Also specific are the minimization problems which arise in the synthesis of relay contact circuits (for example, minimization of the number of contacts, windings, etc. Thus, relay circuits pose their own problems which do not arise in the general theory of finite automata. To our way of thinking, the aim of relay circuit theory consists of studying such types of specific problems and of general methods for the technical realization of finite automata by relay circuits of some type or other.

Since finite automata theory began to be crystallized as an independent scientific discipline only very recently, it is natural that part of the general questions which are important for the understanding of finite automata in general were developed within the purview of relay circuit theory. Due to this, there is ordinarily no distinction made between the general questions bearing on finite automata theory and the questions specific to relay realizations.

The development of the theory of logical devices naturally led to the introduction into consideration of abstract "finite automata" and to the splitting off of finite automata theory as an independent scientific discipline.

10. Concluding Remarks

In designing concrete automatic devices, it is necessary to distinguish several independent steps.

Design begins with the analysis and idealization of the operations which the automatic device must execute. If this idealization leads to a formulation of the operating conditions in terms of discrete time and a finite set of variables, each of which may assume only a finite number of values, then the possibility arises of seeking the automatic device to be designed in the class of finite automata. With this possibility there is closely related a problem subsumed under the general problem of representing events, and the elucidation of what may and may not be implemented by finite automata.

If this question is answered in the affirmative, there arises the second problem, namely, by which equation of type (1) may one describe the finite automaton which satisfies the conditions posed , i.e., what are the tapes of this automaton and of what triads do they consist. This problem relates to the problem of the abstract synthesis of a finite automaton from its given operating conditions.

Even within boundaries of abstract consideration, one may cite a number of ways of realizing automata. One and the same automaton may be made, for example, from elements implementing functional transformations of two-valued or of multi-valued logic, with the use of special delay devices for externally given cycles or without their use if the equilibrium states in abstract neuron nets are employed, etc. The choice among the theoretically different ways of realizing an automation is related to the choice of the automaton's structure, to its abstract assembly.

This entire group of questions comprises the contents of the general theory of finite automata.

Each technical realization of a finite automaton gives rise to its own scientific problems, requires its own methods of analysis and synthesis, the taking into account of the technical special features of the actual apparatus, the economic and other requirements on the design or the circuit.

The application of finite automata theory ends as soon as one has chosen the structure or the net, i.e., as soon as one has written the equations of type (6) of the first part of the present work .

For the problem of the technical realization, the equations of type (6), or any of their equivalents, are the initial data, and the aim here is the engineering choice of

design or circuit which is optimal in some sense (technical or economical).

Certainly, the boundaries between the problems of finite automata theory and the problems of technical realization are not well-defined.

Even in the choice of an abstract structure, one has to take into account the requirements and the special features of the technical realization. But this "infiltration" of technical requirements into the abstract considerations does not impede the detachment of the general theory from the very important, but specific, problems.

A VISUAL-MATRIX METHOD FOR MINIMIZING BOOLEAN FUNCTIONS

A. D. Zakrevskii

(Tomsk)

Translated from Avtomatika i Telemekhanika, Vol. 21, No. 3, pp. 369-373, March, 1960
Original article submitted April 25, 1959

A semiintuitive method is presented for the minimization of Boolean functions which is based on the use of certain properties of visually perceived information. The method is applicable to the minimization of arbitrary Boolean functions with up to 10 to 12 variables, and is particularly effective for the minimization of incompletely defined functions.

One of the most important problems which must be solved in the synthesis of switching circuits— the minimization of the number of circuit elements – is ordinarily solved by transforming the algebraic form of Boolean functions until one has arrived at formulas which are superpositions of minimal numbers of elementary functions.

The difficulties which arise in minimizing arbitrary Boolean functions increase catastrophically fast as the number n of arguments increases, so that a number of methods become inapplicable in practice even for $n > 6$.

The increase in the number of arguments of the function to be minimized may be compensated for either by restricting the class of functions to be considered or by increasing the speed of solution of the minimization problem by using modern computing technology. The realization of these possibilities is the main subject of a large number of published works [1-17].

A common characteristic feature of the contents of a large part of these works is the algorithmization of the process of minimizing Boolean functions. Significantly less attention has been given to the development of methods based on the use of certain properties of the human perception of information which are difficult to translate into algorithms. Despite this, just such methods are necessary for manual minimization of Boolean functions.

The original information on Boolean functions must be presented in compact and readily perceivable form. Since the basic "memory device" for manual minimization is the two-dimensional sheet of paper, the most compact form of representing information in this case will be a two-dimensional—matrix—form. Matrix forms for presenting Boolean functions were used by O. Plekhl' [10], A. Svoboda [18], M. Karnaugh [19] and others.

In these methods, the elements of information concerning the Boolean functions are the functions' values given by sets of elements in two-dimensional space, placed into a single-valued correspondence with the sets of values of the variables. The order of the mutual spatial arrangement of the elements, a matter of indifference in an algorithmic approach, plays an essential role for the visual perception of the matrix by a human being. An advantageous choice of such a mutual spatial disposition of elements, i.e., such a method of coding the spatial elements by sets of values of the variables, is one for which the properties of the Boolean functions which are of interest to us in trying to carry out minimization, would be readily eye-catching.

In the method suggested by A. Svoboda for minimizing Boolean functions, the potential possibilities for minimizing a Boolean function, as represented by a matrix, are expressed by the periodicity properties of that representation. With large numbers of variables, one has to do with the superposition of periodic representations with different periods which is difficult to preceive visually as a whole. In connection with this, A. Svoboda uses lattices (grids), corresponding to the individual variables, by means of which one successively isolates the portions of the matrix which correspond to definite values of these variables.

In the author's opinion, it is easier to perceive visually the symmetry properties of the representation, which gives the possibility of using the superiority of Gestalt perception of the original information, thus dispensing with cards and leading to the successive analysis of the individual portions of the representation.

The visual matrix method of minimizing Boolean functions which the author proposes is semialgorithmic, semiintuitive, so that its practical implementation is required in order to elucidate its superiorities over other methods.

It should be remembered that, for a large number of arguments, due to the complexity of the problem, the minimization of a Boolean function in the general case is considered to be successfully implemented if it has led to a sufficiently minimal algebraic form (i.e., strictly speaking, to a form which is sufficiently close to the absolutely minimal one).

An arbitrary Boolean function $f(x_1, x_2, \ldots x_n)$ can be given by a matrix (α_{ik}) whose binary elements α_{ik} are the function values, while the subscripts i, k are its arguments. The pairs of values of i, k are put into a one-to-one correspondence with the sets of values of the arguments $x_1, x_2, \ldots x_n$, whereby the arguments are, for convenience, divided into two sets of as close to equal

size as possible. Values of the arguments which enter into one of these parts code the values of i, the values of the remaining arguments code the values of k. O. Plekhl' and A. Svoboda coded the natural number i, k by a positional binary code with weight 2^j for the jth place (bit).

For coding the rows and columns of the matrix which represents the Boolean function to be minimized, we shall use a symmetric Gray code which, as will be shown, has certain superiorities over other codes.

Unit ("1") values of a Boolean function will be represented by dots in the corresponding matrix elements, blank elements will correspond to zero function values, and blackened matrix elements will attest that the function is not defined on the sets of argument values corresponding to these elements. The set of all elements thus marked will be called the representation of the function.

TABLE 1

Example 1. Table 1 represents the Boolean function which takes the value "1" on the sets * 00000, 00010, 11011, 01110, 10100, 10110, 00111, is not defined on the sets 10010, 11010, 10001, 01101, 11111 and takes the value "0" on the remaining sets. One may consider that Table 1 represents all $2^5 = 32$ Boolean functions which are defined on all the sets but differ in their values on the sets 10010, 11010, 10001, 01101, and 11111.

We note that when the number of variables does not exceed four, the method suggested here coincides with the method of M. Karnaugh [19] (cf. also [8, 20]), but loses its similarity as the number of variables increases (in Karnaugh's method functions of six variables are represented in three-dimensional space while, for the representation of functions of five variables, Richards [8] suggests carrying out a diagonal decomposition of the elements in the tables representing functions of four variables, etc.).

Let $y = f(f_1, f_2, \ldots, f_m)$ be a Boolean function whose arguments are functions of the binary variables $x_1, x_2, \ldots, x_n$. In order to express y as a function of $x_1, x_2, \ldots, x_n$, it suffices to find, for each set of values of $x_1, x_2, x_3, \ldots, x_n$, the corresponding values of $f_1, f_2, \ldots, f_m$ and then to determine the value of y corresponding to these latter values.

This permits the easy implementation of operations on Boolean functions by means of their matrix forms, represented by tables on tracing paper. The sheets of tracing paper are laid on each other, the function values in the corresponding elements are compared and, in the corresponding element of the result matrix, the resulting value is noted.

The given method is not only applicable to manual computations; by using bit-wise logical operations, one can easily program it for computers.

TABLE 2

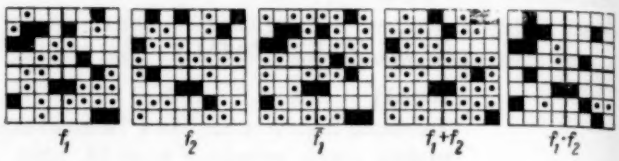

Example 2. Table 2 gives the matrix representations of the incompletely defined functions f_1 and f_2 of six variables, as well as the results of certain operations on them.

Note 1. The character of the representation matrices does not depend on the method of coding their elements if this method is the same for all the interacting matrices, so that the coding was not given here.

Note 2. In obtaining the matrix for $\bar{f}_1$ it was supposed that the inverse (negation) of an undefined value of a binary variable is also an undefined value.

We begin the consideration of the method of minimizing Boolean functions with a comparatively simple case—obtaining the minimal disjunctive form (m.d.f.), while assuming that, in the general case, the function to be minimized is not defined on all the sets of argument values.

In general, obtaining the m.d.f. makes it easier to find other minimal forms, although it may turn out that, in making the transition from the m.d.f. to another form, this latter will not be absolutely minimal.

An algorithm which solves completely the problem posed was described by Yu. I. Zhuravlev [7], but it entails scanning variants, which leads to a very lengthy computational procedure, that hinders its practical employment.

Using the terminology of [7], we shall denote by an interval of the kth rank a sert of matrix elements corresponding to the conjunction of k variables, some of which may enter with a negation sign.

We now define the rules for isolating intervals.

TABLE 3

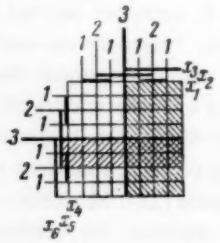

* By a set we mean a conjunction of argument values, for example the set 01000 corresponds to the values $x_1 = 0, x_2 = 1, x_3 = x_4 = x_5 = 0$.

1. Vertical lines in the table which separate elements corresponding to different values of x_1 we shall call axes of symmetry of the first rank; lines separating elements corresponding to different values of x_2 we shall call axes of symmetry of the 2nd rank, etc. We apply an analogous nomenclature to the table's horizontal lines (cf. Table 3).

2. A set of elements which form a band of elements of width 2^r, the central line of which is axis of symmetry of the rth rank, shall be called a zone of symmetry of this axis. (The hatched boxes on Table 3 indicate zones for the first rank horizontal axis and second rank vertical axis.)

3. Each element in the table for a Boolean function of n variables is an nth-rank interval.

A set of two kth-rank intervals is an interval of the (k-1)th rank if the intervals are symmetric with respect to some axis of symmetry and are found completely within its zone of symmetry.

We remark that, since the minimum width of a band of symmetry equals two, it follows that two series of elements forming a rectangle are always intervals; analogously, four series of elements forming a square are always intervals.

The task of obtaining the minimal disjunctive form of a Boolean function reduces to finding such a decomposition of the function representative into intervals for which the sum of the ranks of all the intervals will be minimal. The decomposition is obtained by such a covering by intervals of all the table elements corresponding to unit function values for which interval intersections are admitted, and covering by intervals of elements on which the function is undefined, but not admitting the covering of elements which correspond to zero function values.

Example 3. To find the m.d.f. of the function

$$f(a, b, c) = ab + bc + \bar{a}c.$$

By successively marking with dots the elements of the intervals which correspond to the conjunctions ab, bc, and $\bar{a}c$, we obtain the representation of the function (cf. Table 4, a).

From the visual perception of the representation it becomes obvious that the advantageous decomposition of the representation is into the two intervals corresponding to the conjunctions ab and $\bar{a}c$ (Table 4, b). Thus easily do we obtain the m.d.f. of the original function f(a, b, c) = $= ab + \bar{a}c$.

The special convenience of the visual method comes to the fore in the minimization of incompletely defined functions.

Example 4. To find the m.d.f. of the function whose representation is shown in Table 5.

The series of coverings of the representation by intervals is shown in Table 5, given only to elucidate the decomposition principle, since in practice one of the original matrices can be avoided by successively covering the representation by intervals and by blackening the elements which fall in intervals. With a little practice, one can carry out the decomposition of the representation mentally.

The result of the decomposition gives the m.d.f. of the function to be minimized.

$$f = x_1\bar{x}_2\bar{x}_3 + \bar{x}_2\bar{x}_3\bar{x}_6 + \bar{x}_3x_5\bar{x}_6 + x_1x_4 + x_2x_3\bar{x}_5.$$

As this example shows, the visual estimate of the representation permits one to find the optimal variant of the incompletely defined function more rapidly than may be done with algebraic methods [6].

In certain cases, the algebraic form of the original Boolean function which contains a minimal number of variable symbols may be obtained in the form of a product of two disjunctive forms.

TABLE 4

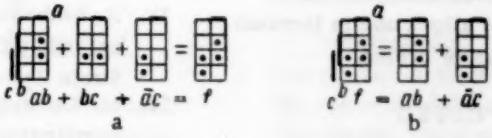

TABLE 5

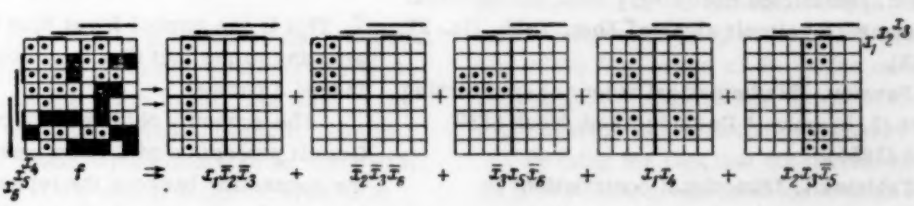

TABLE 6

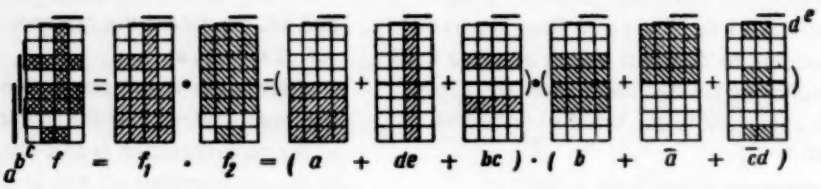

Example 5. (Taken from R. K. Richards' book [8], page 70.) To find the minimal algebraic form of the Boolean function f = ab + ac̄d + bc + bde + ade + c̄de. The function's representation is given as the intersection of two other representations, f_1 and f_2, easily decomposed into intervals (Table 6). The final result, f = (a + bc + de) (b + a + cd), contains nine variable symbols.†

The material herein presented allows the following conclusions to be drawn:

1. The matrix representation of Boolean functions in which the matrix rows and columns are coded by the variables' values in a Gray code has the convenience of immediate visual perception of certain properties of the function represented, the correct estimate of which is necessary in the finding of the optimal way to minimize. Visual analysis of the representation allows one to estimate the possibilities of minimization presented by the representation by degrees of regularity of the representation's elements, the criterion for which is the symmetry of the elements' mutual positioning.

2. Being intuitive to a certain extent, the visual matrix method of minimizing Boolean functions was designed for using certain properties, difficult to render in algorithmic form, of visual perception, thus allowing, without recourse to computing technology, the implementation of complicated transformations of the original function for its minimization. With a little practice, the minimization of Boolean functions of five or six variables may easily be done mentally (if the representation of the function is in front of one's eyes), while making notes on the representation elements during the minimization process allows one to increase the number of variables up to ten or twelve.

LITERATURE CITED

1. M. A. Gavrilov, Theory of Relay Contact Circuits [in Russian] (Izd. AN SSSR, 1950).
2. V. I. Shestakov, "The algebra of two-terminal networks, constructed exclusively from two-terminal constituents (A—circuit algebra)," Zhur. Tekh. Fiz. 11, 6 (1941).
3. G. N. Povarov, "Mathematical theory of synthesizing contact (1, k)-poles," Doklady Akad. Nauk SSSR 100, 5 (1955).
4. S. V. Yablonskii, "Functional constructions in k-valued logic," Inst. Matem. 51 (1958).
5. E. K. Voishvillo, "Method of simplifying truth function expressions," Nauchn. Dokl. Vyssh. Skoly. Filosophskie Nauki No. 2 (1959).
6. V. N. Roginskii, "Taking unused states into account in synthesizing relay contact circuits," Avtomatika i Telemekhanika 15, 3 (1954).
7. Yu. I. Zhuravlev, "On the separability of subsets of the vertices of an n-dimensional unit cube," Trudy Inst. Matem. 51 (1958).
8. R. K. Richards, Arithmetic Operations in Digital Computers (Van Nostrand, Princeton, 1955).
9. "Synthesis of electronic computing and control circuits" (Harvard Computation Laboratory, 1951).
10. O. Plekhl', Electromechanical Switching and Switching and Switching Apparatus [in Russian] (Énergoizdat, 1959).
11. C. E. Shannon, "The synthesis of two-terminal switching circuits," Bell Syst. Tech. J. 28, 1 (1949).
12. W. V. Quine, "The problem of simplifying truth functions," Am. Math. Monthly 59, 8 (1952).
13. E. W. Veitch, "A chart method for simplifying truth functions," Proc. Assoc. Comput. Mach. No. 2 and 3 (1952).
14. E. J. McCluskey, "Minimization of Boolean functions," Bell Sys. Tech. J. 35, 6 (1956).
15. B. Harris, "An algorithm for determining minimal representation of a logic function," Trans. IRE EC-6 2 (1957).
16. J. P. Roth, "Algebraic topological methods for the synthesis of switching systems. I," Trans. Am. Math. Soc. 88, 2 (1958).
17. G. Epstein, "Synthesis of electronic circuits for symmetric functions," Trans. IRE EC-7, 1 (1958).
18. A. Svoboda, "Grafico-mechanicke pomücky uzivane při analise a synthese kontaktovych obvodů," Stroje Zpracov. inform. 4 (1956).
19. M. Karnaugh, "The map method for synthesis of combinatorial logic circuits," Trans. AIEE 72, Part I (1953).
20. N. B. Acred, "Control circuits design," Electronic Eng. 29, No. 358 (1957).

† This is one symbol fewer than in Richards' result, attesting to the fact that the solution of this problem is indeed a puzzle.

The economy obtained is a consequence of the Gestalt perception of the representation which allows the connection between the representation elements to be taken into account in the search for the optimal variant of its decomposition.

GENERALIZED PROPORTIONALITY CONDITIONS OF ELECTROMAGNETIC SYSTEMS

(GEOMETRY OF ELECTROMAGNETIC SYSTEMS)

A. S. Tulin

(Moscow)

Translated from Avtomatika i Telemekhanika, Vol. 21, No. 3, pp. 374-383, March,1960
Original article submitted November 5 , 1959

Questions of proportionality of electromagnetic devices are propounded. Geometric regularities, related to the conditions of rational use of electromagnetic energy, are used. As a result, there are found many optimal configurations from which, in correspondence with the technical and economic requirements, the actual configuration is chosen in each specific instance.

In devices which use electromagnetic energy, the basic design element is the electromagnetic system, which is a ferromagnetic magnetic circuit with one or several windings.

The electromagnetic system of an electromagnetic device is a function of the device's purpose. Thus, for example, there are electromagnetic systems for transformers, chokes, magnetic amplifiers, relays, and other electromagnetic mechanisms, among which can be included electrical machines.

Despite the variety of the physical forms taken by electromagnetic systems, they have something in common, which speaks for the efficacy of a generalized consideration of the fundamental regularities which are valid for all electromagnetic devices.

For this generalized consideration of electromagnetic systems, we use the fact that any electromagnetic system is some geometric figure whose absolute and relative dimensions are determined by the physical laws concerning the use of electromagnetic energy.

We are justified in calling the set of questions as to the geometry and physics of electromagnetic systems the "geometry of electromagnetic systems."

Basic Postulates of the Geometry of Electromagnetic Systems

Questions as to the geometry of electromagnetic systems in their generalized form have not yet been treated in the literature, so that it is necessary to first consider certain postulates and, for convenience of exposition, to introduce some terms from electromagnetic system theory.

First of all, it is necessary to introduce the concept of the absolute magnitude of an electromagnetic system.

The necessity for this arises in all cases when it is required to compare different electromagnetic systems among themselves. Such comparisons can be made with sufficient simplicity if the electromagnetic systems to be compared are completely similar. In all other cases, this comparison gives rise to well-known difficulties.

We shall henceforth take, as the absolute magnitude of an electromagnetic system, the sum of the volumes of its active materials, i.e., the sum of the volumes of its windings and magnetic circuit. With this, any change in the dimensions of the electromagnetic system without any concomitant change in the sum of the volumes of its active materials will be considered as a change of its relative dimensions with retention of its absolute magnitude. Conversely, we shall consider that a change in an electromagnetic system's absolute magnitude corresponds to a change wherein all linear dimensions change while the conditions of geometric similarity are retained. Finally, if a change in the dimensions of an electromagnetic system is not accompanied by a retention of the conditions of geometric similarity and, simultaneously, the sum of the volumes does not remain a constant, we shall then consider that, in this case, both the absolute magnitude and the relative dimensions of the electromagnetic system have changed.

As the relative linear dimensions of an electromagnetic system, we take its linear dimensions divided by a fixed one of them.

Corresponding to the concepts of absolute magnitude and relative dimensions of an electromagnetic system are the concepts of the absolute and relative parameters of this system. As the relative (or reduced) parameters we take the absolute parameters divided by the absolute magnitude of the electromagnetic system. With this, if the parameters which interest us are proportional to the first powers of linear dimensions, then their reduction will be implemented by a division by the cube root of the sum of the first powers of the active materials' volumes. For a quadratic dependency, the aforementioned sum will be raised to the second power , etc.

By using the fact that the parameters of electromagnetic devices can be reduced to an arbitrary number of turns of their windings, we shall consider their windings

to be reduced to the one-turn form. In this case, instead of the cross section and length of a circuit's winding, we shall consider its mean length and total cross section, with account taken of the corresponding space factor.

Naturally, all parameters of electromagnetic systems are the corresponding functions of the geometric dimensions of these systems and of the properties of the active materials. For convenience of exposition, we shall henceforth, instead of such expressions as "a geometric function of the magnetic circuit's magnetic conductance," use "the magnetic circuit's geometric conductance," "the geometric impedance of the winding," and also "geometric coefficient. . ." or "geometric constant. . .," etc.

The nonlinearity of ferromagnetic materials ordinarily introduces significant complication into the theory of elemectromagnetic devices, but it is not mandatory to take these nonlinearities into account in the theory of the geometry of electromagnetic systems. The explanation of this is that the geometry of electromagnetic systems is concerned with the regularities imposed on the relative (or reduced) parameters, in the aforementioned sense, of electromagnetic systems, and these reduced parameters do not depend on the properties of any material. As will become clear in the sequel, the materials' properties, while having no infleunce on the choice of relative dimensions of electromagnetic systems, influence completely its absolute dimensions.

We should make particular mention of the questions in our generalized consideration of electromagnetic systems which deal with the classification of systems into those with closed or with open magnetic circuits. Thus, for example, a transformer has a closed, and an electromagnetic relay an open, magnetic circuit.

The author initially will consider all electromagnetic systems in the closed magnetic circuit mode (the mode of a short-circuited magnetic circuit). The transition from closed to open magnetic circuits does not render it necessary to change the optimal geometric relationships obtained when considering closed magnetic circuit modes. The proof of this assumption in particular cases of electromagnetic system employment engenders no particular difficulty, and is in good agreement with experience.

The consideration of proportionality of electromagnetic systems with closed magnetic circuits eliminates the necessity of taking magnetic flux leakage into account, which also simplifies the problem.

The reduction of windings to one turn and the ignoring of flux leakage lead to an equivalence between current and ampere-turns, and also between magnetic flux and flux linkages.

Energetic Bases of Electromagnetic Systems

The use of electromagnetic energy in any electromagnetic device is related to the property of the electromagnetic system of accumulating energy obtained from a source of electric current. This energy is then partially or completely utilized, and is partially converted to a source of supply or is lost in the form of various energy dissipations.

As the characteristic of this property of electromagnetic systems, we can use the quantity of accumulated energy divided by the power used in maintaining the static state of the energy stored in the system. To find this parameter we shall use regularities which exist for dc circuits, but it should be kept in mind with this that the parameter in which we are interested does not depend on the nature of the current.

As is well-known, when the windings of an electromagnetic system are connected to a dc source, a transient response ensues for which the following equation is valid:

$$ui\,dt = i^2 r\,dt + i\,d\psi. \tag{1}$$

Equation (1) shows that all the energy from the source consists of two parts, one of which is consumed in thermal losses in the windings, while the other serves to change the system's magnetic state. At the termination of the transient response, the current and the magnetic flux assume constant values. The energy which continues to be supplied from the source is now consumed solely by the thermal losses in the windings. These losses determine the power which goes to maintain the static state of electromagnetic energy accumulated in the electromagnetic system during the transient response. This power, defined in terms of the steady-state value of current $\dot{I}$ and the electric conductance g_M of the windings, equals

$$P = \frac{I^2}{g_M}. \tag{2}$$

The quantity of electromagnetic energy stored in the electromagnetic system during the transient response is defined by the expression

$$W_L = \int_0^{\psi} i\,d\psi. \tag{3}$$

To find the differential magnetic flux which appears in Expression (3), we use the well-known dependency which exists between the magnetizing force of magnetic flux and magnetic conductance. With this, and also using (2), we obtain

$$W_L = \frac{1}{2} P g_M g_c, \tag{4}$$

from whence

$$\frac{W_L}{P} = \frac{1}{2} g_M g_c = k G_M G_c, \tag{5}$$

where G_M and G_c are the geometric conductances of, respectively, the windings and the closed magnetic circuit, and k is a proportionality factor which takes into account the adopted units of measurement, the space factors of the winding cross section and the magnetic circuit, the specific conductance and permeability of the materials of the windings and the magnetic circuit, and other quantities relating the windings' electric

conductance and the magnetic circuit's magnetic conductance with the geometric dimensions of the electromagnetic system.

By dropping the factor $\underline{k}$ from (5), we obtain a function of the electromagnetic system's geometric dimensions which characterizes this system's property of accumulating electromagnetic energy. With this, we obtain

$$\gamma = G_M G_C = \frac{S_M S_C}{L_M L_C}, \qquad (6)$$

Here, S_M and S_C are the cross sections of the winding and of the magnetic circuit, and L_M and L_C are their mean lengths.

As is clear from (6), to improve the properties of electromagnetic systems, it is necessary, in choosing their geometric dimensions, to attempt to increase the product of the cross sections of the winding and magnetic circuit, and to decrease the product of their lengths. This is the basic law of the theory of electromagnetic systems. However, (6) cannot be used for comparing different electromagnetic systems among themselves, since the quantity defined by this formula depends not only on the relative, but also on the absolute, dimensions of the electromagnetic systems. To eliminate the dependence on absolute quantities, we use the relative value of the parameter of interest to us. We obtain with this

$$\xi = \frac{1}{\sqrt[3]{Q^5}} \frac{S_M S_C}{L_M L_C}, \qquad (7)$$

where Q is the sum of the volumes of the active materials, i.e., the absolute magnitude of the electromagnetic system.

In the theory of the geometry of electromagnetic systems, (7) is one of the fundamentals. In the sequel, this formula will be used for the analysis of the proportionalities of the geometric forms of electromagnetic systems. The parameter defined by (7) is called the "geometric constant" of the electromagnetic system.

The introduction of the concept of the geometric constant into the analysis of proportionality of electromagnetic systems allows geometric function (6) of any electromagnetic device to be presented in the form of two factors, one of which is determined by relative, the other by absolute, dimensions of the electromagnetic

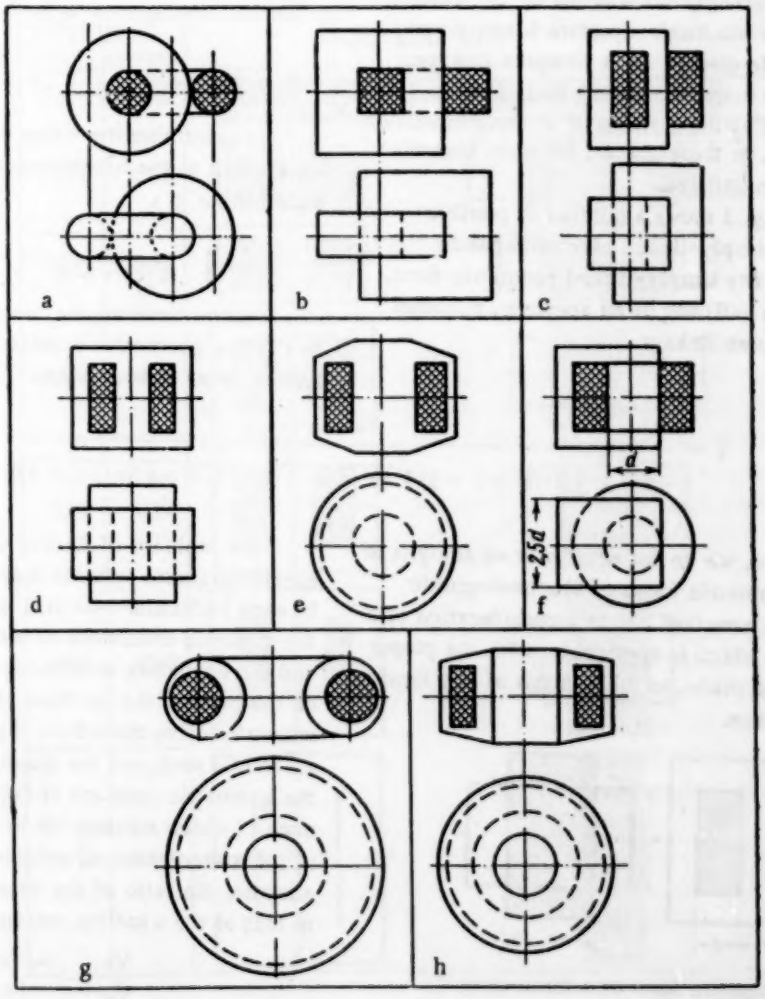

Fig. 1. Certain possible geometric forms of electromagnetic systems.

system, i.e., in the case of the geometric function given by (6), we shall have

$$\gamma = \xi \sqrt[3]{Q^2}. \tag{8}$$

As is obvious, for a given magnitude of the electromagnetic system's geometric function γ, to decrease the expenditure of active materials, i.e., to decrease the quantity Q, it is necessary to try to maximize the geometric constant ξ.

However, it should be taken into account with this that the prices of the materials of the windings and of the magnetic circuit are different, so that it is necessary to attempt to realize, not an absolute decrease in the sum of the volumes of the windings and the magnetic circuit, but a reduction of the total cost of the electromagnetic system's active materials.

Linkages of Geometric Dimensions of Electromagnetic Systems

Electromagnetic systems, in their geometric aspect, are complicated figures which consist of linkages of simpler figures of windings and magnetic circuits.

Linkage between windings and magnetic circuits may be simple or complex. In a simple linkage, the entire aperture of the magnetic circuit is filled by the winding's cross section, and the winding's aperture is completely filled by the magnetic circuit. In a complex linkage, between winding and magnetic circuit there remain certain spaces, filled by the surfaces of winding insulation or by other windings, or these spaces, for some reason or another, may remain unfilled.

As examples, Fig. 1 shows a number of possible geometric forms of simply-linked electromagnetic systems. Certainly, any simply-linked geometric form, with any permissible unfilling of an aperture, becomes a figure with a complex linkage.

In our task here, we do not enter into an analysis of all the possible geometric forms of electromagnetic systems. We limit ourselves just to a consideration of a method of analysis which is applicable, with the proper specifications being made, to the analysis of any form and of any type of linkage.

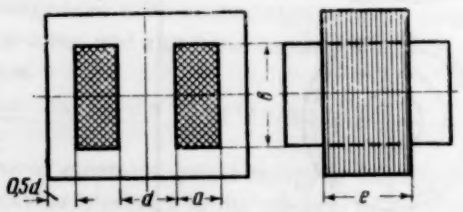

Fig. 2. Geometric form of a three-core electromagnetic system.

For this purpose, as an example, we consider the geometric form of an electromagnetic system as shown in Fig. 2.

As is clear, the given form has four dimensions, the absolute values of which are denoted by a, b, d, and e.

To obtain relative dimensions, we relate all the remaining dimensions to one selected absolute dimension. For example, as such a fundamental dimension, we take the width a of the magnetic circuit's aperture. In this case, the relative dimensions of height, width of core section, and magnetic circuit thickness will equal, respectively,

$$\frac{b}{a} = c, \quad \frac{d}{a} = m, \quad \frac{e}{a} = k.$$

With the notation chosen the cross sections and lengths of the windings and magnetic circuit will equal

$$S_м = a^2 c, \quad S_c = a^2 mk, \tag{9}$$

$$L_м = 2a(m + k + 2), \quad L_c = 2a(m + c + 1). \tag{10}$$

Knowing the cross sections and the lengths, we determine the volumes of the windings and magnetic circuits and then, by adding these volumes, we find the quantity which we have called the absolute magnitude of the electromagnetic system. For this, we get

$$Q = 2a^3 [c(m + k + 2) + mk(m + c + 1)]. \tag{11}$$

To determine the value of the parameter which we have taken as the fundamental one, we solve the last equation for a:

$$a = \sqrt[3]{\frac{Q}{2[c(m + k + 2) + mk(m + c + 1)]}}. \tag{12}$$

We now have all the data necessary for determining, by (7), the geometric constant of the electromagnetic system under consideration. This constant equals

$$\xi = \frac{mck}{(m + k + 2)(m + c + 1)\sqrt[3]{16^2 [c(m + k + 2) + mk(m + c + 1)]^2}} \tag{13}$$

The problem of finding the optimal proportions of electromagnetic systems does not have a unique solution. In each particular case it is necessary to take into account the concrete conditions of use of electromagnetic energy and the economic requirements. This bears first of all on the ratio of the volumes of the electromagnetic system's active materials. By bearing this fact in mind, we should seek, not the general case of the maximum of the geometric constant of (13), but its particular cases, each of which corresponds to some previously given ratio of the aforementioned volumes. With the notation we have adopted, the ratio of the volume of the magnetic circuit to that of the windings equals

$$\frac{Q_c}{Q_м} = \frac{mk(m + c + 1)}{c(m + k + 2)}. \tag{14}$$

By solving this last equation for one of the relative dimensions, and then substituting the value obtained in (13), we would have the capability, by computing the partial derivatives with respect to the relative dimensions, to determine the optimal values of these dimensions, which would correspond to the maximum geometric constant for the previously given constant ratio of the volumes of the active materials. However, this path to a solution leads to significant complexity, so that we shall solve this problem by finding the maximum of the

TABLE 1

m	0.0	0.25	0.5	1.0	1.5	2.0	3.0	10.0	15.0
k	3.0	3.0	2.84	3.0	3.16	3.45	3.9	6.95	10.0
c	0.5	1.0	1.3	2.0	2.67	3.36	4.7	15.0	22.0
Q_c . %	0.0	24.4	36.5	50.0	58.0	63.5	71.0	86.5	90.5
$\xi \cdot 10^3$	0.0	2.76	4.48	4.78	4.85	4.55	4.12	2.2	1.51

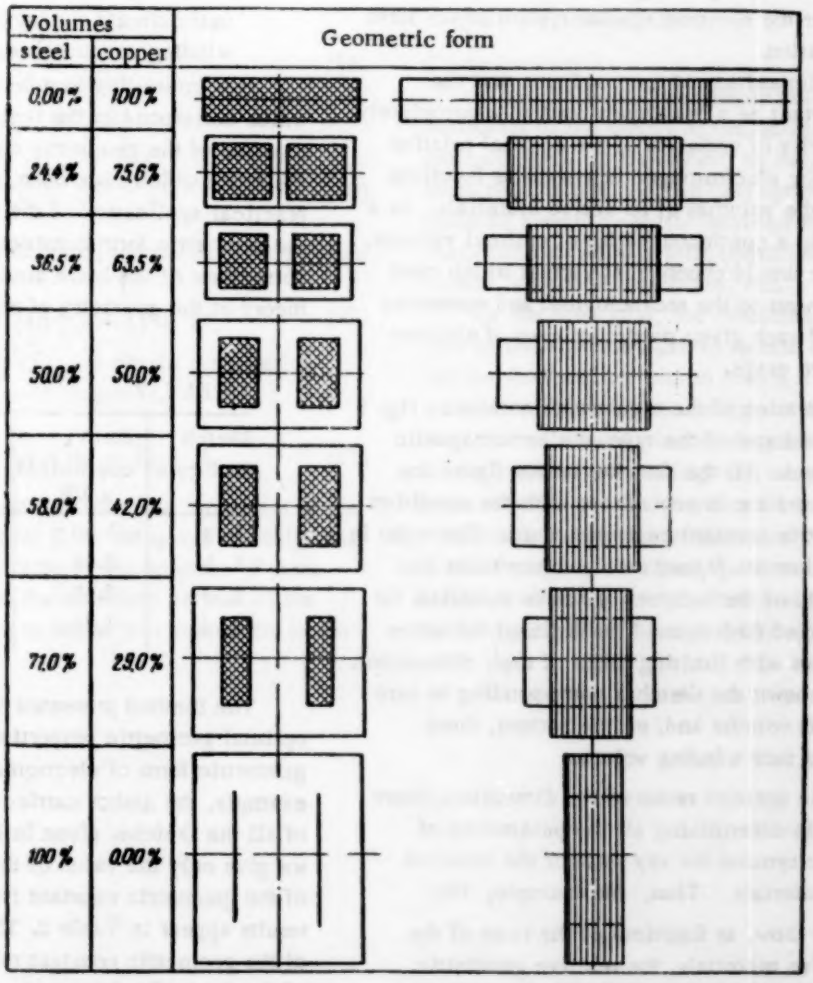

Fig. 3. Series of optimal geometric forms of three-core electromagnetic systems for various ratios of winding and magnetic circuit volumes.

geometric constant of interest to us for a constant value of one of the relative dimensions, which is equivalent to the condition that the ratio of the volumes be constant, although the magnitude of this ratio itself is not given explicitly in this case. As the constant quantity, we take the relative dimension $\underline{m}$, since the ratio of the winding and magnetic circuit volumes depends most heavily on this dimension.

By analyzing (13) for an extremum by the method of partial derivatives, we obtain the following optimal values of the relative dimensions $\underline{k}$ and $\underline{c}$ for a constant value of dimension $\underline{m}$:

$$k = \frac{m+2}{4}\left[1 + \sqrt{1 + \frac{24c}{m(m+c+1)+c}}\right], \quad (15)$$

$$c = \frac{m+1}{4}\left[1 + \sqrt{1 + \frac{24mk}{m+k+2+mk}}\right]. \quad (16)$$

Joint solution of (15) and (16) leads to cumbersome computation, so that we solve this problem by the method of successive approximations. The results are given in Table 1, where we also give the volume of the magnetic circuit as a percentage of the total volume of active material plus the corresponding maximum of the geometric constant for the electromagnetic system of the form under consideration.

Thus, the imposition of the condition that the geometric constant be a maximum leads to a completely definite regularity of variation of the optimal relative dimensions of the electromagnetic system as functions of the ratio of the volumes of its active materials. As a result, we obtain a continuous series of optimal variants, from which one should choose that variant which most completely answers to the technological and economic requirements of each given particular case of electromagnetic system usage.

As an illustration of the regularities obtained, Fig. 3 shows a series of forms of the type of electromagnetic system considered. All the sketches on the figure are drawn to scale and are in accordance with the condition that the geometric constant be a maximum. The order in which the sketches are placed on the figure takes into account the ratio of the volumes of active materials for a constant value of their sum. The limits of the series show the sketches with limiting ratios of their dimensions. On the top are shown the sketches corresponding to zero magnetic circuit volume and, on the bottom, those corresponding to zero winding volume.

Knowing the optimal ratios of the dimensions, there is no difficulty in determining all the parameters of electromagnetic systems for any ratio of the volumes of the active materials. Thus, for example, the curves of Fig. 4 show, as functions of the ratio of the volumes of active materials, the relative geometric conductances of the windings and magnetic circuit as well as their product, i.e., the geometric constant of the electromagnetic system under consideration.

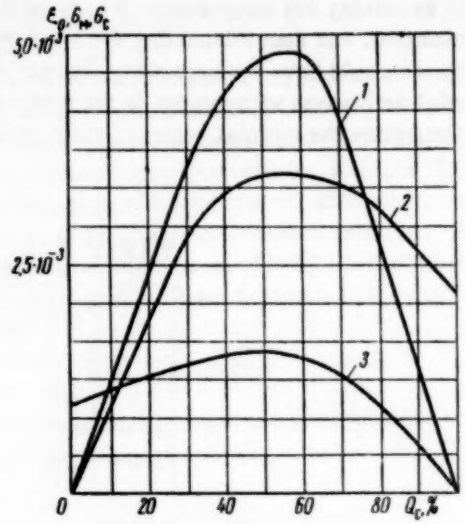

Fig. 4. Geometric conductance of windings and magnetic circuit plus the geometric constant of a three-core electromagnetic system as functions of the ratio of winding and magnetic circuit volumes. 1 is the geometric constant, 2 is the magnetic circuit conductance, and 3 is the winding conductance.

It is interesting to note that the geometric ratios which correspond to the regions of the maximum of the maxima of the geometric constant (Figs. 3 and 4) are the ratios which have been most widely used in the practical application of the electromagnetic systems of the geometric form considered. This substantiates the correctness of the basic assumptions we have made for the theory of the geometry of electromagnetic systems.

TABLE 2

Sketch on figure	Form coefficient $\times 10^3$	Sketch on figure	Form coefficient $\times 10^3$
1. a	3.40	1. e	6.70
1. b	2.46	1. f	5.00
1. c	3.62	1. g	8.00
1. d	4.85	1. h	6.40

The method presented here for the analysis of optimal geometric proportions is applicable to any geometric form of electromagnetic systems. Thus, for example, the author carried out the corresponding analysis of all the sketches given in Fig. 1. Omitting similarities, we give only the value of the maximum of the maxima of the geometric constant for each of these sketches. The results appear in Table 2. The maximum of the maxima of the geometric constant may serve as the characteristic of the form of an electromagnetic system, for which reason we call this parameter the "form coefficient" of an electromagnetic system.

Economics of Electromagnetic Systems

In choosing some variant from the series of optimal design variants of an electromagnetic system (cf., for example, Fig. 3) for some particular case, one must take into account, not only technological, but also economic requirements.

Thus, economic considerations, while having no effect on the general regularities of the geometry of electromagnetic systems, have an effect, in each particular case, on the system's geometric proportions. It should be kept in mind with this, that the basis of the economic influence is the difference in prices of the winding and of the magnetic circuit materials of the electromagnetic system. With identical prices per unit volume of these materials, the economic requirements would cease to be operative.

The cost of an electromagnetic system, defined by the costs of its active materials, equals

$$A = Q_M t_M + Q_c t_c, \tag{17}$$

where Q_M and Q_c are the winding and magnetic circuit volumes, and t_M and t_c are the unit volume costs of, respectively, the windings and the magnetic circuit.

The ratio of unit volume cost of winding to that of magnetic circuit equals

$$t_0 = \frac{t_M}{t_c}. \tag{18}$$

By introducing the coefficient

$$n = \frac{Q_M}{Q_M + Q_c} = \frac{Q_M}{Q}, \tag{19}$$

and by taking (18) into account, we transform Expression (17) to the form

$$A = Qt_c[n(t_0 - 1) + 1]. \tag{20}$$

By dividing (20) by Qt_c, we obtain the relative cost of the electromagnetic system, i.e.,

$$A_0 = \frac{A}{Qt_c} = n(t_0 - 1) + 1. \tag{21}$$

As is clear, the relative cost when the prices of the active materials are equal (i.e., for $t_0 = 1$) is unity, and does not depend on the ratio of the volumes of these materials. In this case, the optimum variant of the electromagnetic system to use is that one which corresponds to the maximum geometric constant. When these prices are not equal, a change in the ratio of the volumes of active materials changes both the geometric constant of the electromagnetic system and its cost. In this case, to choose the optimum variant of electromagnetic system to be used, one should aim at the minimum ratio of the relative cost to the geometric constant, i.e.,

$$A_\xi = \frac{A_0}{\xi} = \frac{n(t_0 - 1) + 1}{\xi}. \tag{22}$$

Thus, for example, from the data of Table 1, if no account is taken of differences in active material costs, i.e., for $t_0 = 1$, the optimal variant of the electromagnetic system to use is the one for which the winding volume is 42 % of the total volume of active materials. If the price of the winding material is, for example, 20 times as high as the magnetic circuit material, then from the data of Table 1 and from (22), we find that the optimal variant for this case is the one where the winding volume is 24% of the total volume of active material in the electromagnetic system.

What has already been said sufficiently adumbrates the principal interrelationships which exist between geometric proportions and the economics of electromagnetic systems.

Conclusion

In this paper we touched on only the most general postulates of the theory of the geometry of electromagnetic systems. In the future, by basing ourselves on these regularities, we can find optimal relationships for standard electromagnetic devices: transformers, electromagnetic relays, magnetic amplifiers, induction relays, chokes, electrical machines, etc.

As the final goal, the consideration of any configuration of the electromagnetic system of any electromagnetic device should allow one to obtain a continuous series of optimal variants of the configuration considered, the sequence of these variants being determined by the ratio of the volumes of windings and magnetic circuit. The study of such a series provides the capability of establishing the interdependencies of the relative dimensions and the technical-economic parameters which are of decisive value in choosing the physical design of the electromagnetic device from this series in each specific case.

RELAY WINDING OVERHEATING AND HEAT TRANSMISSION COEFFICIENT AS FUNCTIONS OF AMBIENT AIR TEMPERATURE

M. I. Vitenberg

(Leningrad)

Translated from Avtomatika i Telemekhanika, Vol. 21, No. 3, pp. 384-392, March, 1960
Original article submitted November 30, 1959

The paper deals with relay winding overheating and heat transmission coefficient as functions of ambient air temperature. Empirical formulas are derived for determining the magnitude of relay winding overheating and relay heat transmission coefficient.

1. Winding Overheating

The excess of relay winding temperature over the ambient medium's temperature is ordinarily determined under normal conditions for an air temperature of +20°C. However, relays are frequently used under conditions where there are large oscillations of the ambient temperature – from -60 to +60°C– and special types of relays are used at temperatures up to +125°C and higher.

As is well known, with a raising of the winding temperature the heat transmission coefficient (specific heat transmission) increases, since heat transmission by convection depends on a fractional power of the overheating temperature, while heat transmission by radiation is proportional to the difference of the fourth powers of the absolute temperatures of the winding and of the ambient air. Therefore, with identical magnitudes of power dissipation, overheating of a relay winding is decreased as the ambient air temperature increases.

The working life of relay insulation is determined by the greatest magnitude of the working temperature. Consequently, it is necessary to know, as accurately as possible, the relay winding overheating for the highest ambient air temperature. Measurement of relay winding overheating with increased temperature is ordinarily carried out experimentally in a thermostat, for which a great deal of time is required. Moreover, these measurements are usually distinguished by their low accuracy, due to the significant relative errors in

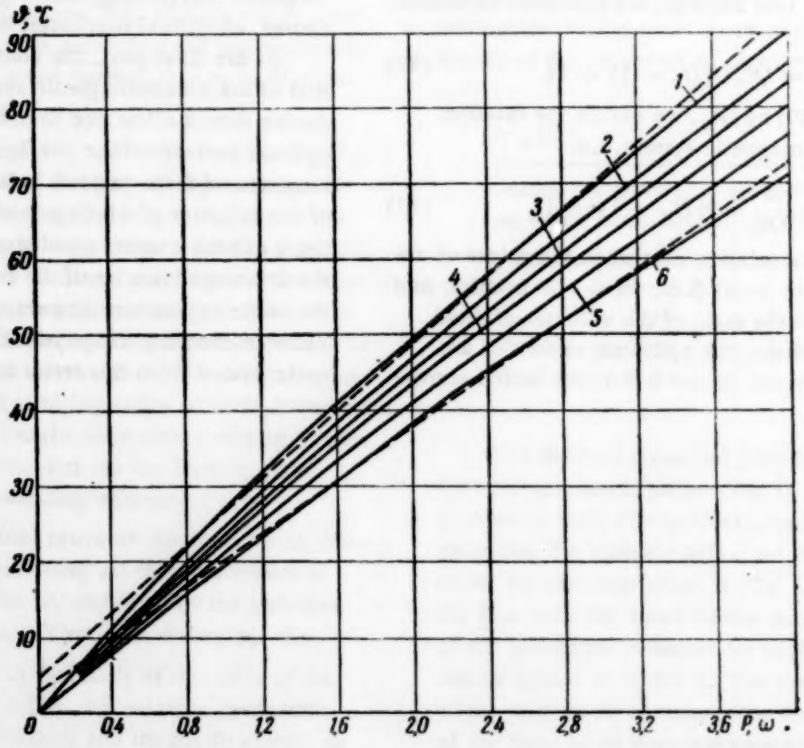

Fig. 1. *1* — $\vartheta_0 = 21°$ C, *2* — $\vartheta_0 = 44°$C, *3* — $\vartheta_0 = 65°$ C, *4* — $\vartheta_0 = 84°$ C, *5* — $\vartheta_0 = 105°$ C, *6* — $\vartheta_0 = 141°$ C.

determining the winding overheating temperature for an increased temperature of the ambient air.

Thus , for example, with ambient temperature of 100°C and winding overheating temperature of 30°C, an error of 2% (2°C) , in measuring the temperatures of winding and air gives a relative error of about 13% in determining the temperature of the relay winding overheating.

Relay winding overheating temperature can be found more accurately by analytical means.

Figure 1 gives curves showing excess of relay winding temperature over ambient temperature as a function of the power applied for small-size-type RMU relay, taken off experimentally for various ambient temperatures up to +141°C .

The measurements were carried out in a 500-watt dessicator with automatic temperature regulation within the limits of +30 to +200°C with an error no greater than ± 3 % . The working chamber of the dessicator had a diameter of 300 mm and a length of 290 mm.

The dimensions of the relay types tested were: for type RMU, 24.7 x 38.5 x 41 mm, for type RÉS10, 11.1 x x 16.5 x 26 mm and, for type RKN, 25.6 x 56.5 x 97 mm.

The relay weights were: for type RÉS10, 6 g, for type RMU, 70 g and, for type RKN, 290 g.

The relay specimens had wire windings with brand PÉTKM heat-resistant insulation. The winding temperatures were measured by a copper-constantan thermocouple. To eliminate heat leakage at the relay supports, the relays were suspended by a fine wire in the center of the dessicator.

The ventilation apertures of the dessicator were tightly covered by asbestos plugs, and were used for the outlet of the conductors and the thermocouple.

The air temperature in the dessicator was also measured by a thermocouple,which was placed at the level of the specimen relay at a distance of about 30 mm from it. As protection against direct radiation, the thermocouple's junction on the relay's side was shielded by a small fragment of white paper. For each value of supplied power, the relay was immersed for not less than an hour in the given ambient temperature. The actual temperature oscillations in the dessicator did not exceed 2 %. It is clear from Fig. 1 that, in the limits of overheating temperature from 20 to 70°C, the curves differ very little from the straight lines drawn with dashes (the error does not exceed ±1°C). In Fig. 1, the dashed straight lines are shown only for the extreme curves, so as not to complicate the figure.

In the aforementioned limits, the relay winding overheating curves can be approximated by the formula

$$\vartheta = a + bP, \qquad (1)$$

where a is the amount of overheating intercepted by the straight line on the axis of ordinates, and b is the tangent of the slope of this line.

TABLE 1

Ambient temperature θ_0, °C	a, °C	b, °C/ω
21	4.7	21.7
44	4.3	20.9
65	3.8	20.4
84	3.6	19.3
105	3.2	18.6
141	2.8	17.2

The values of the quantities a and b for relay type RMU for different values of ambient air temperature, determined graphically from Fig. 1, are given in Table 1.

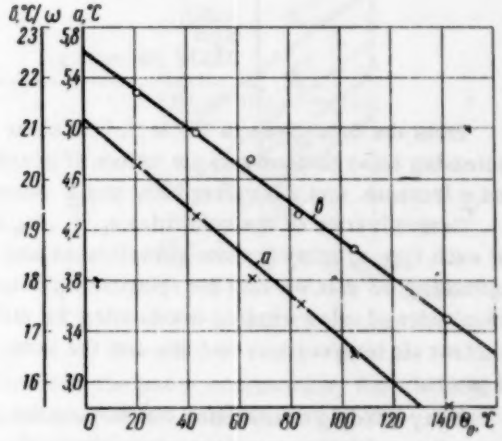

Fig. 2.

From the data of this table, the dependencies of a and b on the ambient temperature were constructed, as shown in Fig. 2. These dependencies are straight lines, which can be expressed by the formulas

$$a = a_0 - c\theta_0, \qquad (2)$$

$$b = b_0 - d\theta_0, \qquad (3)$$

where a_0 and b_0 are the values of a and b for an ambient temperature of 0°C , and c and d are the tangents of the slopes of these lines.

By substituting in (1) the values of a and b from (2) and (3), we obtain a general expression for determining the relay winding overheating temperature as a function of the supplied power and the ambient temperature :

$$\vartheta = a_0 - c\theta_0 + (b_0 - d\theta_0)\,P. \qquad (4)$$

This formula gives sufficient accuracy only in the limits of overheating values from 20 to 70°C, which are the ones most frequently occurring .

The largest errors are obtained at the initial portion of the curve, for overheating temperatures less than 20°C. The accurate determination of such overheating temperatures ordinarily has no practical value.

From Fig. 2 we find the values of quantities a_0, c , b_0, and d for relay type RMU: a_0 = 50.7°C, c= 0.0175 , b_0 = 22.54°C/watt and d = 0.038.

Consequently, for type RMU relay, winding overheating is expressed by the following formula:

$$\vartheta = 5{,}07 - 0{,}0175\,\theta_0 + \\ + (22{,}54 - 0{,}038\,\theta_0)\,P. \qquad (4a)$$

By an analogous procedure, we found the values of the quantities a_0, c, b_0, and d for miniaturized type RÉS10 relay (without cover) and normal type RKN relay.

The values of these quantities are given in Table 2.

TABLE 2

Relay type	S_k, cm²	a_0, °C	c	b_0, °C/cm	d
RÉS10 (without cover)	3.2	6,3	0.0171	71.6	0.126
RMU	22.6	5,07	0.0175	22.54	0.038
RKN	60.2	8,36	0.0238	8.85	0.0167
RÉS10 (in cover)	3.2	3,52	—0.006	91.5	0.103

From the data given in Table 2, it is clear that, with increasing relay dimensions, the values of quantities b_0 and c increase, and the values of b_0 and d decrease.

Determination of the quantities a_0, c, b_0, and d for each type of relay is quite complicated and time-consuming, so that we find the relationship between the magnitudes of relay winding overheating for different ambient air temperatures and one and the same magnitude of power.

Relay winding overheating for one and the same power P and different ambient temperatures θ_{01} and θ_{02} will equal

$$\vartheta_1 = a_0 - c\theta_{01} + (b_0 - d\theta_{01})\,P \text{ and}$$

$$\vartheta_2 = a_0 - c\theta_{02} + (b_0 - d\theta_{02})\,P,$$

from which we find the following expression for relay winding overheating for ambient temperature θ_{02}:

$$\vartheta_2 = \vartheta_1 - (c + Pd)(\theta_{02} - \theta_{01}) = \\ \vartheta_1[1 - \beta(\theta_{02} - \theta_{01})], \qquad (5)$$

where

$$\beta = \frac{c + Pd}{\vartheta_1}.$$

Table 3 gives the values of the temperature overheating coefficient β for various values of power in the winding, and the corresponding relay winding overheating temperatures of relay types RMU, RÉS10 and RKN for these values of power and for ambient temperature +20°C, computed by means of (4) and (6).

Figure 3 shows the curves, constructed from the data of Table 3, of the temperature overheating coefficient

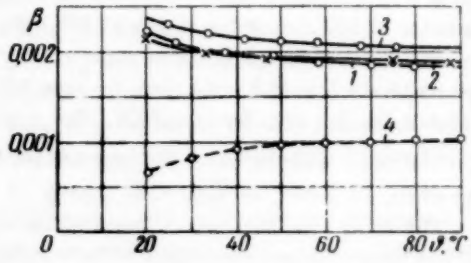

Fig. 3. 1) Relay type RMU; 2) relay type RÉS10 without cover; 3) relay type RKN, 4) relay type RÉS10 in cover.

β as a function of the winding overheating temperature of these types of relays for $\theta_0 = +20°C$. For comparative purposes, the dashed line of Fig. 3 shows the approximate curve for type RÉS10 relay (with cover). It follows from Fig. 3 that the curves for the coefficient β for relay types RMU and RÉS10 (without cover) virtually coincide, and the value of coefficient β for type RKN relay is about 10 % larger.

Type RÉS10 relay, protected by a thin aluminum cover, has a coefficient β of about half the size, due to the poor thermal contact between the relay's magnetic

TABLE 3

Relay type								
RMU			RÉS10 (without cover)			RKN		
P, ω	β	ϑ, °C	P, ω	β	ϑ, °C	P, ω	β	ϑ, °C
0.7	0.00219	19.86	0.2	0.00214	19.77	2	0.00229	24.92
1.0	0.00209	26.5	0.4	0.002005	33.58	3	0.00221	33.43
1.5	0.00199	37.4	0.6	0.001955	47.4	4	0.00216	41.95
2.0	0.00194	48.29	0.8	0.00193	61.22	5	0.00213	50.46
2.5	0.00190	59.22	1.0	0.001905	75.03	6	0.0021	59.0
3.0	0.00188	70.1	1.2	0.001895	88.86	7	0.00208	67.5
						8	0.00207	76.01

circuit and the cover (the relay's pedestal is made of plastic). With air-tight relays having thick steel covers and fastened to a metallic base (pedestal), the magnitude of coefficient β is about the same as for relays unprotected by covers, since the winding of an air-tight relay generally has good thermal contact with the magnetic circuit and with the cover. As the relay winding overheating temperature varies within the limits of 20 to 70°C [the limits of applicability of (4)], the size of coefficient β varies comparatively little (by not more than ± 10 %).

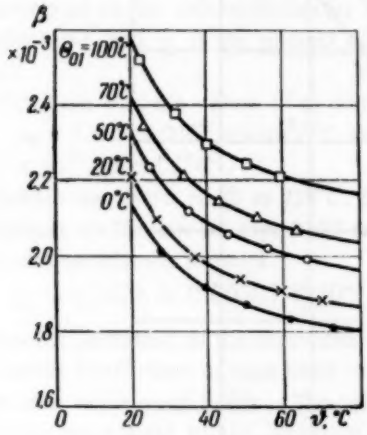

Fig. 4.

The magnitude of coefficient β depends on the initial temperature of the ambient air. Figure 4 gives the curves for the coefficient β as a function of winding overheating for various ambient air temperatures for type RMU relay. By means of these curves, the curves shown on Fig. 5 of coefficient β as a function of ambient air temperature for various heating temperatures were constructed. The curves of Fig. 5, for β within the limits of 0 to 100°C, are practically straight lines, so that coefficient β as a function of initial ambient air temperature with average overheating temperature (ϑ = 40°C) can, for small-size relays (without covers), be expressed by the formula

$$\beta = (1.91 + 0.0036\theta_{01})\,10^{-3}. \qquad (6)$$

Consequently, with a constant magnitude of power, if one knows the winding overheating temperature of small-size relays (without covers) for the ambient temperature θ_{01}, one can, with an accuracy sufficient for practical purposes, determine the overheating of these relays' windings for another ambient temperature θ_{02} by means of the formula

$$\vartheta_2 \approx \vartheta_1 [1 - (1.91 + 0.0036\,\theta_{01})\,10^{-3}\,(\theta_{02} - \theta_{01})]. \qquad (7)$$

If the initial ambient temperature is θ_{01} = 20°C, then

$$\vartheta_2 \approx \vartheta_1 [1 - 0.00198\,(\theta_{02} - 20)]. \qquad (7a)$$

Thus, with an increase of ambient air temperature by 10°C (within the limits of 0 to 100°C), the winding overheating of the relay (without cover), for one and the same value of power, is decreased by about 2%.

Measurements carried out on different types of relays showed that this formula is also valid for higher temperatures of the ambient air (up to 140°C).

2. Heat Transmission Coefficient

The magnitude of the average (nominal) heat transmission coefficient of windings of electromagnetic relays and dc apparatus can be determined from the experimental data by means of the formula [1]

$$q_1 = \frac{P}{\vartheta S_k}, \qquad (8)$$

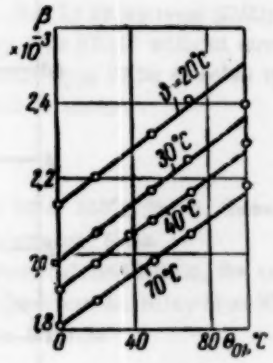

Fig. 5.

where P is the power consumed by the winding, ϑ is the overheating of this winding, and S_k is the computed cooling surface of the relay winding.

Figure 6 gives the experimental curves which show the mean heat transmission coefficient of the winding of a type RMU relay as a function of its overheating for various ambient temperatures. Within the limits of an overheating temperature of 20 to 70°C, these curves differ very little from straight lines. The large scattering of points for overheating values less than 20°C is explained by the inaccuracy of measurements of small temperature drops.

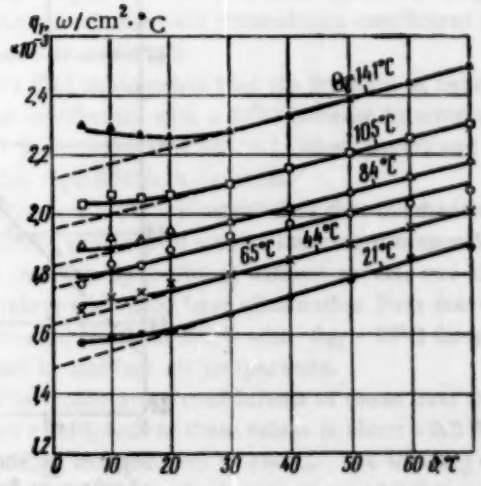

Fig. 6.

a

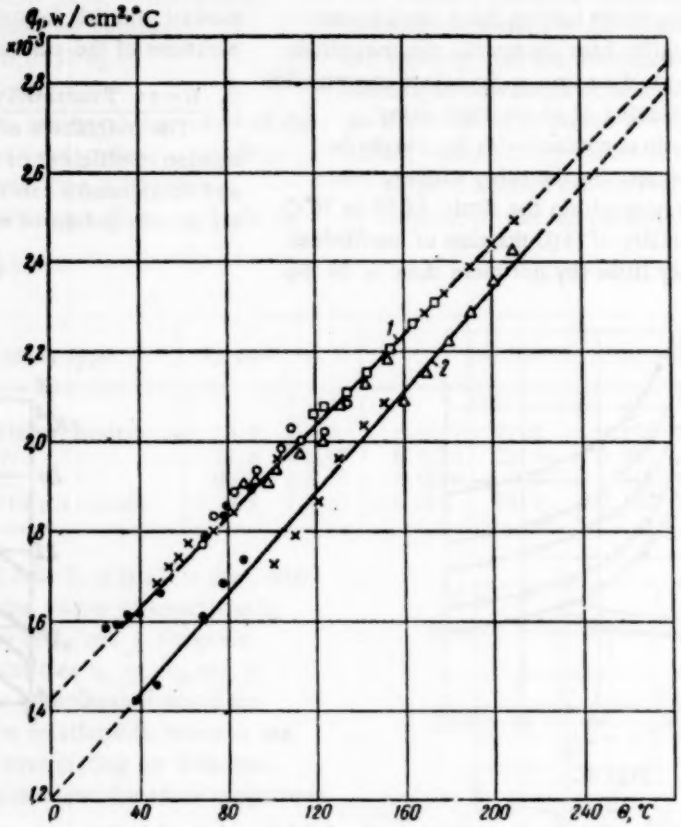

b

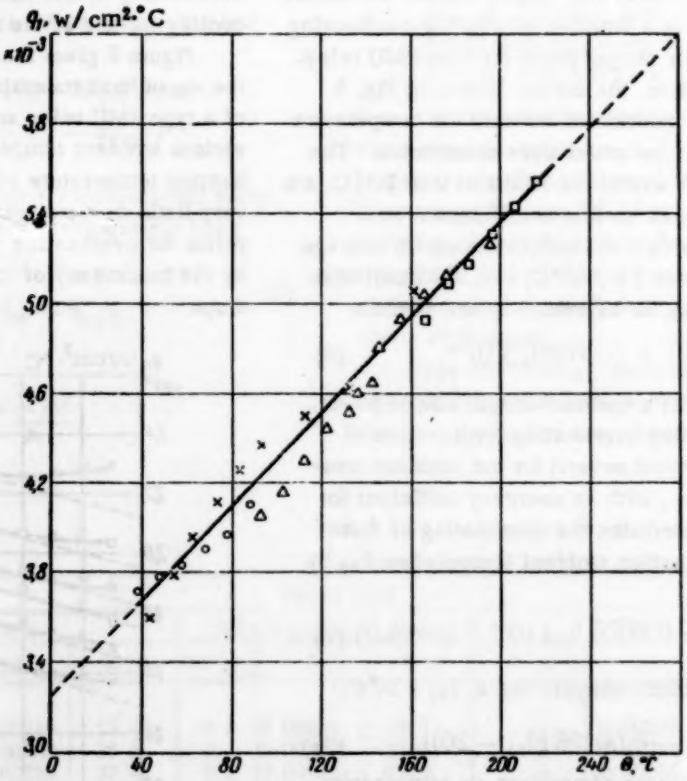

Fig. 7. a shows the mean heat transmission coefficient of relays as functions of winding temperature: 1 is for relay type RMU and 2 is for relay type RKN; b shows the same thing for relay type RÉS10 (without cover).

To elucidate the relationship between relay winding heat transmission and temperature, Fig. 7 shows the constructed relationship of the average heat transmission coefficient of relay windings and the temperature of these windings. Within the limits of 30 to 210°C, this relationship is virtually a linear one which may be expressed by the formula

$$q_1 = q_0 + e\theta = q_0 + e(\theta_0 + \vartheta), \qquad (9)$$

where q_0 is the magnitude of the heat transmission coefficient, intercepted on the axis ordinates by the extension of the straight line, and e is the tangent of the slope of this line.

From Fig. 7 we find the values of q_0 and e for type RMU relay: $q_0 = 1.422 \times 10^{-3}$ w/cm²/°C and $e = 0.00507 \times 10^{-3}$ w/cm²/°C².

Thus, within the limits of 30 to 210°C, the mean heat transmission coefficient for type RMU relay is expressed by the approximate formula

$$q_1 = (1.422 + 0.00507\,\theta)\,10^{-3}. \qquad (9a)$$

The greatest deviation of the individual values of heat transmission coefficient of type RMU relay from the straight line does not exceed 2.2%. The values of q_0 and e for relay types RMU, RÉS10, and RKN are given in Table 4.

TABLE 4

Relay type	q_0, w/cm²·°C	e, w/cm²·°C
RÉS10 (without cover)	$3.24 \cdot 10^{-3}$	$0.01065 \cdot 10^{-3}$
RMU	$1.422 \cdot 10^{-3}$	$0.00507 \cdot 10^{-3}$
RKN	$1.198 \cdot 10^{-3}$	$0.00567 \cdot 10^{-3}$
RÉS10 (in cover)	$2.77 \cdot 10^{-3}$	$0.0045 \cdot 10^{-3}$

The magnitude of the mean heat tramission coefficient for different temperatures θ_1 and θ_2 of the relay winding will be $q_1' = q_0 + e\theta_1$ and $q_1'' = q_0 + e\theta_2$,

from which we find the following expression for the mean heat transmission coefficient of the relay winding for temperature θ_2:

$$q_1'' = q_1' + e(\theta_2 - \theta_1) = q_1'[1 + \gamma(\theta_2 - \theta_1)], \qquad (10)$$

where

$$\gamma = \frac{e}{q_1'}. \qquad (11)$$

Figure 8 shows the curves of the transmission coefficient of the mean heat transmission coefficient γ as a function of winding temperature for relay types RMU, RÉS10, and RKN, computed by means of Formulas (9a) and (11).

It follows from Fig. 8 that the curves of $\gamma = \gamma(\theta)$ for small-size relay types RMU and RÉS10 (without cover) differ very little from each other, and that the value of coefficient γ for type RKN relay is about 25% larger. Type RÉS10 relay, protected by an aluminum cover, has a value of coefficient γ which is about half the size.

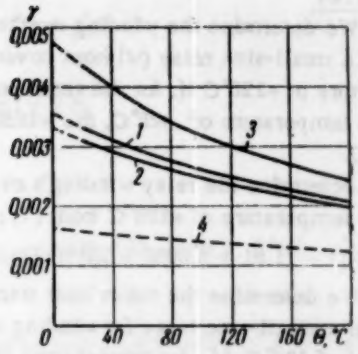

Fig. 8. 1) Relay type RMU; 2) relay type RÉS10 without cover; 3) relay type RKN; 4) relay type RÉS10 in cover.

In the limits of 20 to 160°C for θ, these curves differ very little from straight lines.

In the aforementioned limits, the coefficient as a function of temperature for relay type RMU may be expressed by the formula

$$\gamma = (3.45 - 0.0079\,\theta_1)\,10^{-3}. \qquad (12)$$

Thus, if we know the magnitude of the heat transmission coefficient of small-size type RMU relays (without cover) for winding temperature θ_1, we can, with an accuracy sufficient for practical purposes, determine the heat transmission coefficients of these relays for other winding temperatures θ_2 (in the limits of 20 to 160°C) from the following approximate formula:

$$q_2 \approx q_1[1 + (3.45 - 0.0079\,\theta_1)\,10^{-3}(\theta_2 - \theta_1)]. \qquad (13)$$

If the initial winding temperature is $\theta_1 = 50$°C, then

$$q_2 \approx q_1[1 + 0.00306\,(\theta_2 - 50)]. \qquad (13a)$$

Formula (13a) shows that with a 10°C increase in winding temperature of small-size type RMU relays (without cover), the heat transmission coefficient is increased by about 3%.

We find analogously that the increase in heat transmission coefficient with a 10°C increase in temperature is 2.87 % for relay type RÉS10 (without cover) and 1.5% for relay type RÉS10 in its cover.

Thus, our work has established that overheating temperature of windings of small-size electromagnetic relays (weights up to 300 g) without covers, and also airtight relays with good heat elimination from the windings, is decreased by about 0.2 % with $\theta_{01} = 20$°C for a 1°C increase in ambient air temperature.

The temperature coefficients of mean heat transmission coefficient of these relays is about + 0.3 %/°C for winding temperatures of +50°C. The winding overheating temperature of relays protected by thin covers having poor thermal contact with the windings, is decreased by about a 1%/°C rise in ambient temperature.

Examples

1. We determine the winding overheating temperature of a small-size relay (without cover) for ambient temperature of +125°C if, for the same power and for ambient temperature of +25°C, the winding overheating was 50°C.

We determine the relay winding's overheating with ambient temperature of +125°C from (7):

$$\vartheta_{125} \approx 50\,[1 - (1.91 + 0.0036 \times 25)\,10^{-3}\,(125 - 25)] = 40°\text{C}.$$

2. We determine the mean heat transmission coefficient of a small-size relay for winding temperatures of 40 and of 100°C, if, for temperature 50°C, the heat transmission coefficient equals 1.5×10^{-3} w/cm²/°C.

We determine the relay's heat transmission coefficient by (13):

$$q_{40} \approx 1.5 \times 10^{-3}\,[1 + (3.45 - 0.0079 \times 40)\,10^{-3}\,(40 - 50)] = 1.45 \times 10^{-3}\ \text{w/cm}^2\cdot°\text{C}$$

and

$$q_{100} \approx 1.5 \times 10^{-3}\,[1 + (3.45 - 0.0079 \times 100)\,10^{-3}\,(100 - 50)] = 1.7 \times 10^{-3}\ \text{w/cm}^2\cdot°\text{C}$$

LITERATURE CITED

1. M. I. Vitenberg, "Determination of winding heating of electromagnetic relays," Avtomatika i Telemekhanika 19, 11 (1958).

CERTAIN QUESTIONS IN THE THEORY OF MAGNETIC AMPLIFIERS LOADED BY DC DRIVES

L. V. Safris

(Rostov-on-Don)

Translated from Avtomatika i Telemekhanika, Vol. 21, No. 3, pp. 393-401, March, 1960
Original article submitted November 2, 1959

Equations are derived which characterize the basic modes and peculiarities of operation of a saturated-reactor magnetic amplifier loaded by a dc drive. A simplified method of designing such an amplifier is given.

Introduction

The operation of a magnetic amplifier loaded by a dc motor (MA-M) has its peculiar features. They stem from the fact that the motor, as an energy consumer, presents itself as an impedance and a variable counter-emf whereby, with amplifier control, there is an action on this emf. The presence of the amplifier leads, naturally, to a change in the drive's characteristics. In [1], individual questions in the analysis of such schemes were touched on for one special case. In [2], certain design approaches were adduced. At the same time, there is interest in establishing general regularities characterizing the operation of an MA-M system when its elements are connected in accordance with the scheme of Fig. 1. In the present paper we attempt to fill this void partially. We note that the analogous problem, as applied to a rotary amplifier, and also for the case when control of asynchronous motors is implemented by means of magnetic amplifiers, received consideration in [3-5].

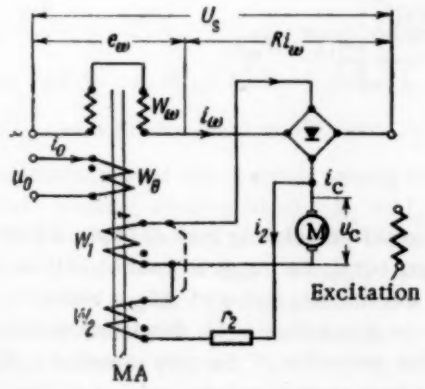

Fig. 1.

As the basis of our investigation, we take the linearization method described in [6, 7]. This method turns out to be particularly effective if one may make the two following assumptions: a) the characteristics of simultaneous core magnetization by constant and variable fields may be approximated by straight line segments ; b) the load curve, expressing the dependency between the variable component of the saturated reactor emf and the load voltage can be replaced by a straight line.

On the strength of the first assumption, we shall suppose that, for amplifier operation, we shall use a linear domain of the magnetization characteristic of the cores, which are made of material of sufficiently high quality. Under these conditions, the increment of the mean value of the working windings' ac current ΔI_ω can be found from the expression [6]

$$\Delta I_\omega = S\Delta I_0 + \frac{\Delta E_\omega}{R_i}. \qquad (1)$$

Here, I_0 is the control current, E_ω is the mean value of the ac windings' emf, S is the slope of the characteristic, and R_I is the amplifier's internal impedance. The last two parameters are defined as follows:

$$S = \sigma \frac{W_0}{W_\omega}, \qquad (2)$$

$$R_i = \frac{\omega \mu_i W_\omega^2 Q}{l}. \qquad (3)$$

W_0 is the number of turns in the control winding, W_ω is the number of turns in the ac winding, Q is the active cross section of the two cores, l is the mean length of the magnetic circuit, $\sigma = \frac{\partial H_\omega}{\partial H_0}$, $\mu_i = \frac{\partial B_\omega}{\partial H_\omega}$, H_0 is the constant (monotonic) component of the magnetic-field strength, H_ω is the "mean" value of the variable component of the magnetic-field strength :

$$H_\omega = \frac{W_\omega I_\omega}{l}, \qquad (4)$$

and B_ω is the "mean" value of the variable component of the magnetic induction:

$$B_\omega = \frac{E_\omega}{\omega W_\omega Q}. \qquad (5)$$

The second assumption derives from the following considerations. It was established in [8] that, with amplifier operation on the counter-emf, the load curve, as a function of material quality, can deviate from the straight line on both sides.

By taking this circumstance into account, as well as the fact that it is desirable to obtain simple graphic expressions, in the first instance mirroring the qualitative side of the phenomena, we shall assume that $E_\omega = U_s - (E_c + RI_\omega)$ and, consequently,

$$-\Delta E_\omega = \Delta E_c + R\Delta I_\omega. \qquad (6)$$

Here, U_s is the mean value of the supply voltage, E_c is the motor's counter-emf, R is the equivalent active impedance of the ac circuit. Figure 2 gives a geometric interpretation of these assumptions. The family of magnetization curves $H_\omega = f_1(H_0, B_\omega)$ is replaced by the dashed-line parallel segments. The linear domain is marked by the coordinates of points 1 and 2 (B_1, H_1 and B_2, H_2). In correspondence with (6), the increments of voltage and emf drops occurring in the system are represented by segments (ab, bc, ce, etc.) whose projections on the axis of abscissas sum arithmetically to emf E_ω.

we can write (6) in the following way:

$$-\Delta E_\omega = \Delta n C_E + R\frac{\Delta M}{C_M}. \qquad (9)$$

Here, $I_c = I_\omega$ is the motor armature's current, $R = r_c + r_a + r_1$, r_c is the impedance of the armature winding and motor brushes, r_1 is the impedance of the amplifier's ac winding.

By substituting (7), (8), and (9) in (1), we obtain

$$\Delta n = \frac{k}{C_E}\Delta I_0 - \frac{\Delta M}{C_M C_E}(R_i + R) =$$

$$K_c \Delta I_0 - \frac{1}{K_r}\Delta M, \qquad (10)$$

where

$$k = SR_i.$$

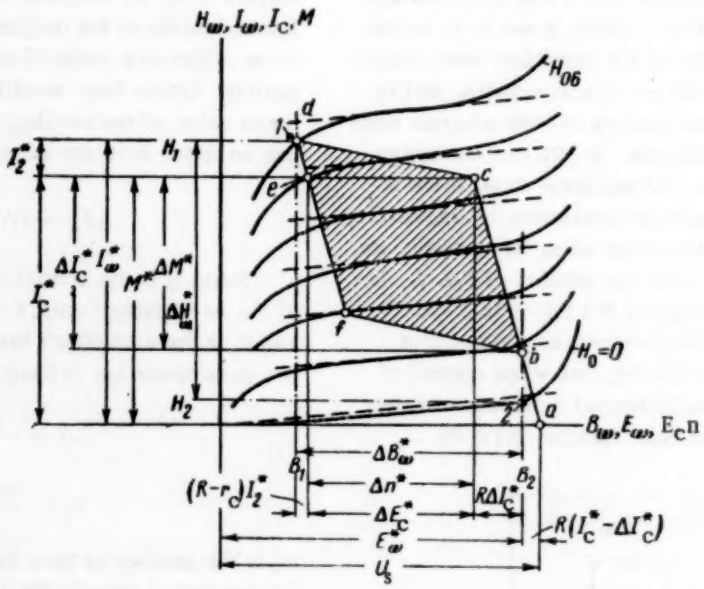

Fig. 2.

Coefficients of Control and Rigidity

We adopt the nomenclature that $K_c = \partial n/\partial I_0$ for $M = \text{const}$ is the control coefficient, and $K_r = -\partial M/\partial n$ for $I_0 = \text{const}$ is the rigidity coefficient. Here, n is motor speed and M is the torque developed by the motor.

We first consider the case when there is no feedback, and we assume that each conducting arm of the rectifier bridge can be replaced by a constant resistance r / 2. The back impedances will be considered infinite.

If we take into account the generally known expressions for dc motors with independent excitation,

$$M = C_M I_c, \qquad (7)$$

$$E_c = C_E n, \qquad (8)$$

It follows immediately from (9) that, all other things being equal, the range of control will be determined by the limiting value of ΔE_ω, which we denote by ΔE^*_ω. According to (5), this latter quantity depends on the properties of the core material (ΔB^*_ω in Fig. 2), its cross section, and the number of turns of the working winding. Since ΔB^*_ω is a constant for a given material, an increase of ΔE^*_ω may be attained by increasing Q and W_ω. Simultaneously, as is clear from (3), R_i will also be increased, which implies an increase in K_c and a decrease in K_r. In view of these circumstances, it is frequently not possible to create an amplifier which, operating in the scheme under consideration, can satisfactorily provide the necessary values of control range and coefficient, and also the rigidity

of the mechanical characteristics. We now show that a system in which the amplifier is used with feedback is free of such a disadvantage.

Effect of Feedback on K_c and K_r

a) Current feedback. Since, in addition to the ampere-turns $W_0\Delta I_0$, the ampere-turns $W_1\Delta I_c$ (Fig. 1) also take part in core magnetization, we then obtain, by adding the proper term to (10),

$$\Delta n = \frac{k}{C_E}\left(\Delta I_0 + \frac{W_1}{W_0}\Delta I_c\right) - \frac{\Delta M}{C_M C_E}(R_i + R), \quad (11)$$

where $R = r_c + r_a + r_1 + r_1$. By taking (7) into account, we obtain, after some simple transformations,

$$\Delta n = \frac{k}{C_E}\Delta I_0 - \frac{\Delta M}{C_M C_E}[R_i(1 - \beta_1 S) + R]. \quad (12)$$

Here, $\beta_1 = W_1 / W_0$ is the feedback coefficient, W_1 and r_1 are, respectively, the number of turns and the impedance of the current feedback winding.

The expression $R_i(1-\beta_1 S)$ can be considered as the equivalent internal impedance of the amplifier with positive current feedback, the magnitude of which can be varied within broad limits by the proper choice of β_1. This statement is well known from the general theory of amplifiers with feedback [9].

Thanks to this, we can obtain the necessary values for K_r, including the value which provides (at least theoretically) absolute rigidity of the mechanical characteristics. The control coefficient does not depend on the current feedback.

b) Voltage feedback. Change of the control coefficient can be obtained by introducing voltage feedback. For this purpose, we use a winding with number of turns W_2, connected in parallel with the motor via resistor r_2. The increment of feedback current will be $\Delta I_2 = \frac{\Delta E_c + \Delta I_c r_c}{r_2}$. and the corresponding ampere-turns are $\Delta I_2 W_2 = W_0\beta_2(\Delta E_c + \Delta I_c r_c)$. Here, $\beta_2 = \frac{W_2}{W_0 r_2}$ — is the feedback coefficient.

The increment of total current passing through the amplifier's working winding equals $\Delta I_\omega = \Delta I_c + \Delta I_2$. Magnetization will be implemented by the positive feedback of ampere-turns $W_0\Delta I_0 + W_2\Delta I_2$. Since the current ΔI_2 does not flow through the motor's armature winding, the component $r_c\Delta I_2$ should be subtracted from the right member of (6), i.e.,

$$-\Delta E_\omega = \Delta E_c + R\Delta I_c + (R - r_c)\Delta I_2. \quad (13)$$

By substituting this last expression in (1) and by taking (7) and (8) into account, we find that

$$\Delta n = \frac{k\Delta I_0}{C_E(1 - \beta_2 k + a)} - \frac{\Delta M}{C_E C_M}\frac{[(R_i + R) - (\beta_2 k - a)r_c]}{(1 - \beta_2 k + a)}, \quad (14)$$

where

$$a = \frac{R_i + R - r_c}{r_2}, \qquad R = r_i + r_a + r_c.$$

Frequently, $r_c(\beta_2 k - a) \ll R_i + R$. Then, we can conclude from (14) that the introduction of positive voltage feedback leads to an increase in K_c and a decrease in K_r. The stability of motor speed will be even worse than with the absence of feedback. With negative feedback, the inverse phenomena will be observed. If $|\beta_2| \to \infty$, then $K_r \to \frac{1}{r_c}$.

c) Combined Feedback. It is clear from an analysis of the two forms of feedback considered that their properties complement each other to a certain extent, and that their joint use must give the very best results. This is an immediate consequence of the following expression, obtained on the basis of the same considerations and methods which we used previously:

$$\Delta n = \frac{k\Delta I_0}{C_E\left[1 - k\left(\beta_2 + \frac{\beta_1}{r_2}\right) + a\right]} - \frac{\Delta M}{C_E C_M}\frac{\left\{R_i + R - k\left[\beta_1\left(1 + \frac{r_c}{r_2}\right) + \beta_2 r_c\right] + a r_c\right\}^*}{\left[1 - k\left(\beta_2 + \frac{\beta_1}{r_2}\right) + a\right]}. \quad (15)$$

Here, $R = r_1 + r_a + r_1 + r_c$. In deriving (15), it was taken into account that the increment of the total constant component of magnetizing force equals $W_0\Delta I_0 + W_1\Delta I_c + (W_1 + W_2)\Delta I_2$, and that ΔE_ω is defined by (13).

The relationships $r_c \ll r_2$, $\beta_1 \ll r_2\beta_2$, $(\beta_2 k - a)r_c \ll R_i + R$ are frequently valid. In this case, (15) can be simplified to

$$\Delta n = \frac{k\Delta I_0}{C_E(1 - \beta_2 k + a)} - \frac{\Delta M}{C_E C_M}\frac{R_i(1 - \beta_1 S) + R}{(1 - \beta_2 k + a)}. \quad (16)$$

By the proper choices of β_1 and β_2, one can attain the necessary values of both the control coefficient and the rigidity coefficient. From this point of view, combined feedback is the most advantageous.

Transient Responses

We first consider the case when there is no feedback. The law of variation of motor speed during the transient response may be found by jointly solving (9) and (10) (written for instantaneous values) and the following equations:

$$\Delta u_0 = r_0\Delta i_0 + W_0 Q\frac{d(\Delta B_0)}{dt}, \quad (17)$$

* The terms β_1/r_2 and r_c/r_2 will be missing if one connects winding W_2 as shown by the dashed line in Fig. 1, which is advantageous for $\beta_2 < 0$.

$$W_0 Q \Delta B_0 = \frac{W_0^2 Q}{l} \mu_c \Delta i_0 - \frac{\nu}{\omega} \frac{W_0}{W_\omega} \Delta e_\omega, \quad (18)$$

$$\Delta M = \Delta M_0 + m\Delta n + J \frac{d(\Delta n)}{dt}. \quad (19)$$

Here, u_0 is the voltage applied to the input of the controlling winding, r_0 is the control circuit's impedance, B_0 is the constant (monotonic) component of magnetic induction. Some explanation should be given a propos of the last equations. Expression (17) derives from Kirchhoff's second law for the control circuit; (18) was borrowed from [6, 7]. Henceforth, to simplify the problem, bearing in mind that the cores are of good quality, we shall assume that $\mu_c = 0$, and we shall denote $\nu W_0 / \omega W_\omega$ by T. Equation (19) expresses Newton's law of motion with the assumption that the static impedance torque of the productive mechanism has two components, one of which is constant (ΔM_0) and the second of which is directly proportional to the speed ($m\Delta n$). On the basis of the equations enumerated, we get

$$\tau_{el}\tau_{mec}\delta \frac{d^2(\Delta n)}{dt^2} + \left[\tau_{el}\left(1 + \frac{m\delta}{K_r}\right) + \right. \quad (20)$$

$$\left. + \tau_{mec}\right] \frac{d(\Delta n)}{dt} + \left(1 + \frac{m}{K_r}\right) \Delta n = K_c \Delta I_0 - \frac{\Delta M_0}{K_r}.$$

Here,

$$\tau_{el} = \frac{K_c T C_E}{r_0}, \quad \tau_{mec} = \frac{J}{K_r},$$

$$\Delta I_0 = \frac{\Delta U_0}{r_0}, \quad \delta = \frac{R K_r}{C_E C_M}.$$

Finding the solution of (20) poses no difficulty. For a qualitative estimate of the possible results, we consider the following particular cases: $\tau_{el} = 0$, $\tau_{mec} \neq 0$, and $\tau_{el} \neq 0$, $\tau_{mec} = 0$. Correspondingly, we obtain the equations

$$\tau_{mec} \frac{d(\Delta n)}{dt} + \left(1 + \frac{m}{K_r}\right) \Delta n = K_c \Delta I_0 - \frac{\Delta M_0}{K_r}$$

and

$$\tau_{el}\left(1 + \frac{m\delta}{K_r}\right) \frac{d(\Delta n)}{dt} +$$

$$+ \left(1 + \frac{m}{K_r}\right) \Delta n = K_c \Delta I_0 - \frac{\Delta M_0}{K_r}.$$

In the first case, the time to establish the number of revolutions is determined by the quantity

$$\frac{\tau_{mec}}{1 + \frac{m}{K_r}} = \frac{J}{K_r + m}, \text{ which will be quite large,}$$

since, in the absence of feedback, K_r is small.

In the second case, the duration of the transient response depends principally on the amplifier lag, and will be characterized by the quantity

$$\frac{K_c T C_E}{r_0} \frac{1 + \frac{mR}{C_M C_E}}{1 + \frac{m}{K_r}}.$$

In investigating transient responses with feedback present, we should, instead of (10), use (16), adding to the latter the terms $W_1 Q d(\Delta B_0)/dt$ and $W_2 Q d(\Delta B_0)/dt$, taking into account the appearance of the corresponding emf, in each of the feedback windings. It was proved in [6] that these emf's can be neglected in the case of current feedback and active load. We assume that this may be done in the present case, bearing in mind the qualitative nature of our estimate. Under these conditions we may, to elucidate the effect of the feedback, use (20), in which the values for K_c and K_r are chosen from (16). It is easily comprehended that an increase in K_r due to positive current feedback or to negative voltage, feedback gives rise to a decrease in τ_{mec} and, consequently, to an acceleration of the transient response. Positive voltage feedback increases K_c and, consequently, τ_{el} as well. However, if r_0 is also simultaneously increased, maintaining the condition $U_0 I_0 = \text{const}$, then τ_{el} will be decreased. Thus, with the assumptions we have made, all forms of feedback are advantageous, in the sense of accelerating the transient response.

We note that if $K_r < 0$, then $\tau_{mec} < 0$ and the term with $d(\Delta n)/dt$ may become negative. In this case, the system exhibits a static instability, the assumption of linearity is unrealistic, and autooscillations will arise in the system, as we have observed in experiments.

Several Remarks Regarding Nonlinearity of Mechanical Characteristics

When low-quality cores are used, the two assumptions made will not hold. In this case, it is impossible to consider the coefficients S and R_i (1) as constants, where their maximum corresponds to a linear domain. With such cores, the load curve cannot be approximated by a straight line, as the second assumption required. In this case, a more suitable approximation is $E_\omega^2 = U_s^2 - (E_c + RI_\omega)^2$, by virtue of which $-dE_\omega = (dE_c + RdI_\omega)(E_c + RI_\omega)/E_\omega$. By denoting $(E_c + RI_\omega)/E_\omega = \alpha$, $R_i/\alpha = R_{i\alpha}$ and $k/\alpha = k_\alpha$, we can find that

$$dn = \frac{k_\alpha}{C_E} dI_0 - \frac{dM}{C_M C_E} (R_{i\alpha} + R) = K_c dI_0 - \frac{dM}{K_r}. \quad (10')$$

Thus, K_c and K_r will depend on the values of α, S, and R_i which, in their turn, are determined by the choice of the working point. The common structure of (10) and (10') allows the basic propositions of the analysis provided earlier to be extended to the given case also, of course, in the neighborhoods of each working point.

We now explain the influence of S and R_i on the linearity of the mechanical characteristics: For this purpose, we determine the relative variation of the rigidity coefficient due to the variation of the internal impedance and of the slope, respectively on dR_i and dS.

Using the expression for K_r from (10), we find that

$$\frac{dK_r}{K_r} \approx -\frac{dR_i}{R_i}.$$

In the absence of feedback, the linearity of the mechanical characteristic will be determined by the constancy of R_i. In the case of positive current feedback

$$\frac{dK_r}{K_r} = -\frac{(1-\beta_1 S)\,dR_i - \beta_1 R_i dS}{Ri(1-\beta_1 S)+R}.$$

If

$$[R_i(1-\beta_1 S)+R]- \quad \text{then}$$

$$K_r \to \infty \text{ and } \frac{dK_r}{K_r} \to \infty.$$

Increasing the rigidity by means of current feedback leads to a sharp manifestation of nonlinearity in the mechanical characteristics. Finally, as was shown earlier, with negative voltage feedback, K_r converges monotonically to its limit $1/r_c$ if $|\beta_2| \to \infty$. In this case, dK_r/K_r will converge to zero. Consequently, negative voltage feedback allows the mechanical characteristic to be linearized and, therefore, is frequently used in combination with positive current feedback. This assertion is confirmed, in particular, by the data of the experimental investigation given in [2].

Design Considerations

The order followed in designing amplifiers will be different, depending on the problem posed and the data originally given, which must be sufficient and which must be compatible. The consideration of all the questions related to design goes beyond the limits of the present work. Here, we limit ourselves to illustrating how the expressions given earlier may be employed in design work.

Let there be given the nominal parameters and operating mode of the motor, M^*, I^*_c, C_M, n^*, the voltage on the brushes U^*_c, r_c, and C_E, the limiting variation of torque and number of rotations ΔM^* and Δn^*, the core parameters μ_1, σ, B_1, B_2, H_1, and H_2 or the corresponding family of magnetization curves from which these parameters may be determined, and the necessary values of the coefficients K_c and K_r.

We now determine the required volume of cores. This will be used in the best way if, in the process of operation, there are attained the largest admissible values (in the limits of the linear domains) of magnetic induction B_2 and magnetic-field strength H_1. By taking this circumstance into account, we find, on the basis of (5) and (13), that

$$\frac{\Delta E^*_c + R\Delta I^* + (R-r_c)\Delta I^*_2}{\omega W_\omega \Delta B^*_\omega} = Q, \qquad (21)$$

where $\Delta B^*_\omega = B_2 - B_1$. The components of the voltage drop given in the left member of (21) are represented in Fig. 2 by the following segments: the increase in motor emf ΔE^*_c, by segment ce; the voltage drop across all the active impedances due to the increase in drive current $R\Delta I^*_c$, by segment bc; voltage drop due to the current of the voltage feedback $(R-r_c)\Delta I^*_2 \approx (R-r_c) I^*_2$ – by segment ed. Since $I^*_\omega = I^*_c + I^*_2$ (Fig. 2) then from (4), we find that

$$\frac{(I^*_c + I^*_2) W_\omega}{H_1} = l. \qquad (22)$$

It is assumed for this that the inequality $(I^*_c - \Delta I^*_c) W_\omega \geqslant H_2 l$ always holds.

Equations (21) and (22) permit the calculation of the active volume of the cores $V = Ql$ if one knows, in addition to the original data, the values of R and I^*_2, i.e., essentially, r_1, r_a, r_1, and r_2. Resistance r_a depends on the rectifier properties and may be found by well-known methods. Amplifier efficiency and volume of copper depend on resistances r_1, r_1, and r_2. Their values can be varied within well-known limits. We assume roughly that $r_i \approx r_1 \approx r_c$, $r_2 \approx (5-10)\frac{U^*_c}{I^*_c}$ and, consequently, $I^*_2 \approx (0{,}2 \text{ to } 0{,}1) I^*_c$. We note that the core volume, found in accordance with (21) and (22) is minimal from the point of view of guaranteeing the magnetic mode. The possibilities of spacing the windings must be verified by additional well-known methods.

By knowing the value of V, we can determine Q or l by giving either the cross section or the mean length of the magnetic circuit. For different ratios of Q/l, we obtain different-size apertures and, to a certain degree, different operating conditions for the cores. The question as to the optimal ratio of Q/l requires a special investigation. As a first approximation, it is advantageous to start with the data given in the table below, obtained on the basis of the recommendations found in [10]:

$V/2, cm^3$	1.0	2.0	10	20	30	60	100	300
$Q/2l$, cm	0.02	0.035	0.05	0.075	0.1	0.15	0.2	0.3

By selecting the value of Q, we find from (21) the number of turns W_ω, and from (3) the magnitude of R_i. Then, using (15), we should determine β_1, β_2, and S for the given K_c and K_r. Since there are three unknowns, one of them should be given, since the necessary control coefficient can be obtained by virtue either of the proper value of W_0 or of W_2. When internal feedback is used, $\beta_1 S \approx 1$. Then, β_2 and S are determined uniquely. Finally, we calculate the supply voltage by the formula $U_s = \omega W_\omega Q B_2 + (I^*_c - \Delta I^*_c)R + (U^*_c - \Delta E^*_c)$, the meaning of which is clear from Fig. 2, on which the particular case is shown when $\Delta E^*_c \approx U^*_c$.

SUMMARY

The analysis of the equations obtained for the MA–M system leads to the following conclusions:

1. When there is no feedback, it is not possible to provide a satisfactory operating mode of the MA–M

system. Introduction of current and voltage feedback can have an effect on the rigidity of the mechanical characteristics and on the control coefficient. The best results can be obtained with the concurrent employment of the aforementioned forms of feedback.

2. Feedback permits the acceleration of the transient response and the linearization of the mechanical characteristics.

3. The expressions obtained may be used for a first-approximation design of an amplifier in accordance with the methodology presented.

LITERATURE CITED

1. R. Kh. Bal'yan, "Push-pull magnetic amplifiers with dc outputs," Avtomatika i Telemekhanika 17, 2 (1956).
2. A. B. Rosenbauli and I. N. Selivokhin, "Construction of the characteristics of a dc drive with choke control," Elektrichestvo No. 10 (1958).
3. S. Ya. Dunaevskii, "On the range of speed control in a motor-generator system with a rotary amplifier," Vestnik elektroprom No. 8 (1951).
4. A. A. Sirotin, "An engineering method of calculating the characteristic of an independently excited motor in systems for the automatic maintenance of speed," Elektrichestvo No. 12 (1954).
5. A. G. Ivakhnenko, Automatic Speed Control of Low Power Asynchronous Motors [in Russian] (Izd AN Ukr SSR, 1953).
6. L. V. Safris, "Designing a magnetic amplifier with linearized magnetization characteristics," Trudy Rostov. Inst. Inzh. Zh.-d. Transporta No. 20 (Transzhelkorizdat, 1956).
7. L. V. Safris, "On the question of transient responses in magnetic amplifiers inductively loaded via rectifiers," Avtomatika i Telemekhanika 19, 3 (1958).
8. N. A. Kaluzhnikov, "On the design of choked magnetic amplifiers, connected on a single-phase rectifier bridge," Avtomatika i Telemekhanika 19, 3 (1958).
9. G. S. Tsykin, Negative Feedback and Its Applications [in Russian] (Svyaz'izdat, 1940).
10. M. A. Rozenblat and O. A. Sedykh, "General principles in the construction production planning of toroidal cores for magnetic amplifiers," Otchet Instituta Avtomatiki i Telemekhaniki AN SSSR (1957).

THE USE OF HALL PICKUPS IN MAGNETIC HEADS

Yu. A. Vasilevskii

(Moscow)

Translated from Avtomatika i Telemekhanika, Vol. 21, No. 3, pp. 402-408, March, 1960
Original article submitted March 4, 1959

This paper reports on the development and experimental investigation of magnetic reading heads based on the Hall effect. The heads have the property that their emf is proportional to the residual carrier flux, in contradistinction to the usual induction-type reading heads in which the emf is proportional to the velocity of flux change. The heads can operate both with magnetic tape and with carriers in the form of drums or disks.

In ordinary magnetic heads for reading or reproducing magnetic recording, there occurs a differentiation of the signal stored on a ferromagnetic carrier. With this, there appear distortions in the amplitude and phase frequency characteristics of the reproduction channel which hinder correct transmission of the signal. Exceptions are sinusoidal signals which, in the given case, do not undergo changes in form if the system is linear. However, even for them there are serious limitations in the range of low audio and infraaudio frequencies.

It is not always possible to tolerate this disadvantage of induction heads, despite their great superiority in other respects. Therefore, there were developed a number of designs of the so-called flux-sensitive heads of the servo system type, whose output emf's are proportional, not to the velocity of change, but to the magnitude of the residual carrier flux. The best known of these are the magnetomodulation head whose operating principle is analogous to a magnetic amplifier (sonde) of the second harmonic type, and the electrobeam head, based on a tube with magnetic deflection of the beam.

The flux-sensitive heads to be considered below, based on the Hall effect, are further developments in this direction. Their operating principle amounts to this, that the residual carrier flux, by means of a magnetic circuit, is applied to a Hall pickup, with the result that at the pickup's output there is generated an emf which is proportional to the magnitude of this flux.

One design of such a head is shown schematically on Fig. 1, a; an over-all view of it is shown in Fig. 1, b. Used in it is an ordinary ring-shaped magnetic circuit, for example, from standard head V-01. The dimensions of core 1 are as follows: length of the leading (reading) slit d_1 = 45 microns; length of the trailing slit d_t = 0.28 mm; outside diameter of the core D_0 = 25 mm; inside diameter D_i = 18 mm. Height of the core assembly is h = 7 mm. The given design is intended to operate with magnetic tape 2 of width 6.35 mm, although it can also operate with a magnetic drum. The Hall pickup 3 is established in the leading slit of the magnetic circuit. Semiconductor pickups of n-type germanium (n-Ge) were used, with dimensions of 6 × 3 × 0.18 mm.

The Hall pickup has a dc supply. The selection of the magnitude of the current turned out to have an essential influence on the head's signal-to-noise ratio. We used the following method to determine the optimum current magnitude. On the carrier there was recorded a sinusoidal signal with a frequency of 125 cps (carrier speed of motion was 38.1 cm/sec) and with a magnitude of residual flux Φ_C = 300 millimaxwells. For the carrier used, this level was about 10 db lower than the saturation level. The pickup's Hall electrodes were supplied directly at the high-ohmic input of the amplifier circuit. Since the pickup's inherent noise is independent, within broad limits, of the magnitude of the signal, the signal-to-noise ratio was determined as the ratio of the indication of

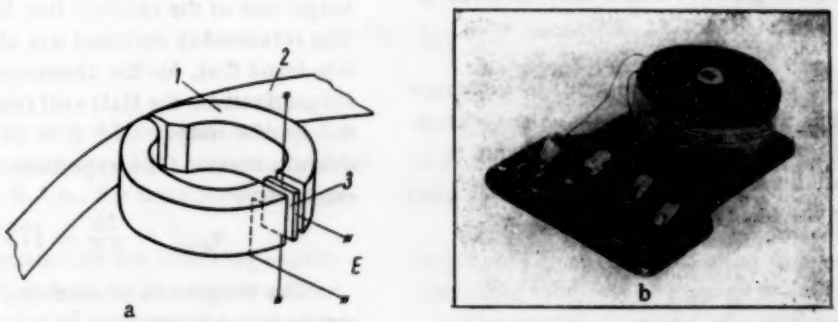

Fig. 1.

the instrument at the output of the amplifier circuit at the time of carrier motion to the instrument's indication for a motionless carrier. This ratio was taken off as a function of the magnitude of the current supplied to the pickup. As a result, it was found that the optimum magnitude of this current for the head under consideration was 8 ma. With such a current, and for an amplifier circuit passband of 20 to 6000 cps, the signal-to-noise ratio was 20.4 db; for a passband of 75 to 150 cps, this ratio was 33.2 db and, for a passband of 25 to 100,000 cps, it equaled 17 db. To eliminate pickup from the constant poles, the current supply circuit for the pickup was carefully screened. A thermal regimen corresponding to the pickup's optimal supply current and to an ambient temperature on the order of 25°C provided prolonged stable operation of the head. For example, the pickup was supplied with current continuously for 48 hours. With this, the operation of the head was periodically verified. No operating changes were observed.

The magnitude of the emf generated by the pickup when it is acted upon by the carrier's magnetic field is related to the head's sensitivity. As a preliminary measure, we found the character of the calculated dependency of the head's sensitivity on the parameters of its magnetic circuit and on the so-called voltage sensitivity of the Hall pickup [1].

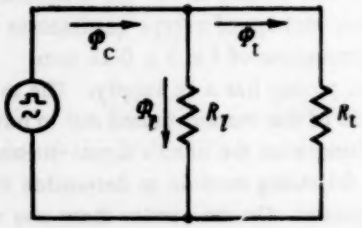

Fig. 2. Simplified equivalent schematic of the head's magnetic circuit. R_l is the reluctance of the leading (reading) slit, R_t is the reluctance of the trailing slit, and Φ_C is the carrier's residual flux.

In a first approximation, the equivalent schematic of the head's magnetic circuit has the form shown in Fig. 2. The emf at the pickup's output may be given as

$$E = \gamma B, \qquad (1)$$

where γ is the Hall pickup's voltage sensitivity (microvolts / gauss) and B is the induction acting on the pickup. In our case, B is the average value of the induction in the trailing slit due to the residual carrier flux Φ_C.

We determine the head's sensitivity from the formula

$$\eta = \frac{E}{\Phi_c} = \frac{E}{B}\frac{B}{\Phi_c} = \gamma\nu, \qquad (2)$$

where ν is a coefficient defined by the parameters of the head's magnetic circuit:

$$\nu = \frac{\Phi_t}{\Phi_c S_t} = \frac{1}{S_t + d/R_l},$$

S_t is the cross section of the flux in the trailing slit, R_l is the reluctance of the leading slit, i.e.,

$$\eta = \frac{\gamma}{S_t + d/R_l}.$$

In the general case, Φ_C is, with certain limitations, an arbitrary function of the space coordinates related to the carrier, and B and E are functions of time corresponding to it.

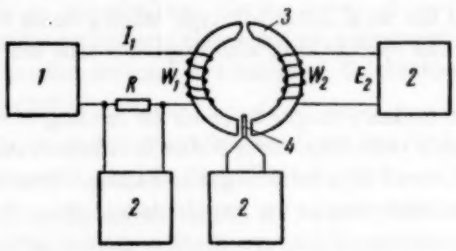

Fig. 3. Scheme for measuring the Hall pickup's sensitivity, with the pickup located in its operating position between the halves of the head's core. 1 is a generator, 2 is a vacuum tube voltmeter, 3 is the head's core, and 4 is the Hall pickup.

The pickup's voltage sensitivity was determined experimentally as shown in Fig. 3. The head's core had two windings: magnetizing winding W_1 and measuring winding W_2. The measure of magnetic induction in the core was taken to be the magnitude of the voltage induced in winding W_2. The ratio of the measured magnitude of the Hall emf E to the corresponding value of induction B gave the mean value of the pickup's voltage sensitivity γ = 116 microvolts/gauss from whence, for the parameters of the magnetic circuit previously enumerated, we found the computed sensitivity of the head:

$$\eta = 204\ \mu v / \mu sec$$

The experimental value of the head's sensitivity was determined by measuring the emf at the pickup's output and seeking the dependency of the emf on the magnitude of the residual flux for an 8 ma supply current. The relationship obtained was close to a linear one. It was found that, for the aforementioned intensity of magnetization, the Hall emf (the equivalent value) at the head's output was E = 52 microvolts. From this was obtained the experimental value of the head's sensitivity:

$$\eta_{exp} = \frac{52}{0.3} = 173\ \mu v / \mu sec$$

The magnitude of induction B in the trailing slit can be found from (2):

$$B = \frac{\eta}{\gamma}\Phi_n = 0.45\ \text{gauss}$$

On the basis of the dynamic range of 20.4 db, found earlier, the head's sensitivity threshold corresponds to a value of induction of

$$B_{min} = \frac{0{,}45}{10^{20.4/20}} = 4.3 \cdot 10^{-2} \text{ gauss}$$

The head's frequency characteristic, obviously, is determined by the frequency characteristics of the two factors in (2). The frequency characteristic of the voltage sensitivity γ was measured by the circuit of Fig. 3 for a constant value of induction B = 3 gauss within the frequency limits of 20 to 200,000 cps. It was found that, within these limits, the voltage sensitivity does not depend on frequency.

In a pickup placed in a variable magnetic field, there is induced an induction emf which is added geometrically to the Hall emf. However, the induced emf can be easily compensated by the proper placement on the core of one of the conductors joining the Hall electrodes to the amplifier circuit. The optimum compensation is chosen as that giving the minimum deviation of the instrument in the circuit of the Hall electrodes at the highest operating frequency. On the basis of the system's linearity and the applicability of the principle of superposition, one can use still another method of isolating the Hall emf from the geometric sum of the two emf's : with the current supplying the pickup switched in, one measures (without compensation) the total emf, after which, with the current switched off, one measures the induced emf. Their geometric difference gives the Hall emf. By such a method, results were obtained which coincided closely with the previous ones until the induced emf exceeded the Hall emf by a factor of more than 3 or 4 . This latter method is effective when the Hall pickups are used as pickups for geometric sums or differences of stimuli, one of which is proportional to the frequency.

The frequency characteristic of coefficient ν is determined by the magnetic and geometric parameters of the core such as, for example, the slit and the frequency-dependent losses, and is not characteristic of the given head .

Since, in the range considered, the pickup sensitivity does not depend on frequency, the head's frequency characteristic is simultaneously the frequency characteristic of the induction in the trailing slit.

The head's experimentally obtained frequency characteristic is shown in Fig. 4. The signal was recorded at a constant writing current but at different frequencies, with a speed of carrier motion of 38.1 cm/sec. Some lifting of the characteristic in the low-frequency range is related to the length of the head contact with the carrier. The fall of the characteristic in the high-frequency range is explained both by slit phenomena and by certain other peculiar characteristics of magnetic recording.

On the other hand, since the Hall emf may be defined in practice as the geometric difference of the

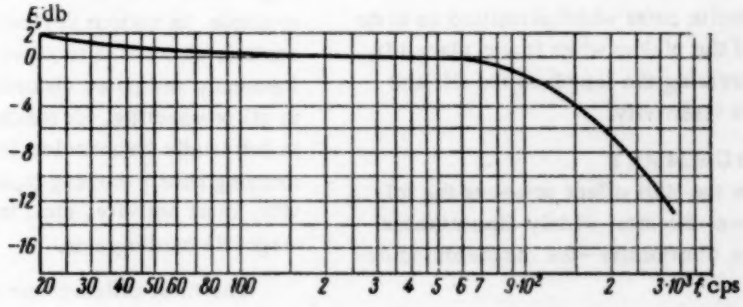

Fig. 4.

total emf and the induced emf, this is confirmed by the form of the proportional dependency (1) between the Hall emf E and the induction B, i.e., the head possesses the property of flux sensitivity.

This latter was illustrated by the following experiments. Recording was read from an immovable carrier. The magnetization intensity of the carrier corresponded to :

1) a sinusoidal signal with a recording wavelength of 16 mm;

2) a pulse signal with a dipole recording length of 10 mm (recording from zero to saturation; a mark-space ratio of 2);

3) a rectangular signal with a dipole recording length also of 10 mm (recording from saturation to saturation; mark-space ratio of 2).

The carrier, by means of a micrometric device, was drawn past the head for a definite distance and then stopped, after which a sensitive galvanometer measured the voltage on the head's Hall electrodes.

The point of reading initiation coincided with the beginning of the recording, for which the initial portion of the recording was made visible by precipitating on the carrier a powder of carbonyl iron from a heptane suspension. As a result of this, there was shown the synphasing of the carrier's surface residual flux and the voltage on the head's Hall electrodes.

We should mention one further trial head design, shown in Fig. 5, a and b. The head's magnetic circuit is open, and the Hall pickup is placed in the reading slit

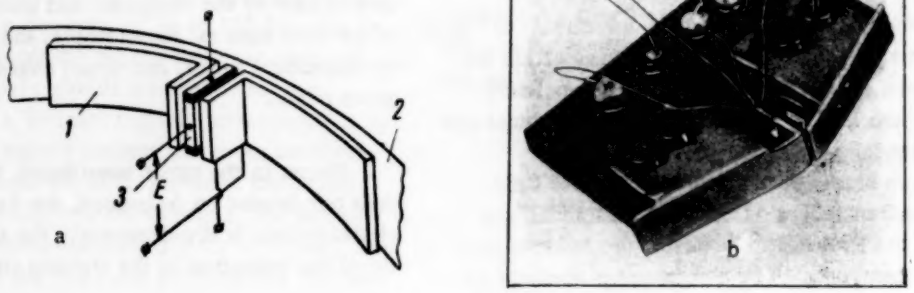

Fig. 5. 1 is the core, 2 is the carrier, 3 is the pickup.

whose length is about 0.35 mm. The design has extended pole shoes (the length of each shoe is 25 mm) and is intended to read recording of long wavelengths. A simplified equivalent schematic of the head's magnetic circuit can be obtained if, in Fig. 2, one sets $R_t = \infty$. As should be expected, with the same pickup, this design has greater sensitivity and a correspondingly better dynamic range than the first design. At a frequency of 40 cps, the increase in sensitivity is about 4 db.

Other heads based on the Hall effect which were investigated differed from the two types considered here only by the core configurations and materials; for example, we used ferrite cores whichpermitted us to do without insulation of the pickup when it was placed in the slit, thereby decreasing the length of the slit and increasing the head's sensitivity.

SUMMARY

A head based on the Hall effect possesses the following advantages over the most widely disseminated type of flux-sensitive transformer—the magnetomodulation head.

1. It permits simplification of the electrical reading scheme.

2. It possesses sensitivity to the direction of the carrier field, i.e., to the polarity of the signal.

3. It can operate in a broad frequency range, in particular, for frequencies of the order of 100 kcps and higher. In this case it is advantageous to use a ferrite magnetic circuit.

4. With heads based on the Hall effect, the danger of random erasure or magnetization of the carrier is excluded.

5. Phase distortion of the signal is virtually eliminated.

6. The requirements on head shielding are reduced.

7. Simplicity of design and small dimensions are provided.

This last quality effectively distinguishes the head based on the Hall effect from the other well-known flux-sensitive head—the head of the electron-beam type.

The Hall pickup is an inductionless transformer, which eases the shielding of such a head in comparision with an ordinary induction head of equal sensitivity.

A head based on the Hall effect may be useful in many cases of special uses of magnetic recording, the importance of which is continuously growing; for example, in various devices of automation and remote control, where it is required to read pulses with minimal frequency and phase distortions; in geology, particularly in oil prospecting, for reading processes which change at infraaudio frequencies; in medicine and biology, for studying slowly varying processes related to brain activity, heart activity, etc., in particular, for reading magnetic cardiograms.

The most efficient use of heads based on the Hall effect is in the frequency range from fractions of a cps to about 100 cps, and for carrier speeds up to 4 to 5 cm/sec, i.e., in those cases where induction heads are practically ineffectual. The basic disadvantage of a head with a Hall pickup for sound reproduction is the relatively small dynamic range. There exist the following ways of improving the dynamic range and other indicators of head quality:

1. Improvement of the technology of preparing Hall pickups, the quality of processing the surfaces and contacts.

2. The use of Hall pickups with non-current-carrying contacts.

3. The use, for pickups, of materials with higher Hall constants.

4. Reduction of the length of the slit in which the Hall pickup is established, which introduces the particular requirement to reduce the width of the pickup. There is interest, in this connection, in film pickups of materials with high voltage sensitivity. These latter can be mounted in the form of a thin film of thickness of 10 to 100 micrometers on the face surface of a ferrite core.

5. The use of magnetic recording carriers with high values of residual flux.

6. Operation with high levels of carrier magnetization, for example, with levels corresponding to the magnetic saturation of the carrier, as occurs in the majority of special applications of magnetic recording.

In conjunction with this, it should be mentioned that, in many cases of special uses of magnetic recording, only a twofold increase of signal over noise is sufficient.

LITERATURE CITED

1. A. R. Regel', Semiconductor Measurers of Magnetic-Field Strength[in Russian] (LDNTP, Leningrad, 1956).

A VOLTAGE DEFLECTION PICKUP BASED ON SEMICONDUCTOR ELEMENTS*

S. V. Kulikov

(Moscow)

Translated from Avtomatika i Telemekhanika, Vol. 21, No. 3, pp. 409-416, March, 1960
Original article submitted August 19, 1959

A description is given of a voltage deflection pickup implemented by semiconductor elements — silicon base diodes, transistors, and thermoimpedances. A design methodology is proposed, and calculated relationships and experimental results are given.

General Remarks

The voltage deflection pickup considered in this paper is designed for use in systems for stabilizing voltage or any quantity which is transformed to a voltage. The special feature of the voltage deflection pickup, shown in Fig. 1 and 2, is its implementation by semiconductor elements. This provides its small weight and size (Fig. 2), reliability, heightened resistance to vibration and shock, and length of useful life .

Type D 810 silicon base diodes D_1 and D'_1, connected in opposite arms of bridge D_1-R_p-R_{11}-D'_1-R_{12}, execute the function of voltage calibration. The voltage to be regulated, E_{reg}, is applied to one of the bridge's diagonals via ballast resistor R_{13}. Connected to the other diagonal of the bridge is a preamplifier of silicon transistors T_1-P102, T'_1-P102, whose output current controls the relay power amplifier, implemented by germanium transistors T_2, T'_2-P13A, T_3 and T'_3-P4D. Thermoimpedances R_{T_1} and R_{T_2} are used to compensate the temperature variations in the scheme.

To obtain, in load impedances R_3 and R'_3 , a signal whose average value would be a continuous function of the input signal for a limited range of variation of the latter, one should connect, instead of resistors R_5 and R'_5, condensers C_1 and C'_1 (shown by dashed lines in Fig. 1),which would provide self-excitation, i.e., the principle of vibration linearization is used. Pulse-width modulation is used in the scheme for deviations of the controlled voltage.

* The results of the investigation described in this paper were discussed in the April, 1959 seminar of the Laboratory of Automation and Remote Control Elements of the IAT AN SSSR .

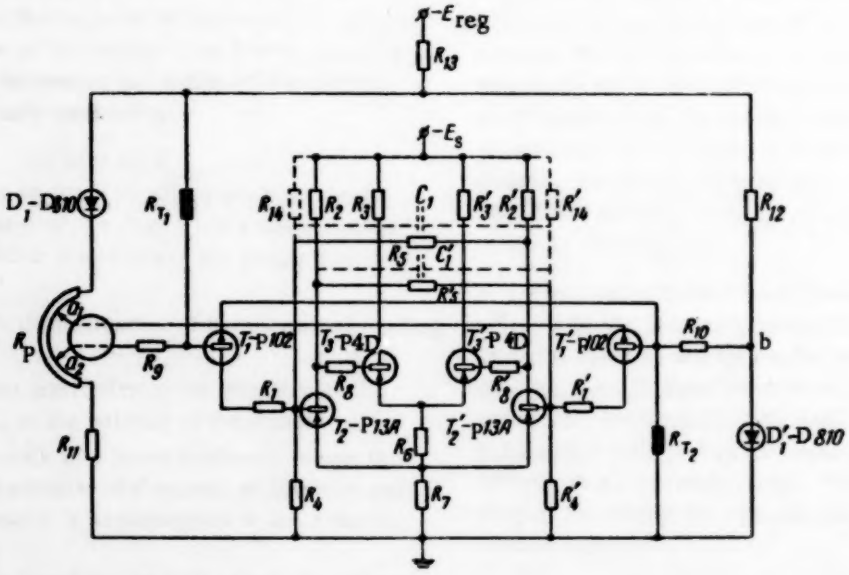

Fig. 1. Simplified schematic of the voltage deflection pickup . $R_1 = R'_1 = 1.2$ kohm; $R_2 = R'_2 = 3.3$ kohm; $R_3 = R'_3 = 100$ ohm; $R_4 = R'_4 = 5.6$ kohm; $R_5 = R'_5 = 15$ kohm; $R_6 = 5$ ohm; $R_7 = 5$ ohm; $R_8 = R'_8 = 1$ kohm; $R_9 = 0$; $R_{10} = 200$ ohm; $R_{11} = 1920$ ohm; $R_{12} = 2100$ ohm; $R_p = 542$ ohm; $R_{a_1\text{-}a_2} = 210$ ohm; $R_{a_1} = 40$ ohm ; $R_{13} = 395$ ohm .

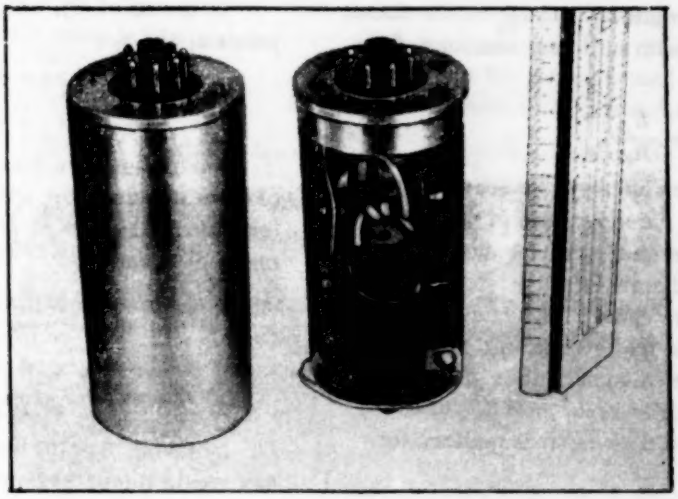

Fig. 2. Outside view of the voltage deflection pickup.

Posing of the Problem

The problem raised in this paper is the presentation of an engineering method of designing the voltage pickup. Relationships are derived which, for given regulated voltage E_{reg}, source voltage E_s and load resistances R_s and R'_s, allow one to determine the remaining circuit parameters for which feasibility of the circuit and its stability under temperature variations would be guaranteed.

In addition, a generalized method is propounded for the analysis of transistor switching circuits.

Method of Investigation

Thanks to the fact that silicon transistors in the cutoff region have insignificant current flowing through the base-collector junction ($I_{co} \leq 1\mu a$), it is possible to design the bridge together with the thermoimpedances R_{T_1} and R_{T_2}, and to implement the additional impedances R_9 and R_{12} separately.

In designing the bridge, the nonlinear base diodes D_1 and D'_1, after the piecewise-linear approximation of their volt-ampere characteristics, are given as "conditionally autonomous" dipoles with emf's E_d and E'_d and with impedances R_d and R'_d (Fig. 3).

The high-ohmic thermoimpedances R_{T_1} and R_{T_2} are presented as current sources I_{T_1} and I_{T_2}.

As a result, we obtain the replacement scheme, shown in Fig. 4, for the bridge. It is calculated by the methods of the linear theory of electrical circuits.

By considering the outputs of transistors T_1 and T'_1 as current sources (in the equilibrium state the currents virtually equal zero), one can compute the relay stages of transistors T_2, T'_2, T_3 and T'_3 separately. The design of the latter is implemented from the conditions of transistor cutoff and saturation, with account taken of temperature variations.

For the computation of the circuit's sensitivity (cf. the Appendix), we introduce the concept of a "conditionally autonomous three-pole," allowing one to take into account the nonlinear properties of the transistor and, at the same time, to use a generalized method of designing linear electrical circuits.

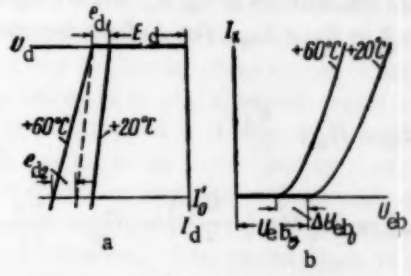

Fig. 3. Volt-ampere characteristics for determining parameters. a is for the silicon base diodes, b is for the silicon transistors.

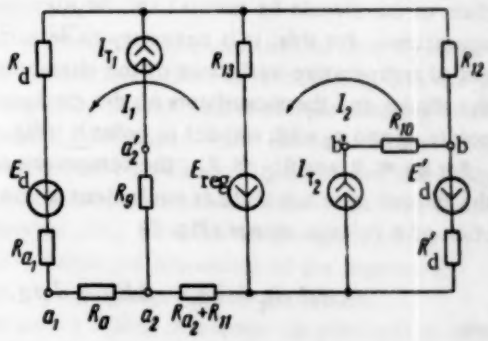

Fig. 4. Equivalent replacement scheme of the nonlinear bridge.

Designing the Nonlinear Bridge

Use of type D808-813 base diodes shows that, for the greatest stability, their operating current I_0 must be of the order of 5 ma.

The magnitude of currents I_{T_1} and I_{T_2} on the circuit of Fig. 4 are determined, with sufficient accuracy, from the equation

$$I_T = \frac{E_d}{R_T}, \tag{1}$$

where E_d is the emf defined by the diode characteristics (Fig. 3), $E_d < E'_d$; R_T is the magnitude of the thermoresistor (the subscript is omitted, since the equation is valid for both diodes and thermoresistors).

The thermoresistors are chosen large enough so that, first of all, operation of the thermoresistors on the linear portion of the volt-ampere characteristic is provided [1] and, secondly, the thermoresistors R_{T_1} and R_{T_2} can be replaced by current sources. This latter is realized for the condition

$$I_0 \geqslant 10 I_T. \tag{2}$$

By neglecting the components of I_T in the bridge, we can find the resistances R_{12}, R_{13} and $R = R_{11} + R_a + R_{a_1} + R_{a_2}$ ($R_p = R_a + R_{a_1} + R_{a_2}$, Fig. 1) from the equations

$$R_{12} = R'_d + \frac{E'_d}{I_0}, \tag{3}$$

$$R = 2\left(R'_d + \frac{E'_d}{I_0}\right) - R_d - \frac{E_d}{I_0}, \tag{4}$$

$$R_{13} = \frac{E_{reg} - 2(I_0 R'_d + E'_d)}{2I_0}, \tag{5}$$

where R'_d is the diode's dynamic impedance.

The remaining unknown resistances, R_a, R_{a_1}, R_{a_2}, and R_{a_3}, are determined from the conditions of equilibrium of the circuit for normal and for elevated temperatures. For this, it is necessary to determine the effect of temperature variations of the characteristics of the diodes and thermoresistors on the displacement of points a_1 and a_2 with respect to point b (Fig. 4).

For $R_d \ll R$ and $R'_d \ll R_{12}$, the temperature variation of the diodes' characteristic is equivalent to the introduction of a voltage source (Fig. 3)

$$e_d = e_{d_1} + e_{d_2} = \Delta E_d + I'_1 r_d, \tag{6}$$

where

$$I'_0 = I_0 + I_T + i_T, \quad e_{d_1} = \Delta E_d, \quad r_d = \Delta R_d, \quad i_T = \Delta I_T.$$

Using the principle of superposition, we determine the effect of temperature variations of the diodes' characteristic from the matrix equation

$$\begin{bmatrix} i_1 \\ i_2 \end{bmatrix} = \begin{bmatrix} R + R_{13} & -R_{13} \\ -R_{13} & R_{13} + R_{12} \end{bmatrix}^{-1} \begin{bmatrix} -e_d \\ +e_d \end{bmatrix}, \tag{7}$$

where i_1 and i_2 are the increments of currents I_1 and I_2 (Fig. 4).

Solving (7), we get

$$i_1 = \Delta I_1 = \frac{(R_{12} + R_{13})\, e_d - R_{13} e'_d}{R(R_{12} + R_{13}) + R_{12} R_{13}}. \tag{8}$$

By means of (8), we determine the displacements of points a_1 and a_2:

$$\begin{aligned} \Delta U'_{ba_2} &= e'_d + i_1 (R - R_a - R_{a_2}), \\ \Delta U'_{ba_1} &= e'_d + i_1 (R - R_{a_1}). \end{aligned} \tag{9}$$

Analogously, we find the displacements due to changes in current I_{T_1} with the condition that $R \gg R_p$ (variation in I_{T_2} has no practical effect on the displacements of a_1 and a_2):

$$\begin{aligned} \Delta U^*_{ba_2} &= -\frac{R(R_a + R_{a_2})(R_{12} + R_{13})}{R(R_{12} + R_{13}) + R_{12} R_{13}}\, i_{T_1}; \\ \Delta U^*_{ba_1} &= \frac{R_a R_{12} R_{13} - R_{a_1} R (R_{12} + R_{13})}{R(R_{12} + R_{13}) + R_{12} R_{13}}\, i_{T_1}. \end{aligned} \tag{10}$$

By taking (8)-(10) into account, one can set up the four equilibrium equations for the two temperatures, by solving which we obtain

$$\begin{aligned} R_a &= \frac{I_{T_1}(\Delta U_{eb_0} + \Delta U'_{eb_0}) + i_{T_1}(U_{eb} + U'_{eb_0})}{I_{T_1} i_1 + I_0 i_{T_1}}, \\ R_9 &= \frac{(I_0 - I_{T_1})(\Delta U_{eb_0} + \Delta U'_{eb_0}) - (i_1 + i_{T_1})(U_{eb_0} + U'_{eb_0})}{I_{T_1} i_1 + I_0 i_{T_1}}, \\ R_{a_2} &= \frac{r_1^2 (U'_0 i_{T_2} - U^*_0 I_{T_2})}{(r_1^2 I_0 - r_2^2 I_{T_1}) i_{T_2} + (r_1^2 i_1 + r_2^2 i_{T_1}) I_{T_2}}, \\ R_{10} &= \frac{(r_2^2 I_{T_1} - r_1^2 I_0) U^*_0 - (r_1^2 i_1 + r_2^2 i_{T_1}) U'_0}{(r_1^2 I_0 - r_2^2 I_{T_1}) i_{T_2} + (r_1^2 i_1 + r_2^2 i_{T_1}) I_{T_2}}, \end{aligned} \tag{11}$$

where

$$\begin{aligned} r_1^2 &= R(R_{12} + R_{13}) + R_{12} R_{13}, \\ r_2^2 &= R(R_{12} + R_{13}), \\ U'_0 &= I_0 R - E'_d - U'_{eb_0} - I_{T_1} \frac{R_{12} R_{13}}{r_1^2} R_a, \\ U^*_0 &= -i_1 R - e'_d + \Delta U'_{eb_0} - i_{T_1} \frac{R_{12} R_{13}}{r_1^2} R_a; \end{aligned}$$

U_{eb_0}, U'_{eb_0}, ΔU_{eb_0} and $\Delta U'_{eb_0}$ are the threshold voltages and their increments, defined for the corresponding triodes T_1 and T'_1 from Fig. 3, b.

As is obvious from (11), for certain special values of the parameters on the right, the magnitudes of resisters R_9, R_{a_1} and R_{10} may turn out to be zero.

Design of Relay Stages (Switching Circuits)

The design of relay stages from transistors T_2, T'_2, T_3 and T'_3 leads to the determination of resistances $R_2 = R'_2$, $R_4 = R'_4$, $R_5 = R'_5$, R_6, R_7, and $R_8 = R'_8$ for known load resistances $R_3 = R'_3$ and supply voltage E_3. The six unknown resistances are found from the cutoff and saturation conditions of transistors T_2, T'_2, T_3 and T'_3 [2] and from two auxiliary relationships, the first of which expresses the condition that there be no shunting of the relay amplifier's input

$$R_4 \geqslant 10 R_{in} \tag{12}$$

(R_{in} can be set at 500 ohm for P13A), the second of which is the condition of insignificant losses in bias resistors R_6 and R_7:

$$10(R_6 + R_7) \leqslant R_3. \tag{13}$$

The cutoff condition for transistors T_2 and T'_2 is written in the form

$$I_{co_2} R_4 \leqslant \frac{E_s R_7}{R_3 + R_6 + R_7}, \tag{14}$$

where I_{co_2} is the temperature collector current of transistor T_2.

The cutoff condition for transistors T_3 and T'_3, neglecting the emitter current I_{e_2} of triode T_2 in resistors R_6 and R_7, is defined by

$$I_{co_3} R_8 \leqslant \frac{E_s R_6}{R_3 + R_6 + R_7}. \tag{15}$$

The saturation condition for triodes T_2 and T'_2, neglecting I_{co_3} and I_{e_2} in R_7, is written

$$\frac{r_a (r_c^3 - r_b^3 R_5) I_{co_2}}{R_5 E_s} \leqslant R_6 R_2 + R_8 (R_3 + R_6) - r_b^2 \left(\frac{R_7}{R_4} + \frac{R_3 + R_6}{\beta_2 R_2} \right), \tag{16}$$

where

$$r_a = R_3 + R_6 + R_7,$$
$$r_b^2 = R_2 R_5 + R_2 R_8 + R_5 R_8,$$
$$r_c^3 = R_2 R_5 R_8,$$

β_2 is the current transmission coefficient of the base of transistor T_2, and I_{c_2} is the saturation current of the collector of transistor T_2.

The saturation condition for transistors T_3 and T'_3 is defined by the inequality

$$\frac{E_s}{\beta_3 (R_3 + R_6 + R_7)} - I_{co_3} \leqslant I_{b_3}, \tag{17}$$

where I_{b_3} is the base current of transistor T_3. We give this condition in expanded form:

$$r_b^2 \left(\frac{E_s}{\beta_3} - I_{co_3} r_a \right) \leqslant E_s (R_3 R_5 + R_6 R_2) - I_{co_2} R_2 R_5 r_a. \tag{17'}$$

By taking, in (14)-(17), the value of I_{co} which corresponds to the heightened temperature, we can arrive at equalities. A huge increase in the right members of (14)-(17) leads to a lowering of the circuit's sensitivity (cf. the Appendix).

When the pickup is used in the autooscillatory mode, the half-period of the autooscillation, with the conditions

$$R_{14} = R'_{14} = \infty, \quad R_7 = 0, \quad R_4 = R'_4 = \infty$$

may be found approximately from the formula

$$T = \frac{C E_s}{I_{co_1} + I_{co_2}} \left[\frac{R_2 R_6 + R_3 R_8 + R_6 R_8}{(R_2 + R_8)(R_3 + R_6)} \right], \tag{18}$$

where I_{co_1} is the collector current of transistor T_1 (T'_1) at equilibrium, the deviations from which are approximately proportional to the relatively small deviations of the regulated voltage E_{reg}.

Experimental Investigation

The voltage-deviation pickup, designed in accordance with the formulas given above for the case of E_{reg} = 24 v and E_s = 27 v, was subjected to experimental investigation. The pickup's basic parameters are given in the caption of Fig. 1. Testing of the pickup in the temperature range from +20 to +60 °C showed that it reacted reliably to deviations of ± 1 volt. The output current in loads R_9 and R'_9 in the cutoff state for a temperature of +60 °C did not exceed 1 ma. The circuit operated reliably on an inductive load (a differential electromagnetic mechanism). With output stages of transistors P4D, the circuit was capable of a switching power of 200 w. The results of an investigation of the pickup in the proportional mode for a self-excitation frequency of 50 cps are shown in Fig. 5.

Conclusions

The theoretical and experimental investigation provided gives a foundation for concluding that the voltage deviation pickup constructed of semiconducting elements was efficiently developed. The essential advantages of the pickup described —its small weight and dimensions, the increased resistance to shock and vibration, the long useful service life, inherent in semiconducting elements—permit the expanding of the domain of applicability of voltage deviation pickups.

The author wishes to express his gratitude to B. S. Sotskov for his valuable advice on the execution of the present work.

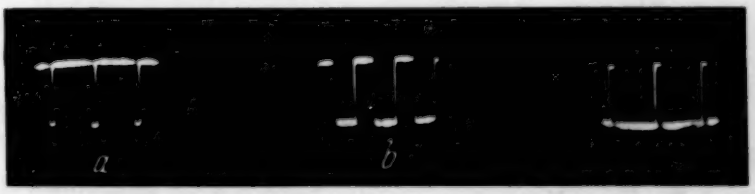

Fig. 5. Oscillograms of pickup output voltages with self-excitation. a is for E_{reg} = 24–0.15 v, b is for E_{reg} = 24 v, and c is for E_{reg} = = 24 + 0.15 v.

APPENDIX

Calculating the Sensitivity of a Relay Scheme

The sensitivity of a relay circuit is defined by the threshold values of controlling current for which the circuit transfers (operates).

In relay schemes constructed of transistors, the currents and voltages on the electrodes of these latter vary within such wide limits that there appear essential nonlinearities in the transistors' properties (cutoff region, saturation and nonlinear active region). However, for a broad class of transistor relay schemes, for definite threshold values of controlling current, it is not necessary to know in detail the nonlinear characteristics of the transistors. It suffices to know the characteristics in the neighborhoods of isolated points, corresponding to the moments of circuit transition points on the boundaries between the cutoff and saturation regions on the one hand, and the active region, on the other.

A nonlinear transistor can be presented as a linear "conditionally autonomous" three-pole (a four-pole with a short-circuited side) for the regions of cutoff and saturation, and also for two (or more) segments of the active region, for example, for the initial (close to the cutoff region) and for the final (close to the saturation region) segments.

Indeed, the behavior of a transistor for constant current in any form of connection (with common emitter, base, collector) is completely described by two nonlinear equations.

For the correspondingly chosen dependent and independent variables, there are six possible variants (systems) of equations. For example, for a circuit with a common emitter, the equations for the dependent base and collector currents have the form

$$I_b = Y_1(U_{eb}, U_{ec}), \quad I_c = Y_2(U_{eb}, U_{ec}),$$

where I_b is the base current, I_c is the collector current U_{eb} is the emitter-base voltage and U_{ec} is the emitter-collector voltage.

On any of the aforementioned segments (in the neighborhood of a point,), one can expand both functions in a Taylor series for two variables, and drop the terms for higher-order derivatives. For example , for the initial portion of the active domain,

$$I_b = \frac{\partial Y_1}{\partial U_{eb}}(U_{eb} - U_{ebI}) + \frac{\partial Y_1}{\partial Y_{ec}}(U_{ec} - U_{ecI}) +$$

$$+ Y_1(U_{ebI}, U_{ecI}), I_c = \frac{\partial Y_2}{\partial U_{eb}}(U_{eb} - U_{ebI}) +$$

$$+ \frac{\partial Y_2}{\partial U_{ec}}(U_{ec} - U_{ecI}) + Y_2(U_{ebI}, U_{ecI})$$

or

$$I_b = Y_{11I}U_{eb} + Y_{12I}U_{ec} + Y_{10I},$$
$$I_c = Y_{21I}U_{eb} + Y_{22I}U_{ec} + Y_{20I},$$

where Y_{11I} , Y_{12I}, Y_{21I} , and Y_{22I} are the nonautonomous transistor parameters for the transistor as a four-pole system of conductances for the initial active segment,

$$Y_{10I} = Y_1(U_{ebI} \quad U_{ecI}) - (Y_{11I}U_{eb\,I} + Y_{12I}U_{ecI}),$$
$$Y_{20I} = Y_2(U_{eb\,I} \quad U_{ecI}) - (Y_{21I}U_{eb\,I} + Y_{22I}U_{ec\,I})$$

are the "conditionally autonomous" parameters of the transistor as a four-pole for the initial active segment.

By using the well-known relationships for nonautonomous and autonomous parameters [3], one can rewrite the parameters obtained in any system of parameters and for any scheme for connecting the transistor. The parameters for the remaining segments are determined analogously.

A "conditionally autonomous" three-pole can be presented in the form of a nonautonomous three-pole (core) with external autonomous dipoles. Such a representation permits the use of the well-developed methods of analyzing schemes with nonautonomous multipoles [4].

By experimental measurements or by determining from static characteristics the aforementioned transistor parameters, one can replace the circuit of Fig. 1 by an equivalent linear replacement circuit including, together with dipoles, multipole elements and sources. The order of circuit design is as follows: For the first step, one determines the transmission coefficient of the portion of the circuit from E_{reg} to the output of the preamplifier (R_1 and R'_1 may be grounded). The second step consists of the determination of the value of collector current of triode $T_1(T'_1)$ which is necessary to operate the relay output stages. For this, the transistors are replaced by "conditionally autonomous" three-poles. As a preliminary step, one determines the collectors' saturation currents, and removes outside the three-pole core the autonomous two-poles. Thereafter, the replacement circuit is constructed.

To determine one (negative) threshold value of the current applied to the input of triode T_2 , it is sufficient to determine the magnitude of it for which the base current of cutoff triode T_2 becomes equal to the boundary base current at the beginning of the active portion; the value of this last current is determined from the triode's forward transmission characteristic.

To determine the second (positive) threshold value of current applied to the input of triode T_2, it is first necessary to find the value of base current of triode T_2 for which saturation of triode T'_2 occurs. For this, after disconnecting and grounding the left end of feedback resistor R_5 (Fig. 1), one sets up the matrix of conductances [Y] (or of impedances [Z]) by the method presented in [4]. By a well-known formula, one determines the current transmission factor from the base of T_2 to load R'_2:

$$K_I = \frac{\Delta_{12}}{\Delta_{22} + R'_2\Delta},$$

where Δ is the determinant of matrix [Y], and Δ_{12} and Δ_{22} are cofactors of the determinant [subscript 1 refers to the input (base of T_2) and subscript 2 refers to the output]. After this, one can determine the base current

of triode T'_2 which corresponds to saturation of T'_1, and thereafter one finds the threshold value of the input current.

In our case, the problem is essentially simplified, since the circuit is symmetric and is controlled only by negative values of the input current, i.e., only one value of threshold current is determined.

We note that the method presented permits one to take into account the effect on relay sensitivity, not only of the transistors' nonlinearities, but also the temperature variations of their parameters. For this, it is necessary to know the transistor characteristics in the operating temperature range.

LITERATURE CITED

1. B. S. Sotskov, "Thermistors and their use in circuits," Avtomatika i Telemekhanika 7, 1 (1948).
2. B. N. Kononov and L. P. Stepanenko, "Scaler circuits built with semiconducting triodes," Atomnaya énergiya No. 4 (1957).
3. É. V. Zelyakh, Fundamentals of the General Theory of Linear Electric Circuits [in Russian] (Izd AN SSSR, 1951).
4. V. P. Sigorskii, Methods of Analyzing Electric Circuits with Multipole Elements [in Russian] (Izd AN Ukr SSR, 1958).

REGARDING THE THEORY OF THIRD-ORDER LINEAR SYSTEMS

Yu. G. Zarenin

(Kiev)

Translated from Avtomatika i Telemekhanika, Vol. 21, No. 3, pp. 417-419, March, 1960
Original article submitted September 28, 1959

The frequency properties of linear third-order systems are considered. The possible types of frequency characteristics are defined and the relationships which uniquely determine their form are found. The results of the investigation are illustrated by diagrams.

Many automatic control systems can be described by linear third-order differential equations with constant coefficients. In spite of this, the theory of third-order systems is still not completely worked out. In particular, there has not yet been obtained an exhaustive solution to the problem of investigating the frequency properties of these systems. The literature is lacking in statements concerning the possible types of amplitude-frequency characteristics for these systems, as well as any information as to how one might determine the exact number of extremal points of these characteristics (not to mention their coordinates), if the coefficients of the system's differential equation are known. Here, we attempt to fill this void.

The investigation of the amplitude-frequency characteristics of third-order systems is divided into three stages.

a) Determine the possible types of these characteristics. As the basis for classifying amplitude-frequency characteristics, it is convenient to take the number of their extremal points.

b) Elucidate the relationships by means of which one might analytically determine, from the form of the system's differential equation, the type of its frequency characteristic.

c) Define the abscissas of the extremal points of the system's amplitude-frequency characteristic in terms of the coefficients of its differential equation.

We write the differential equation of a third-order linear system in the form

$$(Ap^3 + Bp^2 + Cp + D)\varphi = \psi, \tag{1}$$

where p is the differentiation operator, φ is the instantaneous value of some physical quantity at the system's output which is of interest to us, ψ is the instantaneous value of the signal applied to the input and A, B, C, D are constant coefficients.

To obtain the simplest possible relationships in the sequel, it is convenient [1] to divide both sides of (1) by the coefficient of the highest-order derivative. Denoting the new coefficients thereby obtained by $\underline{a}$, $\underline{b}$, $\underline{c}$, and $\underline{d}$, we can write

$$(p^3 + ap^2 + bp + c)\varphi = d\psi. \tag{2}$$

With this, the equation of the amplitude-frequency characteristic has the form

$$K(\omega) = \left|\frac{d}{H(j\omega)}\right| = \frac{d}{\sqrt{(c - a\omega^2)^2 + (b\omega - \omega^3)^2}}. \tag{3}$$

The number of its extremal points equals the number of positive real roots of the first derivative with respect to ω of the radicand in the denominator of (3). After a single differentiation of this expression, we obtain a fifth-order polynomial which contains no free term; corresponding to this one may assert that the first extremum of a third-order system's frequency characteristic lies on the axis of ordinates. In addition to the root $\omega = 0$, the polynomial under consideration has four pairwise conjugate roots. By considering all these roots to be real, we arrive at the conclusion that the maximum possible number of extremal points of the system's amplitude-frequency characteristic equals three. The minimum number of extrema, realized in the case when all four of the aforementioned roots are imaginary, equals one.

Thus, for a third-order system only three types of frequency characteristics are possible (Fig. 1). The dashed lines show frequency characteristics which are, hypothetically, theoretically possible but which, in practice, are not realizable.

Let us consider in more detail the roots of the first derivative of the radicand expression. By differentiating this expression, and introducing the notation

$$b^2 - 2ac = N \text{ and } 2b - a^2 = R, \tag{4}$$

we obtain the polynomial

$$3\omega^5 - 2R\omega^3 + N\omega = 0, \tag{5}$$

the roots of which equal

$$\omega_1 = 0, \quad \omega_{2,3,4,5} = \pm\frac{1}{\sqrt{3}}\sqrt{R \pm \sqrt{R^2 - 3N}}. \tag{6}$$

Discarding the roots less than zero, we obtain the abscissas of the extremal points of the system's amplitude-frequency characteristic:

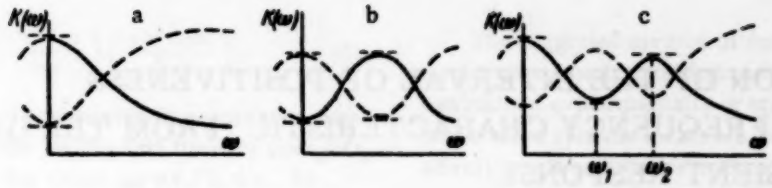

Fig. 1.

$$\omega_1 = 0,\quad \omega_2 = \frac{1}{\sqrt{3}}\sqrt{R+\sqrt{R^2-3N}} \text{ and } \omega_3 = \frac{1}{\sqrt{3}}\sqrt{R-\sqrt{R^2-3N}}. \tag{7}$$

The following conclusions derive from Expressions (7).

1. If $N < 0$ then, independently of the sign of R, frequency ω_3 is imaginary and ω_2 is real. The system's amplitude-frequency characteristic is a curve with two extrema—at the frequencies $\omega = \omega_1 = 0$ and $\omega = \omega_2$ (Fig. 1, b).

2. For $N > 0$ and $R < 0$, both frequencies ω_2 and ω_3 are imaginary. The amplitude-frequency characteristic has only one extremum—at the frequency $\omega = \omega_1 = 0$ (Fig. 1, a). The amplitude-frequency characteristic has the same form in the case when $N > 0$ and $R > 0$ but $R^2 < 3N$.

3. Frequencies ω_2 and ω_3 are both real only if the conditions $N > 0$, $R > 0$, and $R^2 > 3N$ all hold. With this, the amplitude-frequency characteristic has the form of a curve with extrema at the frequencies ω_1, ω_2, and ω_3 (Fig. 1, c).

The conclusions just drawn, together with (7), exhaust the problem of investigating the frequency properties of third-order systems.

For the practical use of these results, it is very convenient to employ a diagram with coordinates N and R (Fig. 2), on which the various hatchings indicate the

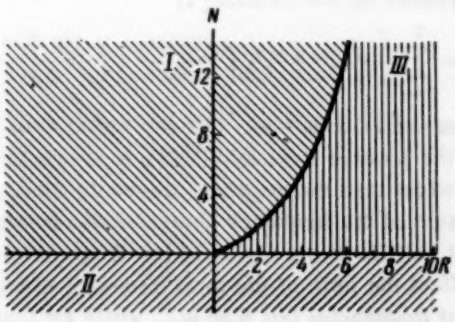

Fig. 2. I is the region of one extremum, II is the region of two extrema, and III is the region of three extrema.

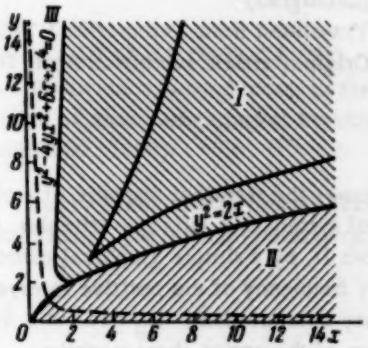

Fig. 3. I is the region of one extremum, II is the region of two extrema, and III is the region of three extrema.

regions corresponding to systems with various types of amplitude-frequency characteristics. Similar to those, like the well-known Vyshnegradskii diagram [1], which permit one, without solving equations, to judge of the stability and character of the transient response of a third-order system, the diagram of Fig. 2 gives a representation of its amplitude-frequency characteristic.

It is interesting to note that the juxtaposition of the diagram proposed by us with the Vyshnegradskii diagram (Fig. 3) graphically illustrates the relationship between the character of a third-order system's transient response and the form of its amplitude-frequency characteristic.

This relationship is implicitly contained in the relationships obtained by Vyshnegradskii and in the relationships given in the present work and, if necessary, could easily be elucidated analytically.

LITERATURE CITED

1. I. A. Vyshnegradskii, "On direct-acting regulators," D. K. Maksvell, I. A. Vyshnegradskii, and A. Stodola, Theory of Automatic Control (the Linearized Problem) [in Russian] (Izd AN SSSR, 1949).

DETERMINATION OF THE INTERVAL OF POSITIVENESS OF THE REAL FREQUENCY CHARACTERISTIC FROM THE GRAPH OF THE TRANSIENT RESPONSE

L. P. Shiniberov

(Leningrad)

Translated from Avtomatika i Telemekhanika, Vol. 21, No. 3, pp. 420-421, March, 1960
Original article submitted April 20, 1959

If one knows the transient response of a closed automatic control system to a unit step stimulus, then one may find from it, by a simple graphical construction, the boundary frequency of the positive interval of the real frequency characteristic ω_p without a detailed determination of the entire characteristic.

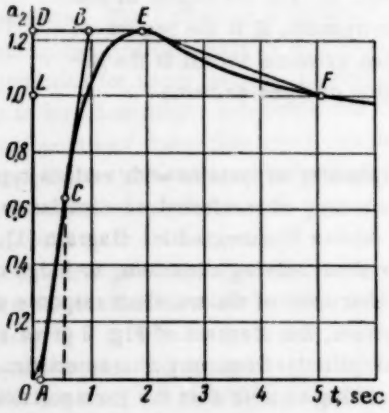

Fig. 1. Determination of ω_p from the graph of the transient response.

We assume that the curve of Fig. 1 is the transient response referred to for the output coordinate $\alpha_2 = f(t)$. On the figure we draw two auxiliary lines: line DE parallel to the axis of abscissas from the axis of ordinates to the maximum point of the transient response, and line AB, coinciding with the majority of points on the ascending (increasing) part of the transient response curve, from the axis of abscissas to line DE. We bisect line AB and find the value of time t_m which corresponds to the midpoint of this line (point C). Then, the boundary frequency of the positive interval can be determined from the formula

$$\omega_p = \frac{\pi}{2t_m}. \qquad (1)$$

In the example given, $\omega_p = \pi/2(0.5) = 3.14\ \text{sec}^{-1}$, which is close to the true value of $\omega_p = 3.20\ \text{sec}^{-1}$.

We now prove the validity of the result obtained.

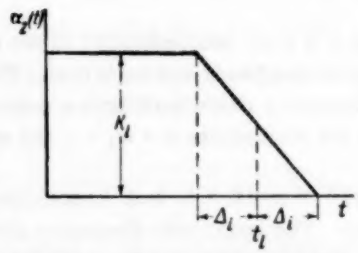

Fig. 2. Typical trapezoidal transient response.

We divide the curve of the transient response, given in Fig. 1, into three parts: 1) the unit step transient response $+1(t)$; 2) the positive trapezoid DEFL lying above the function $+1(t)$ with altitude $K_1 = DL$; 3) the negative trapezoid DBAO with altitude $K_2 = -OD$. From these trapezoidal characteristics it is possible to find the real frequency characteristic of the automatic control system. If we denote the elements of the trapezoidal characteristic as was done in Fig. 2, then in the given case the system's real frequency characteristic $R(\omega)$ will be expressed by the formula [1]

$$R(\omega) = \sum_{i=1}^{2} \left[K_i - \omega K_i t_i \left(\frac{\cos t_i\omega}{t_i\omega} \right) \left(\frac{\sin \Delta_i\omega}{\Delta_i\omega} \right) \right] + 1. \qquad (2)$$

For the value $\omega = \omega_p$, this expression must vanish. Since the positive trapezoid DBEFL is always several times wider than the negative trapezoid DBAO, the maximum of the frequency characteristic constructed from it will lie in the region of low frequencies, and it will affect the form of the total frequency characteristic only for frequencies less than ω_p, while for frequencies close to ω_p or larger than ω_p, it will have a constant value, equal to K_1.

This means mathematically that, for frequencies $\omega > 5/t_1$, the term $\omega K_1 t_1 (\cos t_1\omega/t_1\omega)(\sin \Delta_1\omega/\Delta_1\omega)$ in (2) can be ignored, since it is significantly smaller than $0.1K_1$. Thus, in the neighborhood of frequency ω_p, the real frequency characteristic, when account is taken of the fact that $K_1 + K_2 + 1 = 0$, will be approximately expressed by the formula

$$R(\omega) = -\omega K_2 t_2 \left(\frac{\cos t_2\omega}{t_2\omega}\right)\left(\frac{\sin \Delta_2\omega}{\Delta_2\omega}\right). \qquad (3)$$

The curve for $R(\omega)$ constructed in accordance with (3) will pass through zero for the first time for $\cos t_2\omega / t_2\omega = 0$, which occurs for the value $t_2\omega = \pi/2$, i.e., for

$$\omega = \frac{\pi}{2t_m}, \quad \text{since} \quad t_2 = t_m$$

As is clear, the frequency $\omega = \pi/2t_m$ is the boundary frequency of the positive interval, i.e., (1) is valid.

The value of ω_p thus obtained may serve as an estimate of the cutoff frequency ω_c of the system's logarithmic amplitude characteristic since, as is well known, the logarithmic amplitude characteristic intersects the frequency axis for the values [2]

$$\omega_c = (0.55 - 0.7)\,\omega_p. \qquad (4)$$

The suggested method of determining ω_p gives good results when one is considering transient responses, either determined experimentally or stated as desirable, of power servo systems which are distinguished by comparatively small oscillatory indices: M = 1.1 to 1.4.

For other transfer functions, the error reaches 15 to 20 %, and this method can be used only for an approximate estimate of ω_p.

LITERATURE CITED

1. V. V. Solodovnikov, Introduction to the Statistical Dynamics of Automatic Control System [in Russian] (Gostekhizdat, 1952).
2. A. V. Fateev, Fundamental Linear Automatic Control Theory [in Russian] (Gosénergoizdat, 1954).

PROCESSING EXPERIMENTAL FREQUENCY CHARACTERISTICS

G. I. Monastyrshin

(Moscow)

Translated from Avtomatika i Telemekhanika, Vol. 21, No. 3, pp. 422-428, March, 1960
Original article submitted May 20, 1959

For recording forced oscillations, loop oscillographs are ordinarily used, recording both the stimulus and the reaction of the element. In those cases where the oscillations do not have a perfectly sinusoidal form, oscillogram processing is carried out by means of a harmonic analyzer which separates out the harmonic component of the reaction which has the same frequency as the stimulus; for brevity, we shall henceforth call it simply the reaction's harmonic component.

Figure 1 gives a set of oscillograms of a servo drive's oscillations, established under the action of sinusoidal stimuli of various frequencies and constant amplitudes. On these oscillograms, U is the stimulus and V is the servo drive's reaction. The oscillograms also bear the reaction's harmonic component. The cross on each oscillogram marks the maximum deviation of the servo drive's oscillation from the given harmonic component. We note that, in the example given, not only the sinusoidal character of the oscillation is disrupted, but, as is clear from Fig. 1, its periodicity is also disturbed to a certain extent, so that in the cases of Fig. 1, c and d the harmonic analysis is carried out over an interval of several (two) periods of the stimulus.

The results of the measurements are collected in the table, where ω_i is the angular frequency of the harmonic stimulus, A_i is the stimulus amplitude, B_i is the amplitude of the reaction's harmonic component, φ_i is the phase shift between the stimulus and the reaction's harmonic component and ΔB_i is the maximum deviation of the reaction from its harmonic component.

We remark that the table can be obtained without the intermediary of an oscillograph by means of direct measurements using the method cited in [1].

In what follows we shall not deal with any concrete form of the deviations of the forced oscillations from their harmonic components, but shall deal with the study abstractly, assuming that any character of these deviations is possible with limitations on the modulus of the ΔB_i. Corresponding to such a treatment, the forced oscillations are characterized, not by lines, but by the bands included between two sinusoids, equidistant from the harmonic component of the oscillation, and separated from it by the maximum deviation marked on the oscillograms.

By considering the reaction's harmonic component as the projection of the polar vector $\bar{B}_i$, we can interpret the deviations of actual oscillations from their harmonic components as the projections of an auxiliary vector $\Delta\bar{B}_i$, limited in modulus.

i	ω_i, sec^{-1}	A_i, mm	B_i, mm	φ_i, degrees	ΔB_i, mm
1	3.123	31.0	20.95	— 47°20′	3
2	6.148	31.0	13.83	— 74°03′	4
3	12.45	31.0	7.36	—101°46′	3
4	25.13	31.0	3.61	—138°08′	5

If we abstract from the concrete definiteness of the rotation of this auxiliary vector we obtain, instead of the end of the vector $\bar{B}_i$, a circular smear with radius ΔB_i.

The vector interpretation allows one to note that when $\Delta B_i \ll B_i$ (for our purposes, it suffices in practice if $\Delta B_i < 0.5\, B_i$) the ratio $\Delta B_i : B_i$ is determined approximately both by the maximum relative variation of the harmonic component's amplitude and by the maximum variation of its phase (measured in radians) for which the harmonic oscillations will remain within the limits of the smear defined earlier or, what amounts to the same thing, within the limits of the forced oscillations' bands. In this sense, instead of the lines of the frequency, amplitude and phase characteristics, one can consider the bands of the amplitude and phase characteristics. Figure 2 shows such bands, constructed from the oscillograms of Fig. 1. In the neighborhood of the frequency 4 cps, the bands of the phase characteristic are not bounded due to the fact that the condition on the smallness of ΔB_i does not hold.

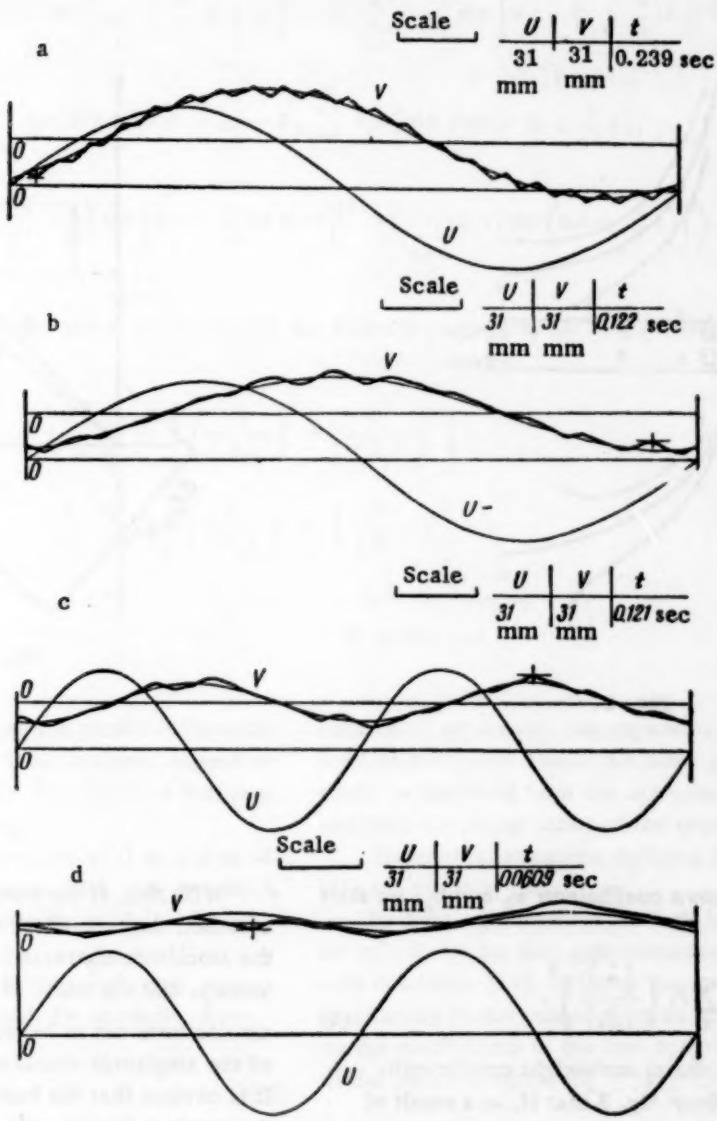

Fig. 1.

In using an element's experimental frequency characteristic, it may turn out to be advantageous to define the system by the differential equation corresponding to these characteristics [2-6]. For example, the problem arises in mathematical modelling of setting up the scheme which reproduces the frequency characteristics.

We assume that the linear differential equation defined by the experimental frequency characteristics has the form

$$\sum_{k=0}^{n} a_k U^{(k)} = \sum_{k=0}^{m} b_k V^{(k)}, \qquad (1)$$

where the $U^{(k)}$ are the stimulus and its derivatives, and the $V^{(k)}$ are the reaction and its derivatives.

As represented on the oscillograms, the stimulus U_i and the reaction's harmonic component V_i may be written in the form

$$U_i = A_i \sin \omega_i t, \qquad (2)$$

$$V_i = B_i \sin (\omega_i t + \varphi_i). \qquad (3)$$

To determine the numerical values of the coefficients a_k and b_k of (1), we use the approximate equation obtained by substituting (2) and (3) in (1):

$$\sum_{k=0}^{n} a_k A_i \omega_i^k \sin \left(\omega_i t + \frac{\pi}{2} k\right) \approx$$

$$\sum_{k=0}^{m} b_k B_i \omega_i^k \sin \left(\omega_i t + \varphi_i + \frac{\pi}{2} k\right). \qquad (4)$$

To provide a graphic representation, we denote the left and right members of (4) by polar vectors $\bar{R}_i$ and $\bar{S}_i$ (Fig. 3).

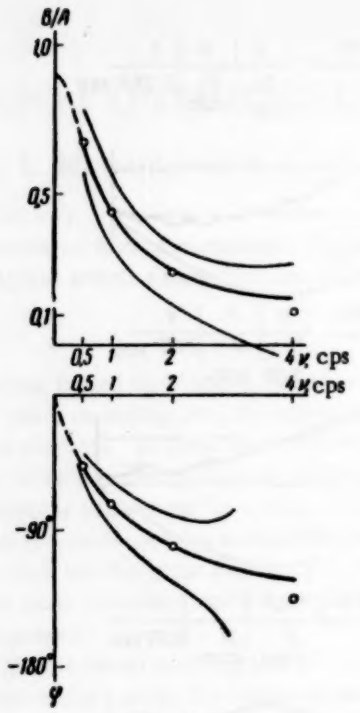

Fig. 2.

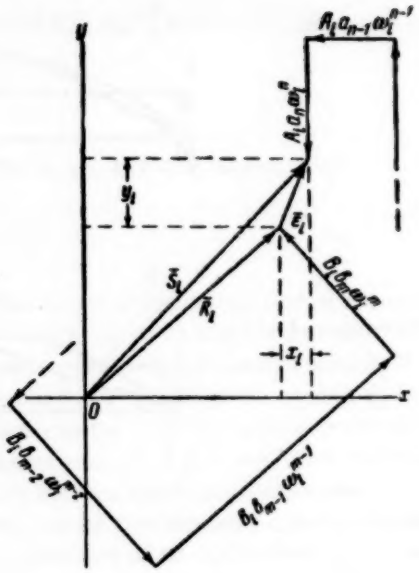

Fig. 3.

To find the unknown coefficients a_k and b_k, we start from the condition

$$\min \sum_i p_i \left(\frac{|\bar{\varepsilon}_i|}{|\bar{R}_i|} \right)^2, \tag{5}$$

where $\bar{\varepsilon}_i = \bar{S}_i - \bar{R}_i$ and the p_i are weight coefficients.

It is easily seen from Fig. 3 that if, as a result of seeking the values of the coefficients of (1), the vectors $\bar{\varepsilon}_i$ lie within the limits of certain circular smears whose radii are in the same ratios to the moduli of vectors $\bar{R}_i$ as the ΔB_i are to the B_i, then the forced oscillations defined by (1), with the values found for the coefficients, lie within the limits of the bands considered earlier.

In correspondence with this, by setting the requirements on the accuracy of the approximation of the frequency characteristics, and omitting the arbitrary coefficient of proportionality, we establish the weight coefficients:

$$p_i = \left(\frac{B_i}{\Delta B_i} \right)^2. \tag{6}$$

If in (6), instead of the quantities ΔB_i, which depend on the frequency of the forced oscillations, we use the quantity $\max \Delta B_i$ and omit the constant factor thereby entailed, then

$$p_i = B_i^2. \tag{7}$$

With this, if the stimulus amplitude is taken to be constant, then the width of the corresponding band of the amplitude characteristic ceases to depend on frequency, and the width of the band of the phase characteristic turns out to be inversely proportional to the value of the amplitude characteristic (for sufficiently small ΔB_i). It is obvious that the bands corresponding to (6) lie inside the bands defined by (7).

We note that (5) for $|\bar{\varepsilon}_i| \ll |\bar{R}_i|$, as may be observed from Fig. 3, is equivalent to the condition

$$\min \sum_i p_i (\Delta_i^2 + \delta_i^2), \tag{8}$$

where the Δ_i are the absolute deviations of the phase characteristic of (1) from the experimental one, measured in radians, and the δ_i are the relative deviations of the amplitude characteristic of (1) from the experimental.

For what follows, it is advantageous to give (5) in the form

$$\min \sum_i p_i \left[\left(\frac{x_i}{|\bar{R}_i|} \right)^2 + \left(\frac{y_i}{|\bar{R}_i|} \right)^2 \right], \tag{9}$$

where x_i and y_i are the projections of vector $\bar{\varepsilon}_i$.

It is easily seen that

$$x_i = A_i \sum_{k=0}^{n} a_k \omega_i^k \sin\left[\omega_i t + \frac{\pi}{2}(k+1)\right] - B_i \sum_{k=0}^{m} b_k \omega_i^k \sin\left[\omega_i t + \varphi_i + \frac{\pi}{2}(k+1)\right], \tag{10}$$

$$y_i = A_i \sum_{k=0}^{n} a_k \omega_i^k \sin\left(\omega_i t + \frac{\pi}{2}k\right) - B_i \sum_{k=0}^{m} b_k \omega_i^k \sin\left(\omega_i t + \varphi_i + \frac{\pi}{2}k\right), \tag{11}$$

$$|\bar{R}_i|^2 = A_i^2\left(\left\{\sum_{k=0}^{n} a_k \omega_i^k \sin\left[\omega_i t + \frac{\pi}{2}(k+1)\right]\right\}^2 + \left[\sum_{k=0}^{n} a_k \omega_i^k \sin\left(\omega_i t + \frac{\pi}{2}k\right)\right]^2\right). \tag{12}$$

With (10), (11), and (12) kept in mind, we shall have the following equations for determining the coefficients sought:

$$\frac{\partial}{\partial a_k}\sum_i p_i\left[\left(\frac{x_i}{|\bar{R}_i|}\right)^2 + \left(\frac{y_i}{|\bar{R}_i|}\right)^2\right] = 0,$$

$$\frac{\partial}{\partial b_l}\sum_i p_i\left[\left(\frac{x_i}{|\bar{R}_i|}\right)^2 + \left(\frac{y_i}{|\bar{R}_i|}\right)^2\right] = 0 \tag{13}$$

$$\begin{pmatrix} k = 1, 2, \ldots, n; & l = 0, 1, 2, \ldots, m \text{ in the case } a_0 = 1 \\ k = 0, 1, 2, \ldots, n; & l = 1, 2, \ldots, m \text{ in the case } b_0 = 1 \end{pmatrix}.$$

Since the quantities following the partial differentiation signs in (13) do not, in the final analysis, depend on t, one can set $t = 0$ in (10), (11), and (12) as a first step, thus simplifying the computations.

If (1) does not contain derivatives of U or V then (13) will be linear since, in the first case, $|\bar{R}_i| = A_i$ (we set a_0 equal to unity) and, in the second, $|\bar{R}_i| \approx |\bar{S}_i| \triangleq B_i$ (we set b_0 equal to unity).

Otherwise, the coefficients being sought can, to a first approximation, be determined, for example, from the condition

$$\min \sum_i |\bar{\varepsilon}_i|^2. \tag{14}$$

To render more exact the solution thus obtained one might determine the quantities $|\bar{R}_i|$ graphically from the vector diagram or by (12) for $t = 0$ and the numerical values of the coefficients of the first approximation, where for the differentiation of the fractions in (13), one differentiates only the numerator (as in the case when the denominator does not depend on the parameter with respect to which the differentiation is being performed), which is possible if the numerator is sufficiently small with respect to the denominator.

Omitting the detailed computations, we give the final expressions determining the coefficients of the equation

$$U + a_1\dot{U} + a_2\ddot{U} + a_3U^{(3)} + a_4U^{(4)} + a_5U^{(5)} = b_0V + b_1\dot{V} + b_2\ddot{V} + b_3V^{(3)} + b_4V^{(4)} + b_5V^{(5)}. \tag{15}$$

In terms of this example, we consider the structure of the formulation which permits one to obtain the analogous formulas for any more complicated case. The case considered apparently encompasses all practically possible particular cases. All these particular cases may easily be obtained from the one considered by simply omitting the proper terms of the expressions provided.

The normal equations defining the coefficients of (15) are given by (16).

In these equations, $p_i k_i^2 = 1$ (it is also possible to set $k_i^2 = 1$) for the first approximation in correspondence with condition (14), and may thereafter be determined graphically in the rendering more accurate of the solution by the coefficients of the first approximation by means of the vector diagram ($k_i^2 = |\bar{R}_i|^{-2}$) or by

$$k_i^2 = A^{-2}_i[(a_1\omega_i - a_3\omega_i^3 + a_5\omega_i^5)^2 + (1 - a_2\omega_i^2 + a_4\omega_i^4)^2]^{-1}. \tag{17}$$

For simpler cases it suffices, in (16), to delete the columns, and the rows symmetric with them about the principal diagonal in the matrix of the unknown coefficients, for the coefficients of the higher derivatives which are lacking in (15). The corresponding terms in (17) are also omitted. In the particular case when there are no derivatives in the left member of (15), there remain only the last six columns of the left side of (16) and, correspondingly, only the six last equations $k_i^2 = A_i^{-2}$, and the problem is significantly simplified. If there are no derivatives in the right member of (15), it is then advantageous to change the problem slightly, setting $b_0 = 1$ and taking a_0 as an unknown. In this case, the simplified normal equations obtained from (16) are analogous to the preceding ones if one first makes the following changes in (16): the b_k are replaced by the

$$
\begin{array}{rrrrrrrrrrrcl}
+a_1\sum_i c_i\omega_i^2 & & -a_3\sum_i c_i\omega_i^4 & & +a_5\sum_i c_i\omega_i^6 & -b_0\sum_i d_i\omega_i & -b_1\sum_i e_i\omega_i^2 & +b_2\sum_i d_i\omega_i^3 & +b_3\sum_i e_i\omega_i^4 & -b_4\sum_i d_i\omega_i^5 & -b_5\sum_i e_i\omega_i^6 & = & 0\\
 & a_2\sum_i c_i\omega_i^4 & & -a_4\sum_i c_i\omega_i^6 & & +b_0\sum_i e_i\omega_i^2 & -b_1\sum_i d_i\omega_i^3 & -b_2\sum_i e_i\omega_i^4 & +b_3\sum_i d_i\omega_i^5 & +b_4\sum_i e_i\omega_i^6 & -b_5\sum_i d_i\omega_i^7 & = & \sum_i c_i\omega_i^2\\
-a_1\sum_i c_i\omega_i^4 & & +a_3\sum_i c_i\omega_i^6 & & -a_5\sum_i c_i\omega_i^8 & +b_0\sum_i d_i\omega_i^3 & +b_1\sum_i e_i\omega_i^4 & -b_2\sum_i d_i\omega_i^5 & -b_3\sum_i e_i\omega_i^6 & +b_4\sum_i d_i\omega_i^7 & +b_5\sum_i e_i\omega_i^8 & = & 0\\
 & -a_2\sum_i c_i\omega_i^6 & & +a_4\sum_i c_i\omega_i^8 & & -b_0\sum_i e_i\omega_i^4 & +b_1\sum_i d_i\omega_i^5 & +b_2\sum_i e_i\omega_i^6 & -b_3\sum_i d_i\omega_i^7 & -b_4\sum_i e_i\omega_i^8 & +b_5\sum_i d_i\omega_i^9 & = & -\sum_i c_i\omega_i^4\\
a_1\sum_i c_i\omega_i^6 & & -a_3\sum_i c_i\omega_i^8 & & +a_5\sum_i c_i\omega_i^{10} & -b_0\sum_i d_i\omega_i^5 & -b_1\sum_i e_i\omega_i^6 & +b_2\sum_i d_i\omega_i^7 & +b_3\sum_i e_i\omega_i^8 & -b_4\sum_i d_i\omega_i^9 & -b_5\sum_i e_i\omega_i^{10} & = & 0\\
-a_1\sum_i d_i\omega_i & +a_2\sum_i e_i\omega_i^2 & +a_3\sum_i d_i\omega_i^3 & -a_4\sum_i e_i\omega_i^4 & -a_5\sum_i d_i\omega_i^5 & +b_0\sum_i f_i & & -b_2\sum_i f_i\omega_i^2 & & +b_4\sum_i f_i\omega_i^4 & & = & \sum_i c_i\\
-a_1\sum_i e_i\omega_i^2 & -a_2\sum_i d_i\omega_i^3 & +a_3\sum_i e_i\omega_i^4 & +a_4\sum_i d_i\omega_i^5 & -a_5\sum_i e_i\omega_i^6 & & +b_1\sum_i f_i\omega_i^2 & & -b_3\sum_i f_i\omega_i^4 & & +b_5\sum_i f_i\omega_i^6 & = & -\sum_i d_i\omega_i\\
a_1\sum_i d_i\omega_i^3 & -a_2\sum_i e_i\omega_i^4 & -a_3\sum_i d_i\omega_i^5 & +a_4\sum_i e_i\omega_i^6 & +a_5\sum_i d_i\omega_i^7 & -b_0\sum_i f_i\omega_i^2 & & +b_2\sum_i f_i\omega_i^4 & & -b_4\sum_i f_i\omega_i^6 & & = & -\sum_i e_i\omega_i^2\\
a_1\sum_i e_i\omega_i^4 & +a_2\sum_i d_i\omega_i^5 & -a_3\sum_i e_i\omega_i^6 & -a_4\sum_i d_i\omega_i^7 & +a_5\sum_i e_i\omega_i^8 & & -b_1\sum_i f_i\omega_i^4 & & +b_3\sum_i f_i\omega_i^6 & & -b_5\sum_i f_i\omega_i^8 & = & \sum_i d_i\omega_i^3\\
-a_1\sum_i d_i\omega_i^5 & +a_2\sum_i e_i\omega_i^6 & +a_3\sum_i d_i\omega_i^7 & -a_4\sum_i e_i\omega_i^8 & -a_5\sum_i d_i\omega_i^9 & +b_0\sum_i f_i\omega_i^4 & & -b_2\sum_i f_i\omega_i^6 & & +b_4\sum_i f_i\omega_i^8 & & = & \sum_i e_i\omega_i^4\\
-a_1\sum_i e_i\omega_i^6 & -a_2\sum_i d_i\omega_i^7 & +a_3\sum_i e_i\omega_i^8 & +a_4\sum_i d_i\omega_i^9 & -a_5\sum_i e_i\omega_i^{10} & & +b_1\sum_i f_i\omega_i^6 & & -b_3\sum_i f_i\omega_i^8 & & +b_5\sum_i f_i\omega_i^{10} & = & -\sum_i d_i\omega_i^5
\end{array}
$$

where $c_i = p_i k_i^2 A_i^2$; $d_i = p_i k_i^2 A_i B_i \sin\varphi_i$; $e_i = p_i k_i^2 A_i B_i \cos\varphi_i$; $f_i = p_i k_i^2 B_i^2$. (16)

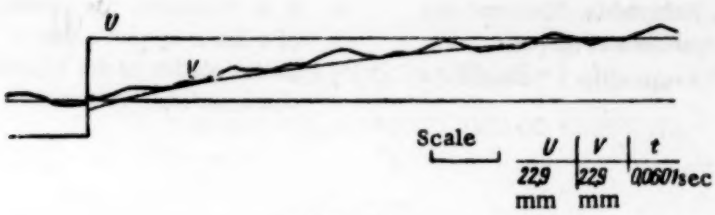

Fig. 4.

a_k and the a_k are replaced by the b_k and, in the expressions for the coefficients c_l, d_l, e_l, and f_l, A_l is replaced by B_l, B_l is replaced by A_l, φ_l is replaced by $-\varphi_l$ and the k_l^2 are defined as B_l^{-2}. One should then retain the six last equations and, correspondingly, the six last columns of the left members of these equations, determining the p_l by (6) or (7).

If, as a result of the computation of the coefficients of (15), the difference between its frequency characteristics and the experimental ones, defined by the harmonic components of the actual oscillations, turns out to be sufficiently small - for example, significantly less than the possible deviations inside the previously defined bands of the forced oscillations - we shall then consider that the problem of determining the linear equation which approximates the experimental frequency characteristics has been successfully solved.

In the concrete example considered, given by Figs. 1 and 2 and by the table, we are investigating an equation of the form

$$U + a_1\dot{U} = b_0V + b_1\dot{V}, \tag{18}$$

for which we shall have the normal equations

$$\begin{aligned}
&a_1\sum_i p_i k_i^2 A_i^2\omega_i^2 - \\
&- b_0\sum_i p_i k_i^2 A_i B_i\omega_i \sin\varphi_i - b_1\sum_i p_i k_i^2 A_i B_i\omega_i^2\cos\varphi_i = 0,\\
&-a_1\sum_i p_i k_i^2 A_i B_i\omega_i \sin\varphi_i + b_0\sum_i p_i k_i^2 B_i^2 = \\
&\qquad = \sum_i p_i k_i^2 A_i B_i\cos\varphi_i,\\
&-a_1\sum_i p_i k_i^2 A_i B_i\omega_i^2\cos\varphi_i + \\
&\qquad + b_1\sum_i p_i k_i^2 B_i^2\omega_i^2 = -\sum_i p_i k_i^2 A_i B_i\omega_i\sin\varphi_i
\end{aligned} \tag{19}$$

Setting the p_l by (6) and taking, in correspondence with (17),

$$k_i^2 = A_i^{-2}(a_1^2\omega_i^2 + 1)^{-1} \tag{20}$$

we obtain, as the result of computing the first and second approximations and the corresponding rounding,

$$a_1 = -0{,}034, \quad b_0 = 1{,}11, \quad b_1 = 0{,}325.$$

The corresponding frequency characteristic is given in Fig. 2. The circles on the figure mark the experimental points, while the heavy lines show the results of the approximation.

It should not be overlooked that the frequency characteristics considered can not determine all the properties of the actual element. Due to this, the question as to the use of such a type of characteristics, and the equations approximating them, can form the subject of a concrete study.

For the example considered, Fig. 4 shows the reaction to a unit step function stimulus, obtained from (18) by computing the values of the coefficients, and the analogous reaction of the actual servo drive.

It may happen that, in practice, one does not succeed in obtaining a sufficiently small error of approximation of the experimental frequency characteristics. For example, these errors may remain beyond the limits of the experimentally defined bands of the forced oscillations. In this case, the question as to the possibility of using the results of the approximation can be decided by fixing the band of the forced oscillations in correspondence with the approximation errors obtained.

We note that a treatment analogous to that presented here is also possible in the case when the experimental results are free from nonlinear deviations, and only measurement errors distort them.

LITERATURE CITED

1. K. V. Zakharov and V. K. Svyatodukh, "An instrument for determining frequency characteristics of nonlinear systems," Avtomatika i Telemekhanika 20, 12 (1959).

2. L. A. Galin, "Determining an instrument's differential equation on the basis of testing for forced oscillations," Prikl. Matem. i Mekhan. No. 10 (1946).

3. G. L. Rabkin, B. A. Mitrofanov, and Yu. O. Shterenberg, "On the determination of the numerical values of the coefficients of the transfer functions of linearized links and systems from experimental frequency characteristics," Avtomatika i Telemekhanika 16, 5 (1955).

4. G. I. Monastyrshin, "Mathematical processing of an experiment for the investigation of an automatic control system," Collection: Questions in Automatic Control Theory [in Russian] (Oborongiz, 1956).

5. A. A. Kardashov and L. V. Kamyushin, "Determining system parameters from experimental (given) frequency characteristics," Avtomatika i Telemekhanika 19, 4 (1958).

6. E. E. Dubnikov, "Determination of the coefficients of a linear system's transfer function from the initial portion of the experimental amplitude-phase characteristic," Avtomatika i Telemekhanika 20, 5 (19

INFORMATION

THE ÉMU-8 ELECTRONIC ANALOG COMPUTER

As the result of the work on improving electronic analog computers and their elements which has been carried on at the Institute for Automation and Remote Control of the Academy of Science of the USSR in conjunction with a collective under the direction of G. N. Grigor'yan, there has been created a new electronic analog computer, type ÉMU-8, production of which has already begun.

Domain of Application of Type ÉMU-8 Electronic Analog Computer

The type ÉMU-8 electronic analog computer is designed for the investigation of linear and nonlinear dynamic systems. Structurally, it is a general-purpose computer capable of real-time operation (joined with elements of actual apparatus) with accelerated and retarded solution processes within the limits of its passband. The computer can be used to greatest effect in the solution of technological problems where the error in giving the original parameters is sufficiently large (from 5 to 10%).

Among these problems may be listed:

1) investigation of the dynamics of automatic control and regulation systems (automated systems, missile control, boiler aggregate regulation, steam turbine control, various automated electric drives, etc.);

2) certain problems of nuclear physics and technology;

3) investigation of combustion processes in internal-combustion engines;

4) investigation of transient responses in complicated electrical circuits;

5) investigations in the area of nonlinear mechanics.

Brief Technical Characteristics of the ÉMU-8*

The ÉMU-8 computer consists of individual building blocks each of dimensions 450 x 460 x 320 mm. Each building block can provide the solution of linear and nonlinear differential equations up to second-order, inclusive.

* For more detailed technical characteristics of the computer plus its functional schematic, see Vestnik Akademii Nauk No. 7 (1958).

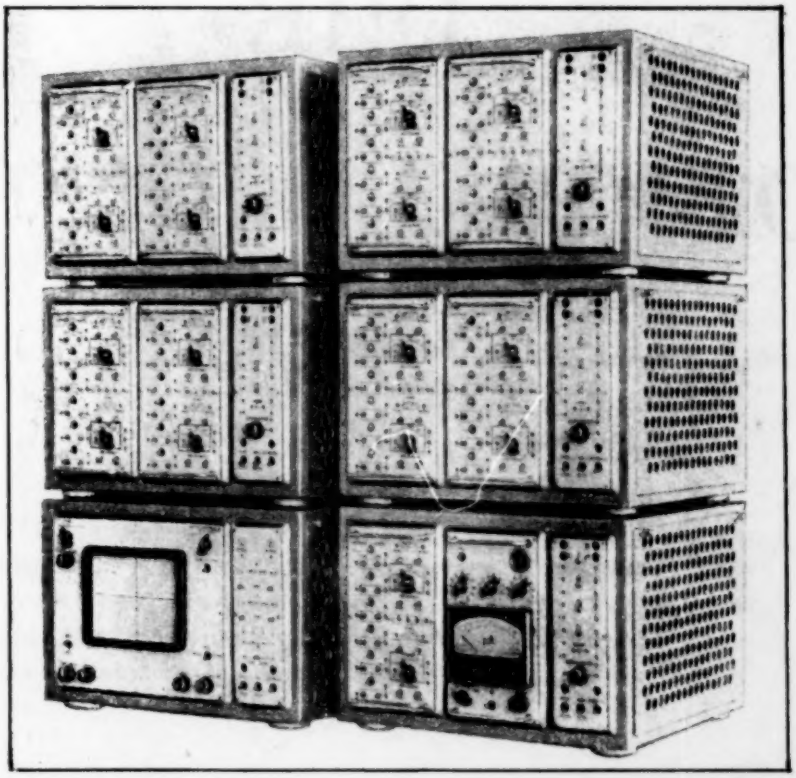

while the standard package of building blocks provides solutions of differential equations up to tenth-order, inclusive. Plug-in units permit the execution of the following mathematical operations: multiplication and division of two independent variables, multiplication by a constant factor, differentiation, integration, reproduction of various nonlinear functions and standard nonlinearities.

The character of the mathematical operations executed is determined by the type of plug-in units, which allows operational amplifiers to be used economically.

By choosing several building blocks with the necessary variants of plug-in units, one can solve problems of various complexity.

In the standard package, five building blocks are used.

Six block indicators are connected to each package to provide visual observation of problem solution.

Each building block is designed in the form of a completely independent instrument, and may be connected directly to a 220v line. The power requirement of each block is about 160w.

Line production of the computer was organized in 1960. The wholesale price of a package is 135,000 rubles.

Bureau of Factory Information